Minor element composition and stable oxygen isotopes of calcareous shells of the dinoflagellate *Thoracosphaera heimii*

Dissertation zur Erlangung des Doktorgrades

der Naturwissenschaften

-Dr. Rer. Nat.-

am Fachbereich 5 – Geowissenschaften

der Universität Bremen

Vorgelegt von

Stefanie Dekeyzer

Bremen, Oktober 2011

Tag des Kolloquiums:

09.02.2012

Gutachter:

Frau PD Dr. Karin Zonneveld

Frau Prof. Dr. Simone Kasemann

Stefanie Dekeyzer
Hollerallee 10-12, 28209 Bremen

31st of October, 2011

Erklärung

Hiermit versichere ich, dass ich

1. die Arbeit ohne unerlaubte fremde Hilfe angefertigt habe,

2. keine anderen als die von mir angegebenen Quellen und Hilfsmittel benutzt habe und

3. die den benutzten Werken wörtlich oder inhaltlich entnommenen Stellen als solche kenntlich gemacht habe.

Stefanie Dekeyzer

Bremen, den 31. Oktober 2011

"The larger the island of knowledge,
the longer the shoreline of mystery."

— Unknown author —

Voor Papa, Mama en Valerie

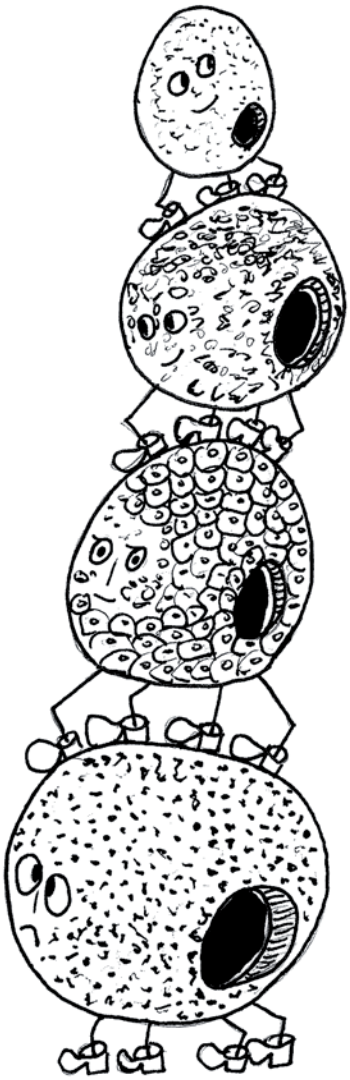

THORACOSPHAERA HEIMII BREMENSIS VULGARIS (courtesy of Jos Dekeyzer)

Acknowledgements

This project was financed by the German Science Foundation (DFG), as a subproject of the International Graduate College 'Proxies in Earth History' (EUROPROX).

First of all, I would like to thank my supervisor PD Dr. Karin Zonneveld for giving me the opportunity to accomplish this PhD thesis. Thanks for her general support, suggestions, comments and advice.

Thanks to Prof. Dr. Patrizia Ziveri, my second supervisor, for allowing me to do part of my research at the Universitat Autònoma de Barcelona, Spain. My research and laboratory work benefitted a lot from your nice comments and suggestions. I also thank you for your constructive comments on previous versions of the manuscripts incorporated in this thesis.

Furthermore I thank Prof. Dr. Simone Kasemann for her willingness to review this thesis.

Being a PhD student would not have been possible without my previous training as a geologist at Ghent University, Belgium. Therefore I would like to thank Prof. Dr. Stephen Louwye and Prof. Dr. Jacques Verniers of the "Department Geology and Soil Science – Research Unit Palaeontology" for their interesting lectures and for supervising my master thesis.

All members of the Historical Geology/Paleontology group (AG Willems) at the University of Bremen are thanked. Special thanks go to my colleagues with whom I shared an office: thank you Ilham Bouimetarhan and Sonja Heinrich for your encouraging words and relaxing coffee breaks. I gratefully acknowledge Ulrike (Uli) Holzwarth and Marion Kohn for having interesting discussions and eruptions of laughter. I also owe Uli many thanks for providing the German summary of this thesis.

During my three years project, I was given the opportunity to join one Meteor and two Poseidon cruises, and to attend many interesting workshops and conferences. I would like to acknowledge all members of the "dinoflagellate science community". Thank you for many interesting discussions and friendly conversations. I especially want to thank Stijn Deschepper, Jan Hennissen, Thomas Verleye and Nicholas Vannieuwenhove. I always enjoyed the funny encounters with you, "my fellow Belgian dino-people", all over the world.

There is 1 person I cannot forget here: Kara Bogus, my dear colleague and friend. Thank you for all the good times we had in the office, on the ship and on our trips. We have been called many names, “the comical duo”, “the dream team”, “an old married couple”, but one thing is for sure: pandas are the best! ☺ We started our PhD on the same day, and yes, we submitted our thesis on the same day. We did it Kara! It felt very reassuring that you were there with me, during every step of the process. I could always turn to you when things were not going as planned and when my dinoflagellate was frustrating the hell out of me.

Unfortunately, I had to say goodbye to my grandmother during the last months of writing my thesis. Dear Oma, I hope you can rest in peace now, wherever you are, together with Opa. I kept my promise to you, I finished in time.

I would also like to thank Giel Demeulemeester. Thank you for taking care of my sister when the distance between Bremen and Wevelgem/Kortrijk seemed like a million kilometers. And thank you again for helping me suprise my parents for Christmas. I will never forget the short car drive in the middle of the night, while trying to get dressed up as a present☺.

Valerie, my dearest little sister. I know you did not allways like the fact that I lived in Bremen and that you wished I was a PhD student in dear old Gent. But, although we couldn’t allways talk about our adventures in person; you were just one phone call/messenger conversation away. Thank you for allways being there for me. Thank you for being my little sister.

And most of all, I would like to thank my parents. Thank you for giving me the chance to pursue my dreams. Thank you for your logistical support. Thank you for supplying me with Belgian chocolate, many times, when you came to Bremen. Thank you for helping me out with house stuff when I barely had the time to sleep. Thank you for fixing my shower☺. And most of all, thank you for your emotional support. You never lost faith in me. Even when I saw no light at the end of the tunnel, your words kept me from giving up. Even when I said, for the umpteenth time, “I don’t think I can do this”, you were the first to tell me otherwise. Papa and mama, I would not have made it without you. Bedankt!

Table of contents

List of figures

CHAPTER 2

CHAPTER 3

CHAPTER 4

CHAPTER 5

CHAPTER 7

CHAPTER 8

CHAPTER 9

List of tables

CHAPTER 7

CHAPTER 8

CHAPTER 9

SUMMARY

The stable oxygen isotope and minor element composition of planktonic microfossils often forms the backbone of paleoceanographic and paleoclimatic studies. The stable oxygen isotope composition of planktonic foraminifera shells provides a well-established tool to reconstruct sea surface temperatures. Also foraminiferal Mg/Ca is widely applied to reconstruct the (calcification) temperature of seawater.

Recently, calcareous cyst producing dinoflagellates, and especially the species *Thoracosphaera heimii*, have gained more interest in paleoenvironmental and paleoclimatic studies. It was suggested that *T. heimii* might have some advantages over other planktonic species consisting of calcium carbonate, such as forminifera and coccolithophores. *T. heimii* has an overall broad geographic distribution, occurring from the polar regions to the tropical areas, and is present in geological records since the Late Cretaceous. Furthermore, it does not bear photosynthetic symbionts, and due to its living depth at a rather stable position in the water column, ontogenetic effects are likely to be minor.

Culture experiments with *T. heimii* documented a clear relationship between their oxygen isotope composition and temperature. Surface sediment samples and down-core studies revealed that *T. heimii* forms a useful tool for temperature reconstructions of the deeper parts of the photic zone. The first part of this thesis focuses on this correlation. A more recent culture experiment on the elemental composition of *T. heimii* shells revealed a strong dependency of shell Sr/Ca on temperature. However, no correlation could be observed between Mg/Ca and temperature. The present study is the first to analyze the minor element to calcium ratios of *T. heimii* shells from surface sediments. This will be the focus of the second part of this thesis.

In order to further establish the stable oxygen isotope composition ($\delta^{18}O$) of *T. heimii* shells as a temperature proxy, it is important to investigate the *T. heimii* $\delta^{18}O$ composition in a natural setting in different hydrographical areas. For the present study, a sample set was compiled with surface sediment samples from the western Indian Ocean offshore Tanzania and from the equatorial and South Atlantic; and seawater temperatures throughout the upper water column (0-200m) were considered. For the Indian Ocean samples, no relationship could be observed between temperature and *T. heimii* $\delta^{18}O$. The temperature signal of *T. heimii* shells in these samples is probably obscured by instrumental and/or environmental influences. For the Atlantic Ocean samples, the temperature – $\delta^{18}O$ correlation slightly improves when temperatures at mixed layer depth, the presumed living depth of *T. heimii*, are considered. This observation supports the

previously proposed idea that the $\delta^{18}O$ composition of *T. heimii* shells has potential as a useful tool to reconstruct temperatures of a specific depth in the water column, notably the mixed layer depth.

Another interesting question to test is whether or not the observations from the culture experiment on the elemental composition of *T. heimii* shells can be transferred to natural sediments. For this, the Mg/Ca, Sr/Ca, Fe/Ca, Mn/Ca and Si/Ca ratios of *T. heimii* shells from surface sediments in the equatorial and South Atlantic were analyzed. The Mg/Ca and Sr/Ca ratios were compared to several environmental parameters of the upper water column, while the Fe/Ca, Mn/Ca and Si/Ca ratios were used as a measure for contamination from the sediment. The first observation was that the Mg/Ca and Sr/Ca values from natural sediments exceed the cultural values by far. Furthermore, highest Mg/Ca values appear in samples which are characterized by highest seawater temperatures. However, Mg/Ca ratios also show a correlation with Fe/Ca, Mn/Ca and Si/Ca, which is an indication for sediment contamination, presumably by adsorbed clay minerals. Sr/Ca is correlated with the carbonate chemistry of the seawater. In contrast to cultured *T. heimii* shells, the Sr/Ca ratios of *T. heimii* shells from natural sediments do not show any correlation with temperature. So far no satisfying explanation can be given for this discrepancy.

Since this was the first time the elemental composition of *T. heimii* shells from surface sediments was analyzed, a question arose to what chemical cleaning protocol should be used. The advantages of commonly applied cleaning protocols for both foraminifera and coccolithophores were combined and applied to *T. heimii* shells from a core top sample. In addition, the sample was processed following the standard cleaning protocol for foraminifera; and following a sequential dissolution protocol, using a Flow-Through (FT) device. Measured Sr/Ca values are quite consistent between different processing and analyzing techniques. Significantly lower Mg/Ca values are obtained when the sample is sequentially dissolved, using the FT device. This is interpreted as evidence for contaminating clay particles, possible trapped inside the small and empty *T. heimii* shells.

ZUSAMMENFASSUNG

Die Zusammensetzung der stabilen Sauerstoffisotope sowie der Mengen- und Spurenelemente in planktonischen Mikrofossilien bildet häufig die Grundlage paläozeanographischer und paläoklimatischer Studien. Dabei stellt die Zusammensetzung der stabilen Sauerstoffisotope in Schalen von planktonischen Formaminiferen ein etabliertes Werkzeug dar, um Meeresoberflächentemperaturen zu rekonstruieren. Auch das Verhältnis von Mg/Ca aus Formaminiferenschalen wird häufig verwendet um die (Kalzifizierungs-) Temperatur von Meerwasser zu rekonstruieren.

In letzter Zeit hat das Interesse an Dinoflagellaten, die kalkige Zysten produzieren, insbesondere an der Art *Thoracosphaera heimii*, zugenommen. Es wird vermutet, daß *T. heimii* einige Vorteile gegenüber anderen kalkigen planktonischen Taxa wie Foraminiferen und Coccolithophoriden haben könnte. *T. heimii* besitzt eine breite geographische Verteilung von den Polarregionen bis in tropische Gebiete und kommt in geologischen Sedimenten seit der späten Kreidezeit vor. Weiterhin besitzt die Art keine photosynthetischen Symbionten und auch ontogenetische Effekte sind aufgrund der relativ konstanten Lebenstiefe in der Wassersäule sehr unwahrscheinlich.

In Kulturexperimenten mit *T. heimii* stellte sich ein eindeutiger Zusammenhang zwischen der Sauerstoffisotopenzusammensetzung in den Schalen und der Temperatur heraus. Oberflächensedimentproben und Sedimentkernuntersuchungen zeigten, daß *T. heimii* ein nützliches Werkzeug für Temperaturrekonstruktionen der tieferen Bereiche der photischen Zone ist. Der erste Teil dieser Dissertation konzentriert sich auf diesen Zusammenhang. Ein aktuelles Kulturexperiment zur Elementzusammensetzung in Schalen von *T. heimii* hat eine starke Abhängigkeit von Sr/Ca von der Wassertemperatur gezeigt. Dahingegen konnte keine Korrelation zwischen Mg/Ca und der Wassertemperatur beobachtet werden. Die vorliegende Studie ist die erste, in der die Zusammensetzung der verschiedener Elemente im Verhältnis zu Calcium in Schalen von *T. heimii* aus Oberflächensedimentproben analysiert wird. Dies ist Thema des zweiten Teils der Dissertation.

Um die stabile Sauerstoffisotopenzusammensetzung ($\delta^{18}O$) von Schalen von *T. heimii* als Temperaturproxy weiter zu etablieren ist es wichtig, die Zusammensetzung von $\delta^{18}O$ von *T. heimii* in ihrer natürlichen Umgebung in verschiedenen hydrographischen Gebieten zu untersuchen. Für die vorliegende Arbeit wurden Oberflächensedimentproben aus dem westlichen Indischen Ozean vor der Küste Tansanias sowie aus dem äquatorialen und südlichen Atlantik ausgewählt; Meerwassertemperaturen der oberen Wassersäule (0-200m) wurden verwendet. Innerhalb der Proben aus dem Indischen Ozean konnte kein Zusammenhang zwischen der Wassertemperatur und

$\delta^{18}O$ von *T. heimii* festgestellt werden. Das Temperatursignal in den Schalen von *T. heimii* aus diesen Proben ist möglicherweise verdeckt durch die Messungen selbst und/oder durch Umwelteinflüsse. Innerhalb der Proben aus dem Atlantik verbessert sich die Korrelation zwischen Temperatur und $\delta^{18}O$ von *T. heimii* etwas wenn die Temperaturen aus der Tiefe der durchmischten Oberflächenschicht, der vermuteten Lebenstiefe von *T. heimii,* berücksichtigt werden. Dies unterstützt die eingangs erwähnte Hypothese, daß $\delta^{18}O$ aus Schalen von *T. heimii* das Potential zu einem nützlichen Werkzeug hat, die Temperatur einer bestimmten Tiefe in der Wassersäule, hier die Tiefe der durchmischten Oberflächenschicht, zu rekonstruieren.

Eine weitere interessante Frage ist, ob die Ergebnisse aus dem Kulturexperiment zur Elementzusammensetzung von *T. heimii* Schalen auf natürlich vorkommende Sedimente übertragbar sind. Zur Beantwortung wurden die Verhältnisse Mg/Ca, Sr/Ca, Fe/Ca, Mn/Ca und Si/Ca in *T. heimii*-Schalen aus Oberflächensedimentproben im äquatorialen und südlichen Atlantik analysiert. Mg/Ca und Sr/Ca wurde mit verschiedenen Umweltparametern aus der oberen Wassersäule verglichen während Fe/Ca, Mn/Ca und Si/Ca als ein Maß für die Kontamination aus den Sedimenten verwendet wurde. Als erstes fällt auf, daß die Werte für Mg/Ca und Sr/Ca aus den Sedimenten bei Weitem über den in Kultur gemessenen Werten liegen. Weiterhin kommen die höchsten Mg/Ca Werte in Probenlokationen vor, die durch höchste Meerwassertemperaturen charakterisiert sind. Allerdings zeigen Mg/Ca Werte auch eine Korrelation mit Fe/Ca, Mn/Ca und Si/Ca, was ein Hinweis auf Kontamination durch das Sediment, vermutlich durch Tonminerale sein könnte. Sr/Ca korreliert mit der Karbonatchemie des Meerwassers. Im Gegensatz zu den *T. heimii* Schalen aus der Kultur zeigen die Sr/Ca Werte von *T. heimii* Schalen aus den Sedimenten keine Korrelation mit der Meerwassertemperatur. Bislang konnte hierfür keine zufriedenstellende Erklärung gefunden werden.

Da in dieser Studie erstmals die Elementzusammensetzung in *T. heimii* Schalen untersucht wurde, stellte sich die Frage, welches chemische Reinigungsprotokoll angewendet werden sollte. Die Vorteile von standardmäßig verwendeten Reinigungsprotokollen für sowohl Foraminiferen als auch Coccolithophoriden wurden kombiniert und auf *T. heimii* Schalen aus den Oberflächensedimentproben angewendet. Außerdem wurden die einzelnen Proben gemäß dem Standard-Reinigungsprotokoll für Foraminiferen aufgearbeitet, gefolgt von einem schrittweisen Lösungsprotokoll, wobei ein sog. Flow-Through (FT) Gerät verwendet wurde.

Im Vergleich zwischen verschiedenen Aufbereitungs- und Analysemethoden sind die gemessenen Sr/Ca Werte relativ konsistent. Signifikant niedrigere Mg/Ca Werte wurden erzielt wenn die Probe unter Verwendung von FT schrittweise gelöst wurde. Dies wird als Hinweis auf potentielle Kontamination durch Tonpartikel interpretiert, die sich möglicherweise in den kleinen leeren *T. heimii* Schalen verfangen.

CHAPTER 1

OBJECTIVES AND OVERVIEW

The main objective of this thesis is twofold:

Stable oxygen isotope composition ($\delta^{18}O$) of *Thoracosphaera heimii*:

Can we gain more information about the $\delta^{18}O$ of *T. heimii* shells in surface sediments?

Is there a difference between different hydrographical areas?

Do we find a correlation with temperature from a specific depth in the upper water column?

Can we improve the use of $\delta^{18}O$ of *T. heimii* shells as a temperature proxy?

→ For this purpose the $\delta^{18}O$ composition of *T. heimii* shells from surface sediments in the western Indian Ocean, and equatorial and South Atlantic was analyzed (Manuscript 1).

Minor element to calcium ratios (ME/Ca) of *Thoracosphaera heimii*:

How can we measure the ME/Ca ratios of *T. heimii* shells in surface sediments?

Do the ME/Ca ratios of *T. heimii* shells from natural sediments differ from culture values?

Can we find any correlation with environmental parameters of the upper water column?

Are the ME/Ca ratios contaminated by the sediment?

→ For this purpose a new cleaning protocol for the elemental analysis of *T. heimii* shells from sediments was developed (Manuscript 3); and the ME/Ca ratios of *T. heimii* shells from surface sediments in the equatorial and South Atlantic were analyzed (Manuscript 2).

To provide the reader with some relevant background information, this thesis is presented with four introductory chapters. **Chapter 2** gives the reader more insights into the wonderful world of dinoflagellates and *Thoracosphaera heimii*. In **Chapter 3**, the reader can find more information about stable oxygen isotope chemistry, while **Chapter 5** reviews the minor element to calcium proxies. Unfortunately, the stable oxygen isotope and minor element composition of *T. heimii* shells has not been studied as extensively as foraminifera tests and coccolithophorid calcite. For the sake of comparison, Chapters 3 and 5 also contain information about the processes affecting foraminiferal and coccolithophorid $\delta^{18}O$ and ME/Ca composition. Since understanding calcification processes is vital to interpret $\delta^{18}O$ and ME/Ca signals, **Chapter 4** gives an overview of biomineralization in foraminifera, coccolithophores and *T. heimii*. Chapter 4 was also added to this thesis out of personal interest in the matter. In Chapter 5 the reader will find additional information about the methods used in this research.

The outcome of this project is presented in three manuscripts, which correspond to **Chapters 6, 7 and 8** of this thesis.

Manuscript 1 – Correlation between temperature and the $\delta^{18}O$ composition of *Thoracosphaera heimii* shells in core top sediments from the Indian and Atlantic Ocean.

This study investigates the correlation between temperature and the stable oxygen isotope composition of *T. heimii* shells in 57 surface sediment samples from the western Indian Ocean offshore Tanzania, and the equatorial and South Atlantic. When reconstructing the upper water column temperatures, unrealistic temperatures are produced when the previously published temperature – $\delta^{18}O$ equation for cultured *T. heimii* is used. When the $\delta^{18}O$ values of *T. heimii* shells are plotted against mean annual water temperatures, no correlation is observed in the Indian Ocean samples. We argue that the $\delta^{18}O$ signal in this area is obscured by river input or contamination by the sediment. For the Atlantic Ocean samples, temperatures at mixed layer depth yield the best correlation. Although further research is necessary to quantify the instrumental, environmental and biological influences, the $\delta^{18}O$ composition of *T. heimii* shells has potential to reconstruct temperatures of a specific depth in the water column, the mixed layer depth.

Manuscript 2 – Sr/Ca and Mg/Ca ratios of *Thoracosphaera heimii* shells in core-top samples from the South and equatorial Atlantic Ocean – A pilot study.

This is the first study to analyze the minor element to calcium ratios of *T. heimii* shells from surface sediments. Mg/Ca and Sr/Ca ratios were compared to several environmental parameters of the upper water column, especially temperature; while the Fe/Ca, Mn/Ca and Si/Ca ratios were used as a measure for sediment contamination. The Mg/Ca and Sr/Ca values from natural sediments show a large range and exceed the values of cultured *T. heimii* shell by far. PCA reveals three hydrographical areas with characteristic Mg/Ca and Sr/Ca ratios. Furthermore, RDA reveals a correlation between Mg/Ca and temperature. However, Mg/Ca ratios are also correlated with Fe/Ca, Mn/Ca and Si/Ca, which is an indication that the Mg/Ca values are contaminated by adsorbed clay particles. RDA also reveals a correlation between *T. heimii* Sr/Ca and the carbonate chemistry of the seawater. In contrast to cultured *T. heimii* shells, the Sr/Ca ratios of *T. heimii* shells from natural sediments do not show any correlation with temperature. So far we do not have a satisfying explanation for this discrepancy. When the extreme Mg/Ca and Sr/Ca values are omitted from the dataset, the remaining core top samples still show a large scatter of Mg/Ca and Sr/Ca.

Manuscript 3 – Comparison between different cleaning protocols to analyze the Mg/Ca and Sr/Ca ratios of *Thoracosphaera heimii* shells from sediments

---

This is the first time the elemental composition of *T. heimii* shells from surface sediments was analyzed. Therefore a question arose as to which chemical cleaning protocol should be used, prior to elemental analysis. Due to the size difference between the small *T. heimii* shells and the bigger foraminifera tests, the widely applied standard cleaning protocol for foraminifera is quite labour intensive, since a centrifuge session is necessary after every cleaning step, in order to prevent the loss of *T. heimii* shells (method 1). Therefore we developed a new cleaning protocol, specifically for *T. heimii* shells from surface sediments (method 2), based on the cleaning protocols for foraminifera and coccolithophores. In addition, *T. heimii* shells were processed following a sequential dissolution protocol, using a Flow-Through (FT) device (method 3). Measured Sr/Ca values are quite consistent between the three different processing and analyzing techniques. Significantly lower Mg/Ca values are obtained when the sample is sequentially dissolved, using the FT device. We interpret this as evidence for contaminating clay particles, possible trapped inside the small and empty *T. heimii* shells.

CHAPTER 2

INTRODUCTION: DINOFLAGELLATES

2.1. General introduction

Dinoflagellates (division Dinoflagellata) are a diverse group of unicellular, eukaryotic organisms (e.g. Evitt, 1985; Fensome *et al.*, 1993). They can be found in a wide range of aquatic environments, from lakes to the open ocean; and in a wide range of climatic zones, from the tropics to the polar regions (e.g. Taylor & Pollingher, 1987; Marret & Zonneveld, 2003; Mathiessen *et al.*, 2005).

Dinoflagellates typically occur as biflagellate motile cells. The longitudinal flagellum, located in the sulcus (Fig. 2.1), mainly acts as a rudder. Most of the propulsive force is provided by the second flagellum, the transverse flagellum, which is coiled and encircles the body along the cingulum (Fig. 2.1). With the aid of these two flagella, dinoflagellates can migrate vertically through the water column in a spiralling motion (e.g. Fensome *et al.*, 1993). This distinctive whirling motion caused by the interaction of two flagella is what gives them their name: *dinos* (Greek) means „whirling“, and *flagellum* (Latin) means „whip, scourge“.

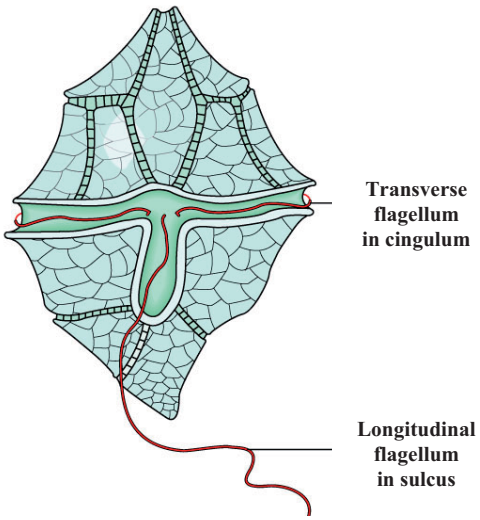

Fig. 2.1 - Schematic drawing of the biflagellate motile dinoflagellate cell (modified from http://classes.midlandstech.edu/carterp/Courses/bio225/chap12/ss3.htm, Copyright © 2004 Pearson Education. Inc., publishing as Benjamin Cummings)

A huge variety of feeding strategies can be observed: autotrophy, heterotrophy, mixotrophy (the organism is either autotroph or heterotroph at different times in their life cycle), parasitism and symbiosis (e.g. Dale, 1983; Gaines & Elbrächter, 1987; Schnepf & Elbrächter, 1992; Jacobson & Anderson, 1986). Most of the 2000 known marine species are autotrophic, i.e. they depend on the availability of light to photosynthesize nutrients (Schnepf & Elbrächter, 1992). This makes dinoflagellates, aside from diatoms, the second most important players in marine primary production (Parsons *et al.*, 1984; Taylor & Pollingher, 1987).

The life cycle of dinoflagellates is complex and involves both sexual and asexual reproduction with motile vegetative cells (thecae) and non-motile cysts (resting cysts, vegetative cysts and temporary cysts), as is summarized in Fig. 2.2. For more details on the life cycle of dinoflagellates, see e.g. Dale, (1986) or Fensome *et al.* (1993). More than 200 species of marine dinoflagellates are known to produce cysts (organic-walled, calcareous or siliceous) as part of their life cycle (Head, 1996). The majority of the cyst-producing dinoflagellates form resting cysts as part of their sexual reproduction cycle. This type of cyst represents a dormant stage during which normal metabolic processes are significantly reduced. They are generally very resistant to unfavorable conditions and preserve very well in the sediments (e.g. Wall & Dale, 1967; Fensome *et al.*, 1993). Being one of the exceptions, the calcareous dinoflagellate *Thoracosphaera heimii* produces vegetative cysts (shells) during their asexual reproduction. In contrast to resting cysts, vegetative cysts are metabolically and/or reproductively active (Fensome *et al.*, 1993). Since *T. heimii* is the focus of this thesis, its life cycle will be described more into detail in Chapter 2.3.

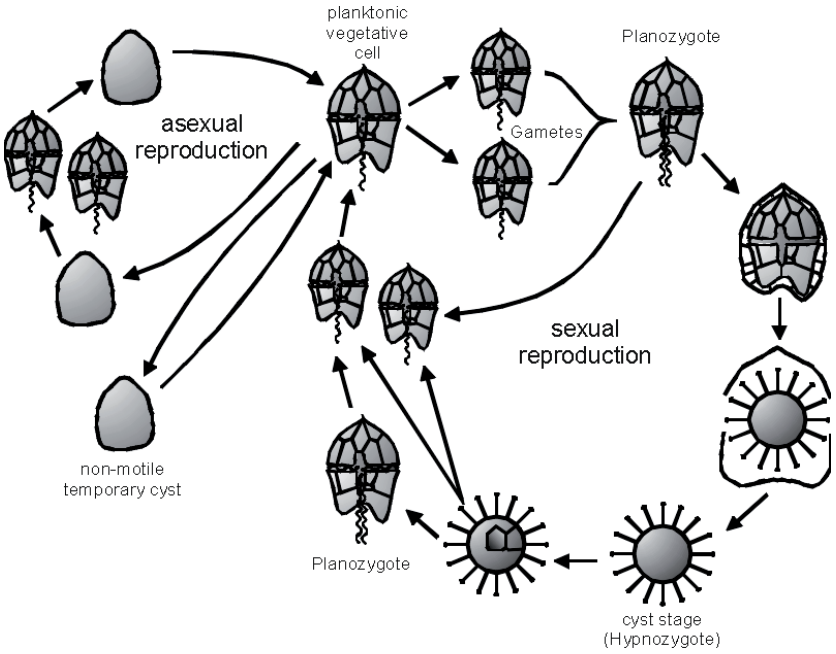

Fig. 2.2 – Schematic life cycle of dinoflagellates showing sexual reproduction (resting cysts) and asexual or vegetative reproduction (vegetative cysts)

Dinoflagellate cysts have many applications. For instance in the petroleum and gas exploration companies and the fishery industries, dinoflagellate cysts are increasingly being used (Zonneveld *et al.*, 2005). And even more important, during the last decades, it has become evident that dinoflagellate cysts form extremely suitable tools for detailed paleoenvironmental and paleoclimatic reconstructions (e.g. de Vernal *et al.*, 2005; Pospelova *et al.*, 2006; Bouimetarhan *et al.*, 2009; Holzwarth *et al.*, 2010).

2.2. Calcareous dinoflagellates

Today there are about 30 modern dinoflagellate species that are known to incorporate calcite crystals into their cyst wall (e.g. Streng *et al.*, 2004; Elbrächter *et al.*, 2008; Zonneveld *et al.*, 2005). Three genera of thecae (motile cells) are described: *Scrippsiella*, *Pentapharsodinium* and *Ensiculifera*, based on the number and form of their cingular plates (Fensome *et al.*, 1993). However, these genera also include species that are not known to produce cysts or produce organic-walled cysts instead of calcareous cysts (D'Onofrio *et al.*, 1999).

Three cyst types are recognized based on the orientation of the crystallographic c-axis, i.e. the vertical axis, of the individual calcite crystals in the cyst wall: tangential, radial or oblique (Fig. 2.3) (e.g. Janofske, 1996). These orientations give characteristic patterns of the interference colours under polarized light in combination with a gypsum plate (Fig. 2.3). Based on the type of the archeopyle, four cyst types can be defined: apical, intercalary, meso-epicystal and epitractal (Fig. 2.4) (e.g. Streng *et al.*, 2004).

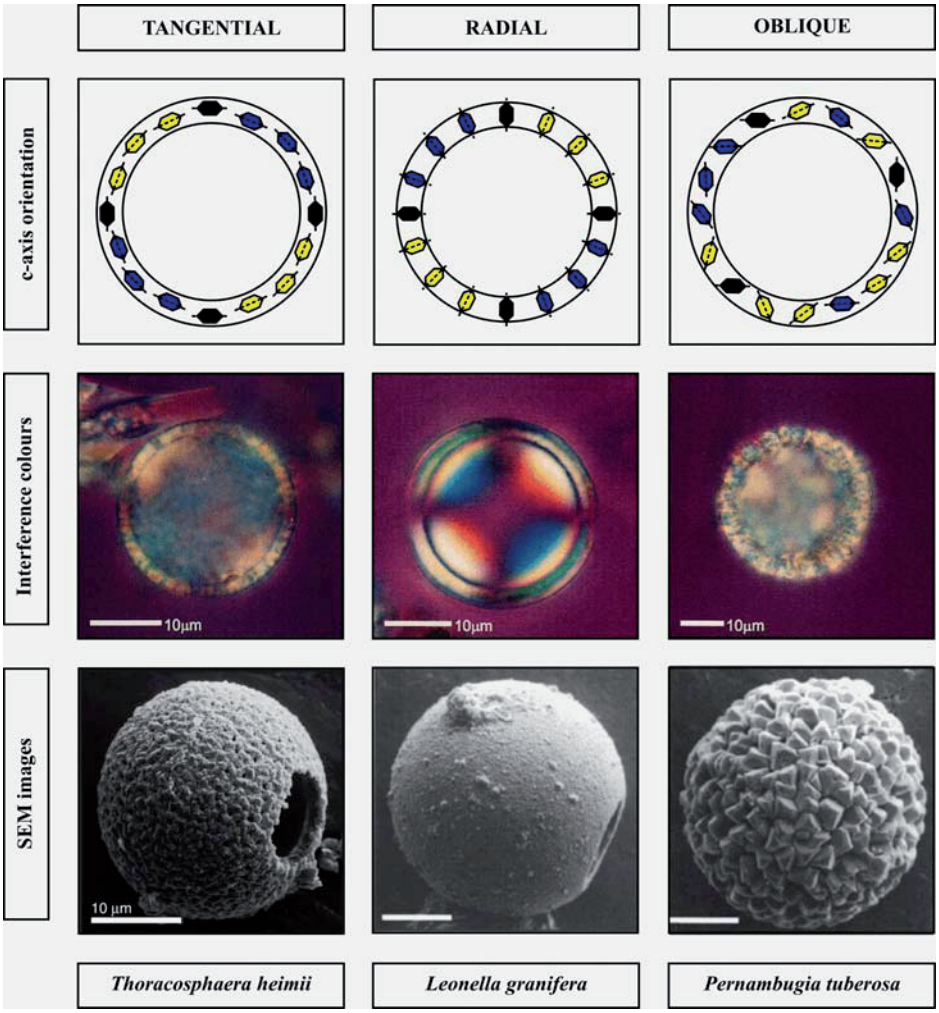

Fig. 2.3

The orientation of the crystallographic c-axis is a morphologically important feature for taxonomy in calcareous dinoflagellate cysts (e.g. Janofske, 1996). C-axis orientation images are drawn after an unpublished lab manual, compiled by Dorothea Janofske and Oliver Esper, Department of Historical Geology and Paleontology (University of Bremen), Interference colour images are taken from the same lab manual. SEM images are taken from Zonneveld *et al.* (2005)

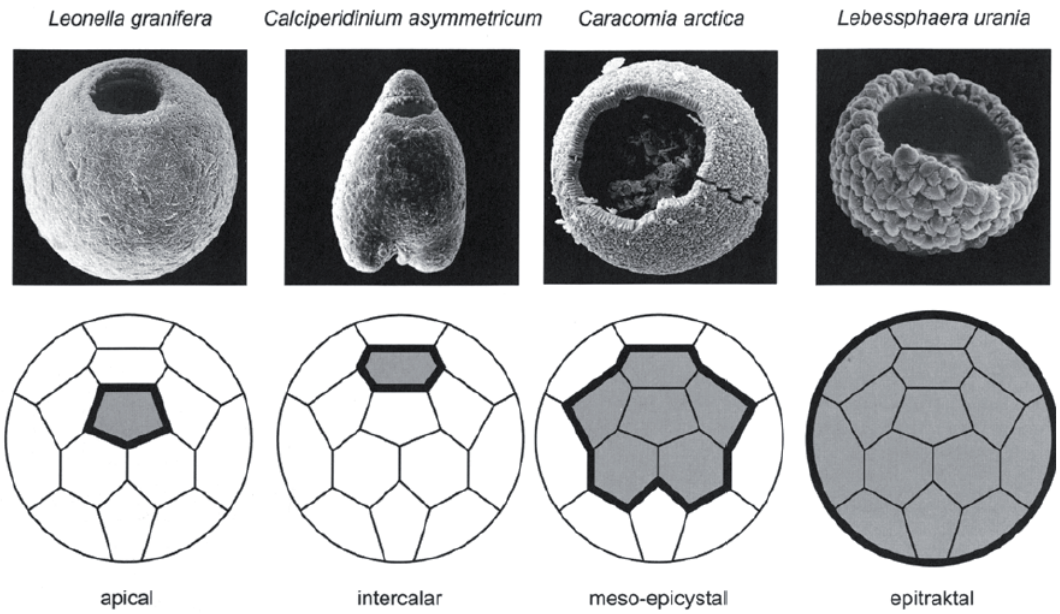

Fig. 2.4 – The archeopyle type is a taxonomically important morphological feature in calcareous dinoflagellate cysts (after Streng *et al.*, 2004) (from Zonneveld *et al.*, 2005)

Sediment trap and surface sediment studies have shown that calcareous dinoflagellate cysts are abundant in tropical, subtropical and temperate oceanic environments, where they often dominate the total dinoflagellate cyst flux to the seafloor (Dale, 1992; Dale & Dale, 1992; Höll, 1998; Höll *et al.*, 1998). For instance in sediments from the equatorial Atlantic, the amount of calcareous dinoflagellate cysts per gram was nearly 50 times higher than the amount of organic-walled dinoflagellate cysts per gram (Höll *et al.*, 1998). Highest diversity of calcareous dinoflagellate species however, can be found in the coastal zones (e.g. Nehring, 1994; Montresor *et al.*, 1998; Vink, 2004). For a detailed overview on the ecology of several calcareous dinoflagellate species, see e.g. Zonneveld *et al.* (2005).

To date, all calcareous cyst producing dinoflagellates are thought to be photosynthetic, i.e. either photoautotrophic or mixotrophic (Tangen *et al.*, 1982; Binder & Anderson, 1987; Montresor *et al.*, 1994). Being primary producers, they are directly influenced by the environmental parameters of the surrounding water masses in the photic zone. Combined with a long geological record since the Late Triassic (Janofske, 1992) and their reactions to long- and short-term, global and local changes, they are very suitable for detailed (paleo-)environmental and (paleo-) oceanographic reconstructions (e.g. Vink *et al.*, 2001; Esper *et al.*, 2004; Meier *et al.*, 2004; Zonneveld *et al.*, 2005; Bison *et al.*, 2007, 2009).

2.3. *Thoracosphaera heimii* (Lohmann) Kamptner

Life cycle

In contrast to other dinoflagellate species producing calcareous cysts, *T. heimii* reproduces asexually and spends most of its life cycle as a vegetative cyst or shell (1-2 in Fig. 2.5), which is presumably haploid (n). After a cell hatches from this calcareous shell (3 in Fig. 2.5), it divides (4 in Fig. 2.5) and forms aplanospores, either directly (6 in Fig.2.5) or via the production of planospores (5 in Fig. 2.5). The aplanospores start to calcify (7 in Fig. 2.5), and weakly calcified cells are capable of mitotic division (b in Fig. 2.5). Sexuality might occur in a separate sexual cycle starting from the planospore stage (c in Fig. 2.5), but was not observed during the experiments (Meier *et al.*, 2007). For a more detailed overview of the life cycle of *T. heimii*, see e.g. Tangen *et al.* (1982) and Inouye & Pienaar (1983). With a reproduction time every 1-2 days, *T. heimii* has a much higher turn-over rate than other (resting) cyst forming species (e.g. Tangen *et al.*, 1982; Dale, 1992).

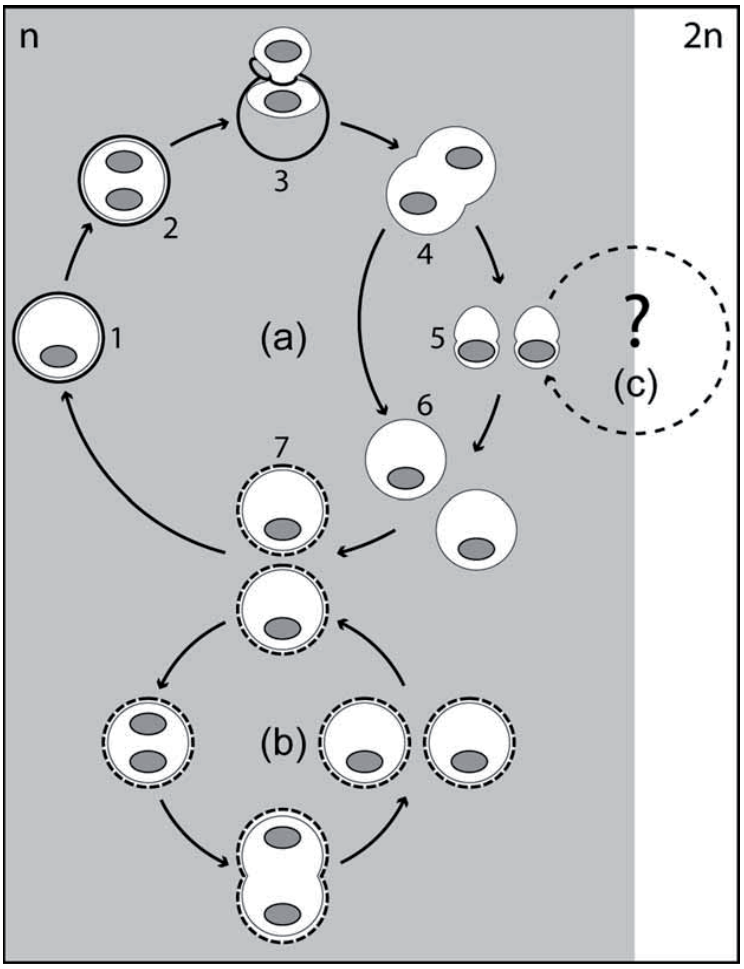

Fig. 2.5 – Life cycle of *Leonella granifera*. *Thoracosphaera heimii* is similar (Meier *et al.*, 2007)

Temperature

Höll *et al.* (1998) reported an overwhelming dominance of *Thoracosphaera heimii* in sediments of the equatorial Atlantic. The content of *T. heimii* shells per gram reached on average 900 times higher values in comparison to the organic-walled dinoflagellate cysts and 18 times higher values in comparison to the other calcareous dinoflagellate cysts. Recent studies have shown that *T. heimii* has a broad geographic distribution and can be observed from sub-polar to tropical environments with highest abundances in subtropical areas (Fig. 2.6; Zonneveld *et al.*, 1999; 2000; Wendler *et al.*, 2002a; Meier & Willems, 2003; Vink, 2004). This is also reflected in culture experiments, which indicate that *T. heimii* has a broad temperature tolerance, with highest growth rates between 14 and 27°C, and maximum growth rates at 27°C (Karwath *et al.*, 2000b).

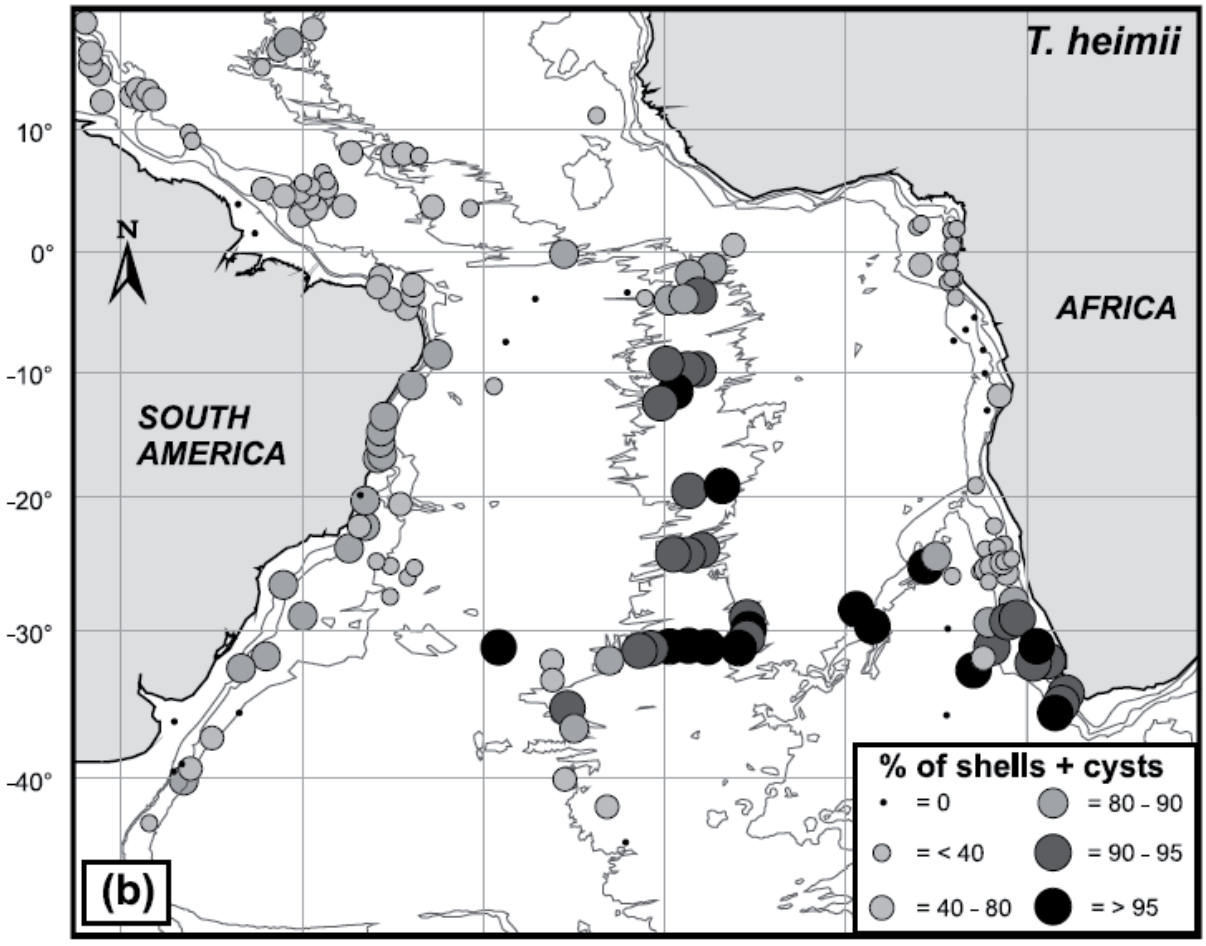

Fig. 2.6 – Surface sediment distribution map of *Thoracosphaera heimii*, as percentage of total dinoflagellate cysts per gram dry sediment (Vink, 2004)

Nutrient availability and stratification

Initial studies on the ecology of calcareous dinoflagellate cysts suggested that enhanced *T. heimii* shell production could be associated with oligotrophic regions, probably related to relatively stratified conditions of the upper water column (Höll *et al.*, 1998, 1999; Vink *et al.*, 2000; Esper *et al.*, 2000). This oligotrophy theory can not always be confirmed. For instance a sediment trap study off the Somalia upwelling area revealed a positive correlation between cyst production and nutrient supply (Wendler *et al.*, 2002b). However, later work showed that stratification of the upper water column and the presence of a well-developed thermocline are probably more important than the trophic state of the upper water column (e.g. Vink *et al.*, 2002; Vink, 2004; Richter *et al.*, 2007). Since, within their research areas, the trophic state of the upper water column also strongly covaries with the development of turbulence, Kohn & Zonneveld (2010) suggested that turbulence may be one of the most important environmental factors negatively influencing cyst production in *T. heimii*. This is in agreement with previous work stating that turbulence in the upper water column is unfavorable for the development of phytoplankton (including the calcareous dinoflagellate *T. heimii*), preventing it from building up a standing stock in the photic zone (e.g. Wendler *et al.*, 2002a, b; Vink, 2004).

Living depth

In the first field study on the vertical distribution of *T. heimii* in the water column, maximum abundances of freshly formed *T. heimii* shells (i.e. shells with cell content or full shells) were observed between 50 and 100m water depth, a depth coinciding with the depth of the thermocline or pycnocline (Karwath *et al.*, 2000a). Although the pycnocline is associated with density differences, it is unlikely that only passive sinking and accumulation are responsible for the high concentrations of full *T. heimii* shells at this depth (Karwath *et al.*, 2000a; Kohn & Zonneveld, 2010). *T. heimii* cycles quickly between its motile and shell phase and therefore is only able to move vertically over a short distance (Inouye & Pienaar, 1983). Therefore Karwath *et al.* (2000a) concluded that *T. heimii* most likely inhabits this lower part of the photic zone, where nutrients are easily accessible from the deep chlorophyll maximum above and where competition with other phytoplankton is less due to reduced light intensities. Based on the data of Karwath *et al.* (2000a), Vink (2004) and Zonneveld (2004) suggested that *T. heimii* shell production may be related to the position of the deep chlorophyll maximum. In a more recent study, Kohn & Zonneveld (2010) observed peaks in the concentration of full *T. heimii* shells at or just above the deep chlorophyll maximum, indicating that calcification of *T. heimii* shells can take place in these water layers.

Seasonality

In culture experiments, *T. heimii* shells are produced throughout the year with the production of about one cyst a day (e.g. Inouye & Pienaar, 1983; Karwath, 2000). This suggests that the production of *T. heimii* shells in natural environments is not restricted to a certain season or to a limited time interval during the year (Zonneveld, 2004). This assumption is supported by, for instance, a sediment trap study off Cape Blanc where *T. heimii* dominates the calcareous dinoflagellate cyst assemblage during an 18-months sampling period (Richter, 2009). However, there are indications that seasonal production of *T. heimii* shells is region dependent: a sediment trap study from the Arabian Sea documents highest accumulation rates of *T. heimii* shells at the end of the SW monsoon (Wendler *et al.*, 2002a, b).

References Chapter 2

Binder, B .J., Anderson, D.M., 1987. Physiological and environmental control of germination in *Scrippsiella trochoidea* (Dinophyceae) resting cysts. *Journal of Phycology* 25, 99-107.

Bison, K.-M., Versteegh, G.J.M., Willems, H., Hilgen, F.J., 2007. Calcareous dinoflagellate turnover in relation to the Messinian salinity crisis in the Eastern Mediterranean Pissouri Basin; Cyprus. *Journal of Micropalaeontology* 26, 103-116.

Bison, K.-M., Versteegh, G.J.M., Orszag-Sperber, F., Rouchy, J.M., Willems, H., 2009. Palaeoenvironmental changes of the early Pliocene (Zanclean) in the eastern Mediterranean Pissouri Basin (Cyprus) evidenced from calcareous dinoflagellate cyst assemblages. *Marine Micropaleontology* 73 (1-2), 49-56.

Bouimetarhan, I., Marret, F., Dupont, L., Zonneveld, K., 2009. Dinoflagellate cyst distribution in marine surface sediments off West Africa (17–6 N) in relation to sea surface conditions, freshwater input and seasonal coastal upwelling. *Marine Micropaleontology* 71 (3–4), 113–130.

Dale, B., 1983. Dinoflagellate resting cysts: "benthic plankton". In: Fryxell, G.A. (Ed.) Survival strategies of the algae. Cambridge University Press, pp. 69-136.

Dale, B., 1986. Life cycle strategies of oceanic dinoflagellates. *Unesco Technical Papers in Marine Science* 49, 65-72.

Dale, B., 1992. Thoracosphaerids: Pelagic fluxes. In: Dale, B. & Dale, A.L. (Eds.). Dinoflagellate Contributions to the Deep Sea. Ocean Biocoenosis Series 5, Woods Hole Oceanographic Institution, Woods Hole, pp. 33-41.

Dale, A.L., Dale, B., 1992. Dinoflagellate contributions to the sediment flux of the nordic seas. In: Dale, B. & Dale, A.L. (Eds.). Dinoflagellate Contributions to the Deep Sea. Ocean Biocoenosis Series 5, Woods Hole Oceanographic Institution, Woods Hole, MA, pp. 45 - 73.

de Vernal, A., Eynaud, F., Henry, M., Hillaire-Marcel, C., Londeix, L., Mangin, S., Matthiessen, J., Marret, F., Radi, T., Rochon, A., Solignac, S., Turon, J.-L., 2005. Reconstruction of sea surface conditions at middle to high latitudes of the Northern Hemisphere during the Last Glacial Maximum (LGM) based on dinoflagellate cyst assemblages. *Quaternary Science Reviews* 24, 897–924.

d'Onofrio, G., Marino, D., Bianco, L., Busico, E., Montresor, M., 1999. Toward an assessment on the taxonomy of dinoflagellates that produce calcareous cysts (Calciodinelloidea, Dinophyceae): a morphological and molecular approach. *Journal of Phycology* 35, 1063-1078.

Ellbrächter, M., Gottschling, M., Hildebrand-Habel, T., Keupp, H., Kohring, R., Lewis, J., Meier, S.K.J., Montresor, M., Streng, M., Versteegh, G.J.M., Willems, H., Zonneveld, K.A.F., 2008. Establishing an agenda for calcareous dinoflagellate research (Thoracosphaeraceae, Dinophyceae) including a nomenclatural synopsis of generic names. *Taxon* 57, 1289-1303.

Esper, O., Zonneveld, K.A.F., Höll, C., Karwath, B., Kuhlmann, H., Schneider, R.R., Vink, A., Weise-Ilho, I., Willems, H., 2000. Reconstruction of palaeoceanographic conditions in the South Atlantic Ocean at the last two Terminations based on calcareous dinoflagellate cysts. *International Journal of Earth Sciences* 88, 680-693.

Esper, O., Versteegh, G.J.M., Zonneveld, K.A.F., Willems, H., 2004. A palynological reconstruction of the Agulhas Retroflection (South Atlantic Ocean) during the Late Quaternary. *Global and Planetary Change* 41, 31-62.

Evitt, W.R., 1985. Sporopollenin dinoflagellate cysts: Their morphology and interpretation. American Association of Stratigraphic Palynologists Foundation, Dallas, 333 pp.

Fensome, R.A., Taylor, F.J.R., Norris, G., Sarjeant, W.A.S., Wharton, D.I., Williams, G.L., 1993. A classification of modern and fossil dinoflagellates. Micropaleontology Special Publication 7. Sheridan Press, Hanover, 351 pp.

Gaines, G., Elbrächter, M., 1987. Heterotrophic nutrition. In: Taylor, F.J.R. (Ed.). The biology of dinoflagellates. Blackwell Scientific Publications, Oxford, pp.224-268.

Head, M.J., 1996. Modern dinoflagellate cysts and their biological affinities. In: Jansonius J., McGregor D.C. (Eds.). Palynology: Principles and applications, American Association of Stratigraphic Palynologists Foundation, Salt Lake City, pp. 1197-1248

Höll, C., 1998. Kalkige und organisch-wandige Dinoflagellatenzysten in spätquartären Sedimenten des tropischen Atlantiks und ihre palökologische Auswertbarkeit. Berichte, Fachbereich Geowissenschaften, Universität Bremen 127, 1-121.

Höll., C., Zonneveld, K.A.F., Willems, H., 1998. On the ecology of calcareous dinoflagellates: the Quaternary eastern Equatorial Atlantic. *Marine Micropaleontology* 33, 1-25.

Höll, C., Karwath, B., Rühlemann, C., Zonneveld, K.A.F., Willems, H., 1999. Palaeoenvironmental information gained from calcareous dinoflagellates: The late Quaternary eastern and western tropical Atlantic Ocean in comparison. *Palaeogeography, Palaeoclimatology, Palaeoecology* 146, 147-164.

Holzwarth, U., Esper, O., Zonneveld, K.A.F., 2010. Organic-walled dinoflagellate cysts as indicators of oceanographic conditions and terrigenous input in the NW African upwelling region. *Review of Paleobotany and Palynology* 159 (1-2), 35-55.

Inouye, I., Pienaar, R.N., 1983. Observations on the life cycle and microanatomy of *Thoracosphaera heimii* (Dinophyceae) with special reference to its systematic position. *South African Journal of Botany* 2, 63-75.

Jacobson, D.M., Anderson, D.M., 1986. Thecate heterotrophic dinoflagellates: feeding behavior and mechanism. *Journal of Phycology* 22, 249-258.

Janofske, D., 1992. Kalkiges nannoplankton, insbesondere kalkige Dinoflagellate-Zysten der alpine Ober-Trias: Taxonomie, Biostratigraphie und Bedeutung für die Phylogenie der Peridinales. Berliner Geowissenschaften Abh. E (4), 1-93.

Janofske, D., 1996. Ultrastructure types in recent “calcispheres”. *Bulletin de l’Institut Océanographique Monaco* 14 (4), 295-303.

Karwath, B., 2000. Ecological Studies on Living and Fossil Calcareous Dinoflagellates of the Equatorial and Tropical Atlantic Ocean. Ph.D. Thesis, Berichte Fachbereich Geowissenschaften, Universität Bremen 152, 175 pp.

Karwath, B., Janofske, D., Willems, H., 2000a. Spatial distribution of the calcareous dinoflagellate *Thoracosphaera heimii* in the upper water column of the tropical and equatorial Atlantic. *International Journal of Earth Sciences* 88, 668-679.

Karwath, B., Janofske, D., Tietjen, F., Willems, H., 2000b. Temperature effects on growth and cell size in the marine calcareous dinoflagellate *Thoracosphaera heimii. Marine Micropaleontology* 39, 43-51.

Kohn, M., Zonneveld, K.A.F., 2010. Calcification depth and spatial distribution of *Thoracosphaera heimii* cysts: Implications for palaeoceanographic reconstructions. *Deep Sea Research Part I: Oceanographic Research Papers* 57 (12), 1543-1560.

Marret, F., Zonneveld, K.A.F., 2003. Atlas of modern organic-walled dinoflagellate cyst distribution. *Review of Palaeobotany and Palynology* 125, 1-200.

Matthiesen, J., de Vernal, A., Head, M.J., Okolodkov, Y.B., Zonneveld, K.A.F., Harland, R., 2005. Modern organic-walled dinoflagellate cysts in Arctic marine environments and their (paleo) environmental significance. *Paläontologische Zeitschrift* 73, 3-51.

Meier, K.J.S., Willems, H., 2003. Calcareous dinoflagellate cysts from surface sediments of the Mediterranean Sea: distribution patterns and influence of main environmental gradients. *Marine Micropaleontology* 48 (3-4), 321-354.

Meier, K.J.S., Zonneveld, K.A.F., Kasten, S., Willems, H., 2004. Different nutrient sources forcing increased productivity during eastern Mediterranean S I sapropel formation as reflected by calcareous dinoflagellate cysts. Paleoceanography 19, 1-12, DOI10.1029/2003PA000895.

Meier, S.K.J., Young, J.R., Kirsch, M., Feist-Burkhardt, S., 2007. Evolution of different life-cycle strategies in oceanic calcareous dinoflagellates. *European Journal of Phycology* 42 (1), 81-89.

Montresor, M., Montesarchio, E., Marino, D., Zingone, A., 1994. Calcareous dinoflagellate cysts in marine sediments of the Gulf of Naples (Mediterranean Sea). *Review of Palaeobotany and Palynology* 84, 45-56.

Montresor, M., Zingone, A., Sarno, D., 1998. Dinoflagellate cyst production at a coastal Mediterranean site. *Journal of Plankton Research* 20 (12), 2291-2312.

Nehring, S., 1994. Spatial distribution of dinoflagellate resting cysts in recent sediments of Kiel Bight, Germany. *Lophelia* 39, 137-158.

Parsons, T.R., Takahashi, M., Hargrave, B., 1984. Biological oceanographic processes. Pergamon Press, Oxford, 330 pp.

Pospelova, V., Pedersen, T.F., de Vernal, A., 2006. Dinoflagellate cysts as indicators of climatic and oceanographic changes during the past 40 kyr in the Santa Barbara Basin, southern California. *Paleoceanography* 21, 1–16.

Richter, D., 2009. Characteristics of calcareous dinoflagellate cyst assemblages in a major upwelling region (NW Africa) – Spatial distribution, fluxes and ecology. PhD thesis, University of Bremen, Department of Geosciences.

Richter, D., Vink, A., Zonneveld, K.A.F., Kuhlmann, H., Willems, H., 2007. Calcareous dinoflagellate cyst distributions in surface sediments from upwelling areas off NW Africa, and their relationships with environmental parameters of the upper water column. *Marine Micropaleontology* 63, 201–228.

Schnepf, E., Elbrächter, M., 1992. Nutritional strategies in Dinoflagellates. A review with emphasis on cell biological aspects. *European Journal of Protistology* 28, 3-24.

Streng, M., Hildebrand-Habel, T., Willems, H., 2004. Archeopyles of fossil calcareous dinoflagellate cysts (Calciodinelloideae). *Journal of Paleontology* 78 (3), 456-483.

Tangen, K., Brand, L.E., Blackwelder, P.L., Guillard, R.R.L., 1982. *Thoracosphaera heimii* (Lohmann) Kamptner is a dinophyte: observations on its morphology and life cycle. *Marine Micropaleontology* 7, 193-212.

Taylor, F.J.R., Pollingher, U., 1987. The ecology of dinoflagellates. In: Taylor, F.J.R. (Ed.). The biology of dinoflagellates. Blackwell Scientific Publications, Oxford, pp. 398-529.

Vink, A., 2004. Calcareous dinoflagellate cysts in South and equatorial Atlantic surface sediments: diversity, distribution, ecology and potential for palaeoenvironmental reconstruction. *Marine Micropaleontology* 50, 43-88.

Vink, A., Zonneveld, K.A.F., Willems, H., 2000. Distributions of calcareous dinoflagellate cysts in surface sediments of the western equatorial Atlantic Ocean, and their potential use in palaeoceanography. *Marine Micropaleontology* 38, 149-180.

Vink, A., Rohlemann, C., Zonneveld, K.A.F., Mulitza, S., Hols, M., Willems, H., 2001. Shifts in the position of the North Equatorial Current and rapid productivity changes in the western Tropical Atlantic during the last glacial. *Paleoceanography* 16 (5), 479-490.

Vink, A., Brune, A., Höll, C., Zonneveld, K.A.F., Willems, H., 2002. On the response of calcareous dinoflagellates to oligotrophy and stratification of the upper water column in the equatorial Atlantic Ocean. *Palaeogeography, Palaeoclimatology, Palaeoecology* 178, 53-66.

Wall, N., Dale, B., 1967. The resting cysts of modern marine dinoflagellates and their paleontological significance. *Review of Paleobotany and Palynology* 2, 349-354.

Wendler, I., Zonneveld, K.A.F., Willems, H., 2002a. Calcareous cyst-producing dinoflagellates: ecology and aspects of preservation in a highly productive oceanic region. In: Clift, P.D., Kroon, D., Gaedicke, C., Craig, J. (Eds.). The tectonic and climatic evolution of the Arabian Sea. Geological Society, London, Special Publications 195, 317-340.

Wendler, I., Zonneveld, K.A.F., Willems, H., 2002b. Production of calcareous dinoflagellate cysts in response to monsoon forcing off Somalia: A sediment trap study. *Marine Micropaleontology* 46, 1-11.

Zonneveld, K., 2004. Potential use of stable oxygen isotope composition of *Thoracosphaera heimii* (Dinophyceae) for upper water column (thermocline) temperature reconstruction. *Marine Micropaleontology* 50, 307-317.

Zonneveld, K.A.F., Höll, C., Janofske, D., Karwath, B., Kerntopf, B., Rohlemann, C., Willems, H., 1999. Calcareous dinoflagellates as palaeo-environmental tools. In: Fischer, G., Wefer, G., (Eds.). Use of Proxies in Paleoceanography: Examples from the South Atlantic, Berlin (Springer), pp. 145-164.

Zonneveld, K.A.F., Brune, A., Willems, H., 2000. Spatial distribution of calcareous dinoflagellates in surface sediments of the South Atlantic Ocean between 13°N and 36°S. *Review of Palaeobotany and Palynology* 111, 197-223.

Zonneveld, K.A.F., Meier, S.K.J., Esper, O., Siggelkow, D., Wendler, I., Willems, H., 2005. The (palaeo-) environmental significance of modern calcareous dinoflagellate cysts: a review. *Paläontologische Zeitschrift* 79 (1), 61-77.

CHAPTER 3

INTRODUCTION: STABLE OXYGEN ISOTOPES

3.1. General introduction

Oxygen (O) is the third most abundant element after hydrogen (H) and helium (He). It is the second most common component of the Earth's atmosphere, taking up 21% of its volume and 23.1% of its mass. It is the major component of the world's oceans (88.8% by mass) and constitutes 49.2% of the Earth's crust by mass.

The element oxygen occurs as three stable isotopes: ^{16}O, ^{17}O and ^{18}O. The nuclei of these heavy and light varieties each have eight protons, but contain a different amount of neutrons (eight, nine or ten). The lightest isotope, ^{16}O, is the most common isotope (natural abundance = 99.759%), followed by the heaviest isotope, ^{18}O, which occurs in much lesser amounts (natural abundance = 0.204%).

The stable oxygen isotope composition of a sample is expressed as the ratio of the heavy oxygen isotope relative to the light isotope: $^{18}O/^{16}O$. When comparing samples however, the differences in this ratio are very small. Therefore, the oxygen isotope ratio $^{18}O/^{16}O$ is always measured relative to an internationally accepted standard. For carbonate samples, the V-PDB standard is used (Cretaceous belemnite formation at Peedee in South Carolina, USA), while for water samples, the V-SMOW standard is used (Vienna Standard Mean Ocean Water).

The oxygen isotope composition is then expressed as the $^{18}O/^{16}O$ ratio of the sample relative to the $^{18}O/^{16}O$ ratio of the standard, an expression which is also known as the δ-notation. δ is multiplied by 1000 to reduce the number of decimals.

$$\delta^{18}O = \left(\frac{\left(\frac{^{18}O}{^{16}O}\right)_{sample} - \left(\frac{^{18}O}{^{16}O}\right)_{standard}}{\left(\frac{^{18}O}{^{16}O}\right)_{standard}} \right) * 1000\ {}^{o}/_{oo}$$

A positive δ value indicates enrichment in ^{18}O, relative to the standard, and conversely, a negative δ value indicates depletion in ^{18}O (or enrichment in ^{16}O).

3.2. Principles of isotopic fractionation

Isotopic fractionation is the partitioning of isotopes between two substances or two phases of the same substance with different isotopic compositions. Isotopic fractionation mainly results from (1) isotope exchange reactions or "equilibrium isotopic fractionation" and (2) kinetic effects or "non-equilibrium isotopic fractionation". Isotope exchange reactions involve the redistribution of isotopes of an element between two phases that are in equilibrium. Processes of equilibrium fractionation are essentially temperature dependent, which is the most important property for geochemical purposes. Kinetic effects cause deviations from equilibrium and are associated with unidirectional and incomplete processes such as condensation or evaporation, crystallization or melting, adsorption or desorption, biologically mediated reactions, and diffusion. In general, the light oxygen isotope (^{16}O) is more mobile and more affected by fractionation processes than the heavy oxygen isotope (^{18}O). The isotopic fractionation between two substances A and B is quantified by the fractionation factor $\alpha = R_A/R_B$, with R_A the $^{18}O/^{16}O$ ratio in substance A, and R_B the $^{18}O/^{16}O$ ratio in substance B (e.g. Bickert, 2000).

3.3. Processes controlling $\delta^{18}O$ of seawater

The oxygen isotopic composition of seawater ($\delta^{18}O_w$) is closely linked with fractionation processes within the hydrological cycle. Schematically, this cycle consists of evaporation at the sea surface, atmospheric vapour transport, precipitation and subsequent return of freshwater to the ocean (via precipitation, river runoff or iceberg melting). Since ^{16}O is lighter, and thus more mobile than ^{18}O, the first water vapour formed during evaporation at low latitudes is enriched in ^{16}O and the residual seawater is enriched in ^{18}O. As the air cools by rising into the atmosphere or moving towards the poles, the water vapour begins to condense and fall as precipitation. During condensation, ^{18}O preferentially enters the liquid (rain), while ^{16}O is being concentrated in the remaining vapour (cloud); a process known as Rayleigh distillation (Rayleigh, 1902). Thus water vapour gradually loses ^{18}O as it travels from the equator to the poles (Fig. 3.1). Also long-term storage of freshwater in aquifers and especially in ice sheets is important for the $\delta^{18}O$ of seawater. Finally, the spatial distribution of oxygen isotopes in the world ocean depends on processes of advection and mixing of water masses from different source regions with different isotopic signatures and the global isotope content of the ocean. A more detailed discussion of the various influences can be found in e.g. Craig & Gordon (1965), Broecker (1974) and Rohling & Cooke (1999).

Since the salinity of seawater is similarly affected by these processes, a correlation exists between salinity and the stable oxygen isotope composition of seawater. For instance Craig & Gordon (1965) and later Fairbanks *et al.* (1992) defined a set of regression equations between salinity and $\delta^{18}O_w$ for several modern water masses. The slopes vary between 0.1 for humid tropical and 1.0 for arid polar surface water masses with a global mean of 0.49. Higher slopes represent areas where evaporation exceeds precipitation, and vice versa (Bickert, 2000).

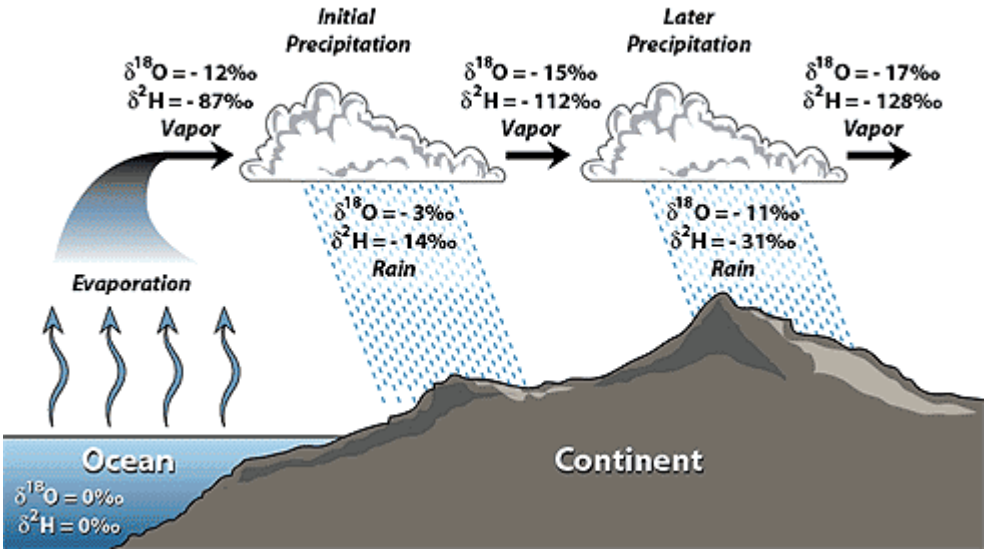

Fig. 3.1 – Oxygen isotopes in the hydrological cycle (http://web.sahra.arizona.edu/programs/isotopes/oxygen.html, based on Hoefs, 1997 and Coplen *et al.*, 2000)

3.4. $\delta^{18}O$ in marine carbonates

Since the oxygen isotope fractionation processes in marine carbonates are a function of temperature, their oxygen isotope composition ($\delta^{18}O$) can be used as a (paleo-)thermometer. Since the pioneering work of Urey (1947), McCrea (1950) and Epstein *et al.* (1953), many temperature – $\delta^{18}O$ equations have been published, and now the $\delta^{18}O$ composition of marine carbonates often forms the backbone of paleoceanographic and paleoclimatic studies. However, oxygen isotopes in carbonates are not only influenced by changes in temperature, they also depend on the oxygen isotope composition of seawater ($\delta^{18}O_w$), which can substantially affect temperature estimates. Therefore, as pointed out by Emiliani (1955) and many others since, it is imperative that the stable oxygen isotope proxy is corrected for $\delta^{18}O_w$. The calculation of temperature from oxygen isotopes is then based on the following quadratic equation:

$$T\ (°C) = a + b*(\delta^{18}O_{calcite} - \delta^{18}O_{seawater}) + c*(\delta^{18}O_{calcite} - \delta^{18}O_{seawater})^2.$$

Ideally, the $\delta^{18}O$ value of a calcareous organism reflects isotopic equilibrium with the surrounding seawater at the ambient temperature. However, offset from equilibrium has been observed for many organisms, and is due to biological, kinetic and/or metabolic effects (e.g. Wefer & Berger, 1991; Waelbroeck *et al.*, 2005). Unless these biological fractionation effects, previously called „vital effects", are accurately known, they decrease the quality of paleoenvironmental reconstructions. However, most paleoceanographic studies have circumvented the problem of biological fractionation by isolating carbonate from a single species and assuming that the vital effect in a given species is constant and does not vary through time (Ziveri *et al.*, 2003).

3.5. Foraminifera

The first empirically derived temperature – $\delta^{18}O$ relationship based on cultured planktonic foraminifera was generated by Erez & Luz (1983) for the symbiotic species *Globigerinoides sacculifer*. After that, many calibrations have followed. For instance, Bouvier-Soumagnac & Duplessy (1985) found a good agreement between the temperature – $\delta^{18}O$ relationships of cultured *Orbulina universa* and specimens collected from seawater. Bemis *et al.* (1998) developed a suite of temperature – $\delta^{18}O$ relationships for cultured *O. universa* and *Globigerina bulloides*. Although the temperature – $\delta^{18}O$ relationship is well characterized in planktonic foraminifera, the calibration equations are species-specific and can only be used for that particular species.

Various studies also reported species-specific deviations of the $\delta^{18}O$ values in foraminiferal tests from those expected for inorganic calcite precipitated in thermodynamic equilibrium with ambient seawater (e.g. Shackleton *et al.*, 1973; Fairbanks & Wiebe, 1980; Duplessy *et al.*, 1981; Bouvier-Soumagnac & Duplessy, 1985; Bemis *et al.*, 1998, Rohling & Cooke, 1999; Zeebe *et al.*, 2008). One fairly well-known biological fractionation effect in foraminiferal calcite is the ontogenetic effect. The majority of modern planktonic foraminifera species migrate vertically through the water column as part of their ontogenetic development; adding new chambers and calcite layers at different water depths (Schiebel & Hemleben, 2005). For instance, the planktonic foraminifera *Globigerina bulloides* calcifies at one depth as a juvenile and then migrates to shallower waters as an adult, where the last chamber is calcified (Spero & Lea, 1996; Bemis *et al.*, 1998). Thus the smallest chambers incorporate a different $\delta^{18}O$ signal compared to the final chamber. The dwelling depths are also species-specific. For instance symbiont-bearing species are restricted to the photic zone, whereas symbiont-barren species can migrate below the photic zone (Schiebel & Hemleben, 2005). Also the seawater carbonate chemistry can significantly affect $\delta^{18}O$

in planktonic foraminifera. This phenomenon has been referred to as the carbonate ion effect (CIE). The CIE is characterized by a decrease in shell $\delta^{18}O$ with increasing [CO_3^{2-}] concentration or pH of the culture medium/seawater, and is likely to be caused by a combination of kinetic effects and [CO_3^{2-}] related variations in the calcification rate. The phenomenon and its possible mechanisms have been extensively discussed in literature and have been described for many foraminifera species (Spero, 1992; Spero & Lea, 1993; Spero *et al.*, 1997; Bijma *et al.*, 1999).

3.6. Coccolithophores

The relationship between temperature and $\delta^{18}O$ has also been studied in coccolithophores (e.g. Ziveri *et al.*, 2003). However, since coccoliths are too small (2-12 μm) to be picked individually under a microscope, as is routinely done for foraminifera, isolating single coccolith species is difficult (Stoll *et al.*, 2001; Stoll & Ziveri, 2002). Furthermore, cultured coccolithophore species show a wide range of vital effects with a range of nearly 5‰ in $\delta^{18}O$ composition (Dudley & Goodney, 1979; Dudley *et al.*, 1980, 1986). According to Ziveri *et al.* (2003), the species-specific vital effects of coccoliths are correlated with cell size and growth rate. Like foraminifera, the carbonate ion effect has been demonstrated, in addition to the temperature effect, for *Calcidiscus leptoporus*, one of the most important calcite producers among coccolithophores (Ziveri *et al.*, 2011).

3.7. *Thoracosphaera heimii*

The stable oxygen isotope composition ($\delta^{18}O$) of *T. heimii* calcite has gained more interest over the past decade. The first studies on the topic indicated that stable oxygen isotopes of *T. heimii* calcite can be used to reconstruct past sea surface temperatures (Friedrich & Meier, 2003, 2006). Zonneveld (2004) measured the $\delta^{18}O$ composition of 21 surface sediment samples from the equatorial and South Atlantic Ocean. When the paleotemperature equation for inorganic calcite by Kim & O'Neil (1997) was applied on the $\delta^{18}O$ composition of the *T. heimii* shells, calculated isotopic temperatures generally reflected mean annual temperatures of the upper water column, notably thermocline depths, which represent the preferred depth habitat of *T. heimii*, as discussed in Chapter 2.3. Therefore, the author suggested that *T. heimii* might precipitate its calcareous shells in equilibrium with seawater.

In culture experiments it was shown there is a clear correlation between the $\delta^{18}O$ composition of *T. heimii* calcite and temperature (Zonneveld *et al.*, 2007): T (°C) = $-6.827*(\delta^{18}O_c-\delta^{18}O_w) - 3.906$ (R = 0.921), with c = calcite and w = water (Fig. 3.2). Furthermore, the authors observed an offset between the temperature – $\delta^{18}O$ relationship for *T. heimii* calcite and the one for inorganic calcite precipitation. The culture study also suggested an inverse pH effect, with heavier oxygen isotope values at higher pH values. This positive relationship was explained by the authors as the presence of external carbonate anhydrase. The efficiency of this enzyme increases rapidly between pH 7.5 to 9, which could result in an increase in CO_2 uptake relative to HCO_3^- with increasing pH (Zonneveld *et al.*, 2007, with all references therein).

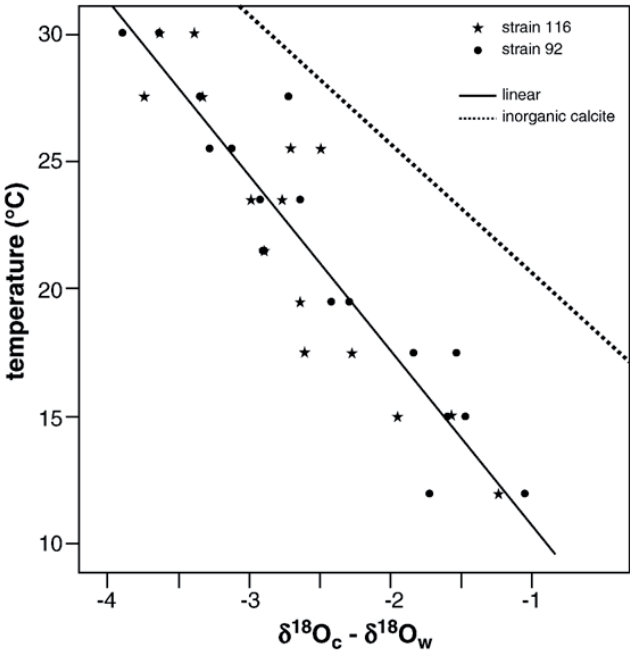

Fig. 3.2 – Correlation between temperature and $\delta^{18}O_c$–$\delta^{18}O_w$ for two strains of *Thoracosphaera heimii* and for inorganic calcite (From Zonneveld *et al.*, 2007).

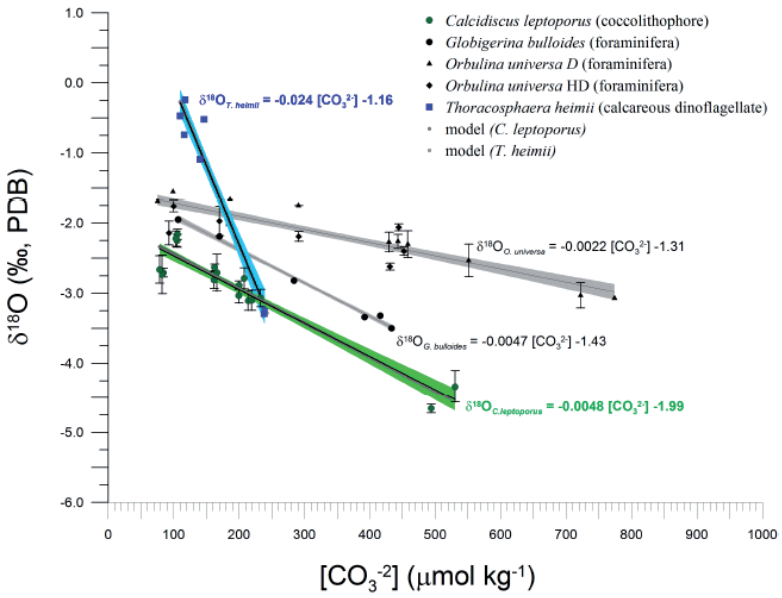

However, a more recent culture experiment revealed a slope of -0.0243 $(\mu mol/kg)^{-1}$ for the $\delta^{18}O/[CO_3^{2-}]$ relationship in *T. heimii* shells (Ziveri *et al.*, 2011) (Fig. 3.3). In comparison to foraminifera and coccolithophores, *T. heimii* has an anomalously steep slope, which suggests a strong biological control on isotope fractionation.

Fig. 3.3 – Effect of $[CO_3^{2-}]$ on $\delta^{18}O$ ($\delta^{18}O_{calcite}$–$\delta^{18}O_{water}$) values of *C. leptoporus* (coccolithophore), *T. heimii* (calcareous dinoflagellate), *O. universa* (HL = foraminifera grown under photosynthetic maximum light levels, D = maintained in the dark) (Spero *et al.*, 1997), and *G. bulloides* (Spero *et al.*, 1997) (lines are linear regression fitted to the data). 1σ confidence bounds are shown for each regression (shaded areas) (From Ziveri *et al.*, 2011)

References chapter 3

Bemis, B.E., Spero, H.J., Bijma, J., Lea, D.W., 1998. Reevaluation of the oxygen isotopic composition of planktonic foraminifera: Experimental results and revised paleotemperature equations. *Paleoceanography* 13 (2), 150-160.

Bickert, T., 2000. Influences of geochemical processes on stable isotope distribution in marine sediments. In: Schulz, H.D., Zabel, M. (Eds.), Marine Geochemistry. Springer, Berlin, pp. 309-333.

Bijma, J., Spero, H.J., Lea, D.W., 1999. Reassessing foraminiferal stable isotope geochemistry: impact of the oceanic carbonate system (experimental results). In: Use of proxies in paleoceanography: examples from the South Atlantic, Fischer, G. (Ed.), Springer Verlag, Berlin, Heidelberg.

Bouvier-Soumagnac., Duplessy, J.-C., 1985. Carbon and oxygen isotopic composition of planktonic foraminifera from laboratory culture, plankton tows and recent sediment: implications for the reconstruction of paleoclimatic conditions and of the global carbon cycle. *Journal of Foraminiferal Research* 15, 302-320.

Broecker, W.S., 1974. Chemical Oceanography. New York: Harcourt Brace Jovanovich.

Coplen, T.B., Herczeg, A.L., Barnes, C., 2000. Isotope engineering: using stable isotopes of the water molecule to solve practical problems. In: Environmental Tracers in Subsurface Hydrology. P.G. Cook, P.G., Herczeg, A.L. (Ed.), Kluwer Academic Publishers, Boston.

Craig, H., Gordon, L.I., 1965. Deuterium and oxygen-18 variations in the ocean and marine atmosphere. In: Tongiorgi, E. (Ed.), Stable isotopes in oceanic studies and paleotemperatures. Consiglio Nazionale Delle Ricerche, Laboratorio di Geologia Nucleare, Pisa, pp. 9-130.

Dudley, W.C., Goodney, D.E., 1979. Oxygen isotope analyses of coccoliths grown in culture. *Deep Sea Research* A26, 495-503.

Dudley, W.C., Duplessy, J.C., Blackwelder, P.L., Brand, L.E., Guillard, R.R.L., 1980. Coccoliths in Pleistocene-Holocene nannofossil assemblages. *Nature* 285, 222-223.

Dudley, W.C., Blackwelder, P., Brand, L., Duplessy, J.C., 1986. Stable isotopic composition of coccoliths. *Marine Micropaleontology* 10, 1-8.

Duplessy, J.C., Blanc, P., Bé, A.W.H., 1981. Oxygen-18 enrichment of planktonic foraminifera due to gametogenic calcification below the euphotic zone. *Science* 213, 1247-1250.

Emiliani, C., 1955. Pleistocene temperatures. *The Journal of Geology* 63 (6), 538-578.

Epstein, S., Buchsbaum, R., Lowenstam, H.A., Urey, H.C., 1953. Revised carbonate-water isotopic composition of coccoliths. *Marine Micropaleontology* 10, 1-8.

Erez, J., Luz, B., 1983. Experimental paleotemperature equation for planktonic foraminifera. *Geochimica et Cosmochimica Acta* 47, 1025-1031.

Fairbanks, R.G., Wiebe, P.H., 1980. Foraminifera and chlorophyll maximum: vertical distribution, seasonal succession, paleoceanographic significance. *Science* 209, 1524-1525.

Fairbanks, R.G., Charles, C.D., Wright, J.D., 1992. Origin of global melt water pulses. In: Taylor, R.E., (Ed.), Radiocarbon after four decades. Springer, New York, pp 473-500.

Friedrich, O., Meier, S.K.J., 2003. Stable isotopic indication for the cyst formation depth of Campanian-Maastrichtian calcareous dinoflagellates. *Micropaleontology* 49 (4), 375-380.

Friedrich, O., Meier, S.K.J., 2006. Suitability of stable oxygen and carbon isotopes of calcareous dinoflagellate cysts for paleoceanographic studies: evidence from the Campanian/Maastrichtian cooling phase. *Palaeogeography, Palaeoclimatology, Palaeoecology* 239 (3-4), 456-469.

Hoefs, J., 1997. Stable Isotope Geochemistry, 4th ed., Springer-Verlag, Berlin.

Kim, S.-T., O'Neil, J.R., 1997. Equilibrium and non-equilibrium oxygen isotope effects in synthetic carbonates. *Geochimica et Cosmochimica Acta* 61, 3461-3475.

McCrea, J.M., 1950. On the isotope chemistry of carbonates and a paleotemperature scale. *The journal of chemical physics* 18 (6), 849-857.

Rayleigh, L., 1902. On the distillation of binary mixtures. Philosophical Magazine (6^{th} series) 4, 521.

Rohling, E.J., Cooke, S., 1999. Stable oxygen and carbon isotope ratios in foraminiferal carbonate. In: Gupta, B.S. (Ed.), Modern foraminifera. Kluwer Academic, Dordrecht, The Netherlands, pp. 239-258.

Schiebel, R., Hemleben, C., 2005. Modern planktic foraminifera. *Paläontologische Zeitschrift* 79 (1), 135-148.

Shackleton, N.J., Wiseman, J.D.H., Buckley, H.A., 1973. Non-equilibrium isotopic fractionation between seawater and planktonic foraminiferal tests. *Nature* 242, 177-179.

Spero, H.J., 1992. Do planktonic foraminifera accurately record shifts in the carbon isotopic composition of sea water $\sum CO_2$? *Marine Micropaleontology* 19, 275-285.

Spero, H.J., Lea, D.W., 1993. Intraspecific stable isotope variability in the planktic foraminifera *Globigerinoides sacculifer*: Results from laboratory experiments. *Marine Micropaleontology* 22, 221-234.

Spero, H. J., Lea, D.W., 1996. Experimental determination of stable isotope variability in *Globigerina bulloides*: Implications for paleoceanographic reconstruction. *Marine Micropaleontology* 28, 231-246.

Spero, H.J., Bijma, J., Lea, D.W., Bemis, B.E., 1997. Effect of seawater carbonate concentration on foraminiferal carbon and oxygen isotopes. *Nature* 390, 497-500.

Stoll, H.M., Ziveri, P., 2002. Methods for separation of monospecific coccolith samples from sediments. *Marine Micropaleontology* 46, 209-221.

Stoll, H.M., Encinar, J.R., Alonso, J.I.G., Rosenthal, Y., Probert, I., Klaas, C., 2001. A first look at paleotemperature prospects from Mg in coccoliths carbonate: cleaning techniques and culture measurements. *Geochemisrty, Geophysics, Geosystems* 2, 2000GC000144.

Urey, H.C., 1947. The thermodynamic properties of isotopic substances. *Journal of the Chemical Society*, 562-581.

Waelbroeck, C., Mulitza, S., Spero, H., Dokken, T., Kiefer, T., Cortijo, E., 2005. A global compilation of late Holocene planktonic foraminiferal relationship between surface water temperature and $\delta^{18}O$. *Quaternary Science Reviews* 24, 853-868.

Wefer, G., Berger, W.H., 1991. Isotope paleontology: Growth and composition of extant calcareous species. *Marine Geology* 100, 207-248.

Zeebe, R.E., Bijma, J., Hönisch, B., Sanyal, A., Spero, H.J., Wolf-Gladrow, D., 2008. Vital effects and beyond: a modeling perspective on developing palaeoceanographical proxy relationships in foraminifera. Geological Society, London, Special Publications 303, 45-58.

Ziveri, P., Stoll, H., Probert, I., Klaas, C., Geisen, M., Ganssen, G., Young, J., 2003. Stable isotope "vital effects" in coccolith calcite. *Earth and Planetary Science Letters* 210, 137-149.

Ziveri, P., Thoms, S., Probert, I., Geisen, M., Langer, G., 2011. A universal carbonate ion effect on stable oxygen isotope ratios in unicellular planktonic calcifying organisms. *Biogeosciences Discussions* 8, 7575-7591, doi:10.5194/bgd-8-7575-2011.

Zonneveld, K., 2004. Potential use of stable isotope composition of *Thoracosphaera heimii* (Dinophyceae) for upper water column (thermocline) temperature reconstruction. *Marine Micropaleontology* 50 (3-4), 307-317.

Zonneveld, K.A.F., Mackensen, A., Baumann, K.-H., 2007. Stable oxygen isotopes of *Thoracosphaera heimii* (Dinophyceae) in relationship to temperature; a culture experiment. *Mar. Micropal.* 64 (1-2), 80-90.

CHAPTER 4
INTRODUCTION: BIOMINERALIZATION & MG, SR INCORPORATION

4.1. General remarks

Biomineralization refers to the processes by which living organisms form minerals. During these processes, the organism exerts a certain control over mineral formation, thus precipitation is not strictly thermodynamically controlled. This distinguishes biomineralization from inorganic or abiotic mineralization, and often results in very unusual external morphologies of the biominerals. Biominerals often have very specific properties such as shape, size and crystallinity. Another characteristic of biominerals is that many are actually composites or agglomerates of biological (or organic) and mineral (or inorganic) compounds. In many organisms, the crystals exist as small bodies distributed within a complex framework of macromollecular frameworks (e.g. Weiner & Dove, 2003).

The most abundant biominerals are the calcium carbonate minerals. Of the eight known polymorphs of $CaCO_3$, seven are crystalline and one is amorphous. Calcite, aragonite and vaterite are pure calcium carbonate ($CaCO_3$); monohydrocalcite and the stable forms of amorphous calcium carbonate contain one water molecule per calcium carbonate ($CaCO_3.H_2O$). One of the major challenges in the field of biomineralization is to understand the mechanism(s) how biological systems determine which polymorph will precipitate (e.g. Weiner & Dove, 2003).

Having the same electrical charge as calcium (Ca^{2+}), magnesium (Mg^{2+}) and strontium (Sr^{2+}) may substitute for Ca^{2+} in the calcium carbonate crystal structure. However, the relatively large diameter of the Sr^{2+} ion prevents it from fitting into the calcite crystal lattice as easily as it lodges in the aragonite crystal lattice. Thus aragonite contains more Sr^{2+} than calcite (e.g. Stanley, 2006). Furthermore, the incorporation of Mg^{2+} in the calcite crystal inhibits crystal growth (Davis *et al.*, 2002). Biomineralization and incorporation of trace elements is species specific. Very little is known about these processes in the calcareous dinoflagellate *T. heimii*. Therefore, in order to have a better understanding and for comparison purposes, an overview of the biomineralization in foraminifera and coccolithophores is provided.

4.2. Foraminifera

Based on their shell (test), foraminifera can be divided into four groups. The first and second group have organic tests and agglutinated tests (composed of particles collected by the organism and inserted in the test). These two groups are not considered as performing biomineralization and hence will not be discussed here. The other two groups precipitate $CaCO_3$ tests and are known as the imperforate (or porcelaneous) foraminifera and the perforate (or calcitic radial) foraminifera. Here, only the biomineralization of the perforate foraminifera will be reviewed, since they dominate the oceans today. (Erez, 2003).

The perforate foraminifera tests can be very simple with one or only a few chambers, or they can be complex with many chambers arranged in various three-dimensional configurations. The name "perforate foraminifera" is derived from the fact that the tests of this group are covered with numerous microscopic pores (from a few microns up to 10 μm). These pores are sealed by an organic plug that prevents the internal cytoplasm from flowing out of the test (Hemleben *et al.*, 1989). Larger openings in the tests are called apertures. The apertures of earlier chambers (also called foramens) are connected, thus forming a continuous space where the internal cytoplasm is connected with the external pseudopodia. These pseudopodia are fine strands of cytoplasm that form a complex network and are important for several life functions of these organisms such as food gathering, movement, respiration, extraction of waste and shell building. (Erez, 2003).

One major feature found in many perforate foraminifera is their lamination: every time the organism builds a new chamber, it covers its entire pre-existing shell with a new layer of calcite. Therefore each newly added chamber is composed of two layers of calcite: primary calcite (~10%), which outlines the new chamber, and secondary calcite (~90%), that covers both the new chamber and the entire existing test (Fig. 4.1). Although the bulk of the foraminiferal calcite is composed of this secondary calcite, little is known about its calcification mechanism: e.g. pores and possible spines are not covered by the secondary calcite (Erez, 2003). As a general overview of the primary and secondary calcification in calcitic radial foraminifera the mechanisms proposed by Erez (2003) will be described.

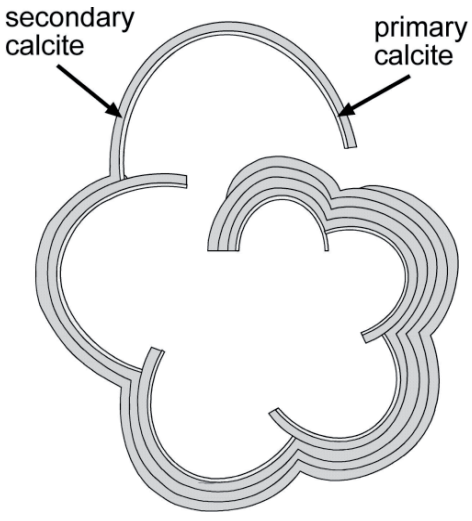

Fig. 4.1 – Lamination scheme in perforate foraminifera (Erez, 2003)

Primary calcification

In order to create a new chamber, the presence of pseudopodia is absolutely essential (A in Fig. 4.2). First, the pseudopodia start to envelop a bulb of seawater, forming an intracellular seawater vacuole, a process called endocytosis (B in Fig. 4.2). Seawater vacuolization is the basis from which calcification starts. Next, the pseudopodia will cover the entire organism, a process called self-vacuolization (C in Fig. 4.2), resulting in a clear separation of intralocullar and extralocullar cytoplasm. The organism now isolated itself from its surrounding environment and primary calcification will occur in the thus delineated space. Meanwhile, small vacuoles are being transported from the initial seawater vacuole to the sites of primary calcification (D in Fig. 4.2). The next step is the formation of an organic matrix in the shape of the newly formed chamber, which indicates a strong biological control over the shape of the shell. This thin organic layer is often called the primary organic membrane (POM) and can sometimes be recovered from fossil samples (foram linings). Not much is known about the role of this POM in the calcification process of foraminifera, but it is often suggested that this organic matrix will serve as a template for nucleation. The last step in the primary calcification is the precipitation of small $CaCO_3$ crystals (microspherulites) on both sides of the POM (E in Fig. 4.2). During this entire process there is an intensive involvement of the pseudopodia, with strong cytoplasmic and vacuole streaming. (Erez, 2003).

Secondary calcification

More and smaller vacuoles start to appear in the extralocullar cytoplasm, still originating from the large initial seawater vacuole. These vacuoles are transported by a pseudopodial network to the sites of secondary calcification, which are still in the delimited space. The vacuoles surround the growing primary calcite crystals and are then exocytosed into the delimited space where calcite is precipitated over the entire existing shell (F in Fig. 4.2). This secondary calcite is made of multilayered calcite platelets that have a radial appearance with their c-axes (vertical axes of the crystals) perpendicular to the test wall, a structure known as “calcitic radial” (Hansen & Reiss, 1972; Bellemo, 1974). These units form the secondary lamination and are responsible for the bulk of the skeleton deposition. (Erez, 2003).

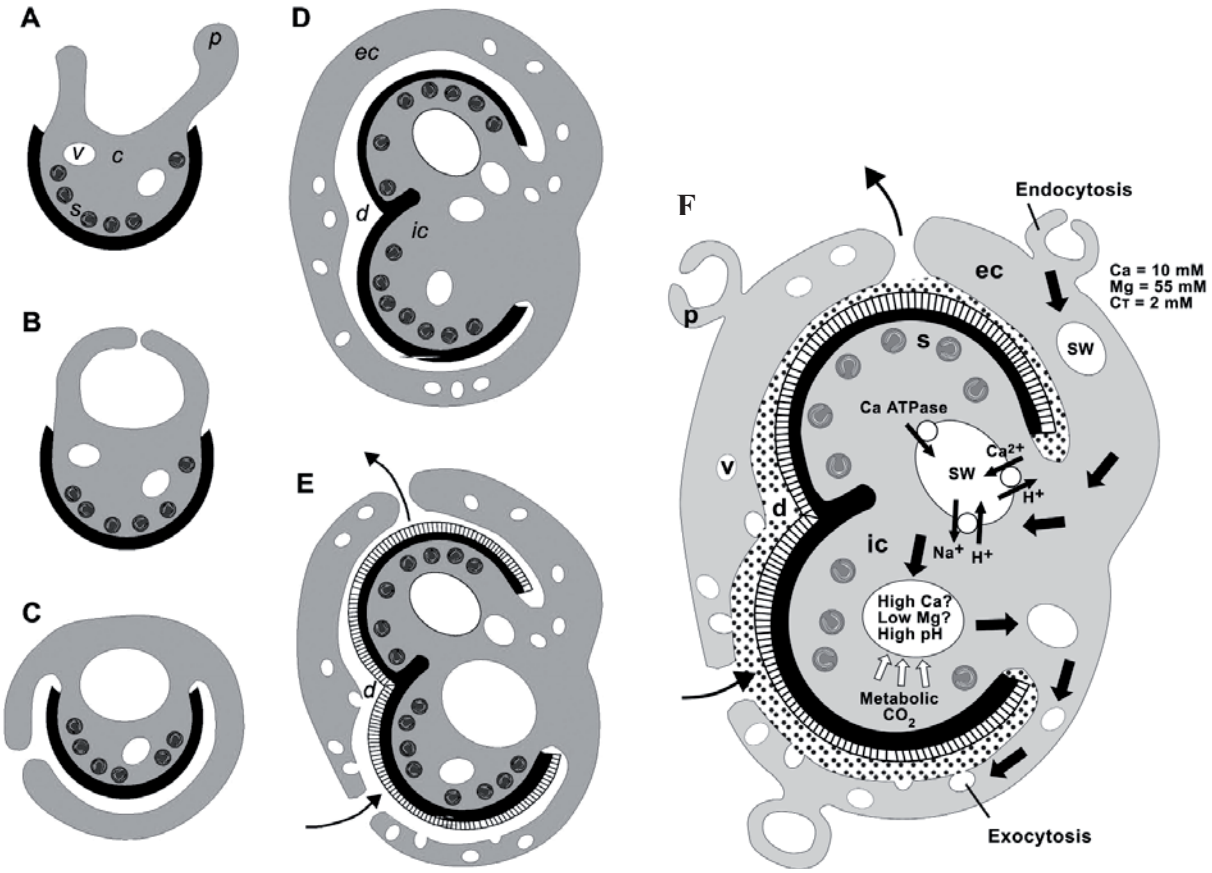

Fig. 4.2 – Schematic presentation of primary (A-E) and secondary (F) calcification in perforate foraminifera (Erez, 2003) – The black cup represents the $CaCO_3$ shell which is exposed to the seawater – s: symbiotic algae, p: pseudopodia, v: vacuole, c: cytoplasm, d: delimited space, ic: intralocullar cytoplasm, ec: extralocullar cytoplasm, sw: seawater

Trace element incorporation

Although surface seawaters are supersaturated with respect to calcite, spontaneous crystal nucleation and growth are prevented by the high concentrations of magnesium in modern-day seawater (Davis *et al.*, 2002; de Nooijer *et al.*, 2009). Despite this fact, planktonic foraminifera generally produce calcite with a low Mg content (1-10 mmol/mol; Elderfield *et al.*, 1996). This low-Mg calcite can only be precipitated if the foraminifera effectively discriminate between Mg^{2+} and Ca^{2+} after seawater vacuolization, most likely by actively removing Mg^{2+} from the seawater vacuoles prior to calcite precipitation (Zeebe & Sanyal, 2002). The seawater vacuoles are thus being altered by the organism during the biomineralization process (Erez, 2003). This discrimination between Mg^{2+} and Ca^{2+} supposedly leads to the production of an intracellular Ca-pool with a very low Mg/Ca ratio from which the calcite will be precipitated (Zeebe & Sanyal, 2002). Carbonate is stored in a separate intracellular pool (e.g. Erez, 2003).

De Nooijer *et al.* (2009) demonstrated that planktonic foraminifera are able to elevate the pH at the site of calcification by at least one unit above seawater pH (8.2) and, thereby, can overcome precipitation-inhibition at high Mg concentrations. However, since planktonic foraminifera precipitate their calcite from an internal fluid with a very low Mg/Ca ratio (Zeebe & Sanyal, 2002), this is not the most important effect of the pH elevation. An elevated pH also promotes conversion from bicarbonate into carbonate (Zeebe & Wolf-Gladrow, 2001). At modern surface seawater pH (8.2), ~90% of the dissolved inorganic carbon (DIC) is present in the form of HCO_3^-. When the pH is elevated with one unit (9.2), ~90% of DIC is present as CO_3^{2-}, resulting in a 9-fold increase of the calcite saturation state (Ω) of the seawater, approximately doubling the precipitation rate (Lopez *et al.*, 2009).

Inter-species and intra-test variability

Inter-species variability in foraminiferal Mg/Ca is generally correlated with the calcification depth of the foraminifera species: shallow dwellers (e.g. *G. ruber* and *G. sacculifer*) have high Mg/Ca ratios, whereas deep dwellers (e.g. *G. tumida* and *G. dutertrei*), have relatively low Mg/Ca ratios (Rosenthal & Boyle, 1993). Many foraminifera species also continue to calcify while migrating vertically through the water column, thus incorporating the Mg signal from different depths in their tests. The Mg/Ca composition of the foraminifera test thus represents a weighted average of calcite layers formed at different depths/temperature (Rosenthal & Linsley, 2007). Differences in Mg/Ca can also exist between different size fractions of the same species (Anand *et al.* 2003). Furthermore, it has been observed that different parts of the foraminiferal calcite shell have different concentrations in trace elements: some parts are enriched, while other parts are depleted (Szafrenek & Erez, 1993; Nürnberg *et al.*, 1996; Eggins *et al.*, 2003; Sadekov *et al.*, 2005). Erez (2003) summarized the above mentioned studies and described the tests of planktonic foraminifera as thick secondary calcite, which is low in Mg, S and perhaps other trace elements, sandwiched between primary calcite and gametogenic calcite (when present), which are both richer in trace elements. Sr does not seem to be distributed heterogeneously in the foraminifera test. Since high Mg calcite is more soluble than low-Mg calcite (Morse & MacKenzie, 1990), the primary and gametogenic calcite are more soluble than the secondary calcite. This dissolution of the Mg-rich phases could be a major concern in the use of foraminiferal Mg as a proxy for dissolution (Brown & Elderfield, 1996).

4.3. Coccolithophores

Biomineralization

Coccolithophores are covered by calcium carbonate plates, called coccoliths. One of the most distinctive aspects of the biomineralization of coccolithophores is that they produce two very different coccolith types in their life cycle. *Heterococcoliths*, produced during the diploid (2N) phase, show radial symmetry and consist of a limited number (< 100) of calcite crystals which can have very complex shapes. *Holococcoliths*, produced during the haploid (N) phase, lack the radial symmetry of the heterococcoliths and are composed of many (100s to 1000s) small (0,1 µm) calcite crystallites. Exceptions exist, e.g. some genera, such as *Pleurochrysis* and *Emiliania*, only produce heterococcoliths and are non-calcifying in the haploid phase (Young & Henriksen, 2003).

Here, only the biomineralization of heterococcoliths will be discussed, since this is the most common type of coccolith. In contrast to foraminifera, where calcification occurs extracellularly, coccolithophores are characterized by intracellular calcification. Within the coccolithophore, coccolith growth occurs in coccolith vesicles (CV in Fig. 4.3) derived from the Golgi body. The calcification site is isolated from the seawater by a complex membrane system: the plasma membrane (PM in Fig. 4.3) and the coccolith vesicle membrane (around CV in Fig. 4.3) (Young & Henriksen, 2003).

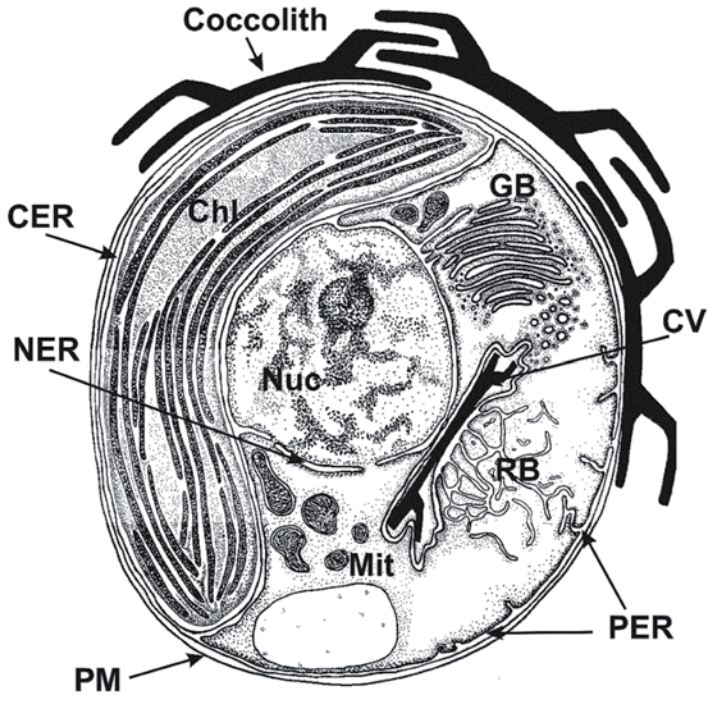

Fig. 4.3

Diagrammatic representation of the endomembrane system in a coccolithophore cell (Brownlee & Taylor, 2004; drawn with reference to Manton & Leedale (1969) and Klaveness (1972)) – Nuc: nucleus, Mit: mitochondria, Chl: chloroplast, PM: plasma membrane, GB: Golgi Body, CV: coccolith vesicle, RB: reticular body, PER: peripheral endoplasmic reticulum, NER: nuclear endoplasmic reticulum, CER: chloroplast endoplasmic reticulum

As an example of coccolithophorid biomineralization, the coccolith development of *Pleurochrysis carterae*, one of the most well-studied coccolithophores, will be discussed; as was worked out in detail by van der Wal *et al.* (1983) (Fig. 4.4). Note that other coccolithophore species have other biomineralization mechanism.

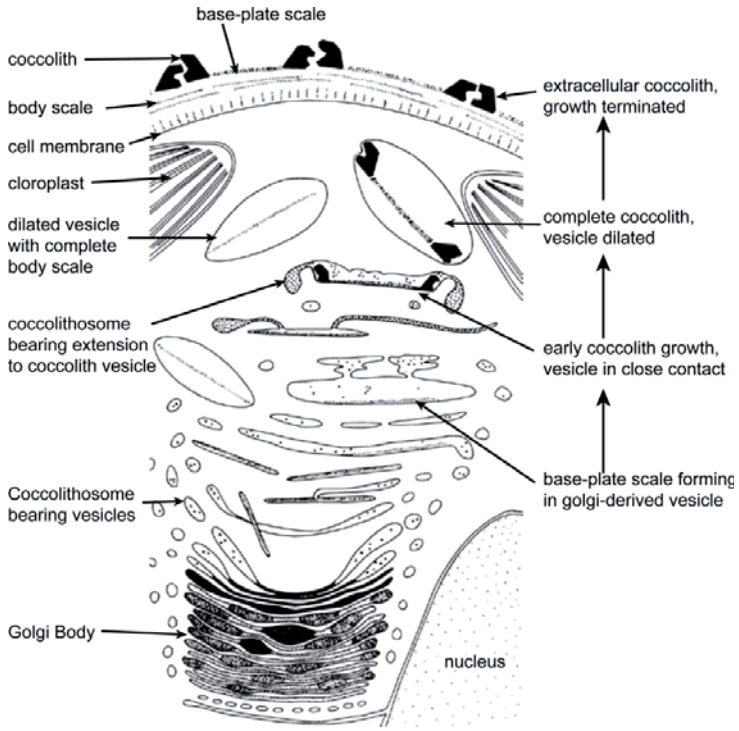

Fig. 4.4 – Coccolithogenesis in *Pleurochrysis carterae*. Van der Wal *et al.* (1983) in Young & Henriksen (2003).

The biomineralization process starts with the formation of an organic base-plate scale within the coccolith vesicle. This organic scale has a microfibrous structure and is composed of coccolith-associated polysaccharides (CAP's). The coccolith vesicles can develop rather complex forms, with extensions containing dense particles, called coccolithosomes. These extensions are probably derived from coccolithosome-bearing vesicles that attach themselves to the coccolith vesicles. Coccolithosomes have been shown to be complexes of acidic polysaccharides with calcium ions. Around the periphery of the organic base-plate scale, nucleation of calcite crystals occurs, followed by crystal growth upward and outward to form the complete coccolith. At an early growth stage, the vesicle is still in close contact with the coccolith. During coccolith growth, the vesicle gradually expands, and, after the coccolith is completed, a dense organic coating, derived from the CAP's, is visible around the coccolith crystals. As a final step, the coccolith vesicle membrane fuses with the cell membrane (exocytosis). When the coccolith is placed extracellularly, a polysaccharide mat stays on top of the coccolith, thus preventing further extracellular (inorganic) precipitation and dissolution (Young & Henriksen, 2003).

Minor element incorporation

Many mechanisms have been proposed for the transport pathways of calcium and minor elements from seawater to the site of calcification inside the coccolith vesicle. Here, the simplest mechanism for *Emiliania huxleyi* will be described (Gussone *et al.*, 2006; Fig. 4.5). In seawater, calcium is present as dissolved Ca^{2+} (Ca_{aq}). At the coccolithophore cell surface, the water layer surrounding the calcium ion is stripped off (dehydration), and Ca^{2+} is transported into the cell through Ca-selective channels (Brownlee & Taylor, 2004). Channels are small pores through which transport occurs as diffusion. Also other ions, such as Sr^{2+} and Ba^{2+} can migrate through these channels. After rehydration and redehydration, practically all of the Ca^{2+} ions are then removed from the cytoplasm by Ca pumps and transferred into cell organelles (e.g. endoplasmic reticulum or Golgi body), into coccolith vesicles or are guided out of the cell. The portion of Ca^{2+} that is transported is indicated by the black slices in the pie charts in Fig. 4.5. Ca pumps are enzym-like proteins and use adenosine triphosphate (ATP) as energy source (Gussone *et al.*, 2006). Every organel thus has its own special isotopic and elemental composition.

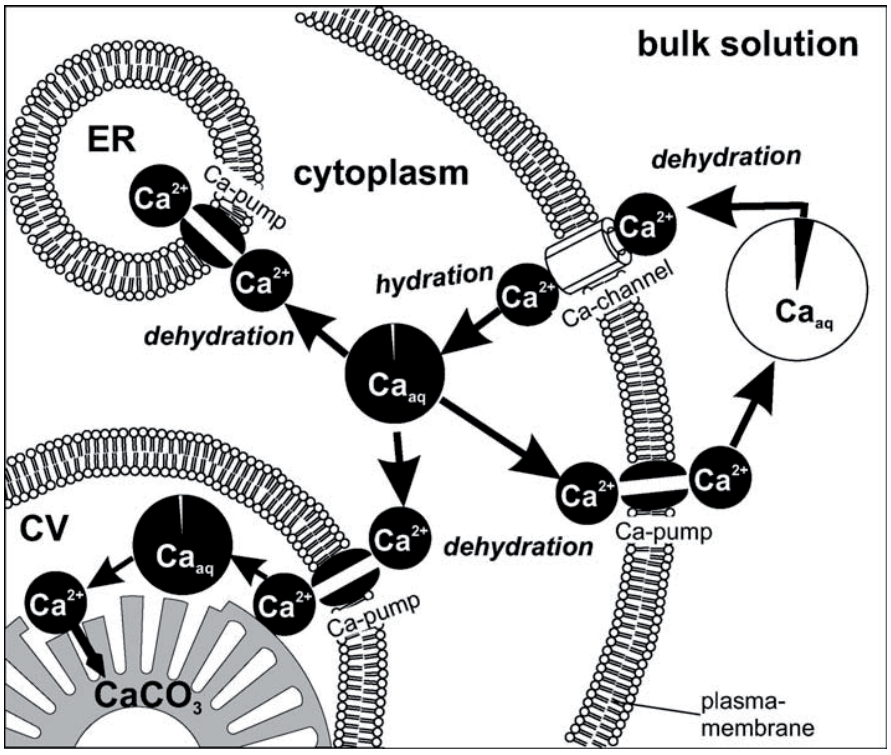

Fig. 4.5 – Proposed calcium transport pathways in *Emiliania huxleyi* from seawater to the calcification site (Gussone *et al.*, 2006). The portion of Ca that is transported is indicated by the black slices in the pie charts.

Inter-species variability

Although it was conventionally believed that all modern coccolithophore species secrete low-Mg calcite (<4 mol% Mg substituting for Ca) in modern seawater (Siesser, 1971, 1977; Miliman, 1974), Stanley *et al.* (2005a,b) and Stanley (2006) discovered that two out of three cultured coccolithophore species (*Pleurochrysis carterae* and *Ochrosphaera neopolitana*) secreted coccoliths of high-Mg calcite (>4 mol% Mg substituting for Ca) in an experimental setup with seawater of modern composition (Mg/Ca = 5.2 mmol/mol). As the ambient Mg/Ca ratio was lowered, these two species incorporated progressively less Mg into their coccoliths, and when the ambient Mg/Ca reached 1 mmol/mol ("Cretaceous" seawater), these two species secreted low-Mg calcite. Only one out of three cultured species did not show any correlation between skeletal Mg/Ca and seawater Mg/Ca: *Coccolithus neohelis* secreted low-Mg calcite in each of the experimental water treatments, including seawater of modern composition (Fig. 4.6; Stanley *et al.*, 2005a,b; Stanley, 2006). This would suggest that *P. carterae* and *O. neopolitana* have less control over the Mg incorporation in the calcite crystal lattice than *C. neohelis*, i.e. their biomineralogical control could be partly overridden by ambient seawater chemistry (Ries, 2010). This also implies that the mineralogy (low-Mg vs high-Mg calcite) of some, but not all coccolithophore species varied significantly with seawater Mg/Ca throughout geological time (Ries, 2010).

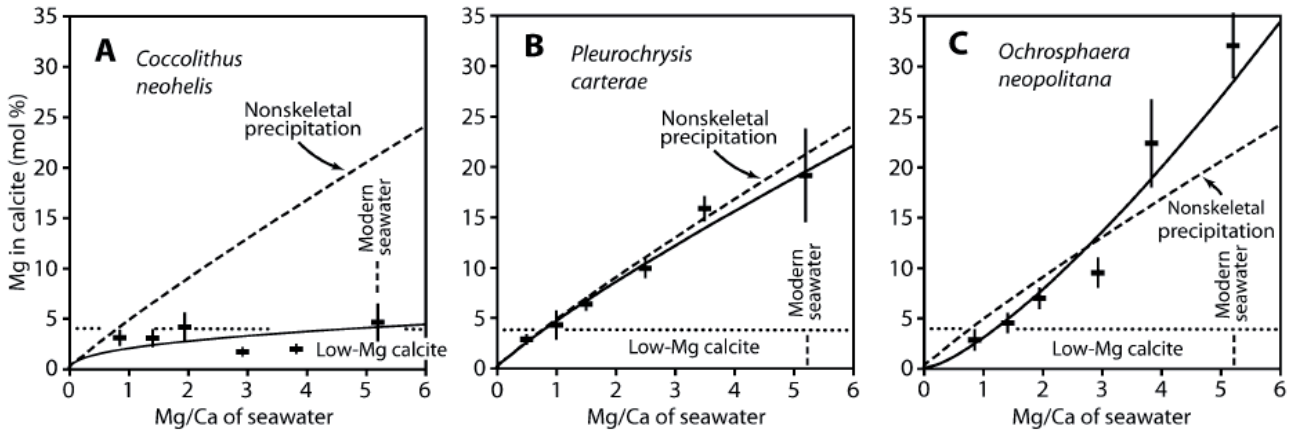

Fig. 4.6 – Magnesium in calcite (mol%) secreted by three coccolithophore species as function of molar Mg/Ca ratio of artifical seawater in which they were grown. Error bars are standard deviations of five measurements. Fitted curves are power functions. Dashed lines depict pattern for inorganic precipitation (Füchtbauer & Hardie, 1976, 1980) (From Stanley *et al.*, 2005b)

4.4. *Thoracosphaera heimii*

Thoracosphaera heimii shells have a very characteristic crystal pattern: polygonal crystals are organized around regularly distributed pseudopores (e.g. Gussone *et al.*, 2010). The tangential orientation of the c-axis (vertical axis) of the individual crystals, gives *T. heimii* a characteristic view under polarized light (Fig. 2.3 in Chapter 2.2; e.g. Janofske, 1996).

Biomineralization process

Currently, limited information is available about the biomineralization mechanisms of the calcareous dinoflagellate *T. heimii*. Using transmission electron microscopy (TEM), Inouye & Pienaar (1983) were able to document *T. heimii* cells in different phases of the calcifying process.

In the initial phase of the calcifying process, vacuoles function as intracellular calcification sites and are separated from the surrounding seawater by several membranes: a cytoplasmic membrane (Cm in Fig. 4.7), a so-called "pellicle layer" (Pl in Fig. 4.7), an inner cell membrane (Icm in Fig. 4.7) and an outer cell membrane (Ocm in Fig.4.7). The vacuoles contain two types of crystals. At the inner side of the vacuoles, the side directed towards the cell centre, cylindrical crystals of unknown composition are present (● in Fig. 4.7A). Most likely, these cylindrical crystals are formed in dictyosomes of the Golgi system. Apart from the cylindrical crystals, the vacuoles also contain small calcium carbonate crystals (◊ in Fig. 4.7B), the first generation of calcite (Inouye & Pienaar, 1983; Gussone *et al.*, 2010).

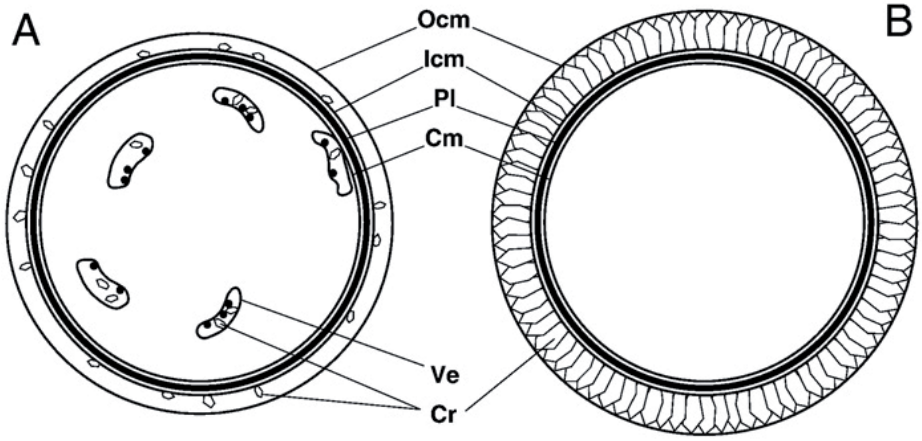

Fig. 4.7 – Two stage biomineralization model of *T. heimii* – A: young cell in the beginning of the calcification process – B: mature cell – Ocm: outer cell membrane – Icm: inner cell membrane – Pl: pellicle layer – Cm: cytoplasma membrane – Ve: vesicle with rounded crystals of unknown composition and calcareous crystals – Cr: calcareous crystals (from Gussone *et al.*, 2010; after Inouye & Pienaar, 1983)

In the next phase of the calcifying process, the vacuoles start migrating towards the cytoplasmic membrane. The primary calcite crystals are transferred into the area between the inner and outer cell membrane, possibly through exocytosis, where a layer of secondary calcite is being precipitated (Fig. 4.7). Initially, crystals occur at places scattered over the cell surface, but rapidly they form the characteristic crystal pattern of *T. heimii* shells. Crystal formation is completed within several hours to maximum three days (Inouye & Pienaar, 1983; Gussone *et al.*, 2010).

Minor element incorporation

To connect the TEM observations of Inouye & Pienaar (1983) with the characteristic elemental (Gussone *et al.*, 2010) and isotopic (Zonneveld *et al.*, 2007) patterns of cultured *T. heimii* shells, Gussone *et al.* (2010) assumed different element and isotope fractionation patterns in two different generations of calcite. Based on a similar temperature dependence of the Sr/Ca ratios of *T. heimii* shells and the coccoliths of *E. huxleyi*, Gussone *et al.* (2010) suggested that the Sr/Ca ratio in *T. heimii* is mainly controlled by a cellular Ca and Sr transport process, as was previously proposed for *E. huxleyi* (Stoll & Ziveri, 2005; Langer *et al.*, 2006). Since the first calcification phase of *T. heimii* shells is secreted under strong cellular control, this implies that the first generation of *T. heimii* calcite, the inner calcite, is Sr-enriched (Fig. 4.8). During the second phase, a Mg-enriched calcite layer is formed, possibly influenced by a seawater dominated fluid (Fig. 4.8; Gussone *et al.*, 2010). In general, it could be stated that the first phase is similar to the biomineralization of coccolithophores, while the second phase is similar to the biomineralization of foraminifera.

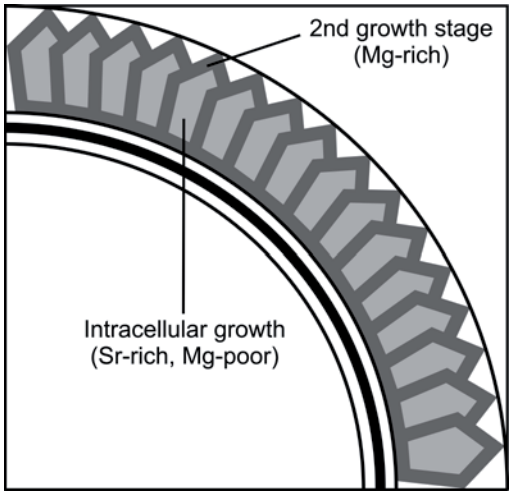

Fig. 4.8 – Minor element incorporation model for *T. heimii* (drawn based on Gussone *et al.*, 2010)

References Chapter 4

Anand, P., Elderfield, H., Conte, M. H., 2003. Calibration of Mg/Ca thermometry in planktonic foraminifera from a sediment trap time series. *Paleoceanography* 18, 1050, doi:10.1029/2002PA000846.

Bellemo, S., 1974. Ultrastructures in recent radial and granular foraminifera. Bull. Geol. Inst. Univ. Uppsala New Series 4, 117-122.

Brown, S.J., Elderfield, H., 1996. Variations in Mg/Ca and Sr/Ca ratios of planktonic foraminifera caused by postdepositional dissolution: Evidence of shallow Mg-dependant dissolution. *Paleoceanography* 11 (5), 543-551.

Brownlee, C., Taylor, A., 2004. Calcification in coccolithophores: A cellular perspective. In: Thierstein, H.R., Young J.R. (Eds.). Coccolithophores – From molecular processes to global impact. New York, Springer, p. 31-49.

Davis, K.J., Dove, P.M., De Yoreo, J.J., 2002. Resolving the controversial role of Mg^{2+} in calcite biomineral formation. *Science* 290, 1134-1137.

de Nooijer, L.J., Toyofuku, T., Kitazato, H., 2009. Foraminifera promote calcification by elevating their intracellular pH. *PNAS* 106 (36), 15374-15378.

Eggins, S., De Deckker, P., Marshall, J., 2003. Mg/Ca variation in planktonic foraminifera tests: Implications for reconstructing palaeo-seawater temperature and habitat migration. *Earth Planetary Science Letters* 212 (3-4), 291-306.

Elderfield, H., Bertram, C.J., Erez, J., 1996. A biomineralization model for the incorporation of trace elements into foraminiferal calcium carbonate. *Earth and Planetary Science Letters* 142, 409–423.

Erez, J., 2003. The source of ions for biomineralization in foraminifera and their implications for paleoceanographic proxies. In: Biomineralization, Dove, P.M., Weiner, S., De Yoreo, J.J., (Eds.). Mineralogical Society of America, Washington, D.C., pp. 115-149.

Füchtbauer, H., Hardie, L.A., 1976. Experimentally determined homogeneous distribution coefficients for precipitated magnesian calcites: application to marine carbonate cements. *Geological Society of America Abstracts with Programs* 8, 877.

Füchtbauer, H., Hardie, L.A., 1980. Comparison of experimental and natural magnesium calcites. Int. As. Sed., Bochum, 167-169.

Gussone, N., Langer, G., Thoms, S., Nehrke, G., Eisenhauer, A., Riebesell, U., Wefer, G., 2006. Cellular calcium pathways and isotope fractionation in *Emiliania huxleyi*. *Geology* 34 (8), 625-628, doi: 10.1130/G22733.1

Gussone, N., Zonneveld, K.A.F., Kuhnert, H., 2010. Minor element an Ca isotope composition of calcareous dinoflagellate cysts of cultured *Thoracosphaera heimii*. *Earth and Planetary Science Letters* 289, 180-188.

Hansen, H.J., Reiss, Z., 1972. Scanning electron microscopy of wall structures in some benthonic and planktonic foraminifera. *Rev. Esp. Micropaleontol.* 4, 169-179.

Hemleben, C., Spindler, M., Anderson, O.R., 1989. Modern Planktonic Foraminifera. Springer-Verlag, New York

Inouye, I., Pienaar, R.N., 1983. Observations on the life cycle and microanatomy of *Thoracosphaera heimii* (Dinophyceae) with special reference to its systematic position. *South African Journal of Botany* 2, 63-75.

Janofske, D., 1996. Ultrastructure types in recent "calcispheres". *Bulletin de l'Institut Océanographique Monaco* 14 (4), 295-303.

Klaveness, D., 1972. *Coccolithus huxleyi* (Lohmann) Kamptner. I. Morphological investigations on the vegetative cell and the process of coccolith formation. *Protistologica* 8, 335-346.

Langer, G., Gussone, N., Nehrke, G., Riebesell, U., Eisenhauer, A., Kuhnert, H., Rost, B., Trimborn, S., Thoms, S., 2006. Coccolith strontium to calcium ratios in *Emiliana huxleyi*: the dependence on seawater strontium and calcium concentrations. *Limnology and Oceanography* 51 (1), 310-320.

Lopez, O., Zuddas, P., Faivre, O., 2009. The influence of temperature and seawater composition on calcite crystal growth mechanisms and kinetics: Implications for Mg incorporation in calcite lattice. *Geochimica et Cosmochimica Acta* 73, 337–347.

Manton, I., Leedale, G.F., 1969. Observations on the microanatomy of *Coccolithus pelagicus* and *Cricosphaera carterae*, with special reference to the origin and nature of coccoliths and scales. *Journal of The Marine Biological Association of the United Kingdom* 49, 1-16.

Milliman, J.D., 1974. Marine carbonates. Springer-Verlag. Berlin. 375 pp.

Morse, J.W., MacKenzie, F.T., 1990. Geochemistry of sedimentary carbonates. Developments in Sedimentology 48. Elsevier Science Publishers.

Nurnberg, D., Bijma, J., Hemleben, C., 1996. Assessing the reliability of magnesium in foraminiferal calcite as a proxy for water mass temperature. *Geochimica et Cosmochimica Acta* 60 (5), 803-814.

Ries, J.B., 2010. Review: geological and experimental evidence for secular variation in seawater Mg/Ca (calcite-aragonite seas) and its effect on marine biological calcification. *Biogeosciences* 7, 2795-2849, doi:10.5194/bg-7-2795-2010.

Rosenthal, Y., Boyle, E.A., 1993. Factors controlling the fluoride content of planktonic foraminifera: an evaluation of its paleoceanographic applicability. *Geochimica et Cosmochimica Acta* 57, 335-346.

Rosenthal, Y., Linsley, B., 2007. Paleoceanography, physical and chemical proxies. Mg/Ca and Sr/Ca paleothermometry. In: Elias, S.A. (Ed.), Encyclopedia of Quaternary Science, Royal Holloway, University of London, U.K., pp. 1723-1731.

Sadekov, A., Yu, S., Eggins, M., De Decker, P., 2005. Characterization of Mg/Ca distributions in planktonic foraminifera species by electron microprobe mapping. *Geochemistry, Geophysics, Geosystems* 6, Q12P06, doi:10.1029/2005GC000973.

Siesser, W.G., 1971. Mineralogy and diagenesis of some South African coastal and marine sediments. *Marine Geology* 10, 15-38.

Siesser, W.G., 1977. Chemical composition of calcareous nannofossils. *South African Journal of Science* 73, 283-285.

Stanley, S.M., 2006. Influence of seawater chemistry on biomineralization throughout phanerozoic time: Paleontological and experimental evidence. *Palaeogeography, Palaeoclimatology, Palaeoecology* 232, 214-236.

Stanley, S.M., Ries, J.B., Hardie, L.A., 2005a. Cretaceous versus modern carbonate sediment mineralogy: evidence from experiments with *Halimeda*. *Geological Society of America Abstracts with Programs* 37, A183.

Stanley, S.M., Ries, J.B., Hardie, L.A., 2005b. Seawater chemistry, coccolithophore population growth, and the origin of Cretaceous chalk. *Geology* 33, 593-596.

Stoll, H., Ziveri, P., 2005. Coccolithophorid-based geochemical paleoproxies. Berlin, Springer, Heidelberg, pp. 529-563.

Szafranek, D., Erez, J., 1993. Chemistry of Mg, SO_4^{2-} , Sr, Na and Cl in live foraminifera shells (abstract). 7th International Symposium On Biomineralization, Monaco. Biomineralization 93, 36.

van der Wal, P., de Jong, E.W., Westbroek, P., de Bruijn, W.C., Mulder-Stapel, AA., 1983. Polysaccharide localization, coccolith formation, and Golgi dynamics in the coccolithophorid *Hymenomonas carterae*. *Journal of Ultrastructure Research* 85, 139-158.

Weiner, S., Dove, P.M., 2003. An overview of biomineralization processes and the problem of the vital effect. In: Biomineralization, Dove, P.M., Weiner, S., De Yoreo, J.J., (Eds.). Mineralogical Society of America, Washington, D.C., pp. 1-31.

Young, J.R., Henriksen, K., 2003. Biomineralization within vesicles: The calcite of coccoliths. In: Biomineralization, Dove, P.M., Weiner, S., De Yoreo, J.J., (Eds.). Mineralogical Society of America, Washington, D.C., pp. 189-215.

Zeebe, R.E., Sanyal, A., 2002. Comparison of two potential strategies of planktonic foraminifera for house building: Mg^{2+} or H^{+} removal? *Geochimica et Cosmochimica Acta* 66, 1159 –1169.

Zeebe, R.E., Wolf-Gladrow, D., 2001. CO_2 in seawater: Equilibrium, kinetics and isotopes. Elsevier Oceanographic Series (Elsevier, Amsterdam).

Zonneveld, K.A.F., Mackensen, A., Baumann, K.-H., 2007. Stable oxygen isotopes of *Thoracosphaera heimii* (Dinophyceae) in relationship to temperature; a culture experiment. *Marine Micropaleontology* 64, 80-90.

CHAPTER 5
INTRODUCTION: MG/CA AND SR/CA PROXIES

5.1. Mg/Ca and Sr/Ca ratios of modern seawater

The Mg/Ca ratio of modern seawater (5.2 mmol/mol) is constant with water depth and shows no ocean to ocean fractionation (Broecker & Peng, 1982). Both Mg (~10 Ma) and Ca (~1 Ma) have relatively long residence times in seawater (Broecker & Peng, 1982). Therefore, on short time scales, i.e. less than one million years, Mg and Ca concentrations of seawater remain stable and paleotemperature equations are not affected by changes in the Mg/Ca ratio of seawater.

The Sr/Ca ratio of modern seawater is 8 mmol/mol (Coggon *et al.*, 2010) and only varies by 2-3% (e.g. de Villiers, 1999). The residence time of strontium in seawater is several million years. The strontium concentration rises somewhat with depth due to the action of acantharians. These organisms precipitate strontium sulphate skeletons, slightly depleting the surface waters of strontium. As these free floating organisms die and settle to the bottom, the deeper waters become enriched in strontium as the skeletons dissolve (de Villiers, 1999).

5.2. Foraminifera

5.2.1. Foraminiferal Mg/Ca

The incorporation of magnesium (Mg) into foraminiferal calcite is temperature dependent: as the substitution of Mg into calcite is an endothermic reaction, the Mg/Ca ratio of foraminiferal calcite is expected to increase with increasing temperature (Rosenthal *et al.*, 1997). At present, the Mg/Ca-temperature calibrations are expressed as an exponential dependence: Mg/Ca (mmol/mol) = $B.e^{AT}$, where A and B are the exponential and pre-exponential constants, respectively, and T is temperature in °C (Rosenthal & Linsley, 2007).

During the last few decades, several Mg/Ca-temperature calibrations have been published for different planktonic foraminifera species, based on culture experiments (Nürnberg *et al.*, 1996 [*Globigerinoides sacculifer*]; Lea *et al.*, 1999 [*Orbulina universa*, *Globigerina bulloides*]; Mashiotta *et al.*, 1999 [*G. bulloides*]; Russell *et al.*, 2004 [*O. universa*]; Langen *et al.*, 2005 [*Neogloboquadrina pachyderma*]), sediment trap time-series (Anand *et al.*, 2003 [multiple

species]) and core-top studies (Elderfield & Ganssen, 2000; Rosenthal & Lohmann, 2002 [multiple species]) (See Fig. 5.1 for the calibration of *G. bulloides* and *G. sacculifer*).

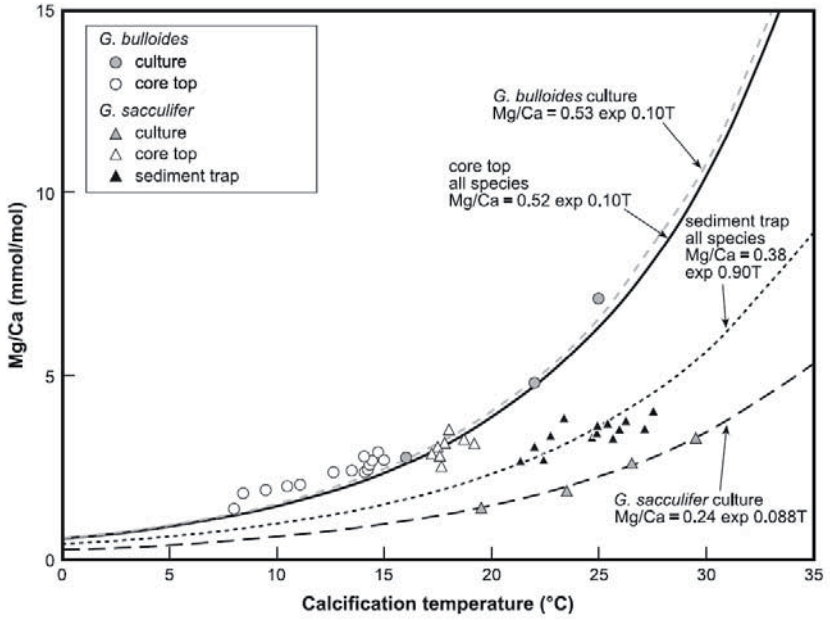

Fig. 5.1 - Relationship between Mg/Ca and calcification temperature determined for two species of planktonic foraminifera (*Globigerina bulloides* and *Globigerinoides sacculifer*) recovered from core-tops, culture experiments and sediment traps. From James & Austin (2008); with data from Elderfield & Ganssen (2000), Anand *et al.* (2003), Lea *et al.* (1999) and Nürnberg *et al.* (1996)

Although planktonic foraminiferal Mg/Ca paleothermometry has become a widely applied tool to reconstruct past sea surface temperatures, it also has been proven that the incorporation of Mg in foraminiferal calcite is controlled by non-temperature effects, biological processes and post-depositional diagenetic alteration.

In foraminiferal culture studies it has been demonstrated that the influence of salinity on planktonic foraminiferal Mg/Ca is rather weak under normal marine conditions, simulated in culture experiments (Nürnberg *et al.*, 1996; Lea *et al.*, 1999; Kisakurek *et al.*, 2008). According to Dueñas-Bohórquez *et al.* (2009), salinity is, after temperature, the second most important control on foraminiferal Mg incorporation, although this effect is still regarded as minor by the authors. Only in a high-salinity setting, e.g. the evaporative Mediterranean Sea Basin, will a salinity effect (possibly in reaction with diagenesis) result in unusually high foraminiferal Mg/Ca values compared to those expected from previous temperature calibrations based on culture experiments (Ferguson *et al.*, 2008).

However, it remains unclear whether salinity itself influences foraminiferal incorporation of Mg or whether it is due to changes in the carbonate chemistry of the seawater/culture medium, associated with changes in salinity: increasing salinity causes total alkalinity (TALK), dissolved inorganic carbon (DIC) and carbonate ion concentration [CO_3^{2-}] of the seawater to increase as well (Dueñas-Bohórquez *et al.*, 2009). It has been noted that the [CO_3^{2-}] of seawater can have an effect on planktonic foraminiferal Mg/Ca ratios (Russel *et al.*, 2004; Mortyn *et al.*, 2005; Kisakurek *et*

al., 2008). Also pH can have an effect on foraminiferal Mg/Ca as was demonstrated in the culture experiments of Lea *et al.* (1999) and Russell *et al.* (2004).

Core top studies along bathymetric transects indicate a systematic decrease in Mg/Ca ratios of planktonic foraminifera with increasing depth, independent of the overlying sea surface temperatures. It was therefore suggested that foraminiferal Mg/Ca is altered by post-depositional dissolution on the seafloor driven by the depth-dependent decrease in carbonate saturation levels (Rosenthal *et al.*, 2000; Dekens *et al.*, 2002).

Inorganic Mg-rich ferromanganese coatings, deposited during diagenesis, have been observed in many foraminiferal studies (e.g. Boyle, 1983; Barker *et al.*, 2003). Ferguson *et al.*, (2008) observed a thin coating (a few μm thick) of high-Mg inorganic calcite on the inside wall of foraminifera. Also Boussetta *et al.* (2011) observed aggregates of rhombohedral crystals that could be interpreted as secondary calcite overgrowths on the foraminifera tests. X-ray diffraction showed that these overgrowths consist of Mg-calcite, thus demonstrating that diagenesis can account for anomalously high foraminiferal Mg/Ca values. Also adsorbed clay particles might contaminate the foraminiferal Mg/Ca ratios (e.g. Boyle, 1983; Barker *et al.*, 2003; Boussetta *et al.*, 2011), since clay contains on average between 1 and 10 weight% Mg (Deer *et al.*, 1992).

5.2.2. Foraminiferal Sr/Ca

Although less pronounced than foraminiferal Mg, the incorporation of Sr into foraminiferal calcite may also show a temperature dependence (Lea *et al.*, 1999; Reichart *et al.*, 2003; Mortyn *et al.*, 2005). A small salinity effect on Sr/Ca has been reported for *O. universa* (Lea *et al.*, 1999). According to Dueñas-Bohórquez *et al.* (2009) however, salinity has no significant influence on the Sr/Ca of *G. sacculifer*. As already mentioned above, a change in salinity results in changing carbonate parameters such as $[CO_3^{2-}]$ (Dueñas-Bohórquez *et al.*, 2009). Similar to Mg/Ca, $[CO_3^{2-}]$ was found to have a positive effect on planktonic foraminiferal Sr/Ca ratios (e.g. Lea *et al.*, 1999; Russell *et al.*, 2004; Mortyn *et al.*, 2005; Kisakurek *et al.*, 2008). When $[CO_3^{2-}]$ of the seawater changes, the carbonate saturation state (Ω) of the seawater also changes, since $\Omega = [Ca^{2+}]*[CO_3^{2-}] / K_{sp}$ (where K_{sp} represents the solubility product at the in situ conditions of temperature, salinity and pressure (Zeebe & Wolf-Gladrow, 2005)). Ω might control the rate of calcite precipitation, which in turn is known to influence trace metal incorporation (Lorens, 1981; Nehrke *et al.*, 2007). Based on culture experiments, Dueñas-Bohórquez *et al.* (2009) therefore suggested that Ω is, after temperature, the main control on foraminiferal Sr incorporation, in contrast to foraminiferal Mg incorporation, where salinity supposedly is the second most dominant control.

5.3. Coccolithophores

5.3.1. Coccolithophorid Sr/Ca

In contrast to foraminifera, the most promising coccolithophorid elemental proxy is Sr/Ca. Stoll & Schrag (2000) were the first to observe that Sr/Ca ratios of core top samples from the equatorial Pacific vary by 15% across the equatorial upwelling zone: Sr/Ca ratios are highest at the equator and decrease towards the poles. They also observed that these variations in coccolithophore Sr/Ca are similar to variations in primary productivity, variations in the $CaCO_3$ rain rate in deep sediment traps and variations in alkenone-based growth rates of coccolithophores in overlying surface waters. Also in culture experiments, Sr/Ca ratios of several coccolithophore species were linked to changes in growth and calcification rates (e.g. Rickaby *et al.*, 2002; Stoll *et al.*, 2002a, b). And although culture experiments also revealed a possible temperature-dependent Sr/Ca partitioning in coccolith calcite (Stoll *et al.*, 2002a, b), the orignial suggestion of Stoll & Schrag (2000), to use coccolith Sr/Ca as a tool for investigating past changes in coccolithophorid productivity, still stands. As such, in several studies, the Sr/Ca ratio of coccolithophore calcite was used as a proxy for past coccolithophore productivity (e.g. Stoll & Schrag, 2001; Billups *et al.*, 2004; Langer *et al.*, 2006).

5.3.2. Coccolithophorid Mg/Ca

Stoll *et al.* (2001) measured Mg/Ca ratios of coccoliths from several cultured coccolithophore species. They suggested that temperature may be an important control on Mg incorporation in coccolithophorid calcite. However, the authors also stated that the potential advantages of a coccolith Mg/Ca paleotemperature proxy may be complicated by cleaning issues, since, compared to foraminifera, coccoliths are much smaller and have a much lower Mg content. More recently, Ra *et al.* (2010) found a species-specific temperature dependence of the Mg/Ca ratios in two cultured coccolithophore species (*Emiliania huxleyi* and *Gephyrocapsa oceanica*). According to the authors however, a difference in absolute Mg/Ca ratios of the two species could complicate the use of coccolithophorid Mg/Ca as a paleothermometer.

5.4. *Thoracosphaera heimii*

So far, only one study has been carried out on the elemental composition of *Thoracosphaera heimii* shells: the culture experiment by Gussone *et al.* (2010).

In the culture experiments of Gussone *et al.* (2010) the Sr/Ca ratios of *T. heimii* shells range between 2.16 and 2.40 mmol/mol. These values are higher than those of planktonic foraminifera (1.2-1.4 mmol/mol; Elderfield *et al.*, 1996) but are similar to those of coccolithophores (1.9-3.2 mmol/mol; Stoll *et al.*, 2002a,b). Furthermore, the Sr/Ca ratios of cultured *T. heimii* shells show a significant correlation with temperature: Sr/Ca (mmol/mol) = 1.95±0.05 + (0.016±0.02)*T (°C) with $R^2 = 0.88$ (Fig. 5.2; Gussone *et al.*, 2010).

Mg/Ca ratios of cultured *T. heimii* shells reveal a relatively large variability: between 2.6 and 7.3 mmol/mol. These values are exceeding those of *Emiliana huxleyi* by one order of magnitude and are within the range of planktonic foraminifera (1-10 mmol/mol; Elderfield *et al.*, 1996). Except for the strong Mg enrichment at the highest temperature (30°C), Gussone *et al.* (2010) found no temperature dependence of the Mg/Ca ratio of cultured *T. heimii* shells (Fig. 5.2). This relatively high Mg concentration at 30°C corresponds to reduced Sr/Ca values and relatively low cyst yields. This is interpreted by Gussone *et al.* (2010) as possibly anomalous growing behaviour of *T. heimii* at high temperatures.

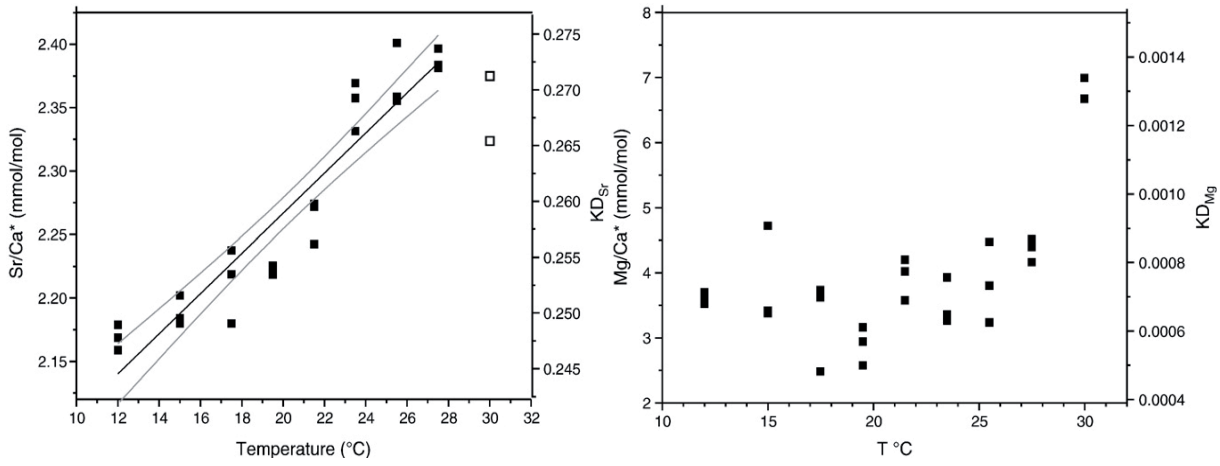

Fig. 5.2 – Left: temperature dependent KD_{Sr} and Sr/Ca ratios of cultured *T. heimii* shells (Gussone *et al.*, 2010) – Right: KD_{Mg} and Mg/Ca ratios of cultured *T. heimii* shells as a function of temperature (Gussone *et al.*, 2010)

References Chapter 5

Anand, P., Elderfield, H., Conte, M. H., 2003. Calibration of Mg/Ca thermometry in planktonic foraminifera from a sediment trap time series. *Paleoceanography* 18, 1050, doi:10.1029/2002PA000846.

Barker, S., Greaves, M., Elderfield, H., 2003. A study of cleaning procedures used for foraminiferal Mg/Ca paleothermometry. *Geochemistry, Geophysics, Geosystems* 4 (9), 8407, doi:10.1029/2003GC000559.

Billups, K., Rickaby, R.E.M., Schrag, D.P., 2004. Cenozoic pelagic Sr/Ca records: Exploring a link to paleoproductivity. *Paleoceanography* 19, doi:1029/2004PA001011.

Boussetta, S., Bassinot, F., Sabbatini, A., Caillon, N., Nouet, J., Kallel, N., Rebaubier, H., Klinkhammer, G., Labeyrie, L., 2011. Diagenetic Mg-rich calcite in Mediterranean sediments: quantification and impact on foraminiferal Mg/Ca thermometry. *Marine Geology* 280, 195-204.

Boyle, E.A., 1983. Manganese carbonate overgrowths on foraminiferal tests. *Geochimica et Cosmochimica Acta* 47, 1815-1819.

Broecker, W.S., Peng, T.H. 1982. Tracers in the Sea, Eldigio, Palisades, N.Y. 690 pp.

Coggon, R.M., Teagle, D.A.H., Smith-Duque, C.E., Alt, J.C., Cooper, M.J., 2010. Reconstructing past seawater Mg/Ca and Sr/Ca from mid-ocean ridge flank calcium carbonate veins. *Science* 327, 1114-117.

Deer, W.A., Howie, R.A., Zussman, J., 1992. An introduction to the rock forming minerals, 2nd ed. Addison-Wesley-Longman, Reading, Mass.

Dekens, P.S., Lea, D.W., Pak, D.K., Spero, H.J., 2002. Core Top Calibration of Mg/Ca in Tropical Foraminifera: Refining Paleo-temperature Estimation. *Geochemistry, Geophysics, Geosystems* 3 (4), 10.1029/2001GC000200.

de Villiers, S., 1999. Seawater strontium and Sr/Ca variability in the Atlantic and Pacific oceans. *Earth and Planetary Science Letters* 171, 623-634.

Dueñas-Bohórquez, A., da Rocha, R.E., Kuroyanagi, A., Bijma, J., Reichart, G.-J., 2009. Effect of salinity and seawater calcite saturation state on Mg and Sr incorporation in cultured planktonic foraminifera. *Marine Micropaleontology* 73, 178-189.

Elderfield, H., Ganssen, G., 2000. Past temperature and $\delta^{18}O$ of surface ocean waters inferred from foraminiferal Mg/Ca ratios. *Nature* 405, 442-445.

Elderfield, H., Bertram, C.J., Erez, J., 1996. A biomineralization model for the incorporation of trace elements into foraminiferal calcium carbonate. *Earth and Planetary Science Letters* 142, 409–423.

Ferguson, J.E., Henderson, G.M., Kucera, M., Rickaby, R.E.M., 2008. Systematic change of foraminiferal Mg/Ca ratios across a strong salinity gradient. *Earth and Planetary Science Letters* 265, 153-166.

Gussone, N., Zonneveld, K.A.F. & Kuhnert, H. 2010. Minor element and Ca isotope composition of calcareous dinoflagellate cysts of cultured *Thoracosphaera heimii*. *Earth and Planetary Science Letters* 289, 180-188.

James, R.H., Austin, W.E.N., 2008. Biogeochemical controls on palaeoceanographic environmental proxies: a review. Geological Society, London, Special Publications 303, pp. 3-32, doi: 10.1144/SP303.2.

Kisakürek, B., Eisenhauer, A., Böhm, F., Garbe-Schönberg, D., Erez, J., 2008. Controls on shell Mg/Ca and Sr/Ca in cultured planktonic foraminiferan, *Globigerinoides ruber* (white). *Earth and Planetary Science Letters* 273, 260-269.

Langen, P.J.v., Pak, D.K., Spero, H.J., Lea, D.W., 2005. Effects of temperature on Mg/Ca in neogloboquadrinid shells determined by live culturing. Geochemistry, Geophysics, Geosystems 6, (doi:10.1029/2005GC000989).

Langer, G., Gussone, N., Nehrke, G., Riebesell, U., Eisenhauer, A., Kuhnert, H., Rost, B., Trimborn, S., Thoms, S., 2006. Coccolith strontium to calcium ratios in *Emiliana huxleyi*: the dependence on seawater strontium and calcium concentrations. *Limnology and Oceanography* 51 (1), 310-320.

Lea, D.W., Mashiotta, T.A., Spero, H.J., 1999. Controls on magnesium and strontium uptake in planktonic foraminifera determined by live culturing. *Geochimica et Cosmochimica Acta* 63, 2369-2379.

Lorens, R., 1981. Sr, Cd, Mn and Co distribution coefficients in calcite as a function of calcite precipitation rate. *Geochimica et Cosmochimica Acta* 45, 553-561.

Mashiotta, T.A., Lea, D.W., Spero, H.J., 1999. Glacial-interglacial changes in Subantarctic sea surface temperature and δ^{18}O-water using foraminiferal Mg. *Earth and Planetary Science Letters* 170, 417-432.

Mortyn, P.G., Elderfield, H., Anand, P., Greaves, M., 2005. An evaluation of controls on planktonic foraminiferal Sr/Ca: comparison of water column and core-top data from a North Atlantic transect. *Geochemistry, Geophysics, Geosystems* 6 (12), Q12007, doi:10.1029/2005GC001047.

Nehrke, G., Reichart, G.J., van Cappellen, P., Meile, C., Bijma, J., 2007. Dependence of calcite growth rate and Sr partitioning on solution stoichiometry: non-Kossel crystal growth. *Geochimica et Cosmochimica Acta* 71 (9), 2240-2249.

Nürnberg, D., Bijma, J., Hemleben, C., 1996. Assessing the reliability of magnesium in foraminiferal calcite as a proxy for water mass temperatures. *Geochimica et Cosmichimica Acta* 60, 803-814.

Ra, K., Kitagawa, H., Shiraiwa, Y., 2010. Mg isotopes and Mg/Ca values of coccoliths from cultured specimens of the species *Emiliania huxleyi* and *Gephyrocapsa oceanica*. *Marine Micropaleontology* 77, 119-124.

Reichart, G., Jorissen, F., Anschutz, P., Mason, P., 2003. Single foraminifera test chemistry records the marine environment. *Geology* 31 (4), 355-358.

Rickaby, R.E.M., Schrag, D.P., Zondervan, I., Riebesell, U., 2002. Growth rate dependence of Sr incorporation during calcification of *Emiliana huxleyi*. *Global Biochemical Cycles* 16, doi:1029/2001GB001408.

Rosenthal, Y., Lohmann, G.P., 2002. Accurate estimation of sea surface temperatures using dissolution-corrected calibration for Mg/Ca paleothermometry. *Paleoceanography* 17, doi: 10.1029/2001PA000749.

Rosenthal, Y., Linsley, B., 2007. Paleoceanography, physical and chemical proxies. Mg/Ca and Sr/Ca paleothermometry. In: Elias, S.A. (Ed.), Encyclopedia of Quaternary Science, Royal Holloway, University of London, U.K., pp. 1723-1731.

Rosenthal, Y., Boyle, E.A., Slowey, N., 1997. Environmental controls on the incorporation of Mg, Sr, F and Cd into benthic foraminiferal shells from Little Bahama Bank: prospects for thermocline paleoceanography. *Geochimica et Cosmochimica Acta* 61, 3633-3643.

Rosenthal, Y., Lohmann, G.P., Lohmann, K.C., Sherrell, R.M., 2000. Incorporation and preservation of Mg in *Globigerinoides sacculifer*: implications for reconstructing O-18/O-16 of seawater. *Paleoceanography* 15, 135–145.

Russell, A.D., Hönisch, B., Spero, H., Lea, D.W., 2004. Effects of seawater carbonate ion concentration and temperature on shell U, Mg and Sr in cultured planktonic foraminifera. *Geochimica et Cosmochimica Acta* 68, 4347-4361.

Stoll, H.M., Schrag, D.P., 2000. Coccolith Sr/Ca as a new indicator of coccolithophorid calcification and growth rate. *Geochemistry, Geophysics, Geosystems* 1, 1-24.

Stoll, H.M., Schrag, D.P., 2001. Sr/Ca variations in Cretaceous carbonates: relation to productivity and sea level changes. *Palaeogeography, Palaeoclimatology, Palaeoecology* 168, 311–336.

Stoll, H.M., Encinar, J.R., Alonso, J.I.G., Rosenthal, Y., Probert, I. & Klaas, C. 2001. A first look at paleotemperature prospects from Mg in coccoliths carbonate: cleaning techniques and culture measurements. *Geochemistry, Geophysics, Geosystems* 2, 2000GC000144.

Stoll, H.M., Klaas, C.M., Probert, I., Encinar, J.R., Garcia Alonso, J.I., 2002a. Calcification rate and temperature effects on Sr partitioning in coccoliths of multiple species of coccolithophorids in culture. *Global and Planetary Change* 34, 153-171.

Stoll, H.M., Ziveri, P., Geisen, M., Probert, I., Young, Y.R., 2002b. Potential and limitations of Sr/Ca ratios in coccolith carbonate: new perspectives from cultures and monospecific samples from sediments. Philos. Trans. R. Soc. Lond. A 360, 719-747.

Zeebe, R.E., Wolf-Gladrow, D., 2005. CO_2 in seawater: equilibrium, kinetics, isotopes. Elsevier Oceanography Series 65, The Netherlands, 346 pp.

CHAPTER 6
MATERIAL AND METHODS

The different methods used in this thesis are described more into detail in Chapters 7, 8 and 9. However, the density-and-size-based method to isolate *Thoracosphaera heimii* shells from sediments, described by Zonneveld (2004), was only cited from literature and will therefore be described in the following section.

Since a single *Thoracosphaera heimii* shell weighs on average 1 ng, one mass spectrometry measurement requires $3x10^4$ individual *T. heimii* shells (Zonneveld, 2004). In contrast to tests of foraminifera, picking of *T. heimii* shells is practically impossible and would be largely time consuming. In order to overcome this problem, Zonneveld (2004) developed a qualitative method to isolate *T. heimii* shells from the sediment, based on particle size and density.

About 1-2 g of dry sediment is dissolved in tap water and homogenized ultrasonically. Since *T. heimii* shells are generally in the size range of 10-20 μm, the dissolved sample is sieved twice through a 20 μm precision sieve to remove particles bigger than *T. heimii*; and through a 10 μm precision sieve to remove particles smaller than *T. heimii*. The fraction between 10 and 20 μm is poured into a large beaker glass and diluted to 1600 ml. Eight 500 ml beaker glasses are each filled with 300 ml tap water and 200 ml of the diluted sample from the large beaker glass. The beaker glasses are left to settle for 10 min. Then, the upper 400 ml of the mixture is carefully discarded using a water jet pump. This step removes particles with a lower sinking rate than the *T. heimii* shells, i.e. particles with a lesser density and non-sperical particles. The residual 100 ml from every 500 ml beaker is collected into the larger beaker glass, diluted to 1600 ml again, and the settling procedure is repeated, at least three times. After every settling step, the sample is checked under a polarized light microscope with a gypsum plate to detect other calcareous particles. Settling is repeated until the sample contains less than 15% calcareous particles other than *T. heimii*. To remove heavier particles than *T. heimii* shells, a decanting step can be applied. However, this was not necessary in the present study. When the sample is pure enough, the sample is filtered through a polycarbonate filter and the filter is oven-dried for 24h at 60°C.

Zonneveld, K., 2004. Potential use of stable isotope composition of *Thoracosphaera heimii* (Dinophyceae) for upper water column (thermocline) temperature reconstruction. *Marine Micropaleontology* 50 (3-4), 307-317.

CHAPTER 7 – MANUSCRIPT 1

Correlation between temperature and the $\delta^{18}O$ composition of *Thoracosphaera heimii* shells in core top sediments from the Indian and Atlantic Ocean

Stefanie P.M. Dekeyzer [a]* & Karin A.F. Zonneveld [a,b]

[a] Universität Bremen, FB 5 – Geowissenschaften, Postfach 330 440, D-28334 Bremen, Germany
[b] MARUM, Universität Bremen, Postfach 330 440, D-28334 Bremen, Germany

*Corresponding author.

E-mail address: stefanie.dekeyzer@uni-bremen.de
Phone: +49 (0) 421 218 65138
Fax: +49 421 218 65159

- Under revision for publication in *Marine Micropaleontology* -

Abstract

Within the present study, we examined the correlation between temperature and the stable oxygen isotope composition ($\delta^{18}O$) of *Thoracosphaera heimii* shells in 57 surface sediment samples from the western Indian Ocean offshore Tanzania, and the equatorial and South Atlantic Ocean. Isotopic temperatures were reconstructed using paleotemperature equations for cultured *T. heimii* and for inorganic calcite, and were compared to natural seawater temperatures. Furthermore, the $\delta^{18}O$ values of the *T. heimii* shells from surface sediments were plotted against sea surface temperatures, temperatures at mixed layer depth and temperature values averaged over 200m water depth. No temperature – $\delta^{18}O$ correlation could be observed for the Indian Ocean samples, possibly due to environmental influences, such as river input. We also observed that for the Atlantic Ocean samples the temperature – $\delta^{18}O$ correlation slightly improves when temperatures at mixed layer depth, the presumed living depth of *T. heimii*, are considered. This supports the suggestion from previous studies that the $\delta^{18}O$ composition of *T. heimii* shells has potential to reconstruct paleotemperatures of a specific depth in the water column, notably the mixed layer depth.

Keywords: calcareous dinoflagellate, *Thoracosphaera heimii*, stable oxygen isotopes, temperature, Indian Ocean, Atlantic Ocean

7.1. Introduction

Today there is a worldwide debate on future climate change. Climate models form a central part in this debate as they have become a practical tool to assess future climate conditions. It has become clear that in order to establish reliable predictions, the water column has to be divided into several artificial layers. Within these model studies, the most important layer is the surface layer which extends from the sea surface until roughly 100m water depth. This layer could be divided more into detail in the upper mixed layer and the lower thermocline. However, climate modellers only very recently started to show interest in the mixed layer depth as a separate layer in the artificial surface layer (e.g. Yeh *et al.*, 2009). A mixed layer depth climatology is necessary in understanding the climatic system and is of primary importance for ocean modellers in validating and improving mixed layer parameterizations and Ocean General Circulation Models (de Boyer Montegut *et al.*, 2004; with all references therein). It is therefore essential to build up an extensive data set, based on water samples and surface sediment samples, with detailed information about the environmental conditions, and especially temperature conditions, of this mixed layer.

Today, the reconstruction of past climates is predominantly based on the use of stable oxygen isotopes and minor element to calcium ratios of organisms which form calcareous remains. In particular the stable oxygen isotope ($\delta^{18}O$) composition of fossil planktonic foraminiferal carbonate has been used for this purpose and has proven to be a very useful tool in paleotemperature reconstructions (e.g. Fischer & Wefer, 1999). Unfortunately, it is not always possible to reconstruct conditions of one specific water depth using foraminifera since several species migrate through the water column (i.e. through different water masses) so that calcification occurs at different water depths. Additionally, some species contain photosynthetic symbionts and other species have seasonal shell production, which also influences the $\delta^{18}O$ composition of the foraminiferal shell calcite and hampers detailed paleotemperature reconstructions (e.g. Spero, 1992; Spero & Lea, 1993, 1996; Bemis *et al.*, 1998; Bijma *et al.*, 1999).

To overcome issues involving the heterotrophic lifestyle of foraminifera, phytoplankton has received increasing interest and has become a succesful tool in paleoclimatic research. For instance, coccolithophores can overcome some of the problems observed for foraminifers: they are primary producers, so they don't contain photosynthetic symbionts. Furthermore, distinct coccolithophore species assemblages prefer to live in certain water depth ranges within the photic zone (e.g. Winter *et al.*, 2002; Boeckel & Baumann, 2008) so that the oxygen isotopic composition of these species will not be altered by vertical migration through the water column. However, for coccolithophores, problems in obtaining monospecific coccolith samples exist.

Another phytoplankton group that recently gained more interest in paleoclimatic studies are the calcareous dinoflagellates and especially the species *Thoracosphaera heimii*. *T. heimii* dominates the calcareous dinoflagellate assemblage in (sub)tropical waters and can relatively easily be isolated from sediments (Zonneveld, 2004). Due to its wide geographic and stratigraphic distribution in sediments, a rather high resistance against calcite dissolution in comparison to other calcareous organisms and a year-round shell production, the $CaCO_3$ vegetative cysts (shells) of *T. heimii* are useful as a proxy archive recording ocean surface conditions e.g. temperature and pH (Karwath, 2000; Karwath *et al.*, 2000; Zonneveld, 2004; Kohn *et al.*, 2011). The most appealing feature of *T. heimii* however, is its living depth, or calcification depth: the depth at which the organism incorporates the isotope signal of the water column into its shell. Kohn & Zonneveld (2010) showed that the presence of full *T. heimii* shells in the water column reflects the living depth of *T. heimii*, since the reproduction cycle of this species is very fast and its motile planktonic forms are able to move vertically over a short distance only (Inouye & Pienaar, 1983). It is now accepted that *T. heimii* thrives in the photic zone with maximal occurences in the upper part and immediately above the deep chlorophyll maximum (DCM) (e.g. Kohn & Zonneveld, 2010). The $\delta^{18}O$ composition of *T. heimii* can therefore be used to reconstruct species-specific temperatures at the depth of the DCM (Zonneveld, 2004).

In comparison to the extensive knowledge available about the $\delta^{18}O$ composition of *T. heimii* in the equatorial and South Atlantic Ocean, no information is available about the western equatorial Indian Ocean. For the present study, *T. heimii* shells were isolated from surface sediment samples offshore Tanzania, and analyzed on their $\delta^{18}O$ composition. We extended the Indian Ocean data set with additional surface sediment samples and published $\delta^{18}O$ data of *T. heimii* shells from surface sediment samples from the equatorial and South Atlantic Ocean (Zonneveld, 2004). Isotopic temperatures were reconstructed using the species-specific paleotemperature equation for *T. heimii* (Zonneveld *et al.*, 2007) and the paleotemperature equation for inorganic calcite (Kim & O'Neil, 1997), and were compared to natural seawater temperatures at different depths in the water column. In addition, the $\delta^{18}O$ values of the *T. heimii* shells from surface sediments were plotted against sea surface temperatures, temperatures at mixed layer depth and temperature values averaged over 200m water depth. Our results will be discussed in terms of instrumental, environmental and biological influences.

7.2. Oceanographic setting

The East African Indian Ocean is influenced by a strong monsoonal system with two distinct monsoon seasons (Fig. 7.1b). The NE monsoon occurs during boreal winter (from November through March) and is characterized by a high-pressure cell over the Tibetan plateaus in central Asia and a low-pressure cell over the Indian Ocean, resulting in northeastern tradewinds across the northern Indian Ocean (Woodberry *et al.*, 1989). During boreal summer (from May through September), the SW monsoon is characterized by a high-pressure cell over the Indian Ocean and Madagascar and a low-pressure cell over the Tibetan plateaus, resulting in an intensification of the southeastern tradewinds of the southern hemisphere. These SE trades blow across the equator, are redirected toward the northeast by the African highlands, and form a strong atmospheric NE blowing jet, often called the Findlater jet (Newell, 1959; Findlater, 1971; Woodberry *et al.*, 1989). During monsoon transitions, around April-May and October-November, wind directions change and short-lived but intense Eastward Equatorial Jets (EEJ) develop (Hastenrath & Greischar, 1991). Meteorologically, the SW monsoon is characterized by high cloud cover, rainfall, river discharge, terrestrial runoff and wind energy, and low solar insolation and temperatures. Oceanographically, the SW monsoon is characterized by cool surface water, a deep thermocline, high water mixing and wave energy, low salinity and high phosphorus. Reversed parameters are observed during the NE monsoon (e.g. McClanahan, 1988).

This monsoonal system and the development of a low level jet also has an effect on the position of the Intertropical Convergence Zone (ITCZ), the area where trade winds from the northern and southern hemisphere meet. During the NE monsoon, the development of the northeastern tradewinds shifts the position of the ITCZ to the south. Whereas during the SW monsoon, the position of the ITCZ is shifted to the north due to the development of the southeastern tradewinds and the NE blowing Findlater jet.

The surface circulation in the study area (Fig. 7.1b) is part of the giant clockwise Indian Ocean Gyre. At the northern tip of Madagascar, the westward flowing South Equatorial Current (SEC) splits into the northward flowing East African Coastal Current (EACC) and the southward flowing Mozambique Current (MC), which continues in the more southern Agulhas current (e.g. Swallow *et al.*, 1991). At the location of the sample sites the surface circulation is dominated by the EACC. Throughout the year the position of the EACC is situated between latitudes 11°S and 3°S and according to Bell (1972) the width of the current is over 160 km. The hydrography of the western Indian Ocean is also strongly influenced by the seasonal reversal of the monsoon trade

winds (e.g. Woodberry *et al.*, 1989; Hastenrath & Greischar, 1991; Lugomela *et al.*, 2001; Schott *et al.*, 2009). During the NE monsoon, the northern part of the EACC meets the southward flowing Somali Current (SC) near 3°S (Schott, 1983; Schott *et al.*, 1988) to form the offshore flowing Equatorial Countercurrent (ECC). This results in the formation of a downwelling area and associated low nutrient waters along Tanzania. During the SW monsoon, the EACC merges into the northward flowing SC and return flow is via the Southwest Monsoon Current coming from the northern hemisphere (e.g. Bell, 1972; Woodberry *et al.*, 1989; Swallow *et al.*, 1991; Schott *et al.*, 2009).

Subsurface waters north of 10°S consist of the Indian Equatorial Water, also called the North Indian High-Salinity Intermediate Water (Wyrtki, 1973). This water mass is formed in the Arabian Sea with some components from the Red Sea and the Persian Gulf. Between 20°S and 40°S, subsurface waters consist of the Indian Central Water. Under this the Antarctic Intermediate Water is positioned. Both the deep and bottom waters are of Atlantic/Antarctic origin.

Along the coast of Tanzania, the Islands of Mafia, Pemba and Zanzibar lay within the path of the EACC, reducing its current velocity, which in turn results in a stable upper water column and low turbulence conditions (Bryceson, 1977). They protect the Pemba Channel, a rather deep (>800 m) graben-like basin between mainland Tanzania and Pemba Island. The upper waters of the Pemba Channel are fed by a large river discharge from the Pangani River, the sediments in the deeper part of this channel predominantly consist of mud or slightly sandy mud. Here pelagic sedimentation only plays a minor role. On the continental slope of Pemba Island and also further south off Mafia Island, the sediment consists of foraminiferal ooze, which indicates a more pelagic sedimentation (Pätzold *et al.*, subm.). Apart from the Pangani River, also the Wami, Rufiji, Mbwemburu and Ruvuma rivers bring large amounts of terrestrial material into the ocean. Previous to Meteor cruise M75-2 heavy rains over southern Tanzania lead to large river input off the Ruvuma River (Pätzold *et al.*, subm.). During Meteor cruise M75-2 a sharply defined plume of suspended sediment, which extended several kilometers offshore, was observed off the Ruvuma River mouth.

The position of the Indian Ocean core top samples is given in Fig. 7.1c; and of the Atlantic Ocean core top samples in Fig. 7.1a. For a detailed description of the oceanographic conditions of the Equatorial and South Atlantic see e.g. Peterson & Stramma (1991) or Wefer *et al.* (1996).

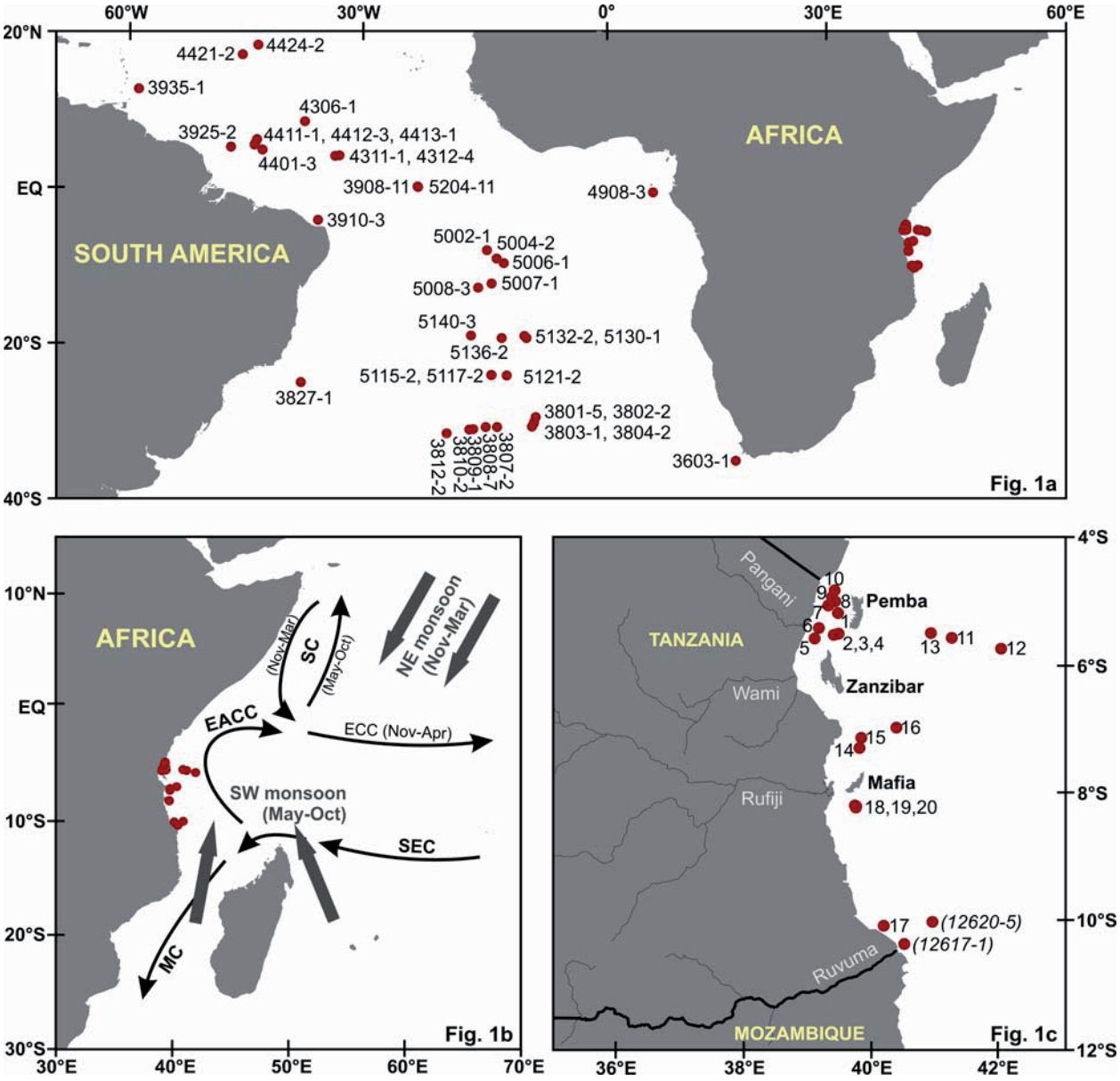

Fig. 7.1 – a) Location of the Atlantic Ocean core tops – b) Oceanography of the western Indian Ocean offshore Tanzania – c) Location of the Indian Ocean core tops (see Table 7.2 for sample numbering; samples GeoB 12617-1 and 12620-5 were excluded from the present study since they contained no *T. heimii* shells)

7.3. Materials and methods

7.3.1. Sample processing and oxygen isotope measurements

To study the isotopic composition of *Thoracosphaera heimii* shells from sediments, 22 core top samples were collected from the western Indian Ocean offshore Tanzania (Fig. 7.1c). Samples were taken by multicorer during Meteor cruise M75-2 between February 7th and 24th 2008 (Pätzold *et al.*, subm.). Samples GeoB 12617-1 and 12620-5 were excluded from the present study since they contained no *Thoracosphaera heimii* shells.

T. heimii was isolated from the upper centimeter of the sediment, starting from 3-4 g of dry sediment, and by using the qualitative density/size based method according to Zonneveld (2004). In summary, within the pre-sieved 10-15 µm fraction, other (calcareous) particles than *T. heimii* can be removed from the sediment by a series of settling and decanting steps. Purification of the samples was tested on a regular basis by polarized light microscope. In general, the calcareous fraction other than *T. heimii* consists of (fragments of) foraminifera, coccoliths, parts of other calcareous dinoflagellate species and parts of larger unidentified calcareous organisms. Percentages of other calcareous particles than *T. heimii* are available for the Indian Ocean core top samples (Table 7.1).

Sample GeoB	% *T. heimii*	% other calcareous dinoflagellates	% foraminifera	% coccolithophores and coccoliths	% unidentified fragments
12601-1	89.69	1.88	2.97	1.25	4.22
12602-3	85.61	2.03	4.95	1.41	6.00
12603-1	84.48	0.99	4.93	1.56	8.05
12604-5	80.65	0.28	3.64	0.91	14.52
12605-2	79.54		15.60	0.33	4.54
12607-1	89.37	0.26	6.69	0.26	3.41
12608-2	94.01		4.13	0.21	1.65
12609-1	88.26	0.44	3.97	0.35	6.97
12611-3	82.79	0.57	15.99		0.65
12612-2	83.21	0.33	16.13	0.16	0.16
12613-2	88.81	1.07	8.26	0.27	1.60
12614-2	93.07		4.47	0.15	2.31
12616-3	94.94	0.42	4.22	0.14	0.28

Table 7.1 – Percentages of *T. heimii* shells, other calcareous dinoflagellates, foraminifera coccolithophores/coccoliths and unidentified calcareous fragments for the Indian Ocean core top samples

Stable oxygen isotopes of *T. heimii* shells were measured at MARUM, Bremen with a Finigan MAT 251 mass spectrometer with an automatic preparation line (Kiel II carbonate device). Standard reproducibility of internal standards is less than 0.07‰ for ^{18}O. Unfortunately, internal variability within each sample cannot be provided, since no replicates were produced. Stable oxygen notations are given in δ values relative to VPDB (Vienna Pee Dee Belemnite). Following Zonneveld (2004), VPDB was converted to VSMOW according to Hut (1987) (eq. 1):

$$\delta^{18}O_{VSMOW} = \delta^{18}O_{VPDB} + 0.27 \qquad \text{(eq. 1)}$$

To expand this dataset, 29 additional core top samples from the equatorial and South Atlantic, taken during previous Meteor cruises (Fig. 7.1a), were treated the same way as described above. In addition, we extended our data set with published $\delta^{18}O$ data of *T. heimii* shells from surface sediment samples from the equatorial and South Atlantic (Zonneveld, 2004) (Table 7.3).

7.3.2. Data collection

To have the whole upper water column represented, environmental parameter data was collected for every 10m between 0 and 200m water depth. These values were separated into two values: a sea surface value (0m) and an average value over 200m water depth. Since the mixed layer depth (MLD) is the depth where highest abundances of *T. heimii* occur (Kohn & Zonneveld, 2010), environmental parameter values were also collected for the MLD.

The annually averaged MLD (m) was derived for every sample location from the Monterey & Levitus (1997) database. This data collection contains monthly MLD fields on a global 1°x1° grid. The MLD fields are computed from climatological monthly mean profiles of potential temperature and potential density based on a temperature change from the ocean surface of 0.5°C. Interpolation of the MLD data for the exact sample locations was done using Ocean Data View (Schlitzer, 2009).

For every sample location, mean annual temperature values (°C) were derived from the World Ocean Atlas 2009 (Locarnini *et al.*, 2010; http://www.nodc.noaa.gov/OC5/WOA09/pr_woa09.html) and interpolated for the sea surface, the mixed layer depth and water depths every 10m between sea surface and 200m with Ocean Data View (Schlitzer, 2009). The 21 water depth values between 0 and 200m were converted into one average temperature value over 200m water depth.

Unfortunately, measured oxygen isotope values of the seawater ($\delta^{18}O_w$) were unavailable for the Indian Ocean sample sites. Therefore $\delta^{18}O_w$ was calculated according to the following two steps. First $\delta^{18}O_w$ and salinity values were taken from the Global Seawater Oxygen-18 Database (Schmidt *et al.*, 1999; http://data.giss.nasa.gov/o18data/). In a 10°x10° square block (2-12°S, 35-45°E) around the Indian Ocean core top samples (blue dots ● in Fig. 7.2), 33 data points of the Global Seawater Oxygen-18 Database were available (red dots ● in Fig. 7.2). Linear regression of these 33 data points yielded the following equation: $\delta^{18}O_w = 0.1075*\text{Salinity} - 3.002$ with $R^2 = 0.79$ (Fig. 7.3b). The dashed lines in Fig. 7.3b show the 95% confidence level. To assess the error of prediction for the regression line, the standard error of the estimate (σ_{est}) was calculated. $\sigma_{est} = \sqrt{(\sum(Y-Y')^2/N)}$, with Y an actual $\delta^{18}O_w$ value, Y' a predicted $\delta^{18}O_w$ value using the regression equation and N the number of pairs of values. For this $\delta^{18}O_w$ – salinity regression equation, σ_{est} = +- 0.32262‰.

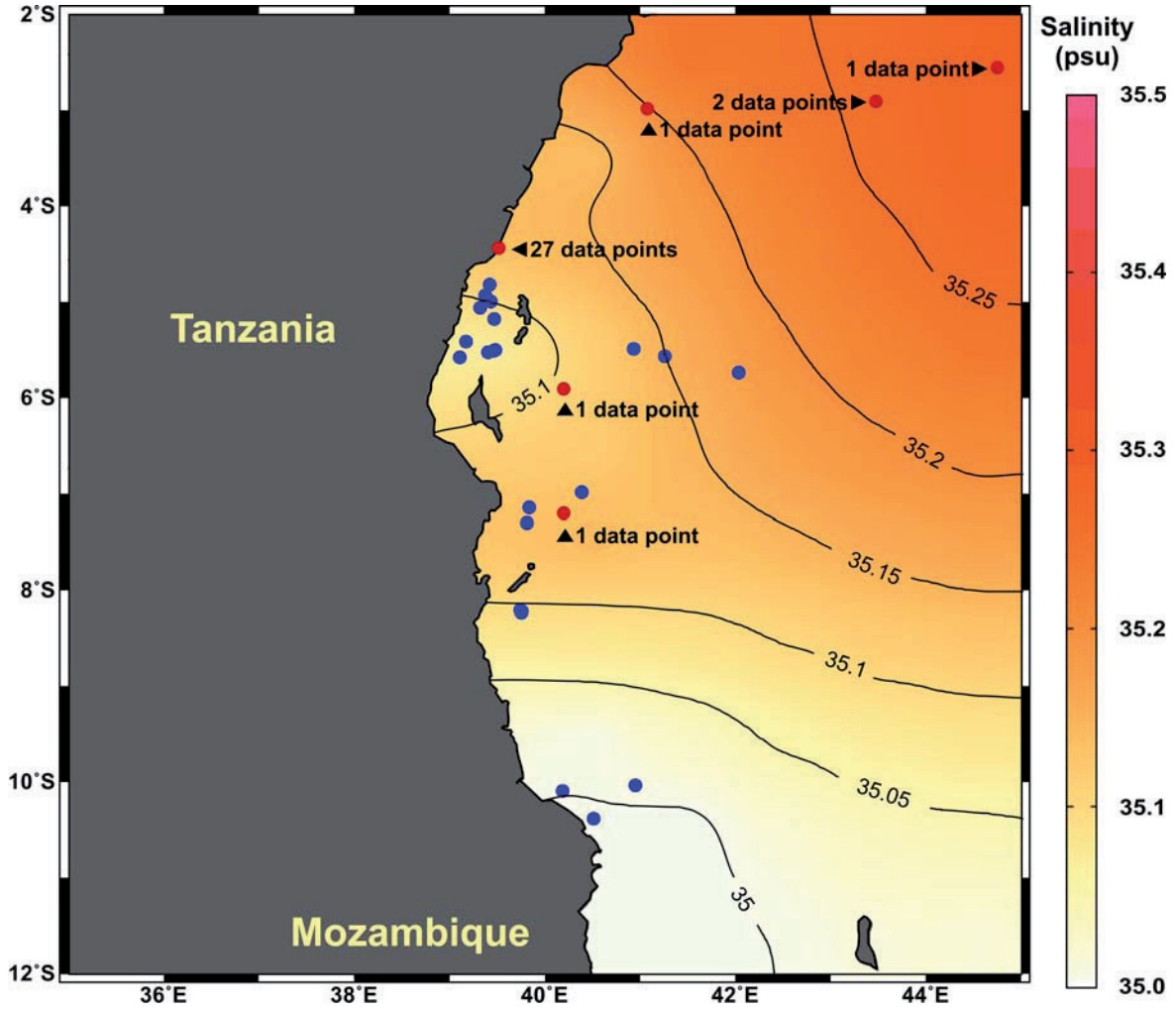

Fig. 7.2 – Visual map of sea surface salinity (World Ocean Atlas 2009) in the western Indian Ocean offshore Tanzania – blue dots ●: core top samples used for the isotopic analysis of *T. heimii* shells – red dots ●: 33 data points from the Global Seawater Oxygen-18 Database used for the establishment of the $\delta^{18}O_w$ -salinity regression equation ($\delta^{18}O_w$ = 0.1075*Salinity - 3.002 with R^2 = 0.789) for the Indian Ocean core top samples

In a second step, mean annual salinity values (psu), interpolated for the sea surface, the mixed layer depth and water depths every 10m between sea surface and 200m with Ocean Data View (Schlitzer, 2009), were derived from the World Ocean Atlas 2009 (Antonov *et al.*, 2010; http://www.nodc.noaa.gov/OC5/WOA09/pr_woa09.html) and plotted into the $\delta^{18}O_w$ – salinity regression equation above to calculate $\delta^{18}O_w$ at sea surface and thermocline depths at every sampling site. A similar calculation was followed for the Atlantic Ocean samples of this study. The aim was to find datapoints of the Global Seawater Oxygen-18 Database in a 10°x10° square block around the core top samples. If this yielded too few datapoints, the grid was expanded. The established $\delta^{18}O_w$ – salinity regression equations used for the different Atlantic Ocean samples are given in Fig. 7.3a. The calculation of $\delta^{18}O_w$ for the additional Atlantic samples is described in Zonneveld (2004).

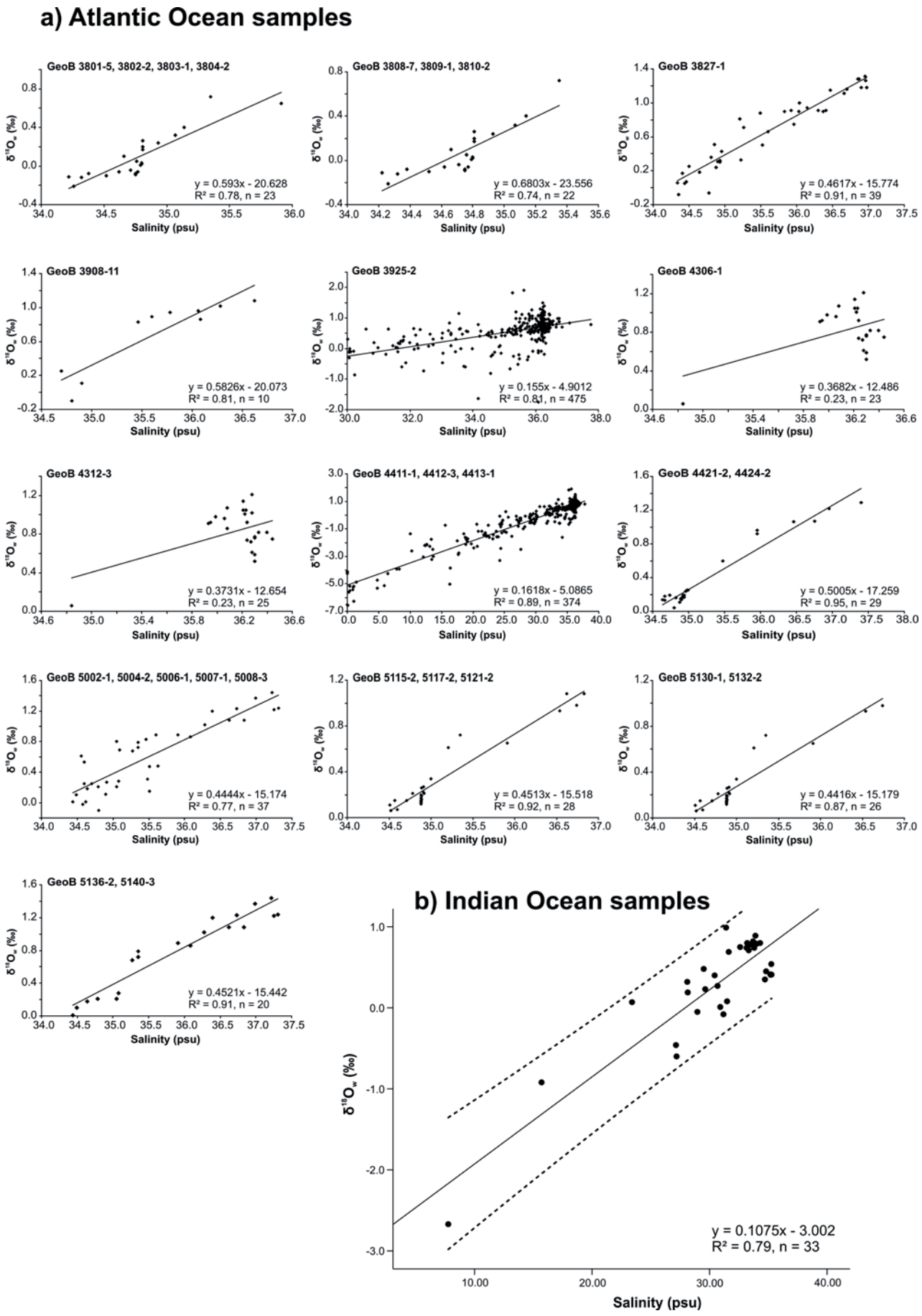

Fig. 7.3 – Correlation between the stable oxygen isotope composition of seawater ($\delta^{18}O_w$, ‰) and salinity (psu) for surface sediment samples in a) the Atlantic Ocean and b) the Indian Ocean. n = the amount of data points taken from the Global Seawater Oxygen-18 Database (Schmidt *et al.*, 1999; http://data.giss.nasa.gov/o18data/)

To investigate the possibility of the carbonate ion effect influencing the $\delta^{18}O$ of *T. heimii*, [CO_3^{2-}] concentrations (µmol/kg) and pH values were obtained from the Goyet *et al.* (2000) database with global alkalinity and total dissolved carbon estimates on a 1°x1° grid. These values were only taken for the mixed layer depth since the mixed layer depth (MLD) is the depth where highest abundances of *T. heimii* occur (Kohn & Zonneveld, 2010).

7.3.3. Calculation of isotopic temperatures

Hypothetical isotopic temperatures were calculated, for the sea surface, the mixed layer depth and a depth averaged over the upper 200m, based on the *T. heimii* oxygen isotope data, the recently published temperature – $\delta^{18}O$ equation for *T. heimii* from culture experiments (Zonneveld *et al.*, 2007) (eq. 2) and the paleotemperature equation for inorganic calcite by (Kim & O'Neil, 1997) (eq. 3)

$$T\ (°C) = -3.906 - 6.827*(\delta^{18}O_c - \delta^{18}O_w),\ R^2 = 0.85 \qquad \text{(eq. 2)}$$

$$T\ (°C) = 16.1 - 4.64*(\delta^{18}O_c - \delta^{18}O_w) + 0.09*(\delta^{18}O_c - \delta^{18}O_w)^2 \qquad \text{(eq. 3)}$$

with $\delta^{18}O_c$ and $\delta^{18}O_w$ being the stable oxygen isotope compositions of *T. heimii* and seawater respectively.

7.3.4. Correlation between temperature and $\delta^{18}O_c$ - $\delta^{18}O_w$ of *T. heimii*

Additionally, we plotted the $\delta^{18}O_c$ - $\delta^{18}O_w$ values of the *T. heimii* shells from the surface sediment samples against sea surface temperature, temperature at mixed layer depth and the temperature averaged over 200m water depth. A linear curve of the form y = a + bx was fitted to the Indian Ocean data set, the Atlantic Ocean data set and the combined data set. As already noted, error bars, representing standard deviations, could not be provided. Therefore, the standard error of the estimate values (σ_{est}) was calculated for each regression equation. The difference between the $\delta^{18}O$ composition of *T. heimii* and the paleotemperature equation for inorganic calcite (Kim & O'Neil, 1997) was also calculated.

Sample GeoB	n° in Fig. 1, 2	Lat (°N)	Lon (°E)	Water depth (m)	MLD (m)	Temperature (°C)			Salinity (psu)			$\delta^{18}O_c$ (‰)[a]		$\delta^{18}O_w$ (‰)[b] (VSMOW)			$\delta^{18}O_c$-$\delta^{18}O_w$ (‰)[c] (VSMOW)			$[CO_3^{2-}]$ (µmol/kg)	pH
						at 0m	at MLD	200m	at 0m	at MLD	200m	(VPDB)	(VSMOW)	at 0m	at MLD	200m	at 0m	at MLD	200m	at MLD	at MLD
12601-1 ♦	1	-5.1735	39.4740	872	42.82	27.24	26.13	20.94	35.18	35.22	35.20	-2.24	-1.97	0.78	0.78	0.78	-2.75	-2.75	-2.75	227.542	8.210
12602-3 ♦	2	-5.4980	39.4852	851	42.41	27.25	26.14	20.95	35.17	35.21	35.20	-1.89	-1.62	0.78	0.78	0.78	-2.40	-2.40	-2.40	226.702	8.207
12603-1 ♦	3	-5.5047	39.4655	825	42.41	27.25	26.14	20.95	35.17	35.21	35.20	-2.09	-1.82	0.78	0.78	0.78	-2.60	-2.60	-2.60	226.682	8.207
12604-5 ♦	4	-5.5187	39.4063	608	42.41	27.25	26.14	20.95	35.17	35.21	35.20	-1.93	-1.66	0.78	0.78	0.78	-2.43	-2.44	-2.44	226.640	8.207
12605-2 ♦	5	-5.5737	39.1073	197	42.41	27.25	26.14	20.96	35.17	35.21	35.20	-1.83	-1.56	0.78	0.78	0.78	-2.33	-2.34	-2.34	226.466	8.208
12606-2 ♦	6	-5.4100	39.1747	355	42.46	27.24	26.14	20.96	35.17	35.21	35.20	-1.89	-1.62	0.78	0.78	0.78	-2.40	-2.40	-2.40	226.910	8.209
12607-1 ♦	7	-5.0570	39.3233	504	43.19	27.24	26.11	20.94	35.18	35.22	35.20	-2.08	-1.81	0.78	0.78	0.78	-2.59	-2.60	-2.59	227.690	8.213
12608-2 ♦	8	-4.9928	39.4332	604	43.54	27.24	26.10	20.93	35.18	35.22	35.20	-2.22	-1.95	0.78	0.78	0.78	-2.73	-2.74	-2.74	227.741	8.213
12609-1 ♦	9	-4.9263	39.3783	453	43.93	27.24	26.07	20.93	35.18	35.22	35.20	-1.87	-1.60	0.78	0.78	0.78	-2.38	-2.38	-2.38	227.709	8.214
12610-3 ♦	10	-4.8167	39.4237	399	44.66	27.23	26.03	20.93	35.18	35.23	35.21	-1.85	-1.58	0.78	0.78	0.78	-2.36	-2.36	-2.36	227.607	8.215
12611-3 ♦	11	-5.5633	41.2622	2786	41.96	27.26	26.15	20.87	35.18	35.22	35.20	-2.29	-2.02	0.78	0.78	0.78	-2.80	-2.81	-2.80	227.289	8.194
12612-2 ♦	12	-5.7325	42.0373	3371	40.75	27.26	26.19	20.83	35.18	35.22	35.20	-2.30	-2.03	0.78	0.78	0.78	-2.81	-2.81	-2.81	227.457	8.187
12613-2 ♦	13	-5.4873	40.9333	2293	42.42	27.25	26.13	20.88	35.18	35.22	35.20	-2.60	-2.33	0.78	0.78	0.78	-3.11	-3.12	-3.11	227.191	8.197
12614-2 ♦	14	-7.2952	39.8127	347	42.74	27.26	26.07	21.10	35.14	35.18	35.19	-1.93	-1.66	0.78	0.78	0.78	-2.43	-2.44	-2.44	222.131	8.189
12615-5 ♦	15	-7.1383	39.8408	446	42.50	27.26	26.09	21.07	35.14	35.18	35.19	-2.11	-1.84	0.78	0.78	0.78	-2.61	-2.62	-2.62	222.624	8.193
12616-3 ♦	16	-6.9785	40.3917	1446	41.96	27.26	26.11	21.02	35.15	35.19	35.19	-2.26	-1.99	0.78	0.78	0.78	-2.77	-2.78	-2.78	223.384	8.194
(12617-1)	This sample was excluded from the present study since it contained no *Thoracosphaera heimii* shells																				
(12620-5)	This sample was excluded from the present study since it contained no *Thoracosphaera heimii* shells																				
12621-1 ♦	17	-10.0915	40.1898	350	41.93	27.22	26.10	21.84	35.07	35.09	35.14	-2.12	-1.85	0.77	0.77	0.78	-2.62	-2.62	-2.63	219.237	8.188
12623-1 ♦	18	-8.2130	39.7610	647	41.75	27.25	26.11	21.29	35.12	35.15	35.18	-2.13	-1.86	0.77	0.78	0.78	-2.64	-2.64	-2.64	220.976	8.176
12624-3 ♦	19	-8.2335	39.7535	651	41.73	27.25	26.11	21.30	35.12	35.15	35.18	-2.16	-1.89	0.77	0.78	0.78	-2.67	-2.67	-2.67	220.945	8.176
12625-1 ♦	20	-8.2005	39.7418	543	41.76	27.25	26.11	21.29	35.12	35.15	35.18	-2.06	-1.79	0.77	0.78	0.78	-2.56	-2.56	-2.57	220.987	8.176

Table 7.2 - Stable oxygen isotope composition of *T. heimii* shells from the Indian Ocean samples (♦) – [a] Measured values of the *T. heimii* shells ($\delta^{18}O_c$; versus VPDB and VSMOW; conversion to VSMOW was done following Zonneveld (2004)) – [b] Calculated stable oxygen isotope composition of seawater ($\delta^{18}O_w$; versus VSMOW) – [c] Stable oxygen isotope values of *T. heimii* corrected for seawater ($\delta^{18}O_c$-$\delta^{18}O_w$; versus VSMOW)

Sample GeoB	n° in Fig. 1, 2	Meteor cruise	Lat (°N)	Lon (°E)	Water Depth (m)	MLD (m)	Temperature (°C)			Salinity (psu)			$\delta^{18}O_c$ (‰)[a]		$\delta^{18}O_w$ (‰)[b] (VSMOW)			$\delta^{18}O_c$-$\delta^{18}O_w$ (‰)[c] (VSMOW)			$[CO_3^{2-}]$ (µmol/kg)	pH
							at 0m	at MLD	200m	at 0m	at MLD	200m	(VPDB)	(VSMOW)	at 0m	at MLD	200m	at 0m	at MLD	200m	at MLD	at MLD
3603-1 ▲	21	M34-1	-35.1217	17.5333	2851	29.66	18.47	17.87	14.82	35.43	35.39	35.21	0.07	0.34	0.51	0.49	0.41	-0.17	-0.15	-0.07	197.624	8.187
3801-5 ■	22	M34-3	-29.5100	-8.3000	4545	48.83	20.58	19.56	17.81	35.98	35.97	35.76	-0.44	-0.17	0.81	0.80	0.68	-0.98	-0.97	-0.85	220.487	8.154
3802-2 ■	23	M34-3	-30.1600	-8.5100	3970	45.27	20.31	19.41	17.59	35.93	35.92	35.72	-0.36	-0.09	0.78	0.77	0.66	-0.87	-0.87	-0.75	218.903	8.152
3803-1 ■	24	M34-3	-30.3500	-8.5700	4173	44.72	20.23	19.35	17.52	35.91	35.91	35.71	-0.35	-0.08	0.77	0.76	0.65	-0.85	-0.84	-0.73	218.297	8.152
3804-2 ■	25	M34-3	-30.7400	-8.7700	3882	43.06	20.06	19.24	17.39	35.88	35.88	35.69	-0.78	-0.51	0.75	0.75	0.64	-1.26	-1.26	-1.15	217.349	8.151
3808-7 ■	26	M34-3	-30.8100	-14.7100	3213	42.68	20.37	19.47	17.62	35.90	35.88	35.73	-0.40	-0.13	0.87	0.86	0.75	-0.99	-0.98	-0.88	221.329	8.153
3809-1 ■	27	M34-3	-31.0500	-16.3300	3470	46.23	20.30	19.27	17.58	35.88	35.86	35.72	-0.75	-0.48	0.85	0.84	0.74	-1.33	-1.32	-1.23	219.733	8.150
3810-2 ■	28	M34-3	-31.1300	-16.8400	3810	45.89	20.28	19.26	17.57	35.87	35.85	35.72	-0.14	0.13	0.85	0.84	0.74	-0.72	-0.71	-0.61	219.605	8.149
3812-2 ▲	29	M34-3	-31.6150	-19.7600	4204	42.46	20.24	19.18	17.61	35.83	35.82	35.71	-0.29	-0.02	0.66	0.66	0.61	-0.68	-0.68	-0.63	216.736	8.102
3827-1 ■	30	M34-3	-25.0300	-38.5483	3842	46.29	23.99	23.36	20.82	36.52	36.68	36.34	-1.18	-0.91	1.09	1.16	1.01	-1.99	-2.07	-1.91	236.692	8.111
3908-11 ■	31	M34-4	-0.0100	-23.4283	3693	38.29	26.83	25.76	19.13	35.75	35.95	35.66	-1.92	-1.65	0.76	0.87	0.70	-2.41	-2.52	-2.35	215.771	8.022
3910-3 ▲	32	M34-4	-4.2450	-36.3467	2361	69.71	27.20	25.54	22.77	36.18	36.36	36.25	-0.77	-0.50	0.97	1.01	0.98	-1.47	-1.51	-1.48	229.426	8.186
3925-2 ■	33	M34-4	5.1433	-47.5300	3198	43.02	27.48	26.90	21.83	35.10	36.07	35.86	-1.01	-0.74	0.54	0.69	0.66	-1.28	-1.43	-1.39	232.155	8.046
3935-1 ▲	34	M34-4	12.6133	-59.3883	1554	45.60	27.54	26.62	23.41	34.90	36.03	36.22	-1.90	-1.63	0.62	0.86	0.90	-2.25	-2.49	-2.53	234.529	8.093
4306-1 ■	35	M38-1	8.3883	-38.0250	3766	39.86	27.01	26.03	19.28	35.76	36.06	35.72	-2.12	-1.85	0.68	0.79	0.67	-2.53	-2.64	-2.51	224.305	8.055
4311-1 ▲	36	M38-1	3.9933	-34.1350	4003	49.42	27.45	26.06	20.14	35.70	35.94	35.65	-2.13	-1.86	0.57	0.66	0.55	-2.43	-2.52	-2.41	235.964	8.198
4312-4 ■	37	M38-1	4.0500	-33.5900	3437	49.16	27.39	26.16	19.99	35.67	35.93	35.66	-1.96	-1.69	0.66	0.75	0.65	-2.34	-2.44	-2.34	235.315	8.062
4401-3 ▲	38	M38-2	4.7900	-43.4590	3396	46.51	27.49	26.61	21.73	35.80	36.05	35.84	-1.71	-1.44	0.90	0.99	0.92	-2.34	-2.43	-2.36	234.400	8.159
4411-1 ■	39	M38-2	5.4300	-44.5000	3300	46.46	27.44	26.68	21.26	35.47	36.07	35.82	-1.97	-1.70	0.65	0.75	0.71	-2.35	-2.44	-2.40	233.903	8.058
4412-3 ■	40	M38-2	5.7200	-44.3600	3767	46.25	27.43	26.64	21.14	35.49	36.07	35.81	-2.30	-2.03	0.66	0.75	0.71	-2.69	-2.78	-2.74	233.926	8.059
4413-1 ■	41	M38-2	6.0900	-44.1900	4295	45.44	27.41	26.60	20.97	35.50	36.07	35.81	-1.87	-1.60	0.66	0.75	0.71	-2.26	-2.35	-2.31	233.813	8.061
4421-2 ■	42	M38-2	16.9900	-46.0100	3176	64.62	25.97	25.20	23.01	36.62	36.96	36.84	-1.08	-0.81	1.07	1.24	1.18	-1.88	-2.05	-1.99	246.059	8.080
4424-2 ■	43	M38-2	18.2000	-44.0200	4779	62.74	25.64	24.86	22.86	36.83	37.07	36.94	-0.35	-0.08	1.17	1.30	1.23	-1.25	-1.38	-1.31	242.310	8.072
4908-3 ▲	44	M41-1	-0.7133	6.8383	3028	14.04	26.74	25.75	18.36	33.65	35.43	34.72	-1.02	-0.75	0.10	0.42	0.64	-0.85	-1.17	-1.39	147.699	8.218
5002-1 ■	45	M41-2	-8.1400	-14.5400	2851	50.61	25.65	24.68	19.55	36.18	36.29	35.89	-1.20	-0.93	0.89	0.94	0.76	-1.82	-1.86	-1.69	208.171	8.028
5004-2 ■	46	M41-2	-9.1700	-13.3400	2790	50.13	25.35	24.56	19.54	36.26	36.37	35.94	-1.25	-0.98	0.93	0.98	0.78	-1.91	-1.96	-1.77	208.703	8.031
5006-1 ■	47	M41-2	-9.7600	-12.3700	3244	50.44	25.12	24.32	19.43	36.31	36.42	35.95	-1.57	-1.30	0.95	0.99	0.79	-2.25	-2.30	-2.09	209.000	8.035
5007-1 ■	48	M41-2	-12.3900	-13.9400	3668	42.89	24.59	24.11	20.06	36.58	36.65	36.18	-1.01	-0.74	1.07	1.10	0.89	-1.80	-1.83	-1.63	226.859	8.073
5008-3 ■	49	M41-2	-12.9300	-15.6900	3407	41.32	24.67	24.24	20.49	36.65	36.71	36.27	-1.00	-0.73	1.10	1.13	0.93	-1.83	-1.85	-1.66	233.418	8.083
5115-2 ■	50	M41-3	-24.1400	-14.0400	3291	24.07	22.83	22.56	19.87	36.48	36.49	36.16	-0.12	0.15	0.94	0.95	0.80	-0.79	-0.80	-0.65	252.577	8.169
5117-2 ■	51	M41-3	-24.1500	-13.9700	3039	24.04	22.82	22.55	19.86	36.48	36.49	36.15	-0.90	-0.63	0.94	0.95	0.80	-1.57	-1.57	-1.42	252.345	8.169
5121-2 ■	52	M41-3	-24.1800	-12.0200	3486	27.25	22.57	22.26	19.62	36.42	36.44	36.11	-0.40	-0.13	0.92	0.93	0.78	-1.05	-1.06	-0.91	248.019	8.166
5130-1 ■	53	M41-3	-19.4000	-9.4600	3166	35.41	22.70	22.24	19.57	36.50	36.49	36.13	-0.65	-0.38	0.94	0.93	0.78	-1.32	-1.32	-1.16	254.940	8.172
5132-2 ■	54	M41-3	-19.1300	-9.7200	3941	37.18	22.76	22.27	19.61	36.51	36.50	36.14	-1.38	-1.11	0.95	0.94	0.78	-2.06	-2.05	-1.90	254.993	8.171
5136-2 ■	55	M41-3	-19.3700	-12.6700	3227	35.23	23.17	22.77	20.16	36.61	36.61	36.25	-1.48	-1.21	1.11	1.11	0.95	-2.32	-2.32	-2.16	262.169	8.176
5140-3 ■	56	M41-3	-19.0500	-16.6100	3660	47.50	23.77	23.11	20.88	36.76	36.73	36.40	-1.09	-0.82	1.18	1.16	1.01	-2.00	-1.98	-1.83	287.556	8.217
5204-11 ▲	57	M41-4	0.0100	-23.4850	3701	38.30	26.79	25.56	19.13	35.80	35.68	35.92	-1.96	-1.69	0.79	0.83	0.74	-2.48	-2.52	-2.43	215.703	8.207

Table 7.3 - Stable oxygen isotope composition of *T. heimii* shells from the Atlantic Ocean samples (■ = this study; ▲ = Zonneveld (2004)) – [a] Measured values of the *T. heimii* shells ($\delta^{18}O_c$; versus VPDB and VSMOW; conversion to VSMOW was done following Zonneveld (2004)) – [b] Calculated stable oxygen isotope composition of seawater ($\delta^{18}O_w$; versus VSMOW) – [c] Stable oxygen isotope values of *T. heimii* corrected for seawater ($\delta^{18}O_c$-$\delta^{18}O_w$; versus VSMOW)

7.4. Results

7.4.1. Stable oxygen isotope composition of *Thoracosphaera heimii*

Stable oxygen isotope values ($\delta^{18}O$) of *T. heimii* shells from the Indian Ocean samples are given in Table 7.2. Measured $\delta^{18}O$ values of the *T. heimii* shells ($\delta^{18}O_c$) in the Indian Ocean samples vary between -2.60 and -1.83‰ (VPDB) or between -2.33 and -1.56‰ (VSMOW). When corrected for the oxygen isotope composition of seawater ($\delta^{18}O_w$), the $\delta^{18}O_c - \delta^{18}O_w$ values of *T. heimii* vary between -3.11 and -2.33‰ (VSMOW) for sea surface conditions, between -3.12 and -2.34‰ (VSMOW) for mixed layer depth conditions and between -3.11 and -2.34‰ (VSMOW) for conditions averaged over 200m water depth.

Table 7.3 contains information about the $\delta^{18}O$ composition of *T. heimii* shells from the Atlantic Ocean samples, both from this study and from the additional samples derived from the dataset of Zonneveld (2004). Measured $\delta^{18}O_c$ values of the *T. heimii* shells in the Atlantic Ocean samples vary between -2.30 and 0.07‰ (VPDB) or between -2.03 and 0.34‰ (VSMOW). When corrected for the oxygen isotope composition of seawater, the $\delta^{18}O_c - \delta^{18}O_w$ values of *T. heimii* vary between -2.69 and -0.17‰ (VSMOW) for sea surface conditions, between -2.78 and -0.15‰ (VSMOW) for mixed layer depth conditions and between -2.74 and -0.07‰ (VSMOW) for conditions averaged over 200m water depth.

7.4.2. Calculation of isotopic temperatures

Calculated isotopic temperatures based on the $\delta^{18}O_c$ - $\delta^{18}O_w$ composition of *T. heimii* from surface sediments and the species-specific paleotemperature equation for *T. heimii* of Zonneveld *et al.* (2007) (dotted line in Fig. 7.4), are lower than the natural mean annual sea surface temperatures (solid line in Fig. 7.4): 10-25°C lower for sea surface conditions (Fig. 7.4a), 9-22°C lower for mixed layer depth conditions (Fig. 7.4b) and 4-19°C lower for conditions averaged over 200m water depth (Fig. 7.4c). Calculated isotopic temperatures based on the $\delta^{18}O_c - \delta^{18}O_w$ composition of *T. heimii* from surface sediments and the paleotemperature equation for inorganic calcite by Kim & O'Neil (1997) (dashed line in Fig. 7.4a, b and c), are lower and higher than the natural mean anual sea surface temperatures (solid line in Fig. 7.4a, b and c): 7°C lower to 4°C higher for sea surface conditions (Fig. 7.4a), 4°C lower to 5°C higher for mixed layer depth conditions (Fig. 7.4b) and 1°C lower to 11°C higher for conditions averaged over 200m water depth (Fig. 7.4c).

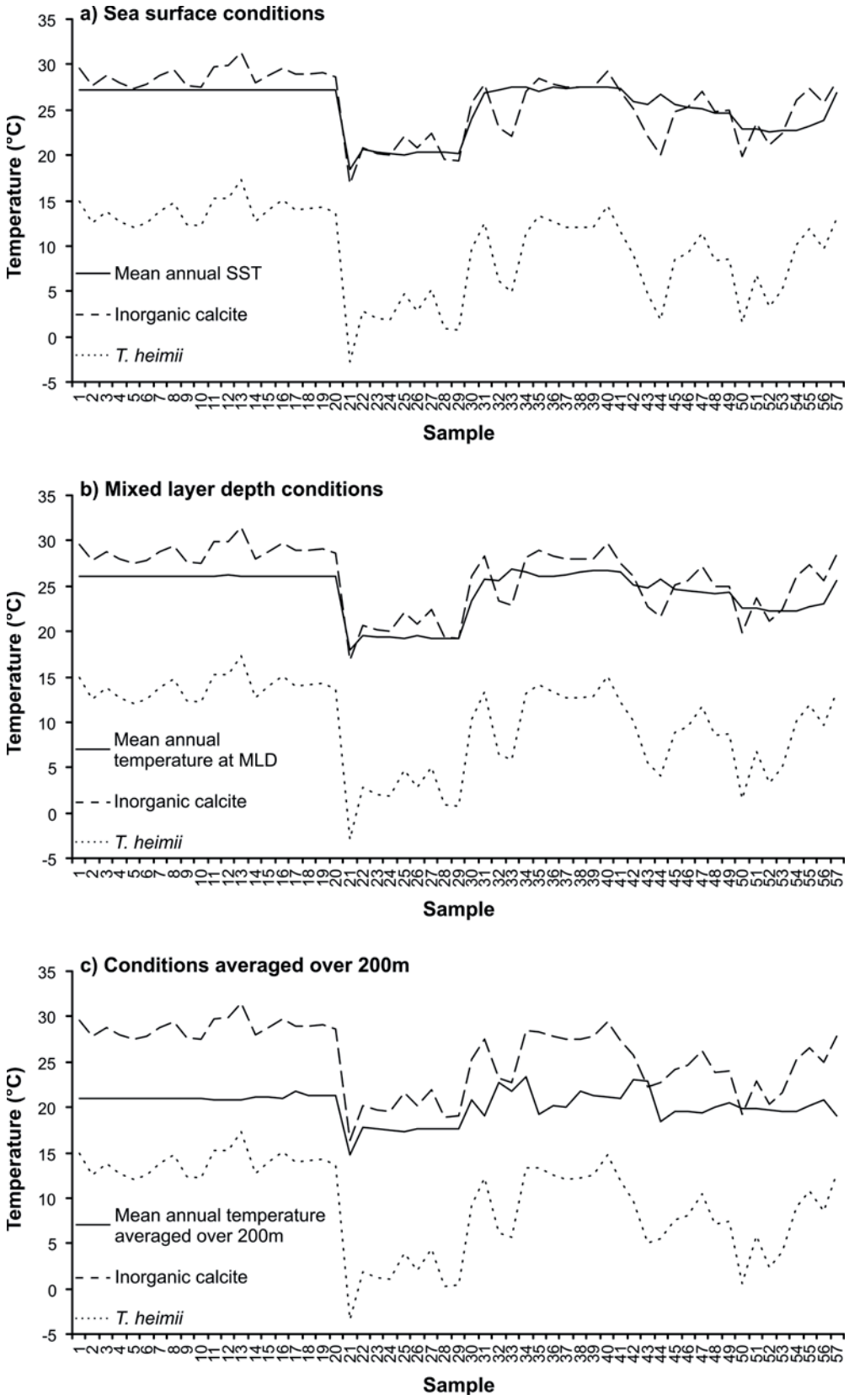

Fig. 7.4 – Reconstruction of isotopic temperatures for (a) sea surface conditions, (b) mixed layer depth conditions and (c) conditions averaged over 200m water depth, based on the *T. heimii* oxygen isotope data, the recently published temperature – $\delta^{18}O$ equation for *T. heimii* from culture experiments by Zonneveld *et al.* (2007) (dotted line in a, b and c) and the paleo-equation for inorganic calcite by Kim & O'Neil (1997) (dashed line in a, b and c). Solid lines in a, b and c depict mean annual temperatures at the corresponding depths. For sample numbering on the x-axis, see Table 7.2 and 7.3.

7.4.3. Correlation between temperature and $\delta^{18}O_c$ - $\delta^{18}O_w$ of *T. heimii*

When the Indian Ocean data is considered separately (yellow diamonds (♦) in Fig. 7.5), no correlation can be observed between temperature and the $\delta^{18}O_c$ – $\delta^{18}O_w$ composition of *T. heimii* shells: $R^2 = 0.01$ for sea surface conditions (Fig. 7.5a), $R^2 = 0.10$ for mixed layer depth conditions (Fig. 7.5b) and $R^2 = 0.002$ for conditions averaged over 200m (Fig. 7.5c).

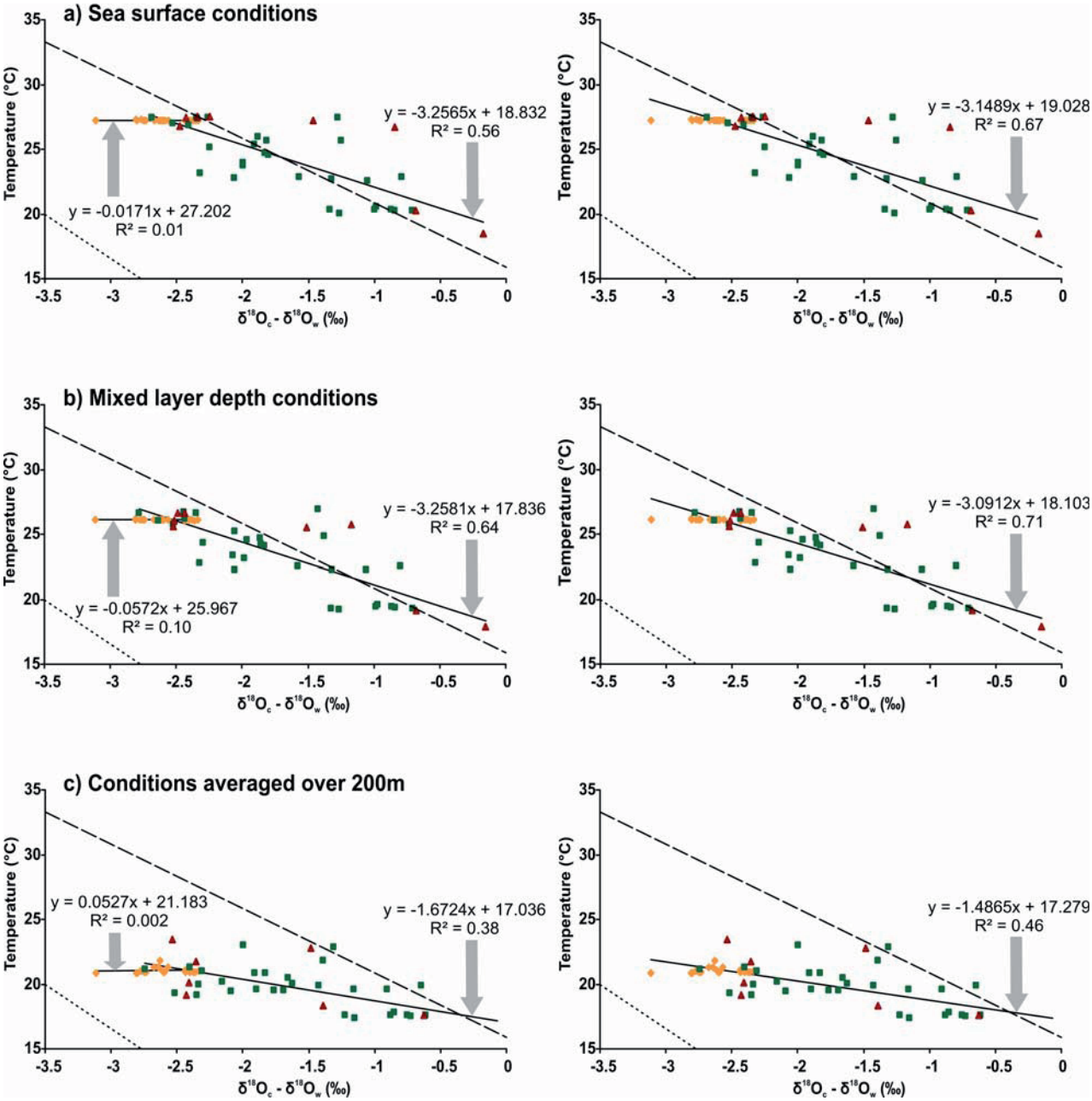

Fig. 7.5 – Correlation between temperature and $\delta^{18}O_c$ - $\delta^{18}O_w$ in *T. heimii* shells from sediments – Yellow diamonds (♦) are the Indian Ocean samples, green squares (■) are the Atlantic Ocean samples from this study and red triangles (▲) are the Atlantic Ocean samples from Zonneveld (2004) – The dotted line represents the paleotemperature equation for *T. heimii* from culture experiments (Zonneveld *et al.*, 2007), the dashed line represents the paleotemperature equation for inorganic calcite (Kim & O'Neil, 1997)

When the Atlantic Ocean data is considered separately, some correlation can be observed between temperature and the $\delta^{18}O_c - \delta^{18}O_w$ composition of *T. heimii* shells (Fig. 7.5; green squares (■) are Atlantic Ocean samples from this study, red trianlges (▲) are Atlantic Ocean sample from Zonneveld (2004)):

Sea surface:	$T(°C) = -3.2565*(\delta^{18}O_c - \delta^{18}O_w) + 18.832$,	$R^2 = 0.56$, $\sigma_{est} = 1.93$
Mixed layer depth:	$T(°C) = -3.2581*(\delta^{18}O_c - \delta^{18}O_w) + 17.836$,	$R^2 = 0.64$, $\sigma_{est} = 1.71$
Averaged over 200m:	$T(°C) = -1.6724*(\delta^{18}O_c - \delta^{18}O_w) + 17.036$,	$R^2 = 0.38$, $\sigma_{est} = 1.49$

with $\delta^{18}O_c$ and $\delta^{18}O_w$ being the stable oxygen isotope compositions of *T. heimii* and seawater respectively. When the combined data set (Indian Ocean and Atlantic Ocean) is considered, some correlation can be observed between temperature and $\delta^{18}O_c - \delta^{18}O_w$ (Fig. 7.5):

Sea surface:	$T(°C) = -3.1489*(\delta^{18}O_c - \delta^{18}O_w) + 19.028$,	$R^2 = 0.67$, $\sigma_{est} = 1.58$
Mixed layer depth:	$T(°C) = -3.0912*(\delta^{18}O_c - \delta^{18}O_w) + 18.103$,	$R^2 = 0.71$, $\sigma_{est} = 1,41$
Averaged over 200m:	$T(°C) = -1,4865*(\delta^{18}O_c - \delta^{18}O_w) + 17.279$,	$R^2 = 0.46$, $\sigma_{est} = 1.21$

with $\delta^{18}O_c$ and $\delta^{18}O_w$ being the stable oxygen isotope compositions of *T. heimii* and seawater respectively.

The difference between the $\delta^{18}O$ composition of the *T. heimii* shells and the values predicted by the paleotemperature equation for inorganic calcite (Kim & O'Neil, 1997) is given in Table 7.4. For the Indian Ocean samples, all $\delta^{18}O_c - \delta^{18}O_w$ values of the *T. heimii* shells are lower than the values predicted for inorganic calcite. For the Atlantic Ocean samples, the majority of the $\delta^{18}O_c - \delta^{18}O_w$ values of the *T. heimii* shells are lower than the values predicted for inorganic calcite. In general, differences with inorganic calcite are smallest for sea surface conditions and largest for conditions averaged over 200m.

7.4.4. Carbonate ion effect

No significant correlation could be found between the $\delta^{18}O_c - \delta^{18}O_w$ composition of *T. heimii* shells in core-top sediments from the Indian and Atlantic Ocean and the carbonate ion concentration $[CO_3^{2-}]$ or the pH of the seawater (Fig. 7.6).

Sample GeoB	$\delta^{18}O$ (*T. heimii* - inorganic calcite) (‰) sea surface	MLD	200m average	Sample GeoB	$\delta^{18}O$ (*T. heimii* - inorganic calcite) (‰) sea surface	MLD	200m average
12601-1 ♦	-0.45	-0.67	-1.73	3827-1 ■	-0.35	-0.55	-0.91
12602-3 ♦	-0.10	-0.32	-1.38	3908-11 ■	-0.19	-0.52	-1.71
12603-1 ♦	-0.30	-0.52	-1.58	3910-3 ▲	0.82	0.45	-0.08
12604-5 ♦	-0.13	-0.36	-1.41	3925-2 ■	1.07	0.81	-0.18
12605-2 ♦	-0.03	-0.26	-1.31	3935-1 ▲	0.11	-0.32	-1.00
12606-2 ♦	-0.10	-0.32	-1.38	4306-1 ■	-0.27	-0.58	-1.84
12607-1 ♦	-0.29	-0.52	-1.57	4311-1 ▲	-0.08	-0.45	-1.55
12608-2 ♦	-0.44	-0.67	-1.72	4312-4 ■	-0.01	-0.35	-1.51
12609-1 ♦	-0.08	-0.31	-1.36	4401-3 ▲	0.01	-0.26	-1.17
12610-3 ♦	-0.06	-0.30	-1.34	4411-1 ■	-0.01	-0.26	-1.32
12611-3 ♦	-0.50	-0.72	-1.80	4412-3 ■	-0.35	-0.60	-1.68
12612-2 ♦	-0.50	-0.72	-1.81	4413-1 ■	0.07	-0.18	-1.28
12613-2 ♦	-0.81	-1.04	-2.10	4421-2 ■	0.16	-0.16	-0.54
12614-2 ♦	-0.13	-0.37	-1.38	4424-2 ■	0.73	0.45	0.11
12615-5 ♦	-0.31	-0.55	-1.57	4908-3 ▲	1.35	0.83	-0.91
12616-3 ♦	-0.47	-0.70	-1.74	5002-1 ■	0.16	-0.08	-0.95
12621-1 ♦	-0.33	-0.55	-1.42	5004-2 ■	0.01	-0.20	-1.03
12623-1 ♦	-0.34	-0.57	-1.55	5006-1 ■	-0.37	-0.58	-1.38
12624-3 ♦	-0.37	-0.60	-1.58	5007-1 ■	-0.03	-0.16	-0.79
12625-1 ♦	-0.26	-0.49	-1.47	5008-3 ■	-0.04	-0.16	-0.73
3603-1 ▲	0.33	0.23	-0.35	5115-2 ■	0.62	0.56	0.15
3801-5 ■	-0.03	-0.24	-0.49	5117-2 ■	-0.16	-0.22	-0.63
3802-2 ■	0.02	-0.16	-0.43	5121-2 ■	0.31	0.24	-0.16
3803-1 ■	0.03	-0.15	-0.42	5130-1 ■	0.06	-0.03	-0.42
3804-2 ■	-0.42	-0.59	-0.87	5132-2 ■	-0.66	-0.76	-1.15
3808-7 ■	-0.09	-0.26	-0.55	5136-2 ■	-0.84	-0.92	-1.29
3809-1 ■	-0.44	-0.65	-0.91	5140-3 ■	-0.39	-0.51	-0.82
3810-2 ■	0.17	-0.03	-0.30	5204-11 ▲	-0.27	-0.56	-1.78
3812-2 ▲	0.20	-0.02	-0.30				

Table 7.2 – Difference between the $\delta^{18}O_c - \delta^{18}O_w$ composition of *T. heimii* shells from sediments and the values predicted using the paleotemperature equation for inorganic calcite by Kim & O'Neil (1997) - ♦ = Indian Ocean samples, ■ = Atlantic Ocean samples (this study) and ▲ = Atlantic Ocean samples (Zonneveld, 2004)

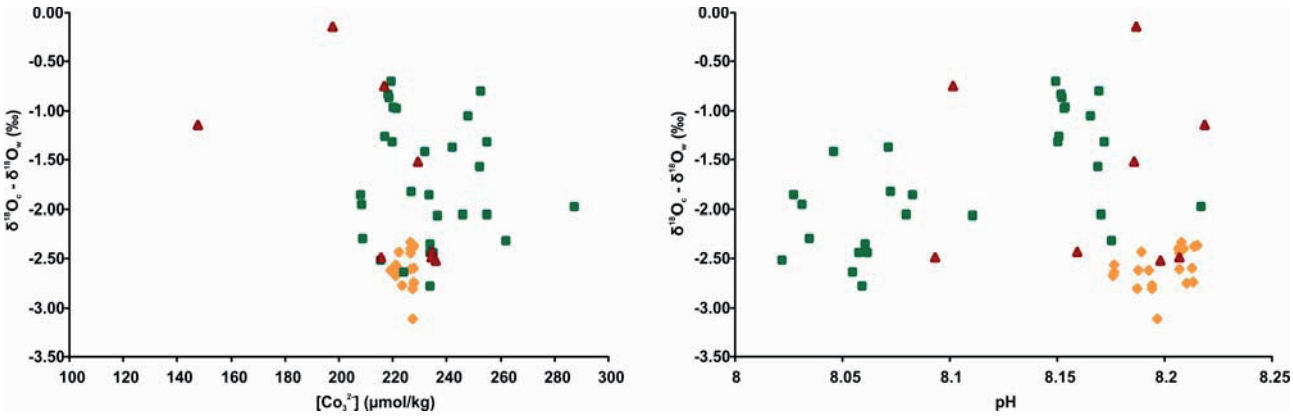

Fig. 7.6 – Correlation between the $\delta^{18}O_c - \delta^{18}O_w$ composition of *T. heimii* shells from sediments with the carbonate ion concentration of the seawater ($[CO_3^{2-}]$) and pH at mixed layer depth – yellow diamonds (♦) are the Indian Ocean samples from this study, green squares (■) are the Atlantic Ocean sample from this study and red triangles (▲) are the additional Atlantic Ocean samples from Zonneveld (2004)

7.5. Discussion

7.5.1. Correlation between temperature and the $\delta^{18}O$ composition of *T. heimii* shells

In an attempt to reconstruct isotopic temperatures based on the $\delta^{18}O$ composition of *Thoracosphaera heimii* shells from core top sediments; two published paleotemperature equations were used: the equation for *T. heimii* from culture experiments by Zonneveld *et al.* (2007) and the equation for inorganic calcite by Kim & O'Neil (1997). In general, the *T. heimii* paleotemperature equation yields reconstructed isotopic temperatures which are 5-25°C lower than the local mean annual temperatures (at sea surface, at mixed layer depth or average temperature values over 200m water depth). Comparable unrealistic isotopic temperatures were already noted by Kohn *et al.* (2011). As a result, the authors suggested that in the culture experiments of Zonneveld *et al.* (2007), an uncontrolled medium – air exchange might have occurred, that caused the physical conditions of the culture medium to remain not completely constant. Since we observed a similar discrepancy, we support the assumption of Kohn *et al.* (2011) to reject the culture experiment-based equation for *T. heimii* of Zonneveld *et al.* (2007). The paleotemperature equation for inorganic calcite (Kim & O'Neil, 1997) yields reconstructed isotopic temperatures which are generally 7°C lower to 11°C higher than the local mean annual temperature (at sea surface, at mixed layer depth or average temperature values over 200m water depth). We also observe that for the Indian Ocean samples and the majority of the Atlantic samples, the $\delta^{18}O_c - \delta^{18}O_w$ values are 0.09-1.35‰ lower than values predicted by the equation for inorganic calcite.

When looking at the correlation between natural temperatures and $\delta^{18}O_c - \delta^{18}O_w$ values in *T. heimii* shells from core top samples, a difference can be noticed between the sample set from the Indian Ocean and the sample set from the Atlantic Ocean. When the Indian Ocean core top samples are considered separately, $\delta^{18}O_c - \delta^{18}O_w$ is not correlated with temperature. This is not surprising since the Indian Ocean samples display a very wide range of $\delta^{18}O_c - \delta^{18}O_w$ values (~0.8‰) for a very narrow range of temperatures (less than 1°C). This is quite unrealistic, since e.g. inorganic calcite and the planktonic foraminifera *Orbulina universa* would show the same $\delta^{18}O_c - \delta^{18}O_w$ range for a range of calcification temperatures as large as ~3.7°C (e.g. Bemis *et al.*, 1998). This might be suggestive of other factors than temperature controlling the $\delta^{18}O$ composition of *T. heimii* shells in core top samples from the western Indian Ocean. The observed offsets in our data set, between *T. heimii* and inorganic calcite, and between the Indian and Atlantic Ocean, will be discussed in terms of instrumental, environmental or biological influences.

7.5.2. Instrumental influences

A potential factor influencing the isotopic signal of *T. heimii* shells is the purification of the samples. Zonneveld (2004) showed that "dirty" samples, i.e. samples that contain more than 15% calcareous particles other than *T. heimii*, gave both positive and negative deviations compared to their purified equivalents. For the Indian Ocean samples within the present study, the total calcareous fraction contains on average 87% *T. heimii* shells. The largest portion of the other calcareous particles consists of foraminifera, i.e. mostly single detached chambers and juvenile foraminifera (on average 7.38%). Also parts of larger unidentified calcareous organisms are quite abundant (on average 4.18%). Less common calcareous particles are (parts of) other calcareous dinoflagellates (on average 0.83%) and coccolithophore and coccolith species (on average 0.58%). Although in general, the requirement for having an accurate *T. heimii* isotope signal is fulfilled (less than 15% other calcareous particles, Zonneveld (2004)), for some individual Indian Ocean samples, *T. heimii* only comprises 80% of the calcareous fraction. Therefore it is possible that the $\delta^{18}O$ composition of the other present species obscure the *T. heimii* signal, perhaps partly causing the large $\delta^{18}O_c - \delta^{18}O_w$ range associated with the very narrow temperature range in the Indian Ocean, or causing the offset with inorganic calcite. To entirely exclude the contaminating effect of other calcareous particles on the *T. heimii* isotope signal, multiple measurements, with different levels of purification are needed.

Another factor that might be of consequence is the calculation of the oxygen isotope composition of sea water ($\delta^{18}O_w$). Since measured $\delta^{18}O_w$ values were not available, we calculated $\delta^{18}O_w$ based on the linear relationship between $\delta^{18}O_w$ and salinity. We are aware that this method might have a high rate of insecurity since for the Indian Ocean study area for instance, only a few data points with measured $\delta^{18}O_w$ and salinity values are available in the Global Seawater Oxygen-18 Database of Schmidt *et al.* (1999). However, we argue that the available $\delta^{18}O_w$ and salinity data display a uniform distribution with a rather high correlation coefficient ($R^2 = 0.79$). We therefore assume that the $\delta^{18}O_w$ – salinity relationship, as established with data points in the Indian Ocean, is representative for the whole research area offshore Tanzania. Although for some Atlantic Ocean samples data points in the Global Seawater Oxygen-18 Database were sparse as well, the correlation between $\delta^{18}O_w$ and salinity is high ($R^2 = 0.74$-0.95). For a few Atlantic Ocean samples however (GeoB 4306-1 and 4312-3) the data points show a large scatter ($R^2 = 0.23$). For these samples, a better relationship needs to be established, which is currently not possible due to the sparsity of data points in the Global Seawater Oxygen-18 Database (Schmidt *et al.*, 1999) at these sample locations.

By calculating the $\delta^{18}O_w$ estimates, we interpolated mixed layer depth, temperature and salinity values with the Ocean Data View VG gridding method (Schlitzer, 2009). Different interpolation methods and programs will off course produce slightly different values and this could have an influence on the calculated isotopic temperatures. However, a discussion about the differences between interpolation methods was not in the scope of this paper.

7.5.3. Environmental influences

Apart from instrumentally induced effects, also environmental processes might influence the $\delta^{18}O$ signal of *T. heimii* shells in surface sediments. For the present study, we analyzed core top samples from two different oceanographic regions, the western Indian Ocean, and the equatorial and South Atlantic, which are characterized by surface currents and water masses with different isotopic composition. Legrande & Schmidt (2006, Fig. 7.7) created a global map for the annual mean surface $\delta^{18}O$ composition of seawater. From this map, it can be derived that the $\delta^{18}O$ values of seawater in the equatorial and South Atlantic are generally higher than in the western Indian Ocean. Therefore it can be assumed that *T. heimii* in Atlantic Ocean waters will precipitate calcareous shells with higher $\delta^{18}O$ values. However, measured $\delta^{18}O$ values of the *T. heimii* shells were corrected for the $\delta^{18}O$ composition of seawater, which should annul the effect of inter-oceanic differences.

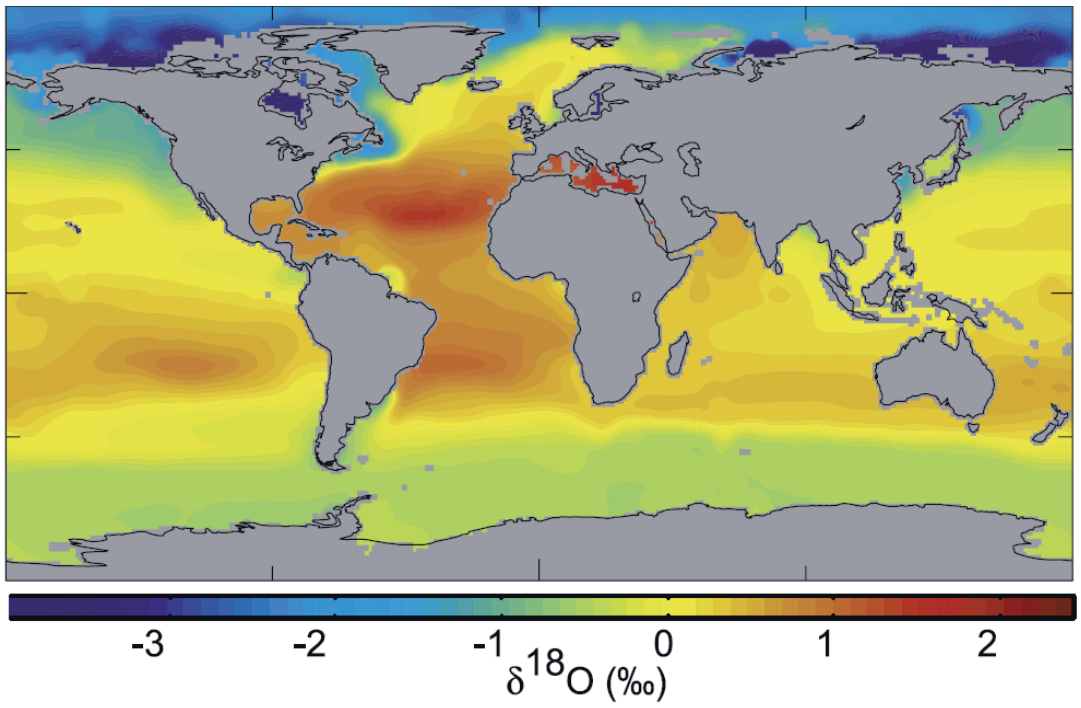

Fig. 7.7 – Global 1°x1° gridded data set of the annual mean surface $\delta^{18}O$ composition of seawater (Legrande & Schmidt, 2006). All $\delta^{18}O$ measurements come from the upper 5 meters of the water column (Schmidt *et al.*, 1999)

In contrast to the Atlantic Ocean samples, the Indian Ocean samples are located in a coastal system, thus influence of freshwater input by local rivers will be more important for the latter samples. Regions in the vicinity of a river mouth are affected by the average isotopic composition of precipitation over the river's catchment area (e.g. Rohling & Bigg, 1998; Rohling & Cooke, 1999). Although currently we do not have specific isotopic data for the Tanzania rivers affecting the sample area (Pangani, Wami, Rufiji and Ruvuma), generally, a low lattitude river system imports freshwater with higher $\delta^{18}O$ values than those of a high latitude river. For example, the average (pre-Aswan dam) Nile River $\delta^{18}O$ composition was near -2‰, whereas the Arctic McKenzie river discharges waters with a composition around -20‰ (e.g. Rohling & Bigg, 1998; Rohling & Cooke, 1999). Since the core top samples from the western Indian Ocean study area are located at low latitudes, we expect that the difference in isotopic composition between the river runoff water and the oceanic water will be minor.

Also a possible seasonal effect on the Indian Ocean samples induced by the monsoon system needs to be considered. In culture experiments *T. heimii* shells are produced throughout the year with the production of about one cyst a day (e.g. Inouye & Pienaar, 1983; Karwath, 2000). This suggests that the production of *T. heimii* shells in natural environments is not restricted to a certain season or to a limited time interval during the year (Zonneveld, 2004). This assumption is supported by, for instance, a sediment trap study off Cape Blanc where *T. heimii* dominates the calcareous dinocyst assemblage during an 18-months sampling period (Richter, 2009). However, there are indications that seasonal production of *T. heimii* shells is region dependent: a sediment trap study from the Arabian Sea documents highest accumulation rates of *T. heimii* shells at the end of the SW monsoon (Wendler *et al.*, 2002a, b). Since our study area, the Indian Ocean offshore Tanzania, is located more south compared to the Arabian Sea, we assume that this seasonal effect is likely to be less pronounced here. Also, the SW monsoon is characterized by high rain fall and river discharge, which is associated with high amounts of suspended material and high turbulence conditions. Turbulence in the upper water column is unfavorable for the development of phytoplankton (including the calcareous dinoflagellate *T. heimii*), preventing it from building up a standing stock in the photic zone (e.g. Wendler *et al.*, 2002a, b; Vink, 2004). Therefore we infer that the increased turbulence in the vicinity of the Ruvuma river mouth at the end of the SW monsoon, as could be observed prior to and during Meteor cruise M75-2 (Pätzold *et al.*, subm.), leads to lowest concentrations of *T. heimii* shells in the water column (Kohn & Zonneveld, 2010) and absence of *T. heimii* shells in the surface sediments (samples GeoB 12617-1 and GeoB 12620-5, this study) and thus that any seasonal effect on *T. heimii* in our study area would be annulled by this phenomenon.

As a last possible environmental influence we need to consider the living depth of *T. heimii*. We observed that the correlation between temperature and the $\delta^{18}O$ composition of *T. heimii* shells from surface sediment samples in the Atlantic Ocean slightly increases when we consider temperatures at mixed layer depth (MLD) instead of sea surface temperatures or temperatures averaged over 200m water depth. The lower limit of the surface mixed layer is characterized by an abrupt density change (pycnocline) or temperature change (thermocline). And these gradients are often co-located with a maximum in chlorophyll-*a* concentration. The upper part of the photic zone and the area immediately above the deep chlorophyll maximum (DCM) is supposedly the living depth of *T. heimii* (Kohn & Zonneveld, 2010). Therefore we used the MLD from the Monterey & Levitus (1997) database as a measure for the depth of the DCM. It should be noted however, that the MLD is not a constant or permanent phenomenon. Temporal variabilities of the MLD can range from diurnally to interannually, including seasonally and interseasonally. Also the spatial variability of the MLD is very large. The MLD can be less than 20 m in the summer hemisphere, while reaching more than 500 m in the winter hemisphere (de Boyer Montégut *et al.*, 2004 with all references therein). Unfortunately, so far no information is available on how these seasonal variabilities of the MLD or DCM effect the isotopic composition of *T. heimii*. But since we assume a year-round production of *T. heimii* shells (see discussion above), the use of annually averaged MLDs can be justified.

7.5.4. Biological influences

To explain the observed offset with inorganic calcite, we also need to consider several biological processes, including calcification, photosynthesis and respiration. For an overview of the effect of these metabolic and kinetic processes, previously referred to as "vital effects", on the $\delta^{18}O$ composition of *T. heimii* shells, see Zonneveld *et al.* (2007). Here we will consider the possibility of the carbonate ion effect (CIE) moderating the $\delta^{18}O$ signal of *T. heimii* shells.

The CIE is characterized by a decrease in shell $\delta^{18}O$ with increasing $[CO_3^{2-}]$ concentration or pH of the culture medium/seawater, and is likely to be caused by a combination of kinetic effects and $[CO_3^{2-}]$ related variations in the calcification rate. The phenomenon and its possible mechanisms have been extensively discussed in literature and have been described for many foraminifera and coccolithophore species (e.g. Spero *et al.*, 1997; Bijma *et al.*, 1999; Zeebe, 1999; Zeebe *et al.*, 1999; Ziveri *et al.*, 2006; Ziveri *et al.*, 2011).

For the calcareous dinoflagellate *T. heimii*, thus far three culture experiments have been carried out to investigate the influence of the carbonate chemistry of the seawater/culture medium. In the study of Zonneveld *et al.* (2007) a positive correlation was found between $\delta^{18}O_c$-$\delta^{18}O_w$ and pH, whereas in the study of Kohn (2009) this correlation was negative. However, as already mentioned at the beginning of this discussion, the results of the culture study of Zonneveld *et al.* (2007) are not entirely trustworthy since several parameters of the culture medium did not remain constant during the experiment. A more recent culture experiment gave a slope of -0.0243 $(\mu mol/kg)^{-1}$ for the correlation between $\delta^{18}O$ and $[CO_3^{2-}]$ (Ziveri *et al.*, 2011). However, for the surface sediment samples in this study, we did not find any correlation between the $\delta^{18}O_c$-$\delta^{18}O_w$ composition of *T. heimii* shells and the $[CO_3^{2-}]$ (or pH) value at mixed layer depth. The Indian Ocean samples show a rather large $\delta^{18}O_c$-$\delta^{18}O_w$ range for a small $[CO_3^{2-}]$ range. Also in the Atlantic Ocean the samples show a large scatter of the data. It is possible that the correlation between $\delta^{18}O$ and $[CO_3^{2-}]$ found in culture experiments (Ziveri *et al.*, 2011) is obscured in natural sediments by processes discussed above. To evaluate the carbonate ion effect on *T. heimii* shells from surface sediments, further research is necessary.

Conclusion

For the present study, we analyzed the stable oxygen isotope ($\delta^{18}O$) composition of *Thoracosphaera heimii* shells from surface sediments in two oceanographic regions: the western Indian Ocean offshore Tanzania, and the equatorial and South Atlantic. The data set was complemented with published *T. heimii* $\delta^{18}O$ data from surface sediment samples in the Atlantic study of Zonneveld (2004). Isotopic temperatures were reconstructed based on the $\delta^{18}O$ composition of *T. heimii* and the culture-based paleotemperature equations for *T. heimii* (Zonneveld *et al.*, 2007) and inorganic calcite (Kim & O'Neil, 1997). These calculated isotopic temperatures differ from the modern mean annual sea surface temperatures. Furthermore, we looked at the correlation between the $\delta^{18}O$ composition of *T. heimii* shells and temperatures of the upper water column. No temperature – $\delta^{18}O$ correlation is present for the Indian Ocean samples, which we explain by a combination of instrumental and environmental influences. For the Atlantic Ocean samples, the temperature – $\delta^{18}O$ correlation slightly improves when temperatures at mixed layer depth, the presumed living depth of *T. heimii*, are considered. This observation supports the proposal of previous studies that the $\delta^{18}O$ composition of *T. heimii* shells has potential as a useful tool to reconstruct paleotemperatures of a specific depth in the upper water column, notably the mixed layer depth.

Acknowledgements

Thanks are given to all cruise participants and the crew of M75-2 for recovering the investigated surface sediment samples. We are also grateful to Monika Segl (Department of Marine Geology, University of Bremen) for carrying out the stable isotope measurements. Kara Bogus (University of Bremen) is thanked for the correction of the English. The manuscript benefitted from helpful and constructing comments of Jürgen Pätzold (MARUM, University of Bremen). We also thank all members of the working group of Historical Geology and Paleontology (University of Bremen) for their general assistance and helpful discussions. This research was carried out within the framework of the International Graduate School: Proxies in Earth History (EUROPROX).

References

Antonov, J.I., Seidov, D., Boyer, T.P., Locarnini, R.A., Mishonov, A.V., Garcia, H.E., 2010. World Ocean Atlas 2009 Volume 2: Salinity. S. Levitus, Ed., NOAA Atlas NESDIS 69, U.S. Government Printing Office, Wahington, D.C., 184 pp.

Bell, B.E., 1972. Marine fisheries. In: Morgan, W.T.W. (Ed.), East Africa: Its people and resources. Oxford University Press, New York, pp. 243-253.

Bemis, B.E., Spero, H.J., Bijma, J., Lea, D.W., 1998. Reevaluation of the oxygen isotopic composition of planktonic foraminifera: experimental results and revised paleotemperature equations. *Paleoceanography* 13(2), 150-160.

Bijma, J., Spero, H.J., Lea, D.W., 1999. Reassessing foraminiferal stable isotope geochemistry: impact of the oceanic carbonate system (experimental results). In: Fischer, G., Wefer, G. (Eds.), Use of Proxies in Paleoceanography. Springer, Berlin, pp. 489-512.

Boeckel, B., Baumann, K.-H., 2008. Vertical and lateral variations in coccolithophore community structure across the subtropical frontal zone in the South Atlantic Ocean. *Marine Micropaleontology* 67, 255-273.

Bryceson, I., 1977. An ecological study of phytoplankton of the coastal waters of Dar Es Salaam. Ph.D. Thesis, University of Dar Es Salaam, Dar Es Salaam, Zanzibar.

de Boyer Montegut, C., Madec, G., Fischer, A.S., Lazar, A., Iudicone, D., 2004. Mixed layer depth over the global ocean: An examination of profile data and a profile-based climatology. *Journal of Geophysical Research* 109, C12003, doi:10.1029/2004JC002378.

Findlater, J., 1971. Mean monthly airflow at low levels over the western Indian Ocean. Geoph. Mem., 115, H.M.S.O., London. 53 pp.

Fischer, G., Wefer, G. (Eds.), 1999. Use of proxies in paleoceanography: examples from the South Atlantic. Springer, Berlin. 735 pp.

Goyet, C., Healy, R.J., Ryan, J.P., 2000. Global distribution of total inorganic carbon and total alkalinity below the deepest winter mixed layer depths. ORNL/CDIAC-127, NDP-076. Carbon Dioxide Information Analysis Center, Oak Ridge National Laboratory, U.S. Department of Energy, Oak Ridge, Tennessee, U.S.A. 40 pp. doi:10.3334/CDIAC/otg.ndp076

Hastenrath, S., Greischar, L., 1991. The monsoonal current regimes of the tropical Indian Ocean: observed surface flow fields and their geostrophic and wind-driven components. *Journal of Geophysical Research* 69(C7), 12 619-12 633.

Hut, G. 1987. Consultants group meeting on stable isotope reference samples for geochemical and hydrological investigations. Report to the Director General of the International Atomic Energy Agency, Vienna, pp. 1-42.

Inouye, I., Pienaar, R.N., 1983. Observations on the life cycle and microanatomy of *Thoracosphaera heimii* (Dinophyceae) with special reference to its systematic position. *South African Journal of Botany* 2, 63-75.

Karwath, B., 2000. Ecological studies on living and fossil calcareous dinoflagellates of the equatorial and tropical Atlantic Ocean. Berichte aus dem Fachbereich Geowissenschaften der Universität Bremen 152, 1-175.

Karwath, B., Janofske. D., Willems, H., 2000. Spatial distribution of the calcareous dinoflagellate *Thoracosphaera heimii* in the upper water column of the tropical and equatorial Atlantic. I*nternational Journal of Earth Sciences* 88, 668-679.

Kim, S.-T., O'Neil, J.R., 1997. Equilibrium and non-equilibrium oxygen isotope effects in synthetic carbonates. *Geochimica et Cosmochimica Acta* 61, 3461-3475.

Kohn, M., 2009. The stable oxygen isotope signal of the calcareous-walled dinoflagellate *Thoracosphaera heimii* as a new proxy for sea-surface temperature. Ph.D. Thesis, Fachbereich 5 – ´Geowissenschaften, Universität Bremen, Germany.

Kohn, M., Zonneveld, K.A.F., 2010. Calcification depth and spatial distribution of *Thoracosphaera heimii* cysts: Implications for palaeoceanographic reconstructions. *Deep-Sea Research I* 57, 1543-1560.

Kohn, M., Steinke, S., Baumann, K.-H., Donner, B., Meggers, H., Zonneveld, K.A.F., 2011. Stable oxygen isotopes from the calcareous-walled dinoflagellate *Thoracosphaera heimii* as a proxy for changes in mixed layer temperatures off NW Africa during the last 45,000 yr. *Palaeogeography, Palaeoclimatology, Palaeoecology* 302, 311-322.

Legrande , A.N., Schmidt, G.A., 2006. Global gridded data set of the oxygen isotopic composition in seawater. *Geophysical Research Letters* 33, L12604, doi:10.1029/2006GL026011.

Locarnini, R.A., Mishonov, A.V., Antonov, J.I., Boyer, T.P., Garcia, H.E., 2010. World Ocean Atlas 2009, Volume 1: Temperature. S. Levitus, Ed., NOAA Atlas NESDIS 68, U.S. Government Printing Office, Washington, D.C., 184 pp.

Lugomela, C., Wallberg, P., Nielsen, T.C., 2001. Plankton composition and cycling of carbon during the rainy season in a tropical coastal ecosystem, Zanzibar, Tanzania. *Journal of Plankton Research* 23(10), 1121-1136.

McClanahan, T.R., 1988. Seasonality in East Africa's coastal waters. *Marine Ecology Progress Series* 44, 191-199.

Monterey, G., Levitus, S., 1997. Seasonal variability of mixed layer depth for the World Ocean. NOAA Atlas NESDIS 14, U.S. Government Printing Office, Washington, D.C., 96 pp. 87 figs.

Newell, B.S., 1959. The hydrography of the British East African coastal waters. Part II. Colonial Office Fishery Publication 12 H.M.S.O. London, 18 pp..

Pätzold, J., Bartholomä, A., Baumann, K.-H., Bouimetarhan, I., Kreuzmann, C., Flemming, B., Groeneveld, J., Hathorne, E., Hüttich, D., Keil, H., Klages, J., Klann, M., Krastel-Gudegast, S., Kühl, B., Kuhlmann, H., Meyer, M., Mulitza, S., Muzuka, A., Niedermeyer, E., Nizou, J., Nyandwi, N., Ochsenhirt, W.-T., Schlömer, A., Schöttke, L., Schulz, M., Shaghude, Y., Stolz, K., Vogel, S., Wilsenack, M., subm. Western Indian Ocean Climate and Sedimentation (WINOCS) PaläoIndik, Part 3, R/V METEOR Cruise No. 75, Leg 2, Dar Es Salaam – Dar Es Salaam (Tanzania). Meteor Berichte, Leitstelle Meteor, Universität Hamburg.

Peterson, R.G., Stramma, L., 1991.Upper-level circulation in the South Atlantic Ocean. *Progress in Oceanography* 26, 1-73.

Richter, D., 2009. Characteristics of calcareous dinoflagellate cyst assemblages in a major upwelling region (NW Africa). Spatial distribution, fluxes and ecology. Ph.D. Thesis, Fachbereich 5 – Geowissenschaften, Universität Bremen, Germany.

Rohling, E.J., Bigg, G.R., 1998. Paleosalinity and $\delta^{18}O$: a critical assessment. *Journal of Geophysical Research* 103, 1307-1318.

Rohling, E.J., Cooke, S., 1999. Stable oxygen and carbon isotope ratios in foraminiferal carbonate. In: Gupta, B.S. (Ed.), Modern foraminifera. Kluwer Academic, Dordrecht, The Netherlands, pp. 239-258.

Schlitzer, R., 2009. Ocean Data View, http://odv.awi.de.

Schmidt, G.A., Bigg, G.R., Rohling, E.J., 1999. Global Seawater Oxygen-18 Database, http://data.giss.nasa.gov/o18data/

Schott, F., 1983. Monsoon response of the Somali Current and associated upwelling. *Progress in Oceanography* 12, 357-381.

Schott, F., Fieux, M., Kindle, J., Swallow, J., Zantopp, R., 1988. The boundary currents east and north of Madagascar 2. Direct measurements and model comparisons. *Journal of Geophysical Research* 93, 4963-4974.

Schott, F.A., Xie, S.-P., McCreary Jr., J.P., 2009. Indian Ocean circulation and climate variability. *Reviews of Geophysics* 47, RG1002.

Spero, H.J., 1992. Do planktonic foraminifera accurately record shifts in the carbon isotopic composition of sea water ΣCO_2? *Marine Micropaleontology* 19, 275-285.

Spero, H.J., Lea, D.W., 1993. Intraspecific stable isotope variability in the planktic foraminifera *Globigerinoides sacculifer*, results from laboratory experiments. *Marine Micropaleontology* 22, 221-234.

Spero, H.J., Lea, D.W., 1996. Experimental determination of stable isotope variability in *Globigerina bulloides*, implications for paleoceanographic reconstruction. *Marine Micropaleontology* 28, 231- 246.

Spero, H.J., Bijma, J., Lea, D.W., Bemis, B.E., 1997. Effect of seawater carbonate concentration on foraminiferal carbon and oxygen isotopes. *Nature* 390, 497-500.

Swallow, J.C., Schott, F., Fieux, M., 1991. Structure and transport of the East African Coastal Current. *Journal of Geophysical Research*, 96(C12), 22245-22257.

Vink, A., 2004. Calcareous dinoflagellate cysts in South and equatorial Atlantic surface sediments: diversity, distribution, ecology and potential for palaeoenvironmental reconstruction. *Marine Micropaleontology* 50, 43-88.

Wefer, G., Berger, W.H., Siedler, G., Webb, D.J., 1996. The South Atlantic: Present and past circulation. Springer, Berlin.

Wendler, I., Zonneveld, K.A.F., Willems, H., 2002a. Calcareous cyst-producing dinoflagellates: ecology and aspects of cyst preservation in a highly productive ocean region. In: Clift, P.D., Kroon, D., Gedicke, C., Craig, J. (Eds.), The Tectonic and Climatic Evolution of the Arabian Sea Region. Geological Society London Special Publications, vol. 195. London, pp. 317-340.

Wendler, I., Zonneveld, K.A.F., Willems, H., 2002b. Production of calcareous dinoflagellate cysts in response to monsoon forcing off Somalia: A sediment trap study. *Marine Micropaleontology* 46, 1- 11.

Winter, A., Rost, B., Hilbrecht, H., Elbrächter, M., 2002. Vertical and horizontal distribution of coccolithophores in the Caribbean Sea. *Geo-Marine Letters* 22, 150-161.

Woodberry, K.E., Luther, M.E., O'Brien, J.J., 1989. The wind-driven seasonal circulation in the southern tropical Indian Ocean. *Journal of Geophysical Research* 94(C12), 17985-18002.

Wyrtki, K., 1973. Physical oceanography of the Indian Ocean. In: Zeitschel, B. (Ed.), The biology of the Indian Ocean. Springer-Verlag, Berlin, pp. 18-36.

Yeh, S.-W., Yim, B.Y., Noh, Y., 2009. Changes in mixed layer depth under climate change projections in two CGCMs. *Climate Dynamics* 33, 199-213.

Zeebe, R.E., 1999. An explanation of the effect of seawater carbonate concentration on foraminiferal oxygen isotopes. *Geochimica et Cosmochimica Acta* 63(13-14), 2001-2007.

Zeebe, R., Bijma, J., Wolf-Gladrow, D.A., 1999. A diffusion-reaction model of carbon isotope fractionation in foraminifera. *Marine Chemistry* 64, 199-227.

Ziveri, P., Probert, I., Stoll, H.M., 2006. Carbonate ion effects on coccolith carbon and oxygen isotopes. American Geophysical Union, Fall Meeting 2006, abstract #PP21C-1718.

Ziveri, P., Thoms, S., Probert, I., Geisen, M., Langer, G., 2011. A universal carbonate ion effect on stable oxygen isotope ratios in unicellular planktonic calcifying organisms. *Biogeosciences Discussions* 8, 7575-7591, doi:10.5195/bgd-8-7575-2011.

Zonneveld, K.A.F., 2004. Potential use of stable oxygen isotope composition of *Thoracosphaera heimii* (Dinophyceae) for upper water column (thermocline) temperature reconstruction. *Marine Micropaleontology* 50, 307-317.

Zonneveld, K.A.F., Mackensen, A., Baumann, K.-H., 2007. Stable oxygen isotopes of *Thoracosphaera heimii* (Dinophyceae) in relationship to temperature; a culture experiment. *Marine Micropaleontology* 64, 80-90.

CHAPTER 8 – MANUSCRIPT 2

Sr/Ca and Mg/Ca ratios of *Thoracosphaera heimii* shells in core top samples from the South and equatorial Atlantic Ocean – A pilot study

Stefanie P.M. Dekeyzer[a]*, Jeroen Groeneveld[b], Ulrike Holzwarth[b] & Karin A.F. Zonneveld[a,b]

[a]Fachbereich 5 – Geowissenschaften, Universität Bremen, Bremen, Germany
[b]MARUM, Universität Bremen, Bremen, Germany

*Corresponding author.

Fax: +49 421 218 65159
E-mail address: stefanie.dekeyzer@uni-bremen.de

Abstract

In this pilot study, the Mg/Ca, Sr/Ca, Fe/Ca, Mn/Ca and Si/Ca ratios of *Thoracosphaera heimii* shells from 31 surface sediments in the equatorial and South Atlantic have been analyzed. The Mg/Ca and Sr/Ca ratios were compared to several environmental parameters of the upper water column, especially temperature; while the Fe/Ca, Mn/Ca and Si/Ca ratios were used as a measure for contamination from the sediments. A difference could be observed between the elemental composition of *T. heimii* shells from natural sediments (this study) and *T. heimii* shells from a previously published culture experiment: natural values are generally higher and show a larger range than culture values. PCA reveals a grouping of the samples: highest Mg/Ca ratios appear in the Amazon Fan area, while highest Sr/Ca ratios appear in the central area of the Subtropical Gyre. RDA reveals a correlation between Mg/Ca and temperature. However, Mg/Ca values also show a correlation with Mn/Ca, Fe/Ca and Si/Ca, which can be an indication for sediment (clay) contamination. RDA also reveals a correlation between Sr/Ca and the carbonate chemistry of the seawater (total alkalinity and carbonate ion concentration [CO_3^{2-}]). In contrast to cultured *T. heimii* shells, the Sr/Ca ratios of *T. heimii* shells from natural sediments do not show any correlation with temperature. So far we do not have a satisfying explanation for this discrepancy. When the extreme Mg/Ca and Sr/Ca values are omitted from this dataset, the remaining core top samples still show a large scatter of Mg/Ca and Sr/Ca.

8.1. Introduction

Today, the minor element to calcium ratios of biogenic carbonates form a major tool for reconstructing past marine environments. Especially the Mg/Ca and Sr/Ca ratios of planktonic foraminifera and coccolithophores are frequently applied in paleoceanography.

Foraminiferal Mg/Ca is widely applied to reconstruct the (calcification) temperature of seawater (e.g. Nürnberg 1995, 2000; Nürnberg *et al.*, 1996, 2000; Lea *et al.*, 1999; Mashiotta *et al.*, 1999; Elderfield & Ganssen, 2000; Dekens *et al.*, 2002). Other variables, however, can influence the temperature proxy signal. For instance seawater salinity (e.g. Nürnberg *et al.*, 1996; Lea *et al.*, 1999; Kisakürek *et al.*, 2008; Ferguson *et al.*, 2008; Dueñas-Bohórquez *et al.*, 2009), pH (e.g. Lea *et al.*, 1999) and carbonate ion concentration ($[CO_3^{2-}]$; e.g. Russell *et al.*, 2004), additionally affect planktonic foraminiferal Mg/Ca. The incorporation of Sr into planktonic foraminiferal calcite may also show a temperature dependence (e.g. Lea *et al.*, 1999; Reichart *et al.*, 2003; Mortyn *et al.*, 2005). Secondary factors can also largely influence the Sr/Ca ratios of planktonic foraminifera tests, such as seawater salinity (Lea *et al.*, 1999), carbonate ion concentration of the seawater ($[CO_3^{2-}]$; e.g. Lea *et al.*, 1999; Russell *et al.*, 2004; Mortyn *et al.*, 2005; Kisakürek *et al.*, 2008) and the carbonate saturation state of the seawater (Ω; Dueñas-Bohórquez *et al.*, 2009).

Since a decade, the Sr/Ca ratio of coccolith calcite has been applied as a proxy for reconstructing past coccolithophore growth rates and consequently reconstructing paleo-primary productivity. A main secondary factor affecting coccolith Sr/Ca ratios are changes in temperature (e.g. Stoll & Schrag, 2000; Stoll *et al.*, 2002a.b; Langer *et al.*, 2006). In analogy with foraminiferal Mg/Ca, Mg/Ca ratios of coccoliths are related to calcification temperature. However, since the Mg content in coccolith calcite is extremely low, there is an issue with the cleaning accuracy (mainly clay removal), thus hampering reliable Mg/Ca measurements (e.g. Stoll *et al.*, 2001).

In comparison to the extensive knowledge available about the elemental composition of foraminiferal and coccolithophorid calcite, very little is known about the minor element to calcium ratios of calcareous dinoflagellate cysts. The only published culture study on this topic revealed that the Sr/Ca ratios of one specific species, *Thoracosphaera heimii*, show a pronounced temperature sensitivity (0.016 mmol/mol $°C^{-1}$), and have the potential to serve as a sea surface temperature proxy (Gussone *et al.*, 2010). No clear temperature dependence was observed for Mg/Ca, except for a strong Mg enrichment at the highest culture temperature (30°C) (Gussone *et al.*, 2010).

Here, we investigate whether or not the observations of the culture experiment by Gussone *et al.* (2010) can be transferred to natural sediments. In this pilot study, we analyzed the elemental composition of *T. heimii* shells in 31 surface sediment samples from the equatorial and South Atlantic. For this purpose, a new cleaning protocol for the elemental analysis of *T. heimii* shells from sediments was developed, based on the cleaning method used for coccoliths, described by Bairbakesh *et al.* (1999) and Stoll & Ziveri (2002). Mg/Ca and Sr/Ca ratios were measured, and compared to several annual average values of several upper water column parameters. We are most interested in a possible correlation with temperature, but also salinity, total alkalinity, pH, the carbonate ion concentration of the seawater, nutrient concentrations and chlorophyll-*a* concentration are being considered. Furthermore, Mn/Ca, Fe/Ca and Si/Ca ratios were measured as a measure for sedimentary influences, i.e. most likely clay contamination.

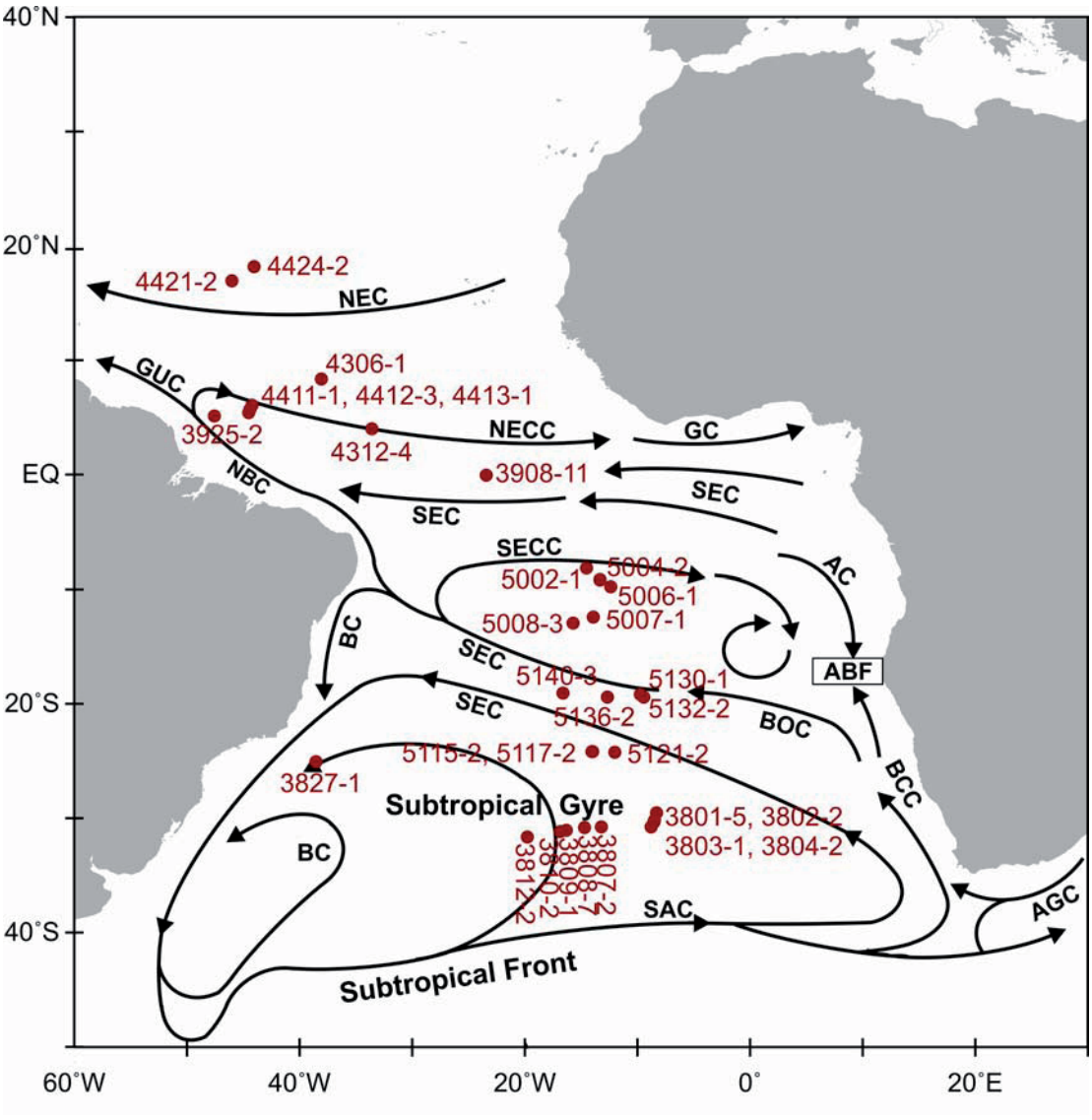

Fig. 8.1 - Surface circulation in the modern equatorial and South Atlantic and sample location

8.2. Surface circulation in the modern equatorial and South Atlantic

Here, we will only give a brief summary of the surface circulation in the South and equatorial Atlantic Ocean (Fig. 8.1). For a more detailed overview, see e.g. Peterson & Stramma (1991) and Wefer *et al.* (1996).

The dominant feature in the South Atlantic Ocean surface circulation is the anticyclonic Subtropical Gyre System, which is confined by the Benguela Coastal Current (BCC) in the east, the South Equatorial Current (SEC) in the north, the Brazil Current (BRC) in the west and the South Atlantic Current (SAC) in the south. The northward flowing BCC, which originates off the Cape of Good Hope, is fed primarily by the SAC but can also receive water from the Agulhas Current (AGC). Along the coast of Namibia, coastal upwelling is driven by the prevailing SE trade winds in the region, resulting in cold, low saline and nutrient-rich waters of the BCC. At around 20°S, the BCC is bending towards the NW, changing names to the Benguela Oceanic Current (BOC) and merging into the SEC, which exhibits increasing temperature and salinity and decreasing nutrient content from east to west. When the SEC reaches the eastern promontory of South America, a small part of the water turns southwards to form the Brazil Current (BRC), whereas the bulk of the flow contributes to the northward flowing North Brazil Current (NBC) and the reversing South Equatorial Counter Current (SECC). Through the BRC, relatively warm, saline and nutrient-poor surface water is transported along the coast of South America, back to the south. At around 40°S, the BRC collides with the cold and relatively fresh northward flowing Falkland Current (FC) and is deflected eastwards to coalesce into the SAC. The SAC is relatively warm compared to the cold, nutrient-rich and relatively fresh Antarctic Circumpolar Current (ACC), which is located more to the south. Both eastward flowing currents (SAC and ACC) are separated by the Subtropical Front.

Intermediate between the equatorial Atlantic and the Subtropical Gyre system, surface ocean circulation is characterized by a small cyclonic gyre circulation system which consists of the north-westward flowing BOC in the south, the eastward flowing SECC in the north and the southward flowing Angola Current (AC) in the east. Southeast of this gyre, the warm equatorial AC waters collide with the colder subtropical BCC waters, resulting in the Angola-Benguela Front (ABF).

In the equatorial Atlantic, surface waters are generally warm and the surface currents are mainly driven by the trade winds. During austral winter, i.e. the season of maximal SE trade wind activity, the SEC and the NBC are at their strongest. The intensification of the trade winds during this season also results in the formation of the eastward flowing North Equatorial Counter Current (NECC) and its continuation into the Guinea Current (GC). During austral summer, the SE trade winds are less intense, resulting in a weakening or even disappearing of the NECC. A northern branch of the SEC is sandwiched between the NECC and the SECC. Towards the Caribbean, the NBC joins the Guiana Current (GUC), both of which account for the net northward transport of surface water from the South Atlantic into the North Atlantic. North of the Equatorial Atlantic surface currents arrangement, nutrient-poor, relatively saline and cool waters, originating from the Canary Current, are transported into the tropics by the westward flowing North Equatorial Current (NEC).

Fig. 8.2 shows the location of the surface sediment samples in correlation to sea surface chlorophyll-*a* concentration (mg/m³). Highest chlorophyll-*a* concentrations occur around the equator and along the shores of the continents.

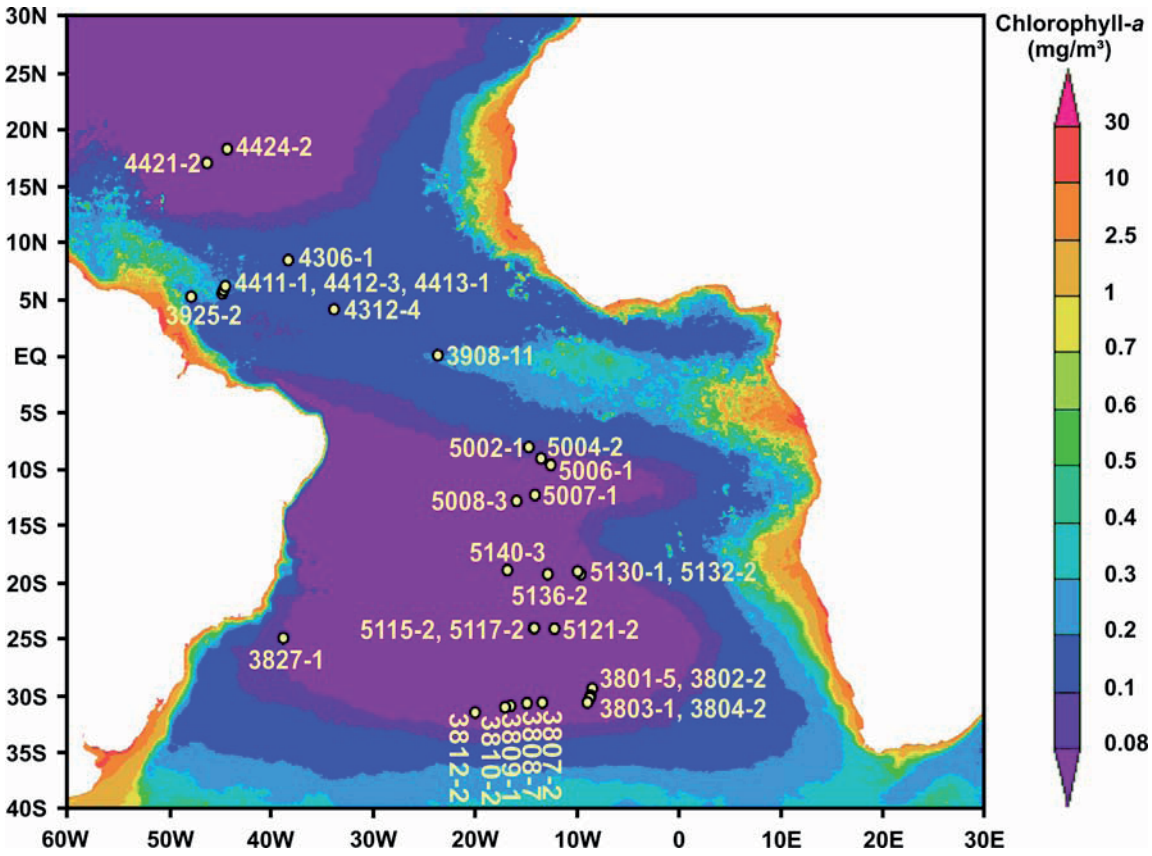

Fig. 8.2 – Sample locations plotted on sea surface chlorophyll-*a* concentration (mg/m³). Chlorophyll-*a* data are an average of monthly data between July 2001 and July 2011, on a 4kmx4km grid. Data is derived from the MODIS-Aqua database (http://gdata1.sci.gsfc.nasa.gov/daac-bin/G3/gui.cgi?instance_id=ocean_month)

8.3. Material and methods

Thirty-one surface sediment samples from the equatorial and South Atlantic Ocean were studied on the minor element to calcium ratios of *Thoracosphaera heimii* shells. Samples were collected by multicorer during several Meteor cruises (Table 8.1).

8.3.1. Sediment preparation and geochemical analysis

The new cleaning protocol for the preparation of calcareous *Thoracosphaera heimii* shells for elemental analysis is based on the cleaning method used for coccoliths described by Bairbakesh *et al.* (1999) and Stoll & Ziveri (2002). For a more detailed description of the method, we refer to Chapter 9 in this thesis. In summary, the protocol consists of six cleaning steps. (1) First, a mixture of bi-distilled water, H_2O_2 and NaClO was added to the sample allowing oxidation of the organic material and allowing disaggregation of the sediment particles. After 10 minutes, more NaClO was added to buffer the oxidation reaction and this was repeated three times. (2) Next, the sample was sieved through a 15 µm precision sieve in order to remove foraminifera and larger calcareous dinoflagellate species. (3) Then, a reductive solution (called "MNX") of bi-distilled water, ammonia and hydroxylamine hydrochloride was added and the sample was placed on a rotating carousel for 24 hours, causing gentle mechanical disaggregation. This reductive treatment removes Mn-Fe-oxide coatings which could have formed in the sediment. (4) After centrifuging and removing the MNX solution, a solution (called "IONX") of bi-distilled water and ammonia was added and again the sample was placed on a rotating carousel for 24 hours. The IONX solution allows an ion exchange reaction of the sample, during which adsorbed cations are removed from the shell wall, and brings the sample more effectively in suspension. (5) After the chemical treatment of the sediment, the sample was sieved through a 10 µm precision sieve and (6) the fraction between 10 and 15 µm was subjected to a series of settling and decanting steps in order to improve the size separation and the removal of coccolith.

The minor element to calcium ratios of the *T. heimii* shells were measured via inductively coupled plasma mass spectrometry (ICP-MS), on a Finnigan ELEMENT sector field instrument in the Department of Analytical Chemistry at the University of Oviedo (Spain). Ratios were measured in pulse-counting mode on dilute solutions (10 ppm Ca). Precision of the analysis is better than 0.4% relative standard deviation.

8.3.2. Upper water column parameters

To have the whole upper water column represented, environmental parameter data was collected for every 10m between 0 and 200m water depth. These values were separated into two values: a sea surface value (0m) and an average value over 200m water depth. Since the mixed layer depth (MLD) is the depth where highest abundances of *T. heimii* occur (Kohn & Zonneveld, 2010), environmental parameter values were also collected for the MLD. For an overview of the upper water column parameters, see Table 8.1.

The annually averaged mixed layer depth (DCM) was derived from the Monterey & Levitus (1997) database. This data collection contains monthly MLD fields on a global 1°x1° grid. The MLD fields are computed from climatological monthly mean profiles of potential temperature and potential density based on a temperature change from the ocean surface of 0.5°C. Interpolation of the MLD for the exact sample locations was done using Ocean Data View (Schlitzer, 2009).

Mean annual temperature (°C), salinity (psu), phosphate (µmol/l), nitrate (µmol/l) and silicate (µmol/l) values were derived from the World Ocean Atlas 2009 (WOA09; http://www.nodc.noaa.gov/OC5/WOA09/pr_woa09.html; Locarnini *et al.*, 2010; Antonov *et al.*, 2010; Garcia *et al.*, 2010). This database contains monthly, seasonal and annual hydrographical data on a global 1°x1° grid. Using Ocean Data View (Schlitzer, 2009), the WOA09 data were interpolated for the exact sample locations, at the desired depths.

Furthermore, total alkalinity (TALK; µmol/kg), total dissolved inorganic carbon (TCO_2; µmol/kg), pH and carbonate ion concentration ($[CO_3^{2-}]$; µmol/kg) values were derived from the Goyet *et al.* (2000) database. This database contains annual mean estimated values of global total alkalinity and total dissolved inorganic carbon, on a 1°x1° grid for the global ocean between 66.5°S and 66.5°N. pH and $[CO_3^{2-}]$ are derived variables in this dataset. Using Ocean Data View (Schlitzer, 2009), the data were interpolated for the exact sample locations, at the desired depths.

Sea surface chlorophyll-*a* concentrations (mg/m^3) were derived from the MODIS-Aqua database on the Giovanni website (http://gdata1.sci.gsfc.nasa.gov/daac-bin/G3/gui.cgi?instance_id =ocean_month). The derived values are an average of monthly data between July 2001 and July 2011, on a 4kmx4km grid.

Sample GeoB	*	Lat (°N)	Lon (°E)	Water depth (m)	Chlorophyll (mg/m³)	SST (°C)	SSS (psu)	TALK (µmol/kg)	TCO_2 (µmol/kg)	pH	$[CO_3^{2-}]$ (µmol/kg)	Phosphate (µmol/l)	Nitrate (µmol/l)	Silicate (µmol/l)
3801-5 ●	1	-29.51	-8.3	4545	0.0582	20.58	35.98	2346.32	2026.41	8.15	224.48	0.2169	0.1001	1.9010
3802-2 ●	2	-30.16	-8.51	3970	0.0613	20.31	35.93	2343.71	2026.79	8.14	222.37	0.2193	0.1037	1.8940
3803-1 ●	3	-30.35	-8.57	4173	0.0618	20.23	35.91	2342.92	2026.91	8.14	221.72	0.2202	0.1052	1.8897
3804-2 ●	4	-30.74	-8.77	3882	0.0654	20.06	35.88	2341.23	2027.10	8.14	220.40	0.2229	0.1103	1.8758
3807-2 ●	5	-30.75	-13.2	2534	0.0625	20.32	35.91	2340.06	2023.04	8.15	222.50	0.2313	0.0748	1.6455
3808-7 ●	6	-30.81	-14.71	3213	0.0594	20.37	35.90	2338.95	2022.70	8.14	222.03	0.2305	0.0719	1.5806
3809-1 ●	7	-31.05	-16.33	3470	0.0562	20.30	35.88	2336.09	2022.88	8.14	220.03	0.2277	0.0750	1.5112
3810-2 ●	8	-31.13	-16.84	3810	0.0578	20.28	35.87	2335.16	2023.02	8.14	219.32	0.2263	0.0769	1.4892
3812-2 ●	9	-31.62	-19.76	4204	0.0625	20.10	35.82	2330.44	2024.26	8.13	215.23	0.2135	0.0951	1.3522
3827-1 ●	10	-25.03	-38.55	3842	0.0787	23.99	36.52	2375.44	2040.49	8.10	235.39	0.1240	0.9650	2.1293
3908-11 ●	11	-0.01	-23.43	3693	0.2070	26.83	35.75	2308.61	1990.33	8.04	224.42	0.1147	0.2046	1.5041
3925-2 ●	12	5.14	-47.53	3198	0.1852	27.48	35.10	2262.11	1901.48	8.11	251.43	0.1733	0.3943	3.8344
4306-1 ●	13	8.39	-38.03	3766	0.1230	27.01	35.76	2246.27	1944.86	8.01	213.64	0.0674	0.2551	1.7884
4312-4 ●	14	4.05	-33.59	3437	0.1203	27.39	35.67	2290.36	1942.19	8.08	243.64	0.0815	0.2896	1.7945
4411-1 ●	15	5.43	-44.5	3300	0.1827	27.44	35.47	2287.44	1933.11	8.08	245.92	0.1454	0.3157	2.8293
4412-3 ●	16	5.72	-44.36	3767	0.2152	27.43	35.49	2285.36	1935.21	8.08	243.42	0.1389	0.2992	2.7808
4413-1 ●	17	6.09	-44.19	4295	0.2251	27.41	35.50	2281.37	1937.00	8.07	239.92	0.1307	0.2815	2.7213
4421-2 ●	18	16.99	-46.01	3176	0.0525	25.97	36.62	2339.92	2001.22	8.05	237.29	0.0554	0.1207	1.4347
4424-2 ●	19	18.2	-44.02	4779	0.0507	25.64	36.83	2351.86	2016.39	8.05	235.69	0.0507	0.1054	1.2752
5002-1 ●	20	-8.14	-14.54	2851	0.1010	25.65	36.18	2321.20	2015.81	8.04	216.74	0.1472	0.1774	1.3731
5004-2 ●	21	-9.17	-13.34	2790	0.0860	25.35	36.26	2327.24	2026.64	8.04	213.92	0.1511	0.1779	1.3513
5006-1 ●	22	-9.76	-12.37	3244	0.0748	25.12	36.31	2332.02	2033.13	8.04	212.85	0.1548	0.1860	1.3348
5007-1 ●	23	-12.39	-13.94	3668	0.0603	24.59	36.58	2363.48	2046.13	8.06	225.32	0.1573	0.1581	1.3108
5008-3 ●	24	-12.93	-15.69	3407	0.0581	24.67	36.65	2374.43	2046.25	8.08	232.28	0.1574	0.1414	1.3197
5115-2 ●	25	-24.14	-14.04	3291	0.0430	22.83	36.48	2382.51	2026.01	8.16	250.00	0.2249	0.1036	1.3258
5117-2 ●	26	-24.15	-13.97	3039	0.0432	22.82	36.48	2382.29	2026.08	8.16	249.80	0.2251	0.1038	1.3297
5121-2 ●	27	-24.18	-12.02	3486	0.0446	22.57	36.42	2377.54	2026.85	8.15	245.93	0.2296	0.1166	1.4221
5130-1 ●	28	-19.4	-9.46	3166	0.0684	22.70	36.50	2379.29	2016.89	8.17	253.83	0.2497	0.2876	1.2197
5132-2 ●	29	-19.13	-9.72	3941	0.0679	22.76	36.51	2381.24	2018.56	8.16	254.09	0.2473	0.2848	1.2050
5136-2 ●	30	-19.37	-12.67	3227	0.0562	23.17	36.61	2391.26	2017.14	8.17	262.03	0.2321	0.1855	1.1267
5140-3 ●	31	-19.05	-16.61	3660	0.0464	23.77	36.76	2408.46	1998.42	8.21	285.93	0.2149	0.1427	1.0616

Table 8.1 (start) – Upper water column parameters at sea surface – FIRST COLUMN: Blue dots (●) = samples with high to extreme Mg/Ca ratios; samples in the Amazon Fan Area – Green dots (●) = samples with high to extreme Sr/Ca ratios; samples in the centre of the Subtropical Gyre – Orange dots (●) = other samples – SECOND COLUMN: * refers to sample numbers in PCA (Fig. 8.3)

Sample GeoB	*	Lat (°N)	Lon (°E)	Water depth (m)	Mixed layer depth (m) - AA	Temperature (°C)	Salinity (psu)	TALK (µmol/kg)	TCO_2 (µmol/kg)	pH	$[CO_3^{2-}]$ (µmol/kg)	Phosphate (µmol/l)	Nitrate (µmol/l)	Silicate (µmol/l)
3801-5 ●	1	-29.51	-8.3	4545	48.83	19.56	35.97	2346.77	2032.52	8.15	220.49	0.1985	0.1807	1.9314
3802-2 ●	2	-30.16	-8.51	3970	45.27	19.41	35.92	2344.43	2032.50	8.15	218.90	0.1999	0.1955	1.9231
3803-1 ●	3	-30.35	-8.57	4173	44.72	19.35	35.91	2343.70	2032.65	8.15	218.30	0.2006	0.2028	1.9178
3804-2 ●	4	-30.74	-8.77	3882	43.06	19.24	35.88	2342.42	2032.77	8.15	217.35	0.2034	0.2173	1.8982
3807-2 ●	5	-30.75	-13.2	2534	41.30	19.52	35.89	2345.15	2029.62	8.15	221.33	0.1957	0.1878	1.5262
3808-7 ●	6	-30.81	-14.71	3213	42.68	19.47	35.88	2345.91	2029.96	8.15	221.62	0.1912	0.1921	1.4429
3809-1 ●	7	-31.05	-16.33	3470	46.23	19.27	35.86	2344.85	2031.70	8.15	219.73	0.1901	0.2226	1.3687
3810-2 ●	8	-31.13	-16.84	3810	45.89	19.26	35.85	2344.21	2031.70	8.15	219.61	0.1893	0.2208	1.3462
3812-2 ●	9	-31.62	-19.76	4204	42.47	19.26	35.83	2339.17	2031.47	8.14	216.08	0.1823	0.1932	1.2335
3827-1 ●	10	-25.03	-38.55	3842	46.29	23.36	36.68	2385.85	2049.92	8.11	236.69	0.1330	1.1298	2.4122
3908-11 ●	11	-0.01	-23.43	3693	38.29	25.76	35.95	2317.11	2013.16	8.02	215.77	0.1898	1.5776	2.1126
3925-2 ●	12	5.14	-47.53	3198	43.02	26.90	36.07	2330.74	2002.23	8.05	232.16	0.1718	0.5755	2.0949
4306-1 ●	13	8.39	-38.03	3766	39.86	26.03	36.06	2296.32	1977.60	8.05	224.31	0.0968	1.2798	1.9027
4312-4 ●	14	4.05	-33.59	3437	49.16	26.16	35.93	2310.21	1975.63	8.06	235.32	0.1736	1.7447	2.3736
4411-1 ●	15	5.43	-44.5	3300	46.46	26.68	36.07	2324.43	1992.59	8.06	233.90	0.1692	0.7914	2.0053
4412-3 ●	16	5.72	-44.36	3767	46.25	26.64	36.07	2323.66	1991.72	8.06	233.93	0.1635	0.8030	1.9807
4413-1 ●	17	6.09	-44.19	4295	45.44	26.60	36.07	2322.01	1990.12	8.06	233.81	0.1541	0.7849	1.9417
4421-2 ●	18	16.99	-46.01	3176	64.62	25.20	36.96	2377.03	2027.37	8.08	246.06	0.0827	0.7529	0.9715
4424-2 ●	19	18.2	-44.02	4779	62.74	24.86	37.07	2381.11	2037.28	8.07	242.31	0.0752	0.6656	0.8887
5002-1 ●	20	-8.14	-14.54	2851	50.61	24.68	36.29	2327.90	2035.01	8.03	208.17	0.1876	1.4667	1.9251
5004-2 ●	21	-9.17	-13.34	2790	50.13	24.56	36.37	2336.14	2042.60	8.03	208.70	0.1737	1.3083	1.8236
5006-1 ●	22	-9.76	-12.37	3244	50.44	24.32	36.42	2342.59	2048.70	8.03	209.00	0.1773	1.3525	1.8173
5007-1 ●	23	-12.39	-13.94	3668	42.89	24.11	36.65	2374.51	2054.11	8.07	226.86	0.1692	0.3570	1.3723
5008-3 ●	24	-12.93	-15.69	3407	41.32	24.24	36.71	2383.05	2052.96	8.08	233.42	0.1648	0.2276	1.2952
5115-2 ●	25	-24.14	-14.04	3291	24.07	22.56	36.49	2386.79	2026.25	8.17	252.58	0.2165	0.0893	1.2888
5117-2 ●	26	-24.15	-13.97	3039	24.04	22.55	36.49	2386.53	2026.33	8.17	252.35	0.2169	0.0895	1.2926
5121-2 ●	27	-24.18	-12.02	3486	27.25	22.26	36.44	2380.89	2026.93	8.17	248.02	0.2237	0.1019	1.3958
5130-1 ●	28	-19.4	-9.46	3166	35.41	22.24	36.49	2380.38	2016.02	8.17	254.94	0.2434	0.3153	1.2888
5132-2 ●	29	-19.13	-9.72	3941	37.18	22.27	36.50	2382.55	2018.23	8.17	254.99	0.2420	0.3199	1.2813
5136-2 ●	30	-19.37	-12.67	3227	35.23	22.77	36.61	2393.40	2018.80	8.18	262.17	0.2327	0.1771	1.1630
5140-3 ●	31	-19.05	-16.61	3660	47.50	23.11	36.73	2411.50	1999.00	8.22	287.56	0.2129	0.1270	1.0942

Table 8.1 (continued) – Upper water column parameters at mixed layer depth – FIRST COLUMN: Blue dots (●) = samples with high to extreme Mg/Ca ratios; samples in the Amazon Fan Area – Green dots (●) = samples with high to extreme Sr/Ca ratios; samples in the centre of the Subtropical Gyre – Orange dots (●) = other samples – SECOND COLUMN: * refers to sample numbers in PCA (Fig. 8.3)

Sample GeoB	*	Lat (°N)	Lon (°E)	Water depth (m)	Temperature (°C)	Salinity (psu)	TALK (µmol/kg)	TCO_2 (µmol/kg)	pH	$[CO_3^{2-}]$ (µmol/kg)	Phosphate (µmol/l)	Nitrate (µmol/l)	Silicate (µmol/l)
3801-5 ●	1	-29.51	-8.3	4545	17.81	35.76	2339.04	2050.95	8.12	203.09	0.2912	1.3810	2.2335
3802-2 ●	2	-30.16	-8.51	3970	17.59	35.72	2337.62	2052.17	8.12	201.28	0.2944	1.4390	2.2174
3803-1 ●	3	-30.35	-8.57	4173	17.52	35.71	2337.20	2052.53	8.12	200.74	0.2957	1.4593	2.2105
3804-2 ●	4	-30.74	-8.77	3882	17.39	35.69	2336.53	2053.28	8.12	199.77	0.2994	1.5079	2.1921
3807-2 ●	5	-30.75	-13.2	2534	17.58	35.72	2339.09	2051.81	8.12	202.48	0.2880	1.3799	1.8580
3808-7 ●	6	-30.81	-14.71	3213	17.62	35.73	2340.00	2051.77	8.13	203.11	0.2853	1.3663	1.7836
3809-1 ●	7	-31.05	-16.33	3470	17.58	35.72	2339.84	2052.22	8.13	202.69	0.2851	1.3986	1.7165
3810-2 ●	8	-31.13	-16.84	3810	17.57	35.72	2339.66	2052.39	8.13	202.45	0.2851	1.4117	1.6968
3812-2 ●	9	-31.62	-19.76	4204	17.47	35.70	2337.60	2053.59	8.12	200.26	0.2839	1.5094	1.5885
3827-1 ●	10	-25.03	-38.55	3842	20.82	36.34	2369.23	2063.29	8.09	216.18	0.2187	1.7830	2.5948
3908-11 ●	11	-0.01	-23.43	3693	19.13	35.66	2324.42	2102.10	7.96	162.78	0.7972	11.3785	5.2738
3925-2 ●	12	5.14	-47.53	3198	21.83	35.86	2331.92	2062.40	8.01	193.07	0.5407	6.6994	4.4213
4306-1 ●	13	8.39	-38.03	3766	19.28	35.72	2310.23	2079.81	7.98	167.69	0.7309	11.4481	5.3613
4312-4 ●	14	4.05	-33.59	3437	19.99	35.66	2318.64	2066.31	8.00	181.86	0.7078	10.2649	5.1138
4411-1 ●	15	5.43	-44.5	3300	21.26	35.82	2326.77	2062.70	8.01	189.36	0.5750	7.7124	4.5565
4412-3 ●	16	5.72	-44.36	3767	21.14	35.81	2326.07	2063.92	8.01	188.12	0.5821	7.9470	4.6043
4413-1 ●	17	6.09	-44.19	4295	20.97	35.81	2325.02	2065.57	8.01	186.38	0.5914	8.2496	4.6676
4421-2 ●	18	16.99	-46.01	3176	23.01	36.84	2380.78	2062.82	8.06	224.79	0.2045	3.0189	1.7431
4424-2 ●	19	18.2	-44.02	4779	22.86	36.94	2386.08	2068.42	8.06	224.70	0.1812	2.6133	1.5054
5002-1 ●	20	-8.14	-14.54	2851	19.55	35.89	2327.22	2104.91	7.95	163.45	0.7459	10.1447	4.5537
5004-2 ●	21	-9.17	-13.34	2790	19.54	35.94	2332.88	2107.28	7.96	165.58	0.7251	9.9706	4.3865
5006-1 ●	22	-9.76	-12.37	3244	19.43	35.95	2336.53	2109.56	7.96	166.45	0.7207	10.0232	4.3522
5007-1 ●	23	-12.39	-13.94	3668	20.06	36.18	2359.26	2099.59	8.01	187.41	0.5590	6.9652	3.1871
5008-3 ●	24	-12.93	-15.69	3407	20.49	36.27	2365.24	2092.71	8.03	195.66	0.5008	5.7184	2.7849
5115-2 ●	25	-24.14	-14.04	3291	19.87	36.16	2374.14	2043.40	8.15	232.18	0.2863	1.0249	1.6635
5117-2 ●	26	-24.15	-13.97	3039	19.86	36.15	2373.89	2043.47	8.15	231.97	0.2866	1.0280	1.6686
5121-2 ●	27	-24.18	-12.02	3486	19.62	36.11	2368.11	2044.09	8.14	227.61	0.2980	1.1568	1.8125
5130-1 ●	28	-19.4	-9.46	3166	19.57	36.13	2366.51	2043.69	8.14	227.18	0.4111	3.2241	2.1858
5132-2 ●	29	-19.13	-9.72	3941	19.61	36.14	2367.82	2045.89	8.13	226.68	0.4138	3.3315	2.1907
5136-2 ●	30	-19.37	-12.67	3227	20.16	36.25	2376.29	2040.77	8.14	235.79	0.3638	2.4377	1.8505
5140-3 ●	31	-19.05	-16.61	3660	20.88	36.40	2389.53	2022.03	8.18	254.48	0.3302	1.8657	1.5982

Table 8.1 (end) – Upper water column parameters averaged over 200m water depth – FIRST COLUMN: Blue dots (●) = samples with high to extreme Mg/Ca ratios; samples in the Amazon Fan Area – Green dots (●) = samples with high to extreme Sr/Ca ratios; samples in the centre of the Subtropical Gyre – Orange dots (●) = other samples – SECOND COLUMN: * refers to sample numbers in PCA (Fig. 8.3)

8.3.3. Statistical methods

Within the performed statistical analyses, the minor element to calcium ratios of the *T. heimii* shells (Mg/Ca, Sr/Ca, Mn/Ca, Fe/Ca and Si/Ca) are considered as five different species. Thus every sample has five species values.

To determine the relationship between target oceanographic parameters and the minor element to calcium ratios of the *T. heimii* calcite, a Detrended Correspondence Analysis (DCA) was performed with CANOCO for Windows version 4.5 (ter Braak & Smilauer, 1998). The current dataset is characterized by a linear relationship between the minor element to calcium ratios and the arbitrary environmental gradients of the DCA, i.e. the minor element to calcium ratios appear to react linearly to changing environmental gradients (e.g. Jongman *et al.*, 1987; Richter *et al.*, 2007; Holzwarth *et al.*, 2010).

Based on the outcome of the initial DCA, a Principal Component Analysis (PCA) and a Redundancy Analysis (RDA) were carried out (also with CANOCO 4.5) to determine potential relationships between the minor element to calcium ratios of the *T. heimii* shells in the sediment and several environmental parameters in the water column. RDA was performed with environmental variable values at sea surface and at mixed layer depth, as well as with an average value over 200m water depth. The data were not transformed.

For the RDA, the ranking of the environmental variables (i.e. the importance of their influence on the distribution of the minor element to calcium ratios) and the detection of co-variance between the environmental parameters is based on the principle of forward selection. Marginal effects represent the amount of variance explained by that variable, uncorrected for possible co-variance; conditional effects represent the amount of variance explained by that particular variable only, after the elimination of co-variance (e.g. Richter *et al.*, 2007; Holzwarth *et al.*, 2010). The significance of each environmental variable was calculated by a Monte Carlo permutation test with 9999 permutations at and above the 5% significance level ($P \leq 0.05$). These tests lower the risk of potential overrepresentation of insignificant variables in the dataset (Richter *et al.*, 2007).

For details on the interpretation of RDA diagrams, we refer to e.g. Jongman *et al.* (1987), Richter *et al.* (2007) and Holzwarth *et al.* (2010). In general: minor element to calcium ratio lines pointing in the same direction indicate that these ratios are positively correlated with each other, i.e. that they are influenced by the same environmental parameters. Lines pointing in opposite directions indicate a negative correlation and perpendicular lines indicate lack of correlation.

8.4. Results

8.4.1. Elemental composition of *T. heimii* calcite in sediments

The minor element to calcium ratios of the *T. heimii* shells are summarized in Table 8.2. Measured Sr/Ca values range between 1.51 and 22.46 mmol/mol, measured Mg/Ca values range between 5.50 and 23.14 mmol/mol, measured Fe/Ca values range between 0.014 and 0.473 mmol/mol, measured Mn/Ca ratios range between 0.021 and 0.921 mmol/mol and measured Si/Ca ratios range between 0.094 and 2.974 mmol/mol.

Sample GeoB	*	Meteor Cruise	Lat (°N)	Lon (°E)	Water depth (m)	Sr/Ca (mmol/mol)	Mg/Ca (mmol/mol)	Fe/Ca (mmol/mol)	Mn/Ca (mmol/mol)	Si/Ca (mmol/mol)
3801-5 ●	1	M34-3	-29.51	-8.30	4545	1.85	9.56	0.185	0.236	0.716
3802-2 ●	2	M34-3	-30.16	-8.51	3970	1.99	6.84	0.083	0.191	0.456
3803-1 ●	3	M34-3	-30.35	-8.57	4173	1.78	7.44	0.237	0.167	0.497
3804-2 ●	4	M34-3	-30.74	-8.77	3882	1.91	5.80	0.146	0.117	0.287
3807-2 ●	5	M34-3	-30.75	-13.20	2534	6.36	6.56	0.151	0.149	0.320
3808-7 ●	6	M34-3	-30.81	-14.71	3213	4.01	6.73	0.108	0.194	0.355
3809-1 ●	7	M34-3	-31.05	-16.33	3470	2.75	6.90	0.149	0.190	0.435
3810-2 ●	8	M34-3	-31.13	-16.84	3810	1.96	7.59	0.228	0.195	0.470
3812-2 ●	9	M34-3	-31.62	-19.76	4204	1.87	7.60	0.228	0.251	0.786
3827-1 ●	10	M34-3	-25.03	-38.55	3842	1.53	19.29	0.162	0.921	2.184
3908-11 ●	11	M34-4	-0.01	-23.43	3693	1.61	5.50	0.057	0.049	0.388
3925-2 ●	12	M34-4	5.14	-47.53	3198	5.41	23.14	0.473	0.469	2.974
4306-1 ●	13	M38-1	8.39	-38.03	3766	1.62	17.25	0.120	0.237	1.083
4312-4 ●	14	M38-1	4.05	-33.59	3437	1.95	8.82	0.062	0.182	0.544
4411-1 ●	15	M38-2	5.43	-44.50	3300	7.23	13.77	0.158	0.176	0.940
4412-3 ●	16	M38-2	5.72	-44.36	3767	2.63	11.45	0.118	0.193	0.848
4413-1 ●	17	M38-2	6.09	-44.19	4295	1.64	20.42	0.242	0.442	1.811
4421-2 ●	18	M38-2	16.99	-46.01	3176	11.32	14.04	0.060	0.272	0.604
4424-2 ●	19	M38-2	18.20	-44.02	4779	1.51	8.95	0.014	0.214	0.611
5002-1 ●	20	M41-2	-8.14	-14.54	2851	2.90	10.35	0.114	0.046	1.113
5004-2 ●	21	M41-2	-9.17	-13.34	2790	3.47	6.93	0.096	0.051	0.580
5006-1 ●	22	M41-2	-9.76	-12.37	3244	4.68	10.97	0.279	0.099	2.909
5007-1 ●	23	M41-2	-12.39	-13.94	3668	5.34	7.27	0.119	0.082	0.181
5008-3 ●	24	M41-2	-12.93	-15.69	3407	12.08	5.51	0.038	0.021	0.094
5115-2 ●	25	M41-3	-24.14	-14.04	3291	22.46	7.90	0.124	0.155	0.227
5117-2 ●	26	M41-3	-24.15	-13.97	3039	13.28	8.78	0.098	0.171	0.281
5121-2 ●	27	M41-3	-24.18	-12.02	3486	7.12	6.20	0.059	0.132	0.142
5130-1 ●	28	M41-3	-19.40	-9.46	3166	1.86	6.92	0.192	0.121	0.268
5132-2 ●	29	M41-3	-19.13	-9.72	3941	3.31	6.31	0.129	0.059	0.133
5136-2 ●	30	M41-3	-19.37	-12.67	3227	16.28	8.76	0.183	0.130	0.219
5140-3 ●	31	M41-3	-19.05	-16.61	3660	9.44	7.13	0.073	0.107	0.141

Table 8.1 – Measured minor element to calcium ratios for *T. heimii* shells from 31 surface sediments in the South and equatorial Atlantic – FIRST COLUMN: Blue dots (●) = samples with high to extreme Mg/Ca ratios; samples in the Amazon Fan Area – Green dots (●) = samples with high to extreme Sr/Ca ratios; samples in the centre of the Subtropical Gyre – Orange dots (●) = other samples – SECOND COLUMN: * refers to sample numbers in PCA (Fig. 8.3)

PCA (Fig. 8.3) reveals two groups of minor element to calcium ratios: Sr/Ca is ordinated perpendicular to Mg/Ca, Fe/Ca, Mn/Ca and Si/Ca, which are ordinated in the same direction. When the different minor element to calcium ratios are compared to each other, we observe a weak correlation between Mg/Ca and Fe/Ca ($R^2 = 0.28$), a slightly stronger correlation between Mg/Ca and Mn/Ca ($R^2 = 0.56$) and a rather high correlation between Mg/Ca and Si/Ca ($R^2 = 0.63$) (no figure). No correlation was observed between Sr/Ca and Fe/Ca, between Sr/Ca and Mn/Ca or between Sr/Ca and Si/Ca (no figure).

Also based on PCA (Fig. 8.3), and in combination with distribution maps of the minor element to calcium ratios (Fig. 8.4), three sample groups (●, ● and ●), with a different elemental composition can be observed. Samples GeoB 3925-2, 4306-1, 4411-1, 4412-3 and 4413-1 show high to extreme Mg/Ca ratios (11.45-23.14 mmol/mol; ● 12, 13, 15, 16 and 17 in Fig. 8.3). These samples generally occur offshore NE Brasil, i.e. in the Amazon Fan area (Fig. 8.4, 8.7). Sample GeoB 3827-1 (● 10 in Fig. 8.3) also shows high Mg/Ca ratios, but is not located in the Amazon Fan area (Fig. 8.4). Samples GeoB 5008-3, 5115-2, 5117-2, 5121-2, 5136-2 and 5140-3 show high to extreme Sr/Ca ratios (7.12-22.46 mmol/mol; ● 24, 25, 26, 27, 30 and 31 in Fig. 8.3). These samples generally occur in the central area of the South Atlantic, i.e. in the central area of the Subtropical Gyre (Fig. 8.4, 8.1). The remainder of the samples show low to intermediate Mg/Ca and Sr/Ca ratios (● in Fig. 8.3) and are not located in a specific hydrographical area (Fig. 8.4).

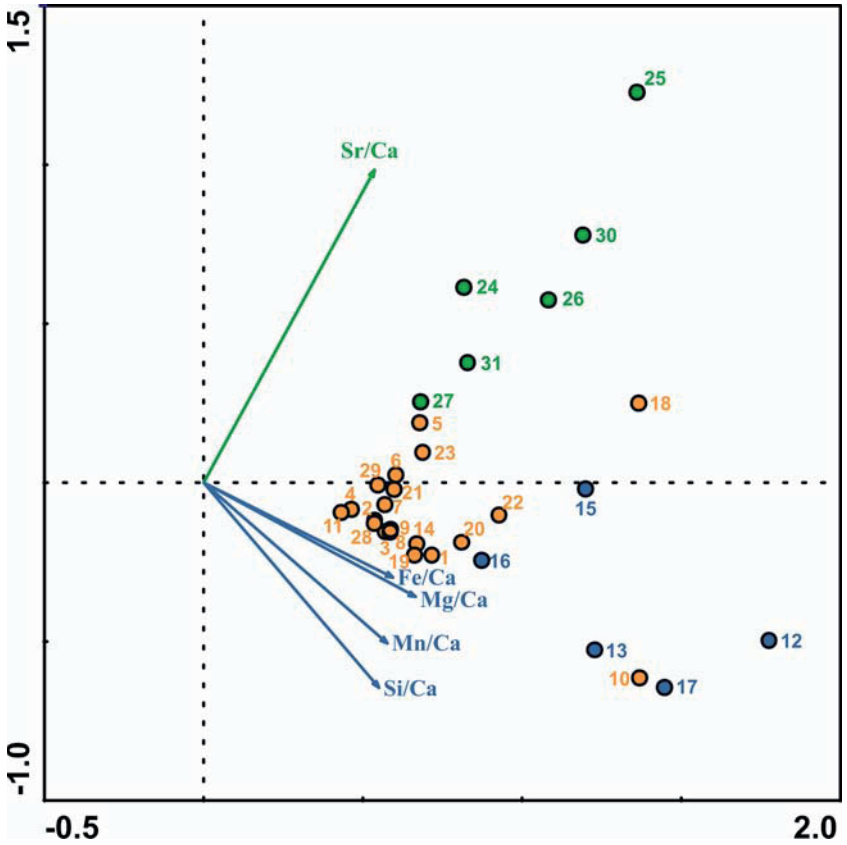

Fig. 8.3 – PCA on the minor element to calcium ratios for *T. heimii* shells from 31 surface sediment samples in the equatorial and South Atlantic – Blue dots (●) = samples with high to extreme Mg/Ca ratios; samples in the Amazon Fan area – Green dots (●) = samples with high to extreme Sr/Ca ratios; samples in the central area of the Subtropical Gyre – Orange dots (●) = other samples

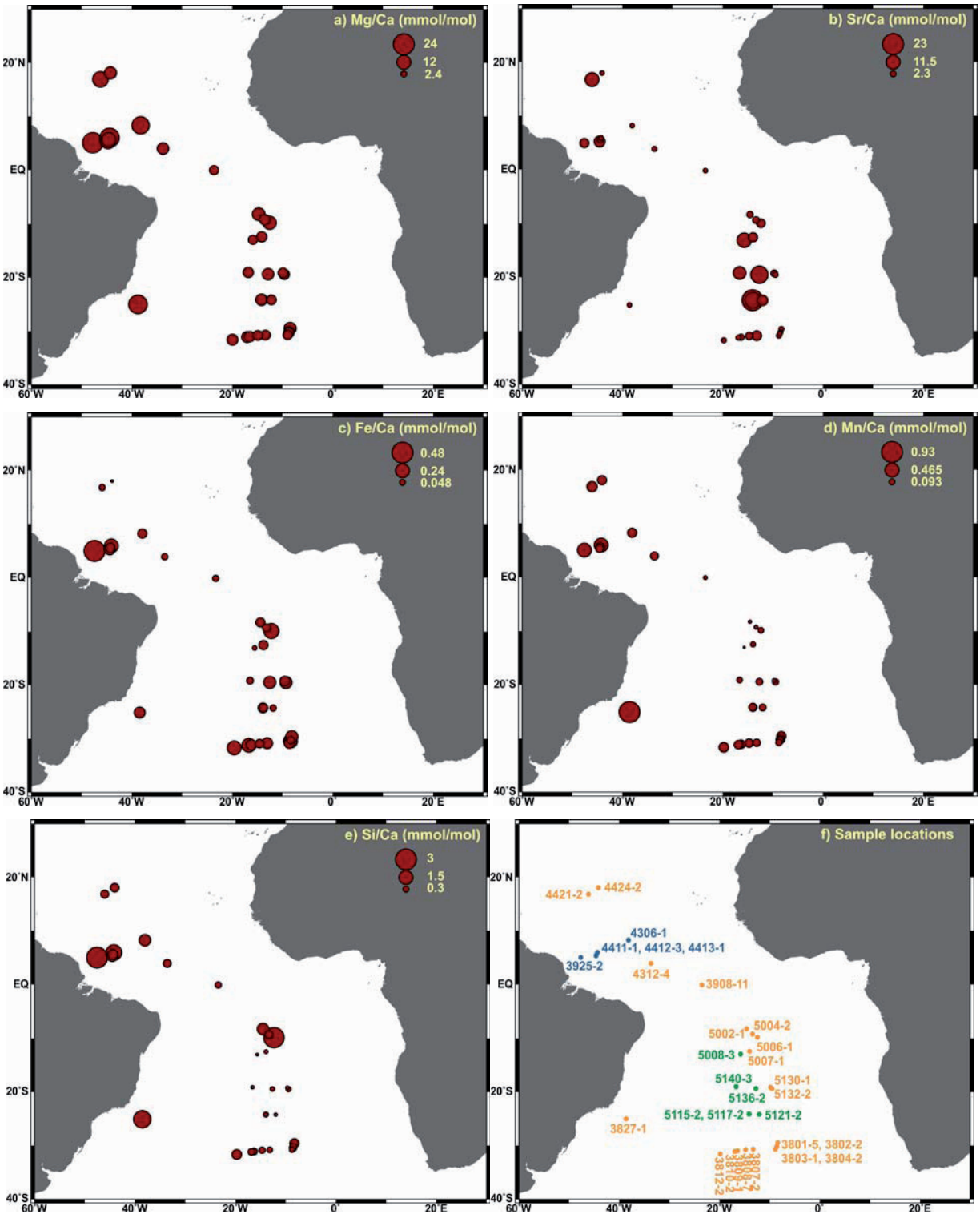

Fig. 8.4 – Geographical distribution maps of a) Mg/Ca, b) Sr/Ca, c) Fe/Ca, d) Mn/C and e) Si/Ca ratios in *T. heimii* shells from surface sediment samples in the equatorial and South Atlantic – Blue dots (●) = samples with high to extreme Mg/Ca ratios; samples in the Amazon Fan area – Green dots (●) = samples with high to extreme Sr/Ca ratios; samples in the central area of the Subtropical Gyre – Orange dots (●) = other samples

a) RDA for environmental paramaters at sea surface (SURF)					
Marginal effects		**Conditional effects**			
Uncorrected for covariance		**Corrected for covariance**			
Name of variable in RDA	**Lambda l**	**Name of variable in RDA**	**Lambda A**	**P value**	**F value**
Silicate	**0.27**	**Silicate**	**0.27**	**0.000**	**10.90**
TALK	**0.26**	**$[CO_3^{2-}]$**	**0.14**	**0.006**	**6.59**
TCO_2	**0.20**	**Nitrate**	**0.08**	**0.034**	**4.20**
Nitrate	**0.20**	SSS	0.05	0.086	2.60
Chlor-*a*	**0.19**	TCO_2	0.05	0.054	3.21
SSS	**0.17**	SST	0.03	0.152	1.97
SST	**0.15**	Chlor-*a*	0.04	0.116	2.41
$[CO_3^{2-}]$	0.14	pH	0.01	0.512	0.63
Phosphate	0.12	TALK	0.00	0.706	0.30
pH	0.11	Phosphate	0.00	0.847	0.15

b) RDA for environmental parameters at mixed layer depth (MLD)					
Marginal effects		**Conditional effects**			
Uncorrected for covariance		**Corrected for covariance**			
Name of variable in RDA	**Lambda l**	**Name of variable in RDA**	**Lambda A**	**P value**	**F value**
TALK	**0.21**	**TALK**	**0.21**	**0.00**	**7.79**
Silicate	**0.20**	**Temperature**	**0.14**	**0.00**	**6.21**
$[CO_3^{2-}]$	**0.16**	**MLD AA**	**0.08**	**0.04**	**3.44**
Temperature	**0.15**	Silicate	0.05	0.10	2.51
Phosphate	0.14	Phosphate	0.05	0.08	2.55
pH	0.14	Nitrate	0.04	0.09	2.53
Nitrate	0.13	pH	0.01	0.55	0.60
MLD AA	0.13	TCO_2	0.03	0.29	1.30
Salinity	0.11	Salinity	0.02	0.35	1.11
TCO_2	0.07	$[CO_3^{2-}]$	0.00	0.93	0.08

c) RDA for environmental parameters averaged over 200m water depth (200m)					
Marginal effects		**Conditional effects**			
Uncorrected for covariance		**Corrected for covariance**			
Name of variable in RDA	**Lambda l**	**Name of variable in RDA**	**Lambda A**	**P value**	**F value**
TALK	**0.20**	**TALK**	**0.20**	**0.001**	**7.07**
Temperature	**0.17**	**Temperature**	**0.19**	**0.000**	**9.18**
$[CO_3^{2-}]$	**0.15**	Phosphate	0.07	0.052	3.02
Silicate	**0.15**	Salinity	0.05	0.054	3.12
pH	0.11	Silicate	0.05	0.103	2.46
Salinity	0.10	TCO_2	0.00	0.676	0.37
Nitrate	0.08	pH	0.04	0.159	1.85
Phosphate	0.05	$[CO_3^{2-}]$	0.01	0.352	1.01
TCO_2	0.04	Nitrate	0.01	0.814	0.21

Table 8.2 – Percentage of variance explained by environmental variables used in the Redundancy Analyses (RDA) for (a) sea surface conditions, (b) mixed layer depth conditions, (c) conditions average over 200m water depth – Chlor-*a* = chlorophyll-*a* concentration, SST = sea surface temperature, SSS = sea surface salinity, TALK = total alkalinity, TCO_2 = total dissolved inorganic carbon; $[CO_3^{2-}]$ = carbonate ion concentration; MLD AA = annual average mixed layer depth (see Table 1 for units) – Marginal effects: bold variables in grey relate to more than 15% of the variance in the minor element to calcium ratios (Lambda l ≥ 0.15) – Conditional effects: Bold variables in grey are significant at the 5% significance level (P ≤ 0.05).

8.4.2. Relation with upper water column parameters

For sea surface conditions, the RDA reveals that the gradients silicate, total alkalinity (TALK), total dissolved inorganic carbon (TCO_2), nitrate, chlorophyll-*a* (Chlor-*a*), salinity (SSS) and temperature (SST) relate to more than 15% of the variance in the minor element to calcium ratios (Lambda $l \geq 0.15$; Table 8.3a; marginal effects). After correcting for covariance, silicate, carbonate ion concentration ($[CO_3^{2-}]$) and nitrate explain the minor element to calcium variance significantly ($P \leq 0.05$; Table 8.3a, conditional effects). Fig. 8.5a shows that for sea surface conditions, Mg/Ca is correlated with sea surface temperature (SST), nitrate, silicate and chlorophyll-*a* (Chlor-*a*) concentrations. Fig. 8.5a also shows that Sr/Ca is correlated with $[CO_3^{2-}]$ for sea surface conditions.

For mixed layer depth conditions, the RDA reveals that the gradients total alkalinity (TALK), silicate, carbonate ion concentration ($[CO_3^{2-}]$) and temperature relate to more than 15% of the variance in the minor element to calcium ratios (Lambda $l \geq 0.15$; Table 8.3b; marginal effects). After correcting for covariance, total alkalinity (TALK), temperature and annual average mixed layer depth (MLD AA) explain the minor element to calcium variance significantly ($P \leq 0.05$; Table 8.3b, conditional effects). Fig. 8.5b shows that for mixed layer depth conditions, Mg/Ca is more correlated with temperature and less correlated with nitrate and silicate than for sea surface conditions. Fig. 8.5b also shows that Sr/Ca is correlated with $[CO_3^{2-}]$ and salinity for mixed layer depths.

For conditions averaged over 200m water depth, the RDA reveals that the gradients total alkalinity (TALK), temperature, carbonate ion concentration ($[CO_3^{2-}]$) and silicate relate to more than 15% of the variance in the minor element to calcium ratios (Lambda $l \geq 0.15$; Table 8.3c; marginal effects). After correcting for covariance, total alkalinity (TALK) and temperature explain the minor element to calcium variance significantly ($P \leq 0.05$; Table 8.3c, conditional effects). Fig. 8.5c shows that for conditions averaged over 200m water depth, Mg/Ca is only weakly correlated with temperature. Fig. 8.5c also shows that Sr/Ca is less correlated with $[CO_3^{2-}]$ and salinity for conditions averaged over 200m water depth than for mixed layer depth conditions.

Since we are mostly interested in a possible relationship between Mg/Ca and/or Sr/Ca and temperature, and since the mixed layer depth (MLD) is the depth where highest abundances of *T. heimii* occur (Kohn & Zonneveld, 2010), a more detailed view of the correlation between temperature at MLD and the Mg/Ca and Sr/Ca ratios is given in Fig. 8.6. No correlation can be observed between Mg/Ca and temperature or between Sr/Ca and temperature. The data show a large scatter compared to the results of cultured *T. heimii* (Gussone *et al.*, 2010) (Fig. 8.6).

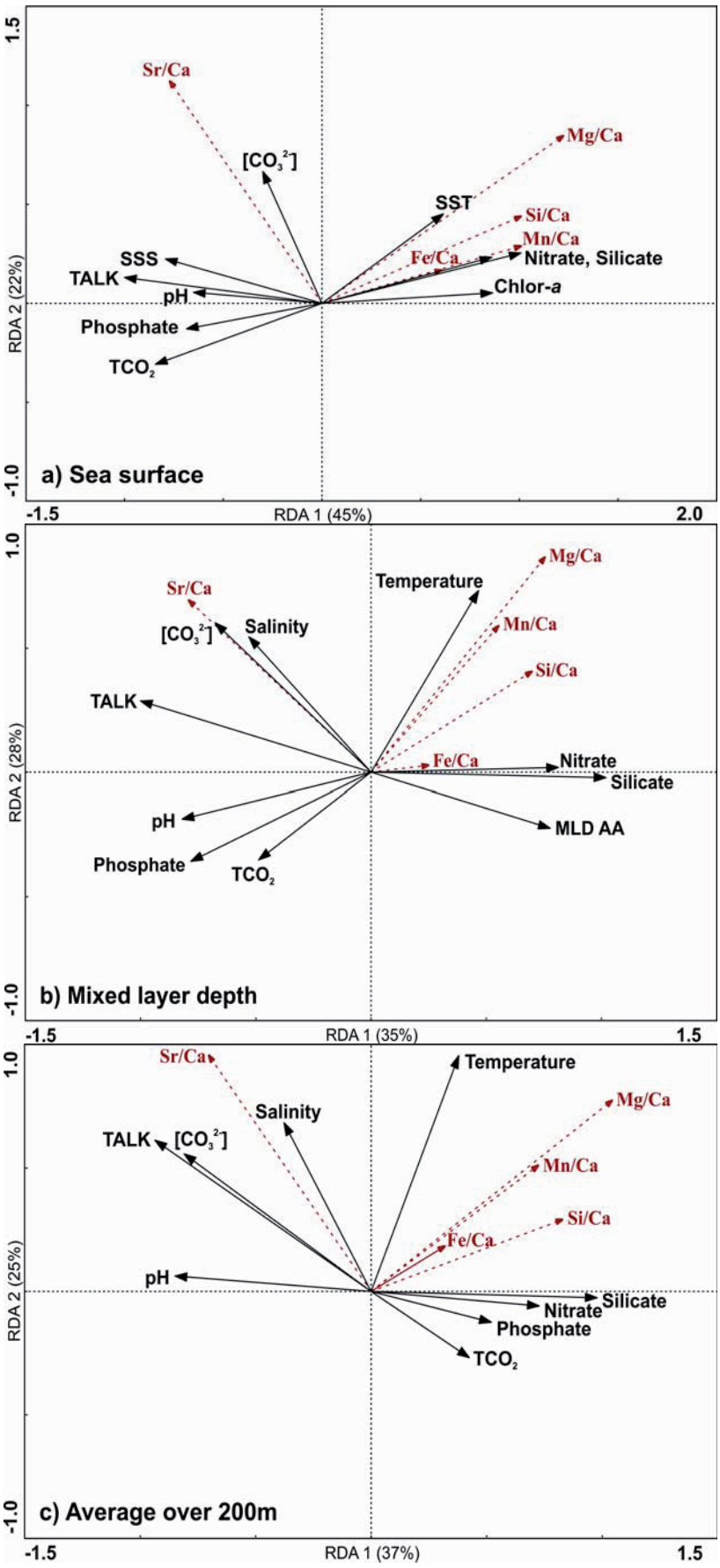

Fig. 8.5 – RDA with environmental parameters for (a) sea surface conditons ($RDA_{surface}$), (b) conditions at mixed layer depth (RDA_{MLD}) and (c) conditions averaged over 200m water depth (RDA_{200m}) – Solid black arrows depict the environmental parameters – Red dashed arrows depict the minor element to calcium ratios, which can be looked at as species in these plots

8.5. Discussion

Both the measured Mg/Ca (5.50-23.14 mmol/mol) and Sr/Ca (1.51-22.46 mmol/mol) ratios of *Thoracosphaera heimii* shells from surface sediments show a large range. Furthermore, the natural values exceed the Mg/Ca (2.6-7.3 mmol/mol) and Sr/Ca (2.16-2.40 mmol/mol) values of cultured *T. heimii* (Gussone *et al.*, 2010) by far (Fig. 8.6). Based on culture experiment data, Gussone *et al.* (2010) suggested a biomineralization mechanism in two phases for *T. heimii*: the major part of the calcite would be precipitated during the first, intracellular phase and is presumably Sr-enriched, while a Mg-enriched calcite layer is formed during the second phase, possibly influenced by a seawater dominated fluid. However, the Mg/Ca ratio of modern seawater is constant around 5.2 mmol/mol (Broecker & Peng, 1982). The Sr/Ca ratio of modern seawater is around 8 mmol/mol (Coggon *et al.*, 2010) and only varies by 2-3% (e.g. de Villiers, 1999). Since both magnesium and strontium are conservative elements, the high variance in both Mg/Ca and Sr/Ca ratios of *T. heimii* shells from the investigated core top samples cannot be due to changes in the Mg/Ca and Sr/Ca values of seawater. An offset with culture values could indicate that additional, natural factors, in the water column and/or in the sediments, have an influence on the shell Mg/Ca and Sr/Ca. In the following chapters, the Mg/Ca and Sr/Ca ratios of the *T. heimii* shells will be compared to several upper water column parameters (especially temperature), and will be discussed in terms of possible contamination by sedimentary processes. Since this is the first study on the elemental composition of *T. heimii* shells from natural sediments, and only one published study on the elemental composition of cultured *T. heimii* shells is available (Gussone *et al.*, 2010), we will also compare our results with published effects on the Mg/Ca and Sr/Ca ratios of foraminifera and coccolithophores.

8.5.1. Mg/Ca

8.5.1.1. Upper water column parameters

In RDA_{MLD}, $RDA_{surface}$, and to a lesser extent in RDA_{200m}, we observe that temperature is influencing the Mg/Ca ratio of *T. heimii* shells from surface sediments. However, when plotting the Mg/Ca values against temperatures at mixed layer depth (the depth where highest abudances of *T. heimii* occur, thus the presumed living depth of *T. heimii*; Kohn & Zonneveld (2010)), no relationship can be observed (Fig. 8.6a). However, we do observe that the highest *T. heimii* Mg/Ca

ratios occur in the core top samples from the Amazon Fan area (▲ in Fig. 8.6a), where seawater temperatures are highest in comparison to the other core top locations analyzed in this study (Table 8.1, Fig. 8.6b). This is in agreement with Gussone *et al.* (2010), who found that Mg/Ca ratios of cultured *T. heimii* shells do not show a pronounced temperature dependence, except for a strong Mg enrichment at the highest temperature (30°C) (Fig. 8.6a). This was interpreted by the authors as possibly anomalous growing behaviour of *T. heimii* at high temperatures. Although we seem to observe a similar phenomenon in natural sediments, currently we have insufficient insights into the biomineralization mechanisms of *T. heimii* to explain this. Furthermore, when the high Mg/Ca values of the Amazon Fan samples are omitted from this study, the Mg/Ca ratios of the remaining samples (▲ and ▲ in Fig. 8.6a) still show no correlation with temperature. We interpret this as an indication that other, more important factors are influencing the Mg/Ca values of *T. heimii* shells in surface sediment samples.

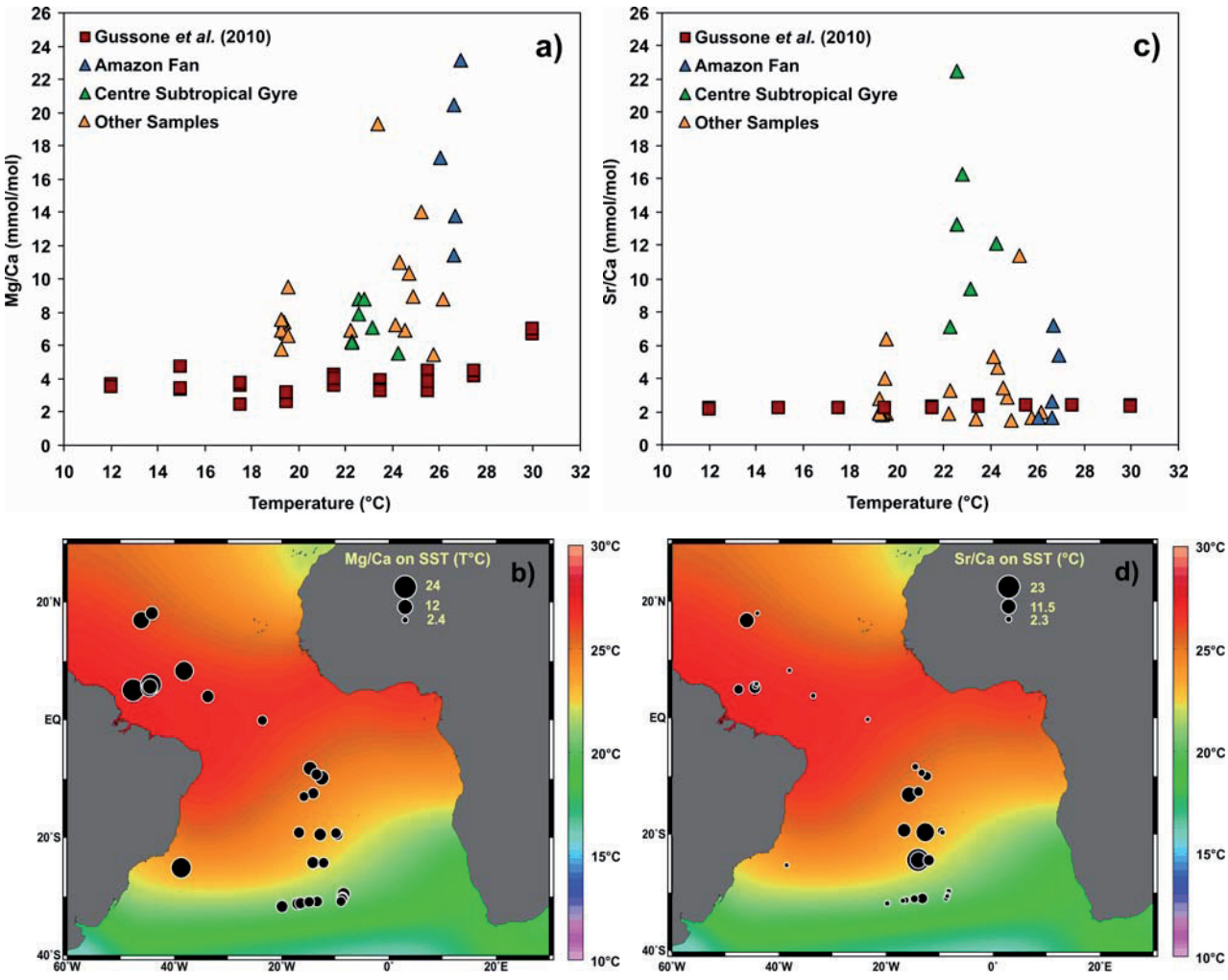

Fig. 8.6 – Mg/Ca (a) and Sr/Ca (c) versus temperature (temperature at mixed layer depth for the surface sediment samples, temperature of the culture medium for the study of Gussone *et al.* (2010)) – Mg/Ca (b) and Sr/Ca (d) ratios of *T. heimii* shells from surface sediments plotted on sea surface temperature (SST, °C)

According to the Redundancy Analyses (RDA), next to temperature, the Mg/Ca values of *T. heimii* calcite are also correlated with nitrate, silicate and chlorophyll-*a*, especially at the sea surface. Since highest Mg/Ca ratios occur in samples in the Amazon Fan area, we suspect that this correlation is the reflection of the sample location: a river outflow area, which is by default characterized by high nutrient and high chlorophyll-*a* concentrations (Fig. 8.7).

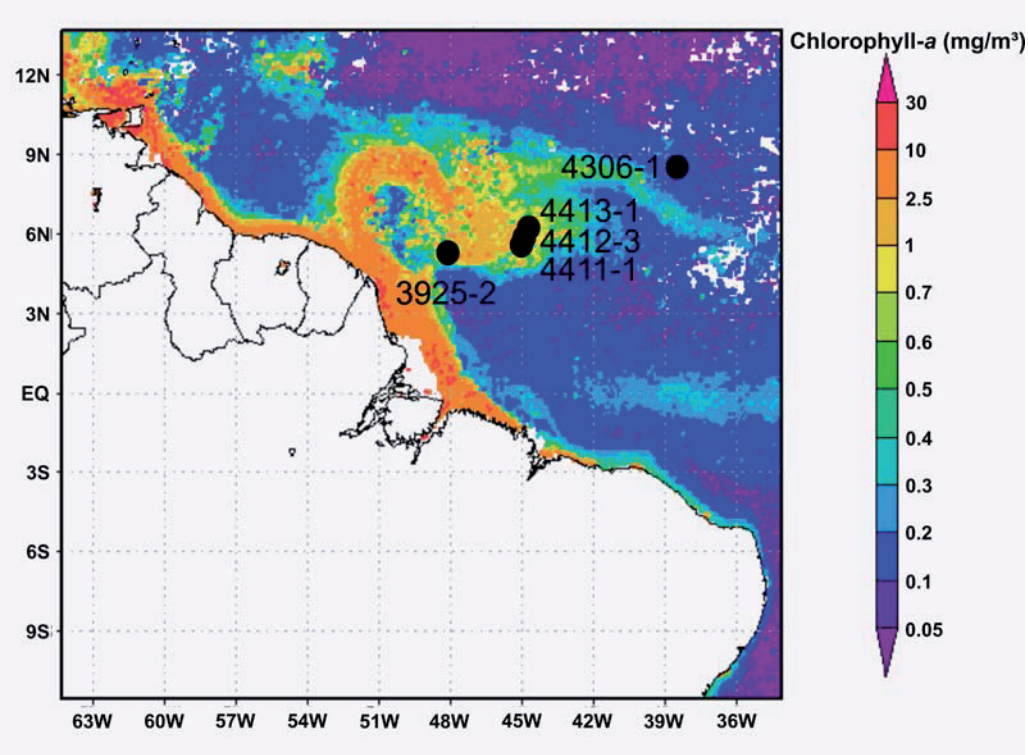

Fig. 8.7 – SeaWIFS image of the Amazon River outflow plume (http://disc.sci.gsfc.nasa.gov/gesNews/agu_oceans_giovanni_presentation) with the location of the surface sediment samples with highest Mg/Ca values

8.5.1.2. Sedimentary processes

In the modern day Atlantic Ocean, the carbonate compensation depth is situated roughly between 4000 and 4500m water depth (Berger, 1976). Except for samples GeoB 3801-5, 3803-1, 3812-2, 4413-1 and 4424-2, all core top samples are well above this dissolution depth. Furthermore, a number of studies have shown that the Mg/Ca content of planktonic foraminiferal tests from deep-sea core tops below the lysocline, decreases with increasing water depth, and hence degree of dissolution, resulting in lower Mg/Ca values (e.g. Rosenthal & Boyle, 1993; Brown & Elderfield, 1996; Elderfield & Ganssen, 2000; Rosenthal *et al.*, 2000). According to Regenberg *et al.* (2006), the onset of Mg^{2+} removal from foraminiferal calcite may even start at a depth with a threshold [CO_3^{2-}] value of 20 mmol/kg, so the dissolution effect might already start above the lysocline. More research is necesarry for the current study, but at first glance it seems that the five core top samples which are located under the lysocline, do not show significantly

lower Mg/Ca values than the other core tops samples. We argue that dissolution had little to no effect on the Mg/Ca ratio of *T. heimii* calcite from the Atlantic Ocean core top samples.

As already stated above, the highest Mg/Ca values of *T. heimii* calcite occur in surface sediment samples in the Amazon Fan area. The Amazon River and its tributaries drain the largest river basin of the world, the Amazon Basin (Mortatti & Probst, 2003), where silicate rocks constitute 96% of the total drainage area (e.g. Amiotte Suchet, 1995; Amiotte Suchet *et al.*, 2003). Therefore, in the Amazon Basin, silicate rock weathering is very common and includes the following two reactions: $CaAl_2Si_2O_8 + 2CO_2 + 3H_2O \rightarrow Al_2Si_2O_5(OH)_4 + 2HCO_3^- + Ca^{2+}$ (Ca-plagioclase into kaolinite) and $Mg_2SiO_4 + 4CO_2 + 4H_2O \rightarrow 2Mg^{2+} + 4HCO_3^- + H_4SiO_4$ (olivine weathering) (e.g. Mortatti & Probst, 2003). Silicate rock weathering produces a lot of clay minerals (e.g. kaolinite and montmorillonite), which find their way to the river plume deposition area. On average, clay minerals contain between 1 and 10 weight% Mg (Deer *et al.*, 1992). Adsorbed clay particles might therefore contaminate the *T. heimii* Mg/Ca ratio, as has also been shown in many foraminiferal studies (e.g. Boyle, 1983; Barker *et al.*, 2003; Boussetta *et al.*, 2011). For foraminiferal calcite, Barker *et al.* (2003), showed that the covariance of Fe/Ca and Mg/Ca is an indication of clay contamination. The observed covariance between the Mg/Ca, Fe/Ca and Mn/Ca ratios of the *T. heimii* shells in the Amazon Fan core top samples (PCA, $RDA_{surface}$, RDA_{MLD} and RDA_{200m}) might therefore be an indication of contamination by adsorbed clay particles, possibly inside the *T. heimii* shells.

Also inorganic Mg-rich ferromanganese coatings, deposited during diagenesis, might contaminate the foraminiferal Mg/Ca ratio (e.g. Boyle, 1983; Barker *et al.*, 2003; Ferguson *et al.*, 2008; Boussetta *et al.*, 2011). These contaminants can be traced by high iron and manganese concentrations: clean, uncontaminated foraminiferal tests should contain 0.1 mmol/mol Mn/Ca and Fe/Ca (Barker *et al.*, 2003). Unfortunately, we do not have similar guidelines for *T. heimii* , since this is the first study on the elemental composition of *T. heimii* shells from surface sediments. However, for the *T. heimii* shells in the Amazon Fan core top samples, Mn/Ca values range between 0.176 and 0.469 mmol/mol and Fe/Ca values range between 0.118 and 0.473 mmol/mol, which are rather high values compared to the other samples in the complete data set.

Since this was the first attempt to measure elemental ratios of *T. heimii* shells from sediments, it is possible that the proposed cleaning protocol does not completely remove Mg-rich ferromanganese coatings or adsorbed clay particles, especially when they are trapped inside the small *T. heimii* shells. However, the effectiveness of the method will be discussed in Dekeyzer *et al.* (in prep., Chapter 9 of this thesis).

8.5.2. Sr/Ca

8.5.2.1. Upper water column parameters

In RDA_{MLD}, RDA_{200m} and to a lesser extent in $RDA_{surface}$, we observe a positive correlation between salinity, seawater carbonate ion concentration ($[CO_3^{2-}]$), total alkalinity (TALK) and the Sr/Ca values of the *T. heimii* shells from core top samples. This is in contrast with Gussone *et al.* (2010) who observed that the Sr/Ca ratios of cultured *T. heimii* shells do not seem to be biased by changes in salinity. A small salinity effect on Sr/Ca (4% increase in Sr/Ca per salinity unit) has been reported for the planktonic foraminifera *Orbulina universa* (Lea *et al.*, 1999). According to Dueñas-Bohórquez *et al.* (2009) however, salinity has no significant influence on the Sr/Ca of *Globigerinoides sacculifer*. Nevertheless, they also noted that it remains unclear whether salinity itself influences foraminiferal incorporation of Sr, or whether it is due to changes in the carbonate chemistry associated with changes in salinity: an increase in salinity results in an increase in the carbonate parameters, such as total alkalinity (TALK), dissolved inorganic carbon (DIC) and seawater carbonate ion concentration ($[CO_3^{2-}]$) (Dueñas-Bohórquez *et al.*, 2009). It has been noted that $[CO_3^{2-}]$ has a positive effect on planktonic foraminiferal Sr/Ca ratios (e.g. Lea *et al.*, 1999; Russell *et al.*, 2004; Mortyn *et al.*, 2005; Kisakürek *et al.*, 2008). Furthermore, Dueñas-Bohórquez *et al.* (2009) suggested that the calcium carbonate saturation state of seawater (Ω) is the main control on foraminiferal Sr incorporation, in contrast to foraminiferal Mg incorporation, where salinity supposedly is the dominant control. When $[CO_3^{2-}]$ of the seawater changes, Ω also changes, since $\Omega = [Ca^{2+}]*[CO_3^{2-}]/K_{sp}$ (where K_{sp} represents the solubility product at the in situ conditions of temperature, salinity and pressure (Zeebe & Wolf-Gladrow, 2005)). Ω might control the rate of calcite precipitation, which in turn is known to influence trace metal incorporation (Lorens, 1981; Nehrke *et al.*, 2007). It is possible that the Sr/Ca values of *T. heimii* shells from surface sediment are affected in a similar way. More research is needed to explain this adequately.

In contrast to Mg/Ca, Sr/Ca is known to be more of a productivity proxy instead of a temperature proxy. Both for culture and sediment studies, it has been documented that the Sr/Ca ratio of coccolithophores changes with coccolithophorid growth rates (e.g. Stoll & Schrag, 2000; Stoll *et al.*, 2002a, b; Rickaby *et al.*, 2002; Stoll & Ziveri, 2005; Langer *et al.*, 2006). In contrast to coccolithophores, no relationship can be observed between the Sr/Ca ratio and cyst production of cultured *T. heimii* (Gussone *et al.*, 2010). For the present study we do not have quantitative cyst/g data. However, Fig. 8.1 and 8.2 show that samples with highest Sr/Ca values (GeoB 5008-3, 5115-2, 5117-2, 5121-2, 5136-2 and 5140-3) are located in the middle of the Subtropical Gyre, an area which is characterized by lowest productivity. According to Gussone *et al.* (2010), the difference

in reaction to high productivity between *T. heimii* and coccolithophores lays in the calcification mechanism of *T. heimii*, which is not a continuous process, in contrast to coccolithophores.

Both $RDA_{surface}$, RDA_{MLD} and RDA_{200m} are characterized by the absence of a correlation between temperature and the Sr/Ca values of the *T. heimii* shells from core top samples. This is in contrast with Gussone *et al.* (2010), who found a large temperature dependence of Sr/Ca in cultured *T. heimii* shells (0.016 mmol/mol per °C) (Fig. 8.6c). We presume that a possible temperature dependence of *T. heimii* Sr/Ca in a natural setting might by obscured due to diagenetic overprint.

8.5.2.2. Sedimentary processes

The samples with highest Sr/Ca ratios (GeoB 5008-3, 5115-2, 5117-2, 5121-2, 5136-2 and 5140-3) are located on the Mid Atlantic Ridge (cruise report of Meteor cruise M41; Schultz *et al.*, 1999). Hydrothermal circulation through the sediments results in the extensive alteration of the primary sediment (e.g. Edmond *et al.*, 1979; Dekov *et al.*, 2008). The altered sediments have been depleted in Sr due to leaching. Therefore, strontium is enriched in the altered sediment pore fluids relative to the non-altered sediments (Dekov *et al.*, 2008). Coogan (2009) describes the behavior of strontium in hydrothermal systems at spreading centers as follows: as ^{87}Sr-rich seawater enters the crust, it is heated and reacts with the basaltic, relatively ^{87}Sr-depleted rocks. This leads to a change in Sr isotopic composition of the rocks and the fluids. In general: vent fluids have Sr isotopic ratios greater than rock values. Perhaps the extreme Sr/Ca values can be explained by leaching of Sr from the basaltic rocks. However, when the locations of these extreme-Sr/Ca samples are compared to a distribution map of hydrothermal vent fields (Fig. 8.8, 8.9, Baker & German, 2004), it seems that these samples are not located in an active hydrothermal field that is currently known. It should be noted that some other samples are located on the Mid Atlantic Ridge as well, but they do not show extreme Sr/Ca values. So far, we have no explanation for this discrepancy.

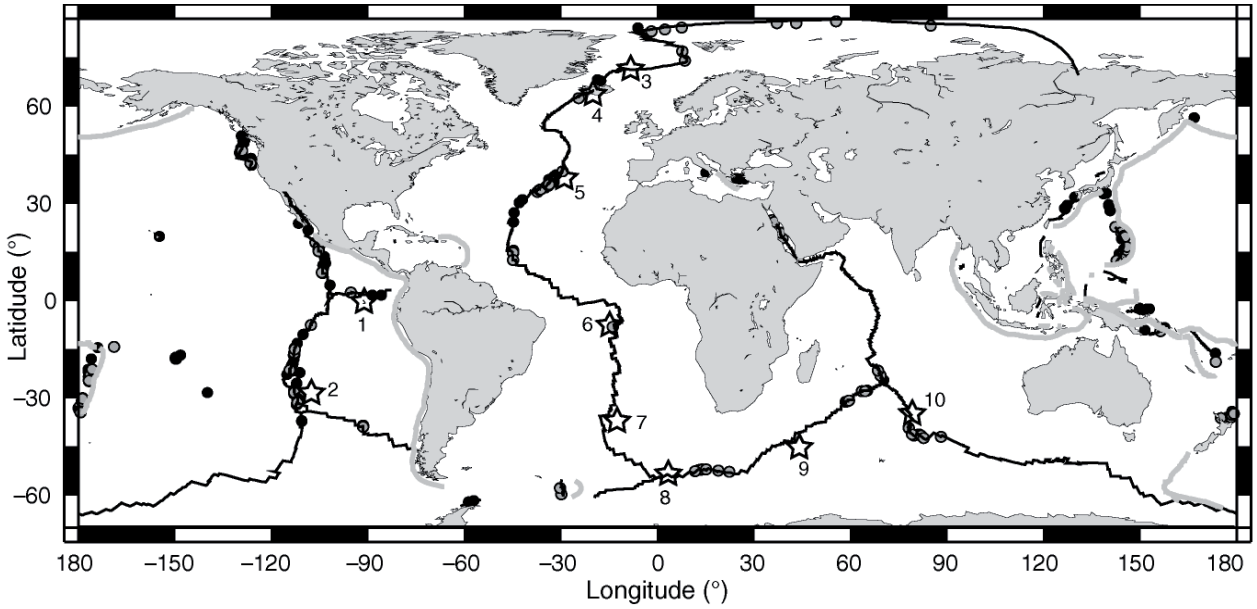

Fig. 8.8 – Distribution of 144 known (black dots) and 133 inferred (gray dots) hydrothermal fields. Solid black lines are the midocean ridge and transform faults, gray lines are subduction zones. Hotspots (open stars) include 1, Galápagos; 2, Easter; 3, Jan Mayen; 4, Iceland; 5, Azores; 6, Ascension; 7, Tristan de Cunha; 8, Bouvet; 9, Crozet; and 10, Amsterdam-St. Paul (From Baker & German, 2004)

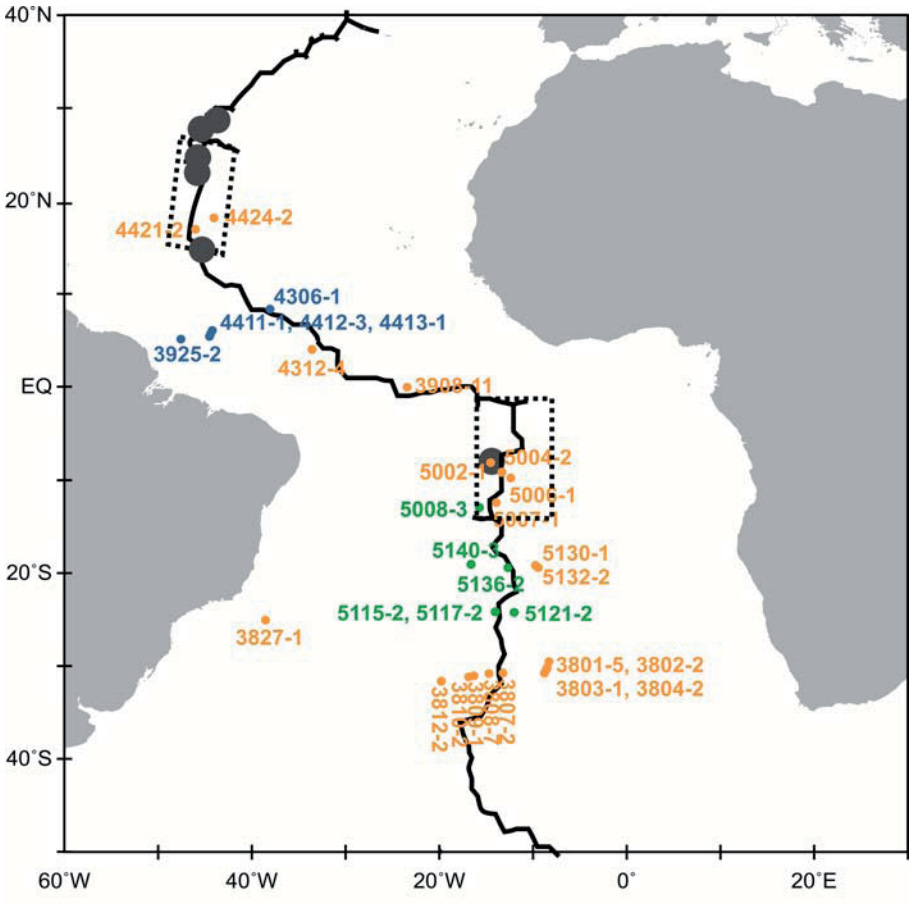

Fig. 8.9 – Sample locations in comparison with hydrothermal field locations (partly redrawn from Baker & German, 2004) – Big gray dots = inferred hydrothermal field locations – Blue dots (●) = samples with high to extreme Mg/Ca ratios; samples in the Amazon Fan area – Green dots (●) = samples with high to extreme Sr/Ca ratios; samples in the central area of the Subtropical Gyre – Orange dots (●) = other samples

8.6. Conclusions

For the current study we analyzed the minor element to calcium ratios of *Thoracopshaera heimii* shells from surface sediments in the equatorial and South Atlantic. Both Mg/Ca and Sr/Ca show a large range and exceed the values of *T. heimii* calcite from cultured specimens by far. Although RDA revealed that *T. heimii* Mg/Ca is influenced by temperature, the only correlation is that highest Mg/Ca values appear in the samples characterized by highest seawater temperature (samples in the Amazon Fan area). When these extreme values are omitted from the data set, no temperature – Mg/Ca relationship can be found. We suspect that the Mg/Ca values are most likely contaminated by adsorbed clay particles, and especially in the Amazon Fan area, where Mg/Ca values reach extreme values. RDA further revealed that *T. heimii* Sr/Ca is correlated with the carbonate chemistry of the seawater. In contrast to cultured *T. heimii*, the Sr/Ca ratios of *T. heimii* shells from natural sediments do not show any correlation with temperature. Although so far we do not have a satisfying explanation for the extreme Sr/Ca values, we suspect that sediment contamination, possibly by hydrothermal activity, might be an important factor. In general, we need also more information about the biomineralization mechanism of *T. heimii* to draw solid conclusions.

Acknowledgements

Thanks are given to all cruise participants and the crews of Meteor cruises M34-3, M34-4, M38-1, M38-2, M41-2 and M41-3 for recovering the investigated surface sediment samples. We are also greatful to Heather Stoll (Department of Analytical Chemistry, University of Oviedo, Spain) for carrying out the minor element to calcium measurements. The manuscript benefitted from helpful and constructing comments of Patrizia Ziveri (Institut de Sciència i Tecnologia Ambientals, Universitat Autònoma de Barcelona, Spain). We also thank all members of the working group of Historical Geology and Paleontology (University of Bremen) for their general assistance. This research was financed by the German Science Foundation (DFG), as a subproject of the International Graduate College Proxies in Earth History (EUROPROX).

References Chapter 8

Amiotte Suchet, P., 1995. Cycle due carbone, érosion chimique des continents et transports vers les oceans. Sci. Géol., Mem. 97 (Strasbourg, 156 pp.)

Amiotte Suchet, P., Probst, J.-L., Ludwig, W., 2003. Worldwide distribution of continental rock lithology: Implications for the atmospheric/soil CO_2 uptake by continental weathering and alkalinity river transport to the oceans. *Global Biogeochemical Cycles*, 1 (2), 1038-1051.

Antonov, J.I., Seidov, D., Boyer, T.P., Locarnini, R.A., Mishonov, A.V., Garcia, H.E., 2010. *World Ocean Atlas 2009 Volume 2: Salinity.* S. Levitus, Ed., NOAA Atlas NESDIS 69, U.S. Government Printing Office, Wahington, D.C., 184 pp.

Bairbakesh, A.N., Jollman, J., Sprengel, C., Thierstein, H.R., 1999. Disintegration of aggregates and coccospheres in sediment trap sanples. *Marine Micropaleontology* 37, 219-223.

Baker, E.T., German, C.R., 2004. On the global distribution of hydrothermal vent fields. In: Mid-ocean ridges: hydrothermal interactions between the lithosphere and oceans. Geophysical Monograph Series 148, C.R. German, J. Lin, and L.M. Parson (Eds.), 245-266.

Barker, S., Greaves, M., Elderfield, H., 2003. A study of cleaning procedures used for foraminiferal Mg/Ca paleothermometry. *Geochemistry, Geosphysics, Geosystems* 4 (9), 8407, doi:10.1029/2003GC000559.

Berger, W.H., 1976. Biogenous deep sea sediments: production, preservation and interpretation. In Riley, J.P. and Chester, R. (Eds). *Chemical Oceanography*, Academic Press, London, pp. 265-388.

Boussetta, S., Bassinot, F., Sabbatini, A., Caillon, N., Nouet, J., Kallel, N., Rebaubier, H., Klinkhammer, G., Labeyrie, L., 2011. Diagenetic Mg-rich calcite in Mediterranean sediments: quantification and impact on foraminiferal Mg/Ca thermometry. *Marine Geology* 280, 195-204.

Boyle, E.A., 1983. Manganese carbonate overgrowths on foraminiferal tests. *Geochimica et Cosmochimica Acta* 47, 1815-1819.

Broecker, W.S. and T.-H. Peng, Tracers in the Sea. 1982, New York: Eldigio press.

Brown, S., Elderfield, H., 1996. Variations in Mg/Ca and Sr/Ca ratios of planktonic foraminifera caused by postdepositional dissolution: evidence of shallow Mg-dependant dissolution. *Paleoceanography*, 11, 543 – 551.

Coggon, R.M., Teagle, D.A.H., Smith-Duque, C.E., Alt, J.C., Cooper, M.J., 2010. Reconstructing past seawater Mg/Ca and Sr/Ca from mid-ocean ridge flank calcium carbonate veins. *Science* 327, 1114-117.

Coogan, L.A., 2009. Altered oceanic crust as an inorganic record of paleoseawater Sr concentration. *Geochemistry, Geophysics, Geosystems* 10 (4), Q04001, doi:10.1029/2008GC002341.

Deer, W.A., Howie, R.A., Zussman, J., 1992. An introduction to the rock forming minerals, 2nd ed. Addison-Wesley-Longman, Reading, Mass.

Dekens, P.S., Lea, D.W., Pak, D.K., Spero, H.J., 2002. Core top calibration of Mg/Ca in tropical foraminifera: Refining paleotemperature estimation. *Geochemistry, Geophysics, Geosystems* 3 (4), 1022, doi:10.1029/2001GC000200.

Dekeyzer, S.P.M., Groeneveld, J., Ziveri, P., Kuhnert, H., Zonneveld, K.A.F. Comparison between different cleaning protocols to analyze the Mg/Ca and Sr/Ca ratios of *Thoracosphaera heimii* shells from sediments. In preparation.

Dekov, V., Scholten, J., Garbe-Schönberg, C.-D., Botz, R., Cuadros, J., Schmidt, M., Stoffers, P., 2008. Hydrothermal sediment alteration at a seafloor vent field: Grimsey Graben, Tjörnes Fracture Zone, north of Iceland. *Journal of Geophysical Research* 113, B11101, doi:10.1029/2007JB005526.

de Villiers, S., 1999. Seawater strontium and Sr/Ca variability in the Atlantic and Pacific oceans. *Earth and Planetary Science Letters* 171, 623-634.

Dueñas-Bohórquez, A., da Rocha, R.E., Kuroyanagi, A., Bijma, J., Reichart, G.-J., 2009. Effect of salinity and seawater calcite saturation state on Mg and Sr incorporation in cultured planktonic foraminifera. *Marine Micropaleontology* 73, 178-189.

Edmond, J.M., Measures, C., McDuff, R.E., Chan, L.H., Collier, R., Grant, B., Gordon, L.I., Corliss, J.B., 1979. Ridge crest hydrothermal activity and the balances of the major and minor elements in the ocean: The Galapagos data. *Earth and Planetary Science Letters* 46, 1-18.

Elderfield, H., Ganssen, G., 2000. Past temperature and $\delta^{18}O$ of surface ocean waters inferred from foraminiferal Mg/Ca ratios. *Nature* 405, 442-445.

Ferguson, J.E., Henderson, G.M., Kucera, M., Rickaby, R.E.M., 2008. Systematic change of foraminiferal Mg/Ca ratios across a strong salinity gradient. *Earth and Planetary Science Letters* 265, 153-166.

Garcia, H.E., Locarnini, R.A., Boyer, T.P., Antonov, J.I., Zweng, M.M., Baranova, O.K., Johnson, D.R., 2010. *World Ocean Atlas 2009, Volume 4: Nutrients (phosphate, nitrate, silicate)*. S. Levitus, Ed. NOAA Atlas NESDIS 71, U.S. Government Printing Office, Washington, D.C., 398 pp.

Goyet, C., Healy, R.J., Ryan, J.P., 2000. Global distribution of total inorganic carbon and total alkalinity below the deepest winter mixed layer depths. ORNL/CDIAC-127, NDP-076. Carbon Dioxide Information Analysis Center, Oak Ridge National Laboratory, U.S. Department of Energy, Oak Ridge, Tennessee, U.S.A. 40 pp. doi:10.3334/CDIAC/otg.ndp076

Gussone, N., Zonneveld, K.A.F. & Kuhnert, H. 2010. Minor element and Ca isotope composition of calcareous dinoflagellate cysts of cultured *Thoracosphaera heimii*. *Earth and Planetary Science Letters* 289, 180-188.

Holzwarth, U., Esper, O., Zonneveld, K.A.F., 2010. Organic-walled dinoflagellate cysts as indicators of oceanographic conditions and terrigenous input in the NW African upwelling region. *Review of Palaeobotany and Palynology* 159, 35-55.

Jongman, R.H.G., ter Braak, C.J.F., van Tongeren, O.F.R., 1987. Data analysis in community and landscape ecology. Centre for Agricultural Publication and Documentation (PUDOC), Wageningen. 229 pp.

Kisakürek, B., Eisenhauer, A., Böhm, F., Garbe-Schönberg, D., Erez, J., 2008. Controls on shell Mg/Ca and Sr/Ca in cultured planktonic foraminiferan, *Globigerinoides ruber* (white). *Earth and Planetary Science Letters* 273, 260-269.

Kohn, M., Zonneveld, K.A.F., 2010. Calcification depth and spatial distribution of *Thoracosphaera heimii* cysts: Implications for palaeoceanographic reconstructions. *Deep Sea Research Part I: Oceanographic Research Papers* 57 (12), 1543-1560.

Langer, G., Gussone, N., Nehrke, G., Riebesell, U., Eisenhauer, A., Kuhnert, H., Rost, B., Trimborn, S., Thoms, S., 2006. Coccolith strontium to calcium ratios in *Emiliana huxleyi*: the dependence on seawater strontium and calcium concentrations. *Limnology and Oceanography* 51 (1), 310-320.

Lea, D.W., Mashiotta, T.A., Spero, H.J., 1999. Controls on magnesium and strontium uptake in planktonic foraminifera determined by live culturing. *Geochimica et Cosmochimca Acta* 63, 2369-2379.

Locarnini, R.A., Mishonov, A.V., Antonov, J.I., Boyer, T.P., Garcia, H.E., 2010. *World Ocean Atlas 2009, Volume 1: Temperature*. S. Levitus, Ed., NOAA Atlas NESDIS 68, U.S. Government Printing Office, Washington, D.C., 184 pp.

Lorens, R., 1981. Sr, Cd, Mn and Co distribution coefficients in calcite as a function of calcite precipitation rate. *Geochimica et Cosmochimica Acta* 45, 553-561.

Mashiotta, T.A., Lea, D.W., Spero, H.J., 1999. Glacial-interglacial changes in Subantarctic sea surface temperature and δ^{18}O-water using foraminiferal Mg. *Earth and Planetary Science Letters* 170, 417-432.

Mortatti, J., Probst, J.-L., 2003. Silicate rock weathering and atmospheric/soil CO_2 uptake in the Amazon basin estimated from river water geochemistry: seasonal and spatial variations. *Chemical Geology* 197, 177-196.

Mortyn, P.G., Elderfield, H., Anand, P., Greaves, M., 2005. An evaluation of controls on planktonic foraminiferal Sr/Ca: comparison of water column and core-top data from a North Atlantic transect. *Geochemistry, Geophysics, Geosystems* 6 (12), Q12007, doi:10.1029/2005GC001047.

Monterey, G., Levitus, S., 1997. Seasonal variability of mixed layer depth for the World Ocean. NOAA Atlas NESDIS 14, U.S. Government Printing Office, Washington, D.C., 96 pp. 87 figs.

Nehrke, G., Reichart, G.J., van Cappellen, P., Meile, C., Bijma, J., 2007. Dependence of calcite growth rate and Sr partitioning on solution stoichiometry: non-Kossel crystal growth. *Geochimica et Cosmochimica Acta* 71 (9), 2240-2249.

Nürnberg, D., 1995. Magnesium in tests of *Neogloboquadrina pachyderma sinistral* from high northern and southern latitudes. *Journal of Foraminiferal Research* 25, 350-368.

Nürnberg, D., 2000, Taking the temperature of past ocean surfaces. *Science* 289, 1698-1699.

Nürnberg, D., Bijma, J., Hemleben, C., 1996. Assessing the reliability of magnesium in foraminiferal calcite as a proxy for water mass temperatures. *Geochimica et Cosmichimica Acta* 60, 803-814.

Nürnberg, D., Müller, A., Schneider, R.R., 2000. Paleo-sea surface temperature calculations in the equatorial east Atlantic from Mg/Ca ratios in planktic foraminifera: A comparison to sea surface temperature estimates from U^k_{37}, oxygen isotopes, and foraminiferal transfer function. *Paleoceanography* 15, 124-134.

Peterson, R.G. & Stramma, L. 1991. Upper-level circulation in the South Atlantic Ocean. *Progress in Oceanography* 26, 1-73.

Regenberg, M., Nürnberg, D., Steph, S., Groeneveld, J., Garbe-Schönberg, D., Tiedemann, R., Dullo, W.-C., 2006. Assessing the effect of dissolution on planktonic foraminiferal Mg/Ca ratios: Evidence from Caribbean core tops. *Geochemistry, Geophysics, Geosystems* 7 (7), Q07P15, doi:10.1029/2005GC001019.

Reichart, G., Jorissen, F., Anschutz, P., Mason, P., 2003. Single foraminifera test chemistry records the marine environment. *Geology* 31 (4), 355-358.

Rickaby, R.E.M., Schrag, D.P., Zondervan, I., Riebesell, U., 2002. Growth rate dependence of Sr incorporation during calcification of *Emiliana huxleyi*. *Global Biochemical Cycles* 16, doi:1029/2001GB001408.

Richter, D., Vink, A., Zonneveld, K.A.F., Kuhlmann, H., Willems, H., 2007. Calcareous dinoflagellate cyst distributions in surface sediments from upwelling areas off NW Africa, and their relationships with environmental parameters of the upper water column. *Marine Micropaleontology* 63, 201-228.

Rosenthal, Y., Boyle, E.A., 1993. Factors controlling the fluoride content of planktonic foraminifera: An evaluation of its paleoceanographic applicability. *Geochimica et Cosmochimica Acta* 57, 335-346.

Rosenthal, Y., Lohmann, G.P., Lohmann, K.C., Sherrell, R.M., 2000. Incorporation and preservation of Mg in *G. sacculifer*: Implications for reconstructing sea surface temperatures and the oxygen isotopic composition of seawater. *Paleoceanography* 15, 135-145.

Russell, A.D., Hönisch, B., Spero, H., Lea, D.W., 2004. Effects of seawater carbonate ion concentration and temperature on shell U, Mg and Sr in cultured planktonic foraminifera. *Geochimica et Cosmochimica Acta* 68, 4347-4361.

Schlitzer, R., 2009. Ocean Data View, http://odv.awi.de.

Schulz, H.D., Devey, C.W., Pätzold, J., Fischer, G., 1999. Geo Bremen/GPI Kiel South Atlantic 1998, Cruise No. 41, 13 February - 13 June 1998. METEOR-Berichte, Universität Hamburg, 99-3, 341 pp.

Stoll, H.M., Schrag, D.P., 2000. Coccolith Sr/Ca as a new indicator of coccolithophorid calcification and growth rate. *Geochemistry, Geophysics, Geosystems* 1, 1-24.

Stoll, H.M., Ziveri, P. 2002. Separation of monospecific and restricted coccolith assemblages from sediments using differential settling velocity. *Marine Micropaleontology* 46, 209-221.

Stoll, H., Ziveri, P., 2005. *Coccolithophorid-based geochemical paleoproxies*. Berlin, Springer, Heidelberg, pp. 529-563.

Stoll, H.M., Encinar, J.R., Alonso, J.I.G., Rosenthal, Y., Probert, I. & Klaas, C. 2001. A first look at paleotemperature prospects from Mg in coccoliths carbonate: cleaning techniques and culture measurements. *Geochemistry, Geophysics, Geosystems* 2, 2000GC000144.

Stoll, H.M., Klaas, C.M., Probert, I., Encinar, J.R., Garcia Alonso, J.I., 2002a. Calcification rate and temperature effects on Sr partitioning in coccoliths of multiple species of coccolithophorids in culture. *Global and Planetary Change* 34, 153-171.

Stoll, H.M., Ziveri, P., Geisen, M., Probert, I., Young, Y.R., 2002b. Potential and limitations of Sr/Ca ratios in coccolith carbonate: new perspectives from cultures and monospecific samples from sediments. Philos. Trans. R. Soc. Lond. A 360, 719-747.

Ter Braak, C.J.F., Smilauer, P., 1998. Canoco reference manual and user's guide for Canocofor Windows. Software for Canonical Community Ordination (version 4), Centre for Biometry, Wageningen. 351 pp.

Wefer, G., Berger, W.H., Siedler, G., Webb, D.J. 1996. The South Atlantic: Present and Past Circulation. Springer, Berlin.

Zeebe, R.E., Wolf-Gladrow, D., 2005. CO_2 in seawater: equilibrium, kinetics, isotopes. Elsevier Oceanography Series 65, The Netherlands, 346 pp.

CHAPTER 9 – MANUSCRIPT 3

Comparison between different cleaning protocols to analyze the Mg/Ca and Sr/Ca ratios of *Thoracosphaera heimii* shells from sediments.

Stefanie P.M. Dekeyzer*[a], Jeroen Groeneveld[b], & Karin A.F. Zonneveld[a,b]

[a]Fachbereich 5 – Geowissenschaften, Universität Bremen, Bremen, Germany
[b]MARUM, Universität Bremen, Bremen, Germany

*Corresponding author.

Fax: +49 421 218 65159
E-mail address: stefanie.dekeyzer@uni-bremen.de

Abstract

For the present study, we processed core top sample GeoB 5008-3 according to the newly proposed cleaning protocol for the elemental analysis of *T. heimii* shells from sediments. In order to evaluate the obtained Mg/Ca and Sr/Ca values, the sample was also processed following the standard cleaning protocol for the elemental analysis of foraminifera, adapted for *T. heimii* shells; and following a sequential dissolution protocol, using a Flow-Through (FT) device. Although the Mg/Ca values of sample GeoB 5008-3, are well within the Mg/Ca range of cultured *T. heimii* shells, the Sr/Ca values of sample GeoB 5008-3 are five to seven times higher than the Sr/Ca values of cultured *T. heimii* shells. The Sr/Ca values obtained with the three different techniques seem to be significant at the 90% confidence level ($p = 0.086$). The Mg/Ca values however differ between the three cleaning techniques. Since lower Mg/Ca values are obtained when the sample is sequentially dissolved, using the FT device, this could be evidence for contaminating clay particles trapped inside the empty *T. heimii* shells.

9.1. Introduction

Although the Mg/Ca and Sr/Ca ratios of other biogenic carbonates, such as foraminifera and coccolithophores, are routinely applied in paleoceanography (e.g. Langer *et al.*, 2006; Mortyn *et al.*, 2005; Stoll *et al.*, 2001), so far only one study has been carried out on the elemental composition of *T. heimii* shells: the culture experiment by Gussone *et al.* (2010). Prior to minor element analysis of the cultured *T. heimii* shells, samples were cleaned following a method previously applied to cultured coccolithophores (Langer *et al.*, 2006; Gussone *et al.*, 2006). In summary: *T. heimii* shells were bleached for 24 hours in a 10% NaClO solution (~ 1% active bleach) to remove organic compounds. When the bleach was removed, samples were washed six times in distilled water. By adding a NH_4OH solution to the distilled water, pH was elevated to 8-9, preventing partial dissolution of the calcareous shells during the cleaning process. The samples were then dissolved in 0.5M HCl (Gussone *et al.*, 2010). However, since this cleaning method is applied on cultured organisms, it only includes an oxidation step, and will therefore not be able to remove non-calcareous particles and/or coatings formed in the sediments. Thus, the chemical cleaning method used by Gussone *et al.* (2010) is not adequate for the chemical cleaning of *T. heimii* shells from sediments.

In our search for an adequate cleaning protocol for *T. heimii* shells from sediments, we also looked at other organisms such as foraminifera and coccolithophores. The standard cleaning protocol for the elemental analysis of foraminifera (Barker *et al.*, 2003) is well established. When applying this protocol on the *T. heimii* shells however, we noticed some difficulties. Being smaller than foraminifera tests, the *T. heimii* shells stay in suspension throughout the whole cleaning process. In order to ensure a minimum loss of *T. heimii* shells, a centrifuge session is needed, before any overlying fluid is removed. This makes the method time consuming and labour intensive.

Next, we applied the cleaning protocol for coccolithophores (Bairbakesh *et al.*, 1999; Stoll & Ziveri, 2002). Since *T. heimii* shells are more or less in the same size range as most coccolithophores, this method is more appropiate. However, different coccolith species are very difficult to separate; therefore the coccolithophore method requires an extensive settling step, which is not necessary for *T. heimii* shells. In the end we adapted the cleaning protocol for coccolithophores by adding some sieving steps and by simplifying the settling step. This adapted cleaning protocol is what we refer to as “the newly proposed cleaning protocol for the elemental analysis of *T. heimii* shells from sediment” in this manuscript. To evaluate this new cleaning protocol, we also analyzed sample GeoB 5008-3 with a Flow-Through sequential dissolution device connected to an ICP-OES.

9.2. Material and methods

9.2.1. Sample collection

For the present study, a sample was required with a high concentration of *Thoracosphaera heimii* shells, in order to facilitate isolation of *T. heimii* shells from the sediment. Sample GeoB 5008-3 was chosen based on the knowledge obtained from previous work (Vink, 2004): the sample contains 80520 *T. heimii* shells/ml.

Sample GeoB 5008-3 (12°55.8'S, 15°41.1'W) was collected from the equatorial Atlantic by multicorer, at water depth 3407 m, during cruise M41-2. According to the cruise report (Schulz *et al.*, 1999), the sample location of sample GeoB 5008-3 is listed as Mid-Atlantic Ridge.

This core-top sample was prepared for elemental analysis using three different methods (see Table 9.1 for sample codes). First, a new cleaning protocol was developed for the preparation of *T. heimii* shells from sediments for elemental analysis. After chemical treatment, the sample was analysed using an ICP-MS (*T. heimii* test in Table 9.1). In addition, the sample was processed using the traditional stepwise cleaning procedure for the preparation of foraminiferal calcite for elemental analysis (Barker *et al.*, 2003), with some modifications for *T. heimii* shells, and analyzed twice using an ICP-MS (Foram Test 1 and Foram Test 2 in Table 9.1). Furthermore the sample was analyzed three times with a flow-through sequential dissolution device (Haley & Klinkhammer, 2002; Groeneveld *et al.*, 2010) connected to an ICP-OES (FT Test 1, FT Test 2 and FT Test 3 in Table 9.1).

9.2.2. New cleaning protocol for the elemental analysis of *T. heimii* shells from sediments

Here we present a new cleaning protocol for the preparation of shells from the calcareous dinoflagellate *Thoracosphaera heimii* from sediments for elemental analysis. The protocol is based on the cleaning method used for coccoliths described by Bairbakesh *et al.* (1999) and Stoll & Ziveri (2002). Additional sieving steps were included and the settling-and-decanting step was modified. In summary, the protocol consists of six steps. First, a mixture of bidistilled water, peroxide and bleach is added to the sample allowing oxidation of the organic material and preventing the formation of sediment aggregates. Next, the sample is sieved through a 15 µm precision sieve in order to get rid of the fraction bigger than 15 µm. Then, a reductive solution of bidistilled water, ammonia and hydroxylamine hydrochloride is added and the sample is placed on a rotating carousel during 24 hours. This reductive treatment removes Mn-Fe-oxide coatings which

could have formed in the sediment. After centrifuging and removing the reductive solution, a solution of bidistilled water and ammonia is added and again the sample is placed on a rotating carousel during 24 hours. This solution allows an ion exchange reaction of the sample and removes adsorbed cations on the shell wall. Afterwards, the sample is sieved through a 10 μm precision sieve in order to get rid of the fraction smaller than 10 μm. In the last step, the sample is subjected to a series of settling and decanting steps in order to get rid of other particles in the 10-15 μm fraction and make the sediment monospecific in *T. heimii* shells. For a detailed overview of the protocol, see Appendix 1.

The minor element to calcium ratios of the *T. heimii* shells were measured via inductively coupled plasma mass spectrometry (ICP-MS), on a Finnigan ELEMENT sector field instrument in the Department of Analytical Chemistry at the University of Oviedo. Ratios were measured in pulse-counting mode on dilute solutions (10 ppm Ca). Precision of the analysis is better than 0.4% relative standard deviation.

9.2.3. Flow-Through sequential dissolution device connected to an ICP-OES

Prior to processing sample GeoB 5008-3 with a Flow-Through (FT) device, *T. heimii* shells were separated from the sediment according to the method described by Zonneveld (2004). In summary: 2,65g of dried sediment was sieved through 10 and 15 μm precision sieves. Then the sediment fraction between 10-15 μm was subjected to a series of settling and decanting steps until this fraction contains less than 15% other calcareous particles than *T. heimii* shells.

To analyze the monospecific *T. heimii* sample with the FT device, three aliquots of around 100 μg were placed on a filter with a mesh size of 0.45 μm. First, the samples were rinsed with buffered Seralpur water, and then HNO_3 was added in small steps to create a gradient of increasing acid strength. During this sequential dissolution protocol, acid is kept constant at each concentration for several minutes, allowing dissolution of a specific calcite phase. While the sample calcite is dissolved, non-calcareous contaminants, such as clay minerals, remain on the filter (Groeneveld *et al.*, 2010).

The FT device is coupled to an Inductively Coupled Plasma Optical Emmision Spectrometer (ICP-OES), allowing online analysis of the sample. Measurements occur every 12-13 seconds, thus resulting in multiple measurements per sample. In the absence of an appropiate *Thoracosphaera heimii* standard, a *Globigerinoides ruber* standard was used with known Mg/Ca and Sr/Ca ratios of 4.12 and 1.37mmol/mol respectively.

Calculation of the Mg/Ca and Sr/Ca values of a sample is based on the linear relationship between Mg and Ca, and Sr and Ca, both for the sample and for the standard. The Mg/Ca and Sr/Ca concentrations of samples GeoB 5008-3 FT Test 1, FT Test 2 and FT Test 3 thus were calculated according to the following principle:

$$Mg/Ca_{standard} / Mg\text{-}Ca\text{-}slope_{standard} = Mg/Ca_{sample} / Mg\text{-}Ca\text{-}slope_{sample}$$
$$Sr/Ca_{standard} / Sr\text{-}Ca\text{-}slope_{standard} = Sr/Ca_{sample} / Sr\text{-}Ca\text{-}slope_{sample}$$

9.2.4. Standard cleaning protocol for the elemental analysis of foraminifera

Prior to processing sample GeoB 5008-3 using the standard cleaning protocol for foraminifera (Barker *et al.*, 2003), *T. heimii* shells were separated from the sediment according to the method described by Zonneveld (2004). In summary: 2.46 g of dried sediment was sieved through 10 and 15 µm precision sieves. Then the sediment fraction between 10-15 µm was subjected to a series of settling and decanting steps until this fraction contains less than 15% other calcareous particles than *T. heimii* shells.

Then, 186 µg of the monospecific *T. heimii* sample was chemically treated using "the stepwise cleaning procedure for the preparation of foraminiferal calcite for elemental analysis" described by Barker *et al.* (2003). Since *T. heimii* shells (10-20 µm) are smaller than foraminifera tests (100-1000 µm), the cleaning protocol had to be adapted by adding a centrifuge session before any overlying solution was removed from the sample vials. For a detailed overview of the modified Barker *et al.* (2003) method, see Appendix 2.

An internal ^{89}Y standard was added prior to elemental analysis. Element concentrations of the dissolved sample were determined on the isotopes ^{43}Ca, ^{25}Mg, ^{88}Sr on a Finnigan Element 2 Inductively Coupled Plasma Mass Spectrometer (ICP-MS), at the Department of Geosciences, University of Bremen, Germany. In contrast to the coupled FT – ICP-OES system, dissolution occurs in a single step prior to analysis and offline measurements yield one element/Ca value per sample, essentially an average over the entire sample. Sample GeoB 5008-3 was measured twice. During the first measurement, the sample was too concentrated ([Ca] = 12473.312 ppb). The sample was diluted until [Ca] = 4421.774 ppb and the measurement was repeated. Analytical errors of the elemental concentrations (standard deviations based on 10 runs) were better than 0.3%.

9.2.5. Statistical methods

Analysis of variance (ANOVA) was used to determine if there is any difference between the mean Mg/Ca values and between the mean Sr/Ca values, obtained with three different methods. An on-line ANOVA calculator was used (Soper, 2011). Mean and standard deviation values used in ANOVA are given in Table 9.1. Since we only have one measurement for the *T. heimii* method (*T. heimii* Test in Table 9.1), this value was used as the mean value and standard deviation was set to be zero for this method.

9.2.6. SEM imagery

In order to detect dissolution effects of the chemical reagents used in the new cleaning protocol for *T. heimii* shells, around 50 mg of bulk sediment was placed in three Eppendorf vials: one with 10 ml distilled water buffered with ammonia, one with 10 ml IONX and one with 10 ml MNX. For distilled water buffered with ammonia and IONX, stubs for scanning electron microscopy (SEM) were prepared after 5 hours, 24 hours and two days. For MNX, SEM stubs were prepared after 16 hours. One bulk sample stub was also prepared, without any chemical treatment.

Sample GeoB 5008-3	Sediment	Method	Mg/Ca (mmol/mol)	Sr/Ca (mmol/mol)	Mg/Ca mean	Mg/Ca SD	Sr/Ca mean	Sr/Ca SD
T.heimii Test	Isolated *T. heimii* shells	New *T. heimii* Protocol	5.51	12.08	5.51	0	12.08	0
Foram Test 1	Isolated *T. heimii* shells	Traditional Foram	5.81	15.62	5.77	0.057	15.280	0.481
Foram Test 2	Isolated *T. heimii* shells	Traditional Foram	5.73	14.94				
FT Test 1	Isolated *T. heimii* shells	Flow Through	5.87	13.63	3.57	1.995	12.393	1.145
FT Test 2	Isolated *T. heimii* shells	Flow Through	2.46	11.37				
FT Test 3	Isolated *T. heimii* shells	Flow Through	2.37	12.18				

Table 9.1 – Measured Mg/Ca and Sr/Ca values for three different methods: T.heimii Test = new cleaning protocol for the elemental analysis of T. heimii shells from sediments, Foram Test = standard cleaning protocol for the elemental analysis of foraminifera (Barker *et al.*, 2003), FT Test = flow-through sequential dissolution device coupled to an ICP-OES – Mg/Ca mean, Mg/Ca SD, Sr/Ca mean, Sr/Ca SD are mean and standard deviation (SD) values used in ANOVA

9.3. Results

9.3.1. New cleaning protocol for the elemental analysis of *T. heimii* shells from sediments

When sample GeoB 5008-3 is chemically treated according to "the new cleaning protocol for the elemental analysis of *T. heimii* shells from sediments", the measured values for Mg/Ca and Sr/Ca are 5.51 and 12.08 mmol/mol respectively (*T. heimii* Test in Table 9.1).

9.3.2. Flow-Through sequential dissolution device connected to an ICP-OES

Sample GeoB 5008-3 was analyzed three times with a Flow-Through sequential dissolution device connected to an ICP-OES (FT Test 1, FT Test 2, and FT Test 3 in Table 9.1). The three sequential dissolution pathways of sample GeoB 5008-3 are shown in Fig. 9.1. The x-axis represents time in seconds. The y-axis represents the concentration of the measured elements – scandium (Sc), calcium (Ca), strontium (Sr) and magnesium (Mg) – in counts per second. Sc is used as a measure for acid strength (HNO_3 concentration).

With increasing time, and increasing acid strength, we observe several peaks, which are simultaneous for Ca, Sr and Mg (Fig. 9.1). These peaks represent a dissolution phase of the sample calcite. When Ca (counts per s) reaches zero, no more calcite is present in the sample. For FT Test 1, FT Test 2 and FT Test 3, these dissolution peaks occur at different time intervals. For sample FT Test 1, we do not observe a distinct dissolution peak: a first peak occurs between 900 and 1200s and a second, broader peak occurs between 1700 and 2600s. For sample FT Test 2, the dissolution peaks occurs between 1300 and 1600s. For sample FT Test 3, the peak occurs a little earlier than for sample FT Test 2, between 700 and 1000s.

Fig. 9.2 shows the correlation between Mg and Ca, and Sr and Ca for the *Globigerinoides ruber* standard that was used. The standard has a known Mg/Ca concentration of 4.12mmol/mol and a known Sr/Ca concentration of 1.37mmol/mol (Table 9.2). During measurements with the ICP-OES, the Mg-Ca-slope of the standard was 0.1972 and the Sr-Ca-slope was 0.17 (Fig. 9.2, Table 9.2).

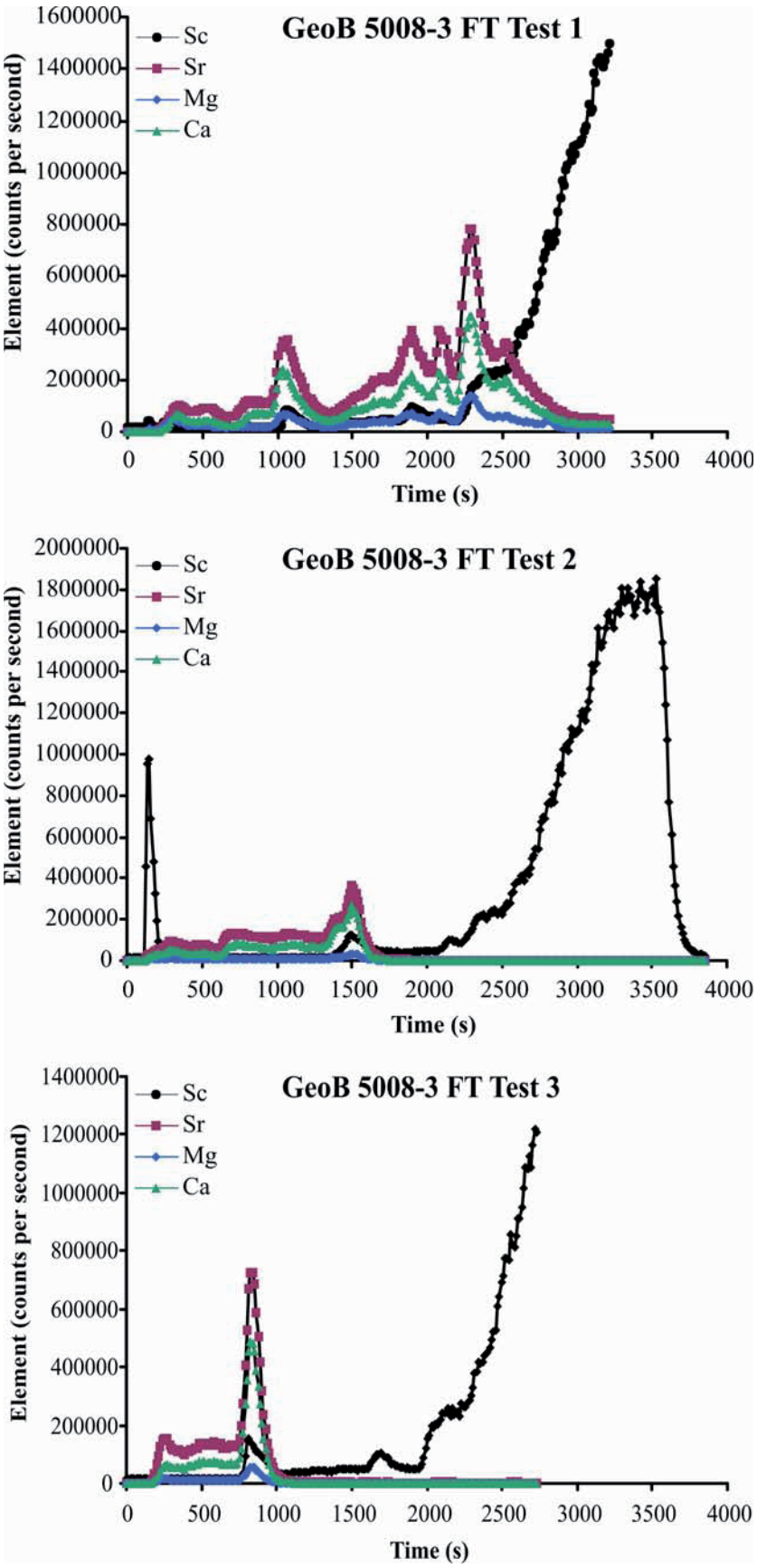

Fig. 9.1 – Sequential dissolution pathways of samples GeoB 5008-3 – The x-axis represents time in seconds, the y-axis represents the concentration of the measured elements (Sc, Ca, Sr and Mg) in counts per second

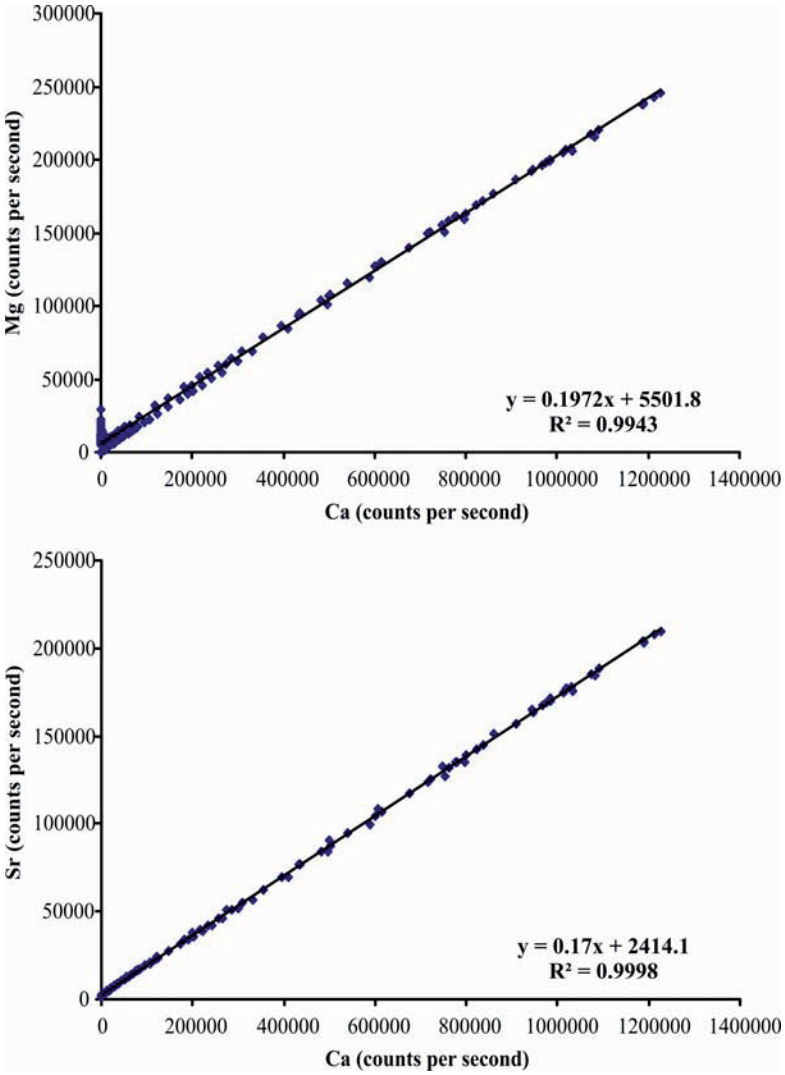

Fig. 9.2 – Correlation between Mg and Ca, and Sr and Ca for the *Globigerinoides ruber* standard

Sample GeoB 5008-3	Mg-Ca-slope$_{standard}$	R^2	Mg/Ca$_{standard}$ (mmol/mol)	Mg-Ca-slope$_{sample}$	R^2	Mg/Ca$_{sample}$ (mmol/mol)
FT Test 1	0.1972	0.9943	4.12	0.2812	0.9518	5.87
FT Test 2	0.1972	0.9943	4.12	0.1179	0.9398	2.46
FT Test 3	0.1972	0.9943	4.12	0.1135	0.9786	2.37
Sample GeoB 5008-3	**Sr-Ca-slope$_{standard}$**	**R^2**	**Sr/Ca$_{standard}$ (mmol/mol)**	**Sr-Ca-slope$_{sample}$**	**R^2**	**Sr/Ca$_{sample}$ (mmol/mol)**
FT Test 1	0.17	0.9998	1.37	1.6916	0.9917	13.63
FT Test 2	0.17	0.9998	1.37	1.4115	0.9792	11.37
FT Test 3	0.17	0.9998	1.37	1.5121	0.9900	12.18

Table 9.2 – Overview of Mg-Ca-slope, Mg/Ca, Sr-Ca-slope and Sr/Ca for the *Globigerinoides ruber* standard and for samples GeoB 5008-3 FT Test 1, FT Test 2 and FT Test 3

Fig. 9.3 shows the correlation between Mg and Ca, and Sr and Ca for samples GeoB 5008-3 FT Test 1, FT Test 2 and FT Test 3. Table 9.2 gives an overview of the Mg-Ca-slope and Sr-Ca-slope for the three test runs of sample GeoB 5008-3. The calculated Mg/Ca values for FT Test 1, FT Test 2 and FT Test 3 were 5.87, 2.46 and 2.37 mmol/mol respectively (Table 9.1, 9.2). The calculated Sr/Ca values for FT Test 1, FT Test 2 and FT Test 3 were 13.63, 11.37 and 12.18 mmol/mol respectively (Table 9.1, 9.2).

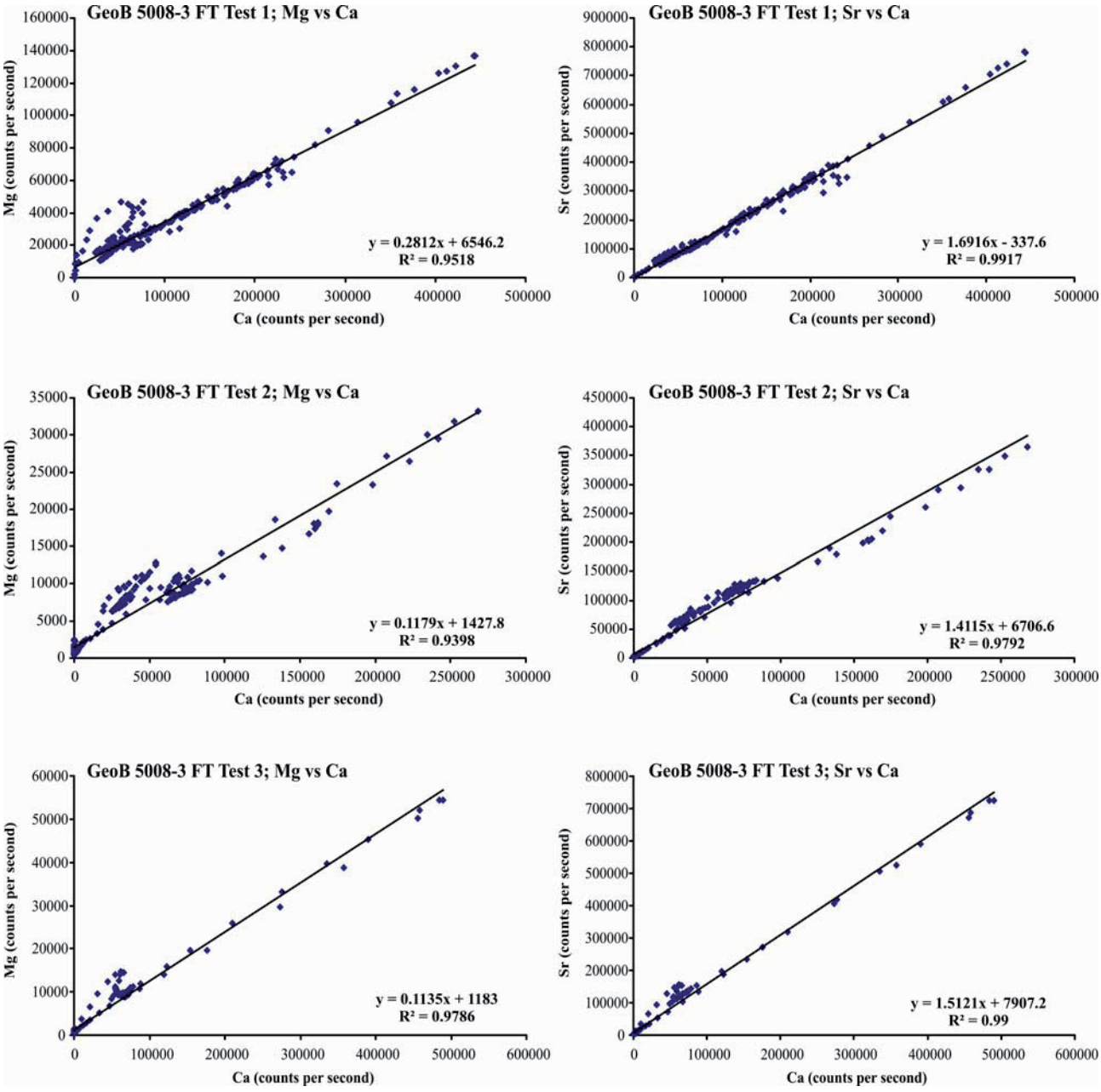

Fig. 9.3 – Correlation between Mg and Ca, and Sr and Ca for samples GeoB 5008-3 FT Test 1, FT Test 2 and FT Test 3

9.3.3. Standard cleaning protocol for the elemental analysis of foraminifera

After chemical treatment according to the standard cleaning protocol for the elemental analysis of foraminifera (Barker *et al.*, 2003), sample GeoB 5008-3 was analyzed with an ICP-MS. During the first measurement (Foram Test 1 in Table 9.1), the sample was too concentrated, and Mg/Ca and Sr/Ca values are 5.81 and 15.62 mmol/mol respectively. During the second measurement (Foram Test 2 in Table 9.1), Mg/Ca and Sr/Ca values are 5.73 and 14.94 mmol/mol respectively.

9.3.4. Statistical methods

Table 9.3 gives the outcome of both ANOVA's, one for the Mg/Ca values and one for the Sr/Ca values. In order for the test to be significant at the 95% confidence level, the p-value needs to be less than or equal to 0.05 ($p \leq 0.05$); in order for the test to be significant at the 90% confidence level, the p-value needs to be less than or equal to 0.10 ($p \leq 0.10$). When considering the Mg/Ca values, the p-value is 0.398, which means that the test is not significant at the 95% or 90% confidence level ($p \geq 0.05$ and $p \geq 0.10$). When considering the Sr/Ca values however, the p-value of 0.086 means that the test is not significant at the 95% confidence level ($p \geq 0.05$), but the test is significant at the 90% confidence level ($p \leq 0.10$).

Anova with Mg/Ca values					
Source of variation:	**SS**	**df**	**MS**	**F**	**p**
Between:	6.744	2	3.372	1.270	0.398
Within:	7.963	3	2.654		
Total:	14.708	5			
Anova with Sr/Ca values					
Source of variation:	**SS**	**df**	**MS**	**F**	**p**
Between:	11.797	2	5.899	6.202	0.086
Within:	2.853	3	0.951		
Total:	14.650	5			

Table 9.3 – ANOVA table – SS = sum of squares, df = degrees of freedom, MS = mean square, F = F-value, p = p-value

9.3.5. SEM imagery

SEM images, taken for the purpose of testing for dissolution effects are summarized in Fig. 9.4. We would like to point out that the sediment did not undergo any sieving or settling prior to SEM imagery; the chemical reagent was added to the bulk sample. Fig. 9.4 is therefore no measure for the purity of the sample.

9.4. Discussion

In foraminiferal studies it has been noted that sample preparation for Sr/Ca analysis does not require the same degree of rigor as is necessary for Mg/Ca analysis; it seems that foraminiferal Mg/Ca values are much more sensitive to contamination than foraminiferal Sr/Ca values (Barker *et al.*, 2003). In the following discussion we will compare Mg/Ca and Sr/Ca values of *Thoracosphaera heimii* shells from one core-top sample, processed and analyzed with three different cleaning techniques. We will make a preliminary attempt to evaluate the effectiveness of the newly proposed cleaning protocol for the elemental analysis of *T. heimii* shells from sediments.

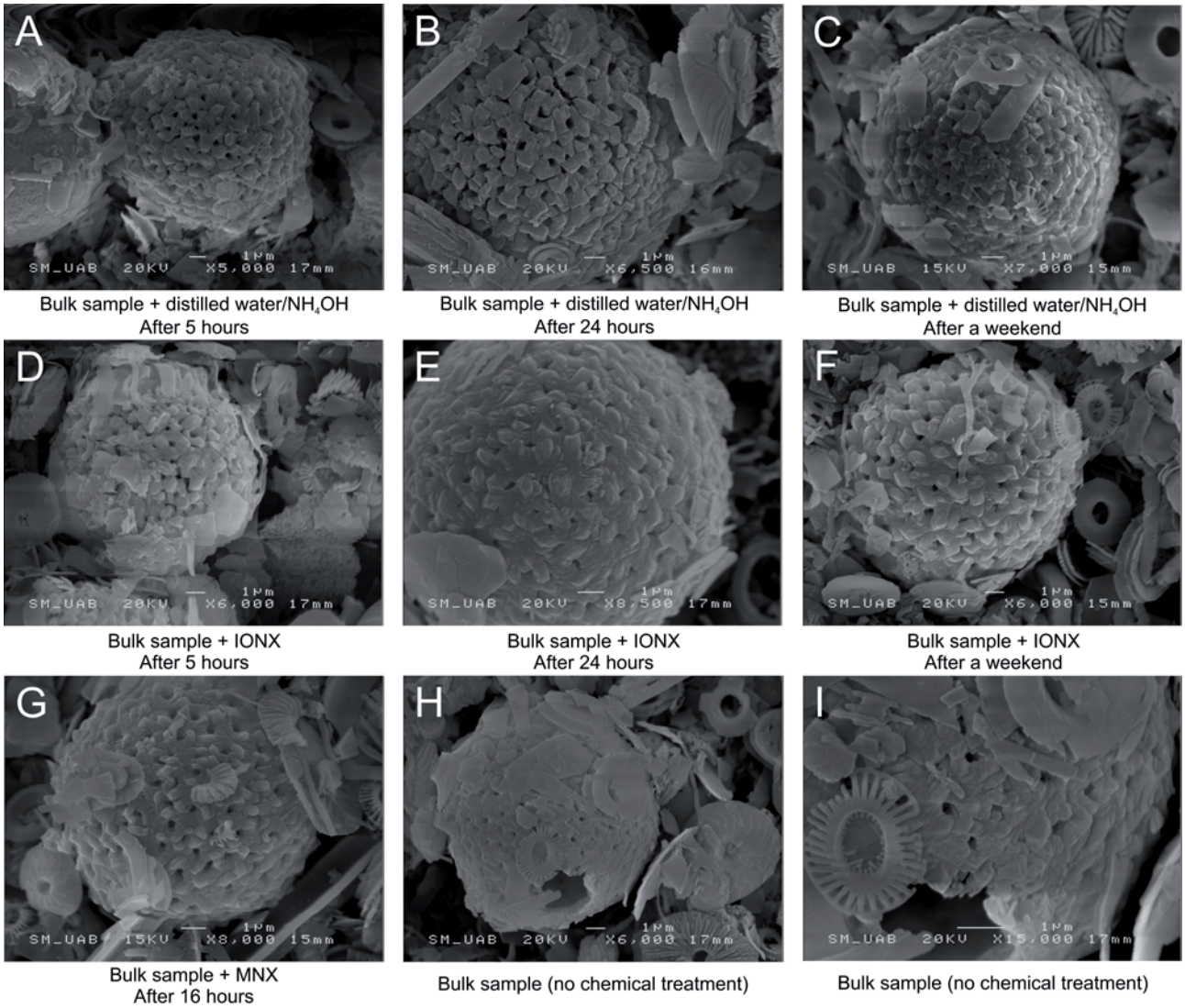

Fig. 9.4 – SEM imagery of possible dissolution effects on *T. heimii* shells from bulk sediment. Please note that this figure is not a measure for the purity of the sample.

9.4.1. Dissolution

Barker *et al.* (2003) found a decrease in the foraminiferal Mg/Ca ratio of up to 10-15%, due to dissolution of the sample carbonate during reductive treatment. Also use of dilute acid leaching to remove adsorbed contaminants caused partial dissolution of the foraminiferal calcite and a corresponding decrease in Mg/Ca (Barker *et al.*, 2003). Since dissolution can severely alter the primary element signal, our first concern was whether or not the different chemical reagents, used in the newly proposed *T. heimii* cleaning protocol, cause the calcium carbonate *T. heimii* shells to dissolve. The three chemical reagents tested were bidistilled water buffered with a few drops of ammonia (NH_4OH), IONX (bidistilled water and NH_4OH) and MNX (bidistilled water, NH_4OH and hydroxylamine hydrochloride).

A preliminary, qualitative assessment of dissolution effects, based on scanning electron microscope (SEM) imagery (Fig. 9.4), shows there is no dissolution of the *T. heimii* shells. Shells from chemically treated bulk sediment (A-G in Fig. 9.4) look similar to shells from untreated bulk sediment (H and I in Fig. 9.4): the characteristic crystal pattern of *T. heimii*, polygonal crystals organised around regularly distributed pseudopores, is very distinct in all SEM images. There also does not seem to be a difference between the duration of the treatment. In order to do a quantitative assessment, more experiments need to be done.

9.4.2. Observed differences in Mg/Ca

All measured Mg/Ca values of sample GeoB 5008-3 are within the Mg/Ca range for cultured *T. heimii* (2.6-7.3 mmol/mol; Gussone *et al.*, 2010). However, within this study, we observe significant differences for Mg/Ca between the three used cleaning protocols. Especially the second and third run with the flow-through device (FT Test 2 and FT Test 3) produced significantly lower Mg/Ca values.

For the measurement of foraminiferal Mg/Ca ratios, it has been shown that the removal of silicate contamination (clay minerals) is the most important step (Barker *et al.*, 2003). On average, clay minerals contain between 1 and 10 weight% Mg (Deer *et al.*, 1992). In an example, foraminiferal Mg/Ca decreased from 10.5 to 2.5mmol/mol during clay removal (Barker *et al.*, 2003). Since this was the first time we chemically treated *T. heimii* shells from sediments for elemental analysis, it is possible that clay particles, adsorbed to the *T. heimii* shell wall, were not adequately removed. However, in order to investigate this further, we need to do more experiments and we need more detailed SEM images.

Another possibility would be the accumulation of clay particles inside the empty *T. heimii* shells. The major difference between our newly proposed cleaning protocol for *T. heimii* shells and the standard cleaning protocol for the elemental analysis of foraminifera, is that foraminifera tests are being crushed prior to analysis, in order to crack open the test chambers. By doing so, the debris trapped inside is released and washed away during several rinsing steps (Barker *et al.*, 2003). Unfortunately, the small size of *T. heimii* shells (10-20 μm) prevents us from doing this. When the chemically treated, uncrushed *T. heimii* shells are dissolved in HNO_3 prior to analysis, possible internal non-calcareous particles will not be dissolved, but will remain in the sample solution and will be measured as well. During the sequential dissolution process of the flow-through method however, the *T. heimii* shells are being dissolved gradually from the outside in. Therefore, any non-calcareous particles that would be trapped inside the *T. heimii* shells stay on the sample filter and are not measured by the ICP-OES. This could explain why the second and third run with the flow-through device produced significantly lower Mg/Ca values than the other two methods. The higher value of the first FT run (FT Test 1) can probably be explained by the formation of a clot. When dissolution does not occur gradually, perhaps it is possible that some non-calcareous particles slip through the filter. Clot formation would also explain why the dissolution time is higher during the first flow-through run, since clots take longer to dissolve.

Another factor to consider is the contribution of Mg from Mn-Fe-oxide coatings. Foraminiferal shells from sediment cores commonly possess a Mn-rich oxide coating formed if Mn^{2+} has been mobilized during anoxic breakdown of organic matter deeper in the sediment column (Boyle, 1983). Barker *et al.* (2003) calculated that the contribution of Mg from these coatings to the Mg/Ca ratio of a typical foraminiferal sample is about 1%. Also diagenesis might have an influence on foraminiferal Mg/Ca. For instance Ferguson *et al.* (2008) observed a thin coating (a few μm thick) of high-Mg inorganic calcite on the inside walls of picked foraminifera from the Eastern Mediterranean. This diagenetic coating has also been reported by Boussetta *et al.* (2011). At first glance, SEM images of cleaned *T. heimii* shells show no evidence of any possible coatings. However, we need more experiments in order to determine whether or not the reductive step in the newly proposed cleaning protocol for *T. heimii* shells from sediments thoroughly removes Mg-rich coatings formed in the sediments. More detailed SEM images and microprobe analyses are needed to determine if coatings are formed on the inner walls of the *T. heimii* shells.

9.4.3. Observed differences in Sr/Ca

Compared to the Sr/Ca value of cultured *T. heimii* shells (2.24-2.49 mmol/mol; Gussone *et al.*, 2010), the Sr/Ca value of sample GeoB 5008-3 is five to seven times higher. Even if clay particles are trapped inside the *T. heimii* shells, as is possibly the case as discussed above, this would not contribute to the Sr/Ca value of the sample, since clay minerals contain insignificant amounts of Sr (Deer *et al.*, 1992). Also Mn-Fe-oxide coatings usually do not contain high Sr amounts. So far we do not have an explanation for the high Sr/Ca value of the *T. heimii* shells in sample GeoB 5008-3, allthough it should be noted that the sample is located at the Mid Atlantic Ridge, thus hydrothermal alteration of the sediment could be a possible determining factor. To get a better understanding we need to do more experiments including samples with lower Sr/Ca values, i.e. within the range of cultured *T. heimii* shells.

The Sr/Ca values of sample GeoB 5008-3 are more significant ($p = 0.086$) than the Mg/Ca values of sample GeoB 5008-3 ($p = 0.398$). This seems to coincide with the observation made in foraminiferal research that sample preparation for foraminiferal Sr/Ca analysis does not require the same degree or rigor as is necessary for foraminiferal Mg/Ca work (Barker *et al.*, 2003).

9.5. Conclusion

In the present study, core-top sample GeoB 5008-3 was processed according to the newly proposed cleaning protocol for the elemental analysis of *T. heimii* shells from sediments. In addition, the sample was also processed following the standard cleaning protocol for the elemental analysis of foraminifera, adapted for *T. heimii* shells; and following a sequential dissolution protocol, using a Flow-Through (FT) device. Although well within the Mg/Ca range of cultured *T. heimii* shells, Mg/Ca values of sample GeoB 5008-3 differ between the three cleaning techniques. Lower Mg/Ca values are being produced when the sample is sequentially dissolved (FT). This could be evidence for contaminating clay particles trapped inside the empty *T. heimii* shells. Sr/Ca values are five to seven times higher than Sr/Ca values in cultured *T. heimii* shells and seem to be more robust than Mg/Ca values.

Acknowledgements

Thanks are given to all cruise participants and the crew of Meteor cruise M41-2 for recovering the investigated surface sediment sample. We are also greatful to Heather Stoll (Department of Analytical Chemistry, University of Oviedo, Spain) and Henning Kuhnert (MARUM, University of Bremen, Germany) for carrying out the minor element to calcium measurements; and to Jeroen Groeneveld (MARUM, University of Bremen, German) for analyzing the sample with the Flow-Through device. We also thank all members of the working group of Historical Geology and Paleontology (University of Bremen) for their general assistance. This research was financed by the German Science Foundation (DFG), as a subproject of the International Graduate College Proxies in Earth History (EUROPROX).

References

Bairbakesh, A.N., Jollman, J., Sprengel, C., Thierstein, H.R., 1999. Disintegration of aggregates and coccospheres in sediment trap samples. *Marine Micropaleontology* 37, 219-223.

Barker, S., Greaves, M. & Elderfield, H. 2003. A study of cleaning procedures used for foraminiferal Mg/Ca paleothermometry. *Geochemistry, Geophysics, Geosystems* 4, 8407, doi:10.1029/2003GC000559.

Boussetta, S., Bassinot, F., Sabbatini, A., Caillon, N., Nouet, J., Kallel, N., Rebaubier, H., Klinkhammer, G., Labeyrie, L., 2011. Diagenetic Mg-rich calcite in Mediterranean sediments: Quantification and impact on foraminiferal Mg/Ca thermometry. *Marine Geology* 280, 195-204.

Boyle, E.A., 1983. Manganese carbonate overgrowths on foraminifera tests. *Geochimica et Cosmichimica Acta* 47, 1815-1819.

Deer, W.A., Howie, R.A., Zussman, J., 1992. An introduction to the rock forming minerals - 2nd edition. Prentice Hall., 712 pp.

Ferguson, J., Henderson, G., Kucera, M., Rickaby, R., 2008. Systematic change of foraminiferal Mg/Ca ratios across a strong salinity gradient. *Earth and Planetary Science Letters* 265, 153-166,

Groeneveld, J., Hathorne, E.C. & Kölling, M. 2010. Using a Flow Through device to reconstruct the thermal gradient in the water column based on *G. inflata* Mg/Ca. *Geophysical Research Abstracts*, Vol. 12, EGU2010-12153.

Gussone, N., Langer, G., Thoms, S., Nehrke, G., Eisenhauer, A., Riebesell, U., Wefer, G., 2006. Cellular calcium pathways and isotope fractionation in *Emiliania huxleyi*. *Geology* 34 (8), 625–628.

Gussone, N., Zonneveld, K., Kuhnert, H., 2010. Minor element and Ca isotope composition of calcareous dinoflagellate cysts of cultured *Thoracosphaera heimii*. *Earth and Planetary Science Letters* 289, 180-188.

Haley, B.A., Klinkhammer, G.P., 2002. Development of a flow-through system for cleaning and dissolving foraminiferal tests. *Chemical Geology* 185, 51-69.

Langer, G., Gussone, N., Nehrke, G., Riebesell, U., Eisenhauer, A., Kuhnert, H., Rost, B., Trimborn, S., Thoms, S., 2006. Coccolith strontium to calcium ratios in *Emiliania huxleyi*: the dependence on seawater strontium and calcium concentrations. *Limnology and Oceanogaphy* 51 (1), 310–320.

Mortyn, G.P., Elderfield, H., Anand, P., Greaves, M., 2005. An evaluation of controls on planktonic foraminiferal Sr/Ca: Comparison of water column and core-top data from a North Atlantic transect. *Geochemistry, Geophysics, Geosystems* 6 (12), Q12007, doi:10.1029/2005GC001047.

Schulz, H.D., C.W. Devey, J. Pätzold and G. Fischer (1999): Geo Bremen/GPI Kiel South Atlantic 1998, Cruise No. 41, 13 February - 13 June 1998. METEOR-Berichte, Universität Hamburg, 99-3, 341 pp.

Soper, D.S., 2011. Analysis of Variance (ANOVA) Calculator – One-Way ANOVA from Summary Data (Online Software). http://www.danielsoper.com/statcalc3.

Stoll, H.M., Encinar, J.R., Alonso, J.I.G., Rosenthal, Y., Probert, I., Klaas, C., 2001. A first look at paleotemperature prospects from Mg in coccolith carbonate: Cleaning techniques and culture measurements. *Geochemistry, Geophysics, Geosystems* 2, 200GC000144.

Stoll, H.M., Ziveri, P., 2002. Separation of monospecific and restricted coccolith assemblages from sediments using differential settling velocity. *Marine Micropaleontology* 46, 209-221.

Vink, A., 2004. Calcareous dinoflagellate cysts in South and equatorial Atlantic surface sediments: diversity, distribution, ecology and potential for paleoenvironmental reconstruction. *Marine Micropaleontology* 50, 43-88.

Zonneveld, K., 2004. Potential use of stable oxygen isotope composition of *Thoracosphaera heimii* (Dinophyceae) for upper water column (thermocline) temperature reconstruction. *Marine Micropaleontology* 50, 307-37.

Appendix 1: New cleaning protocol for the preparation of calcareous *Thoracosphaera heimii* shells for elemental analysis

The cleaning protocol for the preparation of calcareous *Thoracosphaera heimii* shells for elemental analysis is based on the cleaning method used for coccolithophores described by Bairbakesh *et al.* (1999) and Stoll & Ziveri (2002). Some additional sieving steps were included and the settling and decanting step was severely modified.

A1.1. Oxidation step

1. Add 3 ml of bidistilled water to a 45 ml plastic centrifuge tube.
2. Add 3 ml of 5% NaClO.
3. Add 1-2 g of freeze-dried sediment.
4. Add 1 ml of 30% H_2O_2. The reaction will be very strong in samples which are rich in organic material. Be careful that the gaseous build-up does not cause the sediment to bubble out of the tube. Oxidation of the organic material also helps disaggregation of the sample.
5. Place the tube in an ultrasonic bath for 10 seconds.
6. Add 2 ml of 5% NaClO.
7. Place the tube in an ultrasonic bath for 10 seconds.
8. Wait 10 minutes to allow the oxidation reaction to happen
9. Repeat steps (6) to (8) four times. If the sediment contains a lot of organic material, repeat more than four times.

A1.2. Sieving step

1. Wet sieve the sample through a 15 μm precision sieve. Only use bidistilled water buffered with 25% NH_4OH. The calcareous shells of *T. heimii* tend to dissolve when pure bidistilled, without NH_4OH buffer, water is used.
2. Bring the fraction smaller than 15 μm back into the centrifuge tube.

A1.3. Reduction step

1. Prepare the reducing solution ("MNX"): add 50 g of hydroxylamine hydrochloride to a 1000 ml glass flask. Add 600 ml of bidistilled water and 400 ml of 25% NH_4OH.
2. Add 30 ml of MNX to the sediment in the centrifuge tube. Shake and ultrasonicate the sample to make sure all of the sediment is in suspension.

3. Place the tube on a rotating carousel and let it rotate for no longer than 24 hours. Reductive treatment will remove Mn-Fe-oxide coatings on the shell wall which might have been formed in the sediment and contain high amounts of Mg.
4. Centrifuge the sample.
5. Remove and dispose of the overlying solution with a syringe.

A1.4. Ion exchange step

1. Prepare the oxidizing solution ("IONX"): add 65 ml of 25% NH_4OH to a 2000 ml glass flask. Add 1000 ml bidistilled water.
2. Add 30 ml of IONX to the sediment in the centrifuge tube. Shake and ultrasonicate the sample to make sure all of the sediment is in suspension.
3. Place the tube on a rotating carousel and let it rotate for 24 hours. Ion exchange treatment will remove adsorbed cations, especially adsorbed Mg, which is very abundant in clay minerals.
4. Centrifuge the sample.
5. Remove and dispose of the overlying solution with a syringe.

A1.5. Sieving step

1. Wet sieve the sample through a 10 μm precision sieve. Only use bidistilled water buffered with 25% NH_4OH. The calcareous shells of *T. heimii* tend to dissolve when pure bidistilled, without NH_4OH buffer, water is used.
2. Bring the fraction bigger than 10 μm back into the tube. The tube now contains the cleaned sediment fraction between 10 and 15 μm.

A1.6. Settling and decanting step

1. Place the tubes with sediment in the first row of a sample rack.
2. Fill the other rows of the sample rack with empty tubes. Make sure you label everything.
3. Add 30 ml of IONX to the tubes with sediment in the first row of the sample rack. Shake and ultrasonicate the tubes to make sure all of the sediment is in suspension.
4. Place the tubes back in the sample rack and let the sediment settle for 15 minutes.
5. Remove the overlying suspension with a syringe until there is 10 ml of solution left in the tubes. Be sure to take a different syringe for every sample.
6. Transfer the suspension from the syringe into one of the empty tubes.
7. Repeat steps (3) to (6) until the overlying suspension is transparant and all particles are in the settled sediment. Usually repeating the settling six times should be sufficient.
8. Transfer the settled sediment into an Eppendorf vial. The sample is now ready for treatment.

Appendix 2: Stepwise cleaning procedure for the preparation of foraminiferal calcite for elemental analysis by Barker *et al.* (2003), modified for *Thoracosphaera heimii* shells.

Beforehand, samples have been sieved through 10 and 20 µm precision sieves and have been made monospecific in *Thoracosphaera heimii* shells using the method of Zonneveld (2004).

The main problem that had to be overcome when applying the cleaning procedure of Barker *et al.* (2003) on the *Thoracosphaera heimii* samples was the size difference between foraminifera tests (100-1000 µm) and *T. heimii* shells (10-20 µm). The bigger foraminifera tests sink to the bottom of the vial and are visible with the naked eye, whereas the majority of the smaller *T. heimii* shells stay in suspension. In order not to lose too much *T. heimii* shells, the foraminiferal protocol of Barker *et al.* (2003) was adapted to *T. heimii* shells by adding a centrifuge session before any overlying solution is removed from the vials. Centrifuging the samples after every step will make this method much more labor intensive. Several samples can be cleaned at once.

A2.1. Initial cleaning step

1. Add 1 ml of ultrapure water to the samples. It is substantial to use separate pipette tips for adding and removing reagents.
2. Place the sample rack in an ultrasonic bath for one minute.
3. Centrifuge the samples.
4. Remove the overlying solution using a pipette.

A2.2. Removal of clay minerals

1. Add 500 µl of ultrapure water to the samples.
2. Place the sample rack in an ultrasonic bath for one minute. Ultrasonicating the samples will improve removal of clay minerals which are attached very tightly to the shell walls.
3. Centrifuge the samples. It has to be noted that this step contradicts the minimal settling technique to remove clay minerals proposed by Barker *et al.* (2003). However, a centrifuge step is absolutely needed in order not to lose too much *T. heimii* shells (see above).
4. Remove the overlying solution using a pipette.
5. Repeat steps (1) to (4) five times.
6. Add 500 µl of methanol to the samples. The lower viscosity of this reagent in comparison to water should detach clay minerals still attached to the *T. heimii* shells.
7. Place the sample rack in an ultrasonic bath for one minute.
8. Centrifuge the samples.
9. Remove the overlying solution using a pipette.

10. Repeat steps (6) to (9) three times.
11. Add 500 µl of ultrapure water to the samples.
12. Place the sample rack in an ultrasonic bath for one minute.
13. Centrifuge the samples.
14. Remove overlying solution using a pipette.
15. Repeat steps (11) to (13) four to five times.
16. Note: unlike the foraminifera tests, the *T. heimii* shells are not crushed prior to cleaning. Therefore it is likely that some clay minerals inside the shells are still present after treatment.

A2.3. Removal of organic matter = oxidation step

1. Heat the ultrasonic bath to 80°C.
2. Prepare a NaOH – H_2O_2 solution in 50 ml flask: buffer 100 µl 30% H_2O_2 solution with 667 µl 30% NaOH. Add ultrapure water until flask is filled with 50 ml.
3. Add 500 µl of the NaOH – H_2O_2 solution to the samples.
4. Place the sample rack in the pre-heated ultrasonic bath. Ultrasonicate 1 minute, wait 2.5 minutes, ultrasonicate 1 minute, wait 2.5 minutes, ultrasonicate 1 minute, wait 2.5 minutes, ultrasonicate 1 minute. Make sure any gaseous build-up is released so that the vials are not under any pressure.
5. Centrifuge the samples.
6. Remove the overlying solution using a pipette.
7. Repeat steps (3) to (6) two times.
8. Add 1 ml of ultrapure water to the samples.
9. Place the sample rack in an ultrasonic bath for one minute.
10. Centrifuge the samples.
11. Remove the overlying solution by using a pipette.

A2.4. Dissolution of the sample

1. Add 1 ml of 0.075M HNO_3 to the samples.
2. Shake to remove CO_2 and let the reaction take place completely.

CHAPTER 10

CONCLUSIONS AND OUTLOOK

In this thesis we investigated the stable oxygen isotope composition and minor element to calcium ratios of *Thoracosphaera heimii* shells from surface sediments. To answer the two main questions raised at the introduction of this thesis:

Stable oxygen isotope composition ($\delta^{18}O$) of *Thoracosphaera heimii*:

- Can we gain more information about the $\delta^{18}O$ of *T. heimii* shells in surface sediments?
- Is there a difference between different hydrographical areas?

In contrast to the Atlantic Ocean, no temperature – $\delta^{18}O$ correlation could be observed for the Indian Ocean samples. In this area, *T. heimii* $\delta^{18}O$ values show a wide range with a narrow temperature range, suggesting non-temperature (sedimentary) effects are present.

- Do we find a correlation with temperature from a specific depth in the upper water column?

For the core top samples in the Atlantic Ocean, the temperature – $\delta^{18}O$ correlation slightly improves when temperatures at mixed layer depth are considered. This depth is the presumed living depth of *T. heimii*. The depth at which $\delta^{18}O$ is incorporated into its calcareous shell.

- Can we improve the use of $\delta^{18}O$ of *T. heimii* shells as a temperature proxy?

Since the results obtained in this thesis support the suggestions from previous studies, we postulate that the main advantage of the *T. heimii* $\delta^{18}O$ proxy is the possibility to reconstruct temperatures from a specific depth in the water column, notably the mixed layer depth.

Minor element to calcium ratios (ME/Ca) of *Thoracosphaera heimii*:

- How can we measure the ME/Ca ratios of *T. heimii* shells in surface sediments?

This was the first study to look at the elemental composition of T. heimii shells from sediment. Therefore, we developed a new cleaning protocol for the elemental analysis of *T. heimii* shells from sediments, which is based on previously published cleaning protocols for coccolithophores.

- Do the ME/ Ca ratios of *T. heimii* shells from natural sediments differ from culture values?

The Mg/Ca and Sr/Ca ratios in natural sediments show a large range (with extreme values of up to 25 mmol/mol) and exceed the Mg/Ca and Sr/Ca ratios of cultured *T. heimii* by far.

- Can we find any correlation with environmental parameters of the upper water column?

Highest *T. heimii* Mg/Ca ratios occur in the core top samples which are also characterized by highest temperatures. However, these values are also well outside the Mg/Ca range of cultured *T. heimii*. Therefore caution is advised when interpreting these results. *T. heimii* Sr/Ca is possibly correlated with the carbonate chemistry of the seawater. In order to better understand these results, more information about the biomineralization of *T. heimii* is needed.

- Are the ME/Ca ratios contaminated by the sediment?

Although temperature seems to influence *T. heimii* Mg/Ca, the high range in Mg/Ca values most likely can be explained by contaminant phases from the sediment, which were not adequately removed during the chemical cleaning. Flow-Through analysis, using sequential dissolution of the sample, revealed that the sediment contamination is most likely due to clay particles trapped inside the empty *T. heimii* shells. A more rigorous cleaning protocol is needed.

For future studies on the isotopic composition of *T. heimii* shells, it is important to quantify the different non-temperature effects influencing the cyst $\delta^{18}O$ composition. Since the method to isolate *T. heimii* shells from the sediment does not yield samples that are 100% monospecific in *T. heimii*, one should try to assess the $\delta^{18}O$ signal coming from other calcareous particles than *T. heimii*. One way to do so could be to analyze the samples with different levels of purification, as Zonneveld (2004) already did. The other possibility would be to use flow cytometry to separate the *T. heimii* shells from other particles. However, high laboratory costs could be a disadvantage of this technique.

Within this study, minor element to calcium ratios of *T. heimii* shells from surface sediments were measured for the first time. The newly developed cleaning protocol, based on the cleaning protocol for coccolithophores, still has a lot of flaws. Further testing of the method is necessary in order to make sure that contaminating phases from the sediment are removed adequately. Extensive SEM imagery would be very helpful here. I also encourage the use of the Flow-Through device, since it is very likely that the most contaminating particles (clay) are trapped inside the shells. The technique of sequential dissolution dissolves the calcareous shells from the outside in, leaving behind whatever particles are still inside. For this study the Flow-Through was used to measure a sample with extreme Sr/Ca values. In the future, samples with a large range in Sr/Ca and Mg/ca values need to be analyzed as well.

In order to understand the *T. heimii* Mg/Ca and Sr/Ca signals better, more insights are needed into the biomineralization and element incorporation model of *T. heimii*. Culture experiments could further investigate the correlation between the minor element to calcium ratios of *T. heimii* and temperature and/or the carbonate chemistry of the seawater/culture medium. Cultured shells could then be analyzed with e.g. a microprobe to analyze their elemental composition into detail and to examine if the shell wall is indeed built up of two layers of calcite with a different elemental composition, as was suggested by Gussone *et al.* (2010).

As a last suggestion, the elemental composition could be analyzed in *T. heimii* shells from water samples at different depths in the water column. Since no sediment influences are present there, it could be determined if the observed signals are indeed a temperature signal (Mg/Ca) or carbonate chemistry signal (Sr/Ca). The measured values of the shells should be compared to the values of the surrounding water mass.